2021

# Interactions Between Microbial, Neuronal, and Immune Cells in the Digestive System

Fanny Matheis


# INTERACTIONS BETWEEN MICROBIAL, NEURONAL, AND IMMUNE CELLS IN THE DIGESTIVE SYSTEM

A Thesis Presented to the Faculty of
The Rockefeller University
in Partial Fulfillment of the Requirements for
the Degree of Doctor of Philosophy

by
Fanny Matheis
June 2021

# INTERACTIONS BETWEEN MICROBIAL, NEURONAL, AND IMMUNE CELLS IN THE DIGESTIVE SYSTEM

Fanny Matheis, Ph.D.
The Rockefeller University 2021

The intestine is the largest continuous environmental interface of the body. As such, it exerts homeostatic tissue functions, including digestion, sensing and absorption of nutrients, and excretion of waste products. In performing these roles, the intestine faces the unique challenge of remaining tolerant to harmless or beneficial diet- and microbe-derived stimuli, while simultaneously protecting against pathogen invasion. To tackle these challenges, the intestine houses both the body's largest immune compartment, as well as a vast neuronal network, the enteric nervous system (ENS). In concert with the commensal intestinal microbiota, the enteric immune and nervous systems communicate with one another, and this crosstalk was the focus of my thesis work. The studies as presented here are divided into two parts: The first part will focus on the influence of gut microbes on the murine ENS and its functions in host physiology. The second part will investigate the dynamic interplay between gut microbes, neurons and immune cells in the murine intestine during homeostasis and upon microbial perturbations.

The human intestinal tract is home to ~10 trillion commensal microbes (Sender et al., 2016). The microbiota influences key physiological processes including nutrient absorption and lipid metabolism. Further, it has been demonstrated to influence the basal activity of intestine-associated cells, including the excitability of enteric neurons (Furness et al., 2013). Alterations to the composition of the gut microbiota have a potential role in systemic disorders including obesity and diabetes (Ridaura et al., 2013). Yet, the mechanisms underlying these effects of the microbiota, and whether they are mediated by components of the ENS, are still poorly understood. In addition, the cellular circuits and molecular components that mediate gut-to-enteric neuron or gut-to-brain communication remain largely unknown. We thus aimed to determine how commensal microbes influence enteric neurons and their functions to better characterize their role in tissue function and further sought to investigate how disturbances to the microbial composition – during microbial dysbiosis and enteric infections – impact the ENS and host physiology.

Using translating ribosomal affinity purification (TRAP)-sequencing, coupled with confocal microscopy, we found that enteric neurons are functionally adapted to the intestinal segment they occupy. By utilizing germ-free mice, we uncovered a stronger influence of the microbiota on distal intestine neurons, correlating with the region's higher bacterial density. Chronic antibiotic-mediated microbial depletion reinstated our findings in germ-free mice, establishing that specific subsets of enteric neurons, including those expressing the neuropeptide cocaine and amphetamine-regulated transcript (CART), are dependent on the microbiota for their survival. Notably, these changes were not permanent, as colonization of germ-free mice and replenishment of the microbiota of antibiotic-treated mice restored neuronal numbers and neuropeptide levels.

We found that murine enteric infections with different pathogens led to lasting intestinal inflammation, functional disturbances and most notably, rapid and persistent enteric neuron loss driven by a persistent alteration to the microbial composition post-infection; however, restoration of a healthy microbiota was sufficient to induce tissue recovery. Mechanistically, neuronal loss post-infection and following microbial depletion was mediated by a novel form of enteric neuronal cell death, involving the non-canonical inflammasome components NLRP6 and caspase 11.

In further characterizing enteric neuronal populations, we identified a subset of intestinal CART+ neurons that were enriched in the distal intestine and modulated by the microbiota. Through microbial modulation strategies and chemogenetic targeting, we found that these enteric CART+ neurons regulate metabolic parameters including blood glucose and insulin levels. Retro- and anterograde tracing studies revealed that a subset of enteric CART+ neurons send axons to the gut sympathetic ganglion and are synaptically connected to the liver and pancreas. Together, we uncovered a gut-pancreas-liver circuit that regulates glucose metabolism by sensing microbial cues. This peripherally-restricted circuit offers unique neuronal targets for the treatment of metabolic disorders, such as type 2 diabetes, which would bypass central nervous system effects.

We further aimed to better characterize the role of neuro-immune interactions in the context of enteric pathologies, including post-infectious intestinal dysfunction and neuronal damage observed upon enteric infections. We further sought to determine whether a state of tolerance could be induced upon exposure to enteric pathogens, preventing tissue damage during subsequent infections. Finally, we aimed to characterize the role of extrinsic gut-projecting neurons to understand their role in sensing and responding to luminal cues, including enteric infections.

Using cell sorting-independent transcriptomics, confocal imaging, genetic gain- and loss-of-function approaches, surgical lesioning, chemogenetic manipulations, as well as multiple microbial manipulation strategies, we identified a critical role for enteric neuron-macrophage crosstalk in limiting ENS damage induced by a single enteric infection. A population of tissue-resident macrophages residing in close proximity to enteric neurons responded to luminal cues by upregulating a tissue-protective signature, and mediated enteric neuronal protection through adrenergic receptor signaling, and an arginase 1-polyamine program. Notably, we found engagement of macrophage adrenergic receptor signaling to be dependent on local catecholamine release by gut-innervating sympathetic neurons. We further uncovered that these sympathetic neurons on their end are tuned by enteric microbes and microbial products, in that a healthy microbiota suppresses, and absence of a microbiota, dysbiosis and infection enhance their activity. Finally, we found that previous infection with unrelated pathogens prevented infection-induced neuronal loss during subsequent, heterologous infections, suggesting a form of innate immune memory, or “trained tolerance”. Of note, while enteric bacterial and helminth infections induced distinct immune responses, these converged at the level of tissue-protective intestinal macrophages, which mediated enteric neuronal protection, aiding host fitness. Together, this work identified a functional role for interactions between

sympathetic neurons, tissue-resident macrophages and enteric neurons in limiting infection-induced tissue damage.

Overall, the research presented in this work uncovered that the ENS relies on the gut-resident microbiota for its homeostatic tissue function, with influence for local intestinal function and systemic metabolism. Furthermore, through communication with gut-extrinsic sympathetic neurons, tissue-resident macrophages upregulate and maintain a tissue-protective program, which protects enteric neurons from excessive damage during primary enteric infections and prevents cumulative damage during subsequent perturbations.

*To my family,*

*without whom I would never have come this far.*

**ACKNOWLEDGMENTS**

Many people have been instrumental in making this work possible. First, I would like to express my gratitude to my mentor Dr. Daniel Mucida. I am extremely thankful for the experience you have enabled me to have in the lab over the past years. I truly appreciate your guidance and mentorship, and also you having given me the space to branch out and explore wherever science took us over this time. You create an environment of inclusion and collaboration in the lab, which really enables us all to succeed.

I thank all my wonderful collaborators who immediately contributed the work presented in this thesis, and without whom this work would not have been possible. I am particularly grateful to Dr. Paul Muller, who I had the honor of working with closely over the past years ("2 weeks"), and who is an extraordinary scientist, but also wonderful colleague and friend. I truly appreciate all that I have learned from you and from working with you. I would also like to especially thank Drs. Ilana Gabanyi and Christina Graves, as well as Drs. Marc Schneeberger-Pané and Tomasz Ahrends for their contributions to this work.

I would like to further extend my gratitude to all members of the Mucida lab, past and present. To name but a few, Mariya – Dr. – London, thank you so much for being such a wonderful colleague and friend over these past years, for always making time for a tea, dinner or a long walk, and for making sure that I can always, always rely on you. Drs. Angelina Bilate, Juliana Bortolatto and Bernardo Reis, thank you for all your advice, support, empowerment, and friendship over this time. Aneta Rogoz and Yasmeen Khan deserve major credit for tirelessly working to maintain smooth lab operations.

I also want to express my gratitude to Drs. Gabriel Victora, Juan Lafaille and their respective lab members for fruitful discussions during our weekly joint lab meetings, and to the members of the Nussenzweig lab, in particular Dr. Harald Hartweger, for having been wonderful neighbors and colleagues over the years.

I sincerely thank Drs. Paul Cohen and Priya Rajasethupathy, who have provided invaluable support and guidance over these years as my thesis committee, both in terms of scientific expertise and career advice. I would also like to thank Dr. Jakob von Moltke for kindly serving as an external examiner on my thesis defense.

I thank Drs. Sid Strickland and Emily Harms, and the staff of the Dean's office, Cris, Stephanie, Marta, Andrea and Kristen for all your support, advocacy, and behind-the-scene work.

I also wish to thank the staff of the Bio-Imaging Resource Center, in particular Drs. Alison North and Christina Pyrgaki, for all their advice, efforts and support with imaging strategies over the years and for making the imaging core my second home. I am also indebted to the staff of the Comparative Bioscience Center, particularly Sara Gonzales, for taking care of our animals in the most compassionate way.

My most heartfelt gratitude goes to my wonderful family and friends. Most of all, I would like to thank my parents Dietlinde and Günter, my siblings Valerie, Valentin, Leonie, Emilie, and Cécile, and my grandmother Anna for their unconditional love and support,

and never failing to remind me of what really matters in life. No words can truly express how much it all means to me.

I would also like to honor Dr. Jonatan Ersching, a brilliant scientist and wonderful friend. I miss you, today and every day, and just wish you were still here.

Finally, I would like to thank anyone who I did not mention separately, but who somehow influenced my experience during my graduate training over the past years.

## DISCLAIMER

This thesis contains portions of a manuscript and publications written in collaboration with Drs. Daniel Mucida, Paul A. Muller and Tomasz Ahrends. The work as presented was performed in collaboration with the listed co-authors, and is either published or submitted to peer-reviewed journals as indicated below:

### Chapter 1:

Microbial modulation of peripheral neuronal and immune circuitry. **Matheis F** and Mucida D. *Trends in Neurosciences*. Review. Manuscript in preparation.

Gut Macrophages: Key players in intestinal immunity and tissue physiology. Muller PA*, **Matheis F*** and Mucida D. *Curr Opin Immunol* (2019). Review. (* denotes co-first authorship)

### Chapters 2 and 3:

Microbiota-modulated CART+ enteric neurons autonomously regulate blood glucose. Muller PA*, **Matheis F***, Schneeberger M*, Kerner ZJ, Jové V, and Mucida D. *Science.* (2020) (* denotes co-first authorship)

Adrenergic signaling in muscularis macrophages limits infection-induced neuronal loss. **Matheis F***, Muller PA*, Graves CL, Gabanyi I, Kerner ZJ, Costa-Borges D, Ahrends T, Rosenstiel P and Mucida D. *Cell.* (2020) (* denotes co-first authorship)

Enteric pathogens induce tissue tolerance and prevent neuronal loss from subsequent infections. Ahrends T, Aydin B, **Matheis F**, Classon C, Furtado C, Lira SA, Mucida D. Under review in *Cell*.

Microbiota modulate sympathetic neurons via a gut-brain circuit. Muller PA, Schneeberger M*, **Matheis F***, Wang P*, Ilanges A, Kerner ZJ, del Mármol J, Rezende de Castro TB, Perkins M, Han W, de Araujo I and Mucida D. *Nature.* (2020) (* denotes equal contribution)

**TABLE OF CONTENTS**

## LIST OF FIGURES

**CHAPTER 1:**



**CHAPTER 2:**

**CHAPTER 3:**

## LIST OF ABBREVIATIONS

| | |
|---|---|
| 5-HT | 5-hydroxytryptamine, serotonin |
| 5-HT4R | 5-hydroxytryptamine receptor 4 |
| ABX | Antibiotics |
| ACh | Acetylcholine |
| AChR | Acetylcholine receptor |
| ACTH | Adrenocorticotropic hormone |
| AD | Alzheimer's disease |
| Adrb2 | Adrenoceptor beta 2 |
| AgRP | Agouti gene-related peptide |
| AHR | Aryl hydrocarbon receptor |
| AIM2 | Absent in melanoma 2 |
| AMP | Antimicrobial peptide |
| ANNA-1 | Antineuronal nuclear antibody-1 (Anti-Hu) |
| APC | Antigen-presenting cell |
| AR | Adrenergic receptor |
| ARC | Arcuate nucleus of the hypothalamus |
| Arg-1 | Arginase-1 |
| ASC | Apoptosis-associated speck like protein containing a caspase recruitment domain |
| ASF | Altered Schaedler flora |
| ATAC | Assay for Transposase-Accessible Chromatin |
| ATP | Adenosine triphosphate |
| AUC | Area under the curve |
| BA | Bile acid |
| BCG | Bacillus Calmette–Guérin |
| BMP2 | Bone morphogenetic protein 2 |
| BMPRIIα | Bone morphogenetic protein receptor IIα |
| *C. rodentium* | *Citrobacter rodentium* |
| C21 | Compound 21 |
| CARD | Caspase activation and recruitment domain |
| CART | Cocaine- and amphetamine-regulated transcript |
| Cartpt | CART prepropeptide |
| Casp | Caspase |
| CCK | Cholecystokinin |
| Cckar | Cholecystokinin A Receptor |
| CD | cluster of differentiation |
| CG | Celiac ganglion |
| CG-SMG | Celiac-superior mesenteric ganglion (fusion) |
| ChAT | Choline acetyltransferase |
| ChIP | Chromatin immunoprecipitation |
| CPA3 | Carboxypeptidase A3 |
| CREB | cAMP response element-binding protein |

| | |
|---|---|
| CRISPR | Clustered regularly interspaced short palindromic repeats |
| CSF1 | Colony Stimulating Factor 1 |
| CSF1R | Colony Stimulating Factor 1 receptor |
| CTB | Cholera toxin subunit B |
| CysLT2R | Cysteinyl leukotriene receptor 2 |
| cysLT | Cysteinyl leukotriene |
| DAMP | Damage-associated molecular pattern |
| DFMO | Difluoromethylornithine |
| DMN | Dorsal motor nucleus of the vagus nerve |
| DNA | Deoxyribonucleic acid |
| DNBS | Dinitrobenzene sulfonic acid |
| Dpi | Days post infection |
| DREADD | Designer Receptors Exclusively Activated by Designer Drugs |
| DRG | Dorsal root ganglion |
| DSS | Dextran sulfate sodium |
| DTA | Diphtheria toxin fragment A |
| E | Epinephrin (adrenaline) |
| EAN | Enteric-associated neuron |
| EC | Enterochromaffin cell |
| eEAN | Extrinsic enteric-associated neuron |
| EEC | Enteroendocrine cell |
| EGFR | Epidermal growth factor receptor |
| ELAVL3 | ELAV (embryonic lethal, abnormal vision) like RNA binding protein |
| ER | Estrogen receptor |
| Ex-GF | Former GF mouse |
| FFAR | Free fatty acid receptor |
| FLEX | Flip-excision |
| Flox | Flanking by LoxP |
| Fos | Fos proto-oncogene |
| FoxO | Forkhead box O3 |
| FST1 | Follistatin-1 |
| GABA | Gamma aminobutyric acid |
| GALT | Gut-associated lymphoid tissue |
| Gcgr | Glucagon Receptor |
| GF | Germ-free |
| GFP | Green fluorescent protein |
| GI | Gastro-intestinal |
| GIP | Gastric inhibitory polypeptide |
| GITT | Gastrointestinal transit time |
| GLP-1/2 | Glucagon-like peptide-1/2 |
| GLUT | Glucose transporter |
| GO | Gene ontology |

| | |
|---|---|
| GPBAR1 | G Protein-Coupled Bile Acid Receptor 1 |
| GPCR/GPR | G protein-coupled receptor |
| GSDMD | Gasdermin D |
| *H. hepaticus* | *Helicobacter hepaticus* |
| HA | Hemagglutinin |
| HDAC | Histone deacetylase |
| hDTR | Human diphtheria toxin receptor |
| hi | high |
| hM3Dq | $G_q$-coupled human M3 muscarinic DREADD |
| hM4Di | $G_i$-coupled human M4 muscarinic DREADD |
| HPA | Hypothalamic-pituitary-adrenal |
| HSV-1 | Herpes simplex virus 1 |
| i.p. | intraperitoneal |
| i.v. | intravenous |
| IBD | Inflammatory bowel disease |
| IBS | Irritable bowel syndrome |
| ICC | Interstitial cell of Cajal |
| ICE | Interleukin-1 beta (IL-1 beta)-converting enzyme |
| IE | Intraepithelial |
| iEAN | Intrinsic enteric-associated neuron |
| IEC | Intestinal epithelial cell |
| IEL | Intraepithelial lymphocyte |
| IF | Immunofluorescence |
| Ig | Immunoglobulin |
| IGLE | Intraganglionic laminar ending |
| IL | Interleukin |
| IL-R | Interleukin receptor |
| ILC | Innate lymphoid cell |
| IMA | Intramuscular arrays |
| IMG | Inferior mesenteric ganglion |
| IML | Intermediolateral nucleus of the hypothalamus |
| INSL5 | Insulin Like 5 |
| Int | Intermediate |
| IPAN | Intrinsic primary afferent neuron |
| iPHIL | Inducible eosinophil-deficient mice |
| IP-PTT | Intraperitoneal pyruvate tolerance test |
| JG | Jugular ganglion |
| KO | Knockout |
| LAG3 | Lymphocyte Activating 3 |
| Lcn-2 | Lipocalin-2 |
| LFA-1 | Lymphocyte Function Antigen 2 (CD2) |
| Lgr5 | Leucine-rich repeat-containing G-protein coupled receptor 5 |
| LP | Lamina propria |
| LpM | Lamina propria macrophage (i.e., mucosal macrophage) |

| | |
|---|---|
| LPS | Lipopolysaccharide |
| LRR | Leucine-rich repeat |
| LTA | Lipoteichoic acid |
| Ly6C | Lymphocyte antigen 6 complex |
| LysM | Lysozyme M |
| Lyz2 | Lysozyme 2 |
| M cell | Microfold cell |
| mCherry | Monomeric Cherry (red fluorescent protein) |
| MHC II | Major histocompatibility complex II |
| MM | Muscularis macrophage |
| MS | Multiple sclerosis |
| MSK | Mitogen-and stress-activated protein kinase |
| Myd88 | Myeloid differentiation primary response 88 |
| nAChR | Nicotinic acetylcholine receptor |
| NE | Norepinephrine |
| NG | Nodose ganglion |
| NLRP | Nucleotide-binding oligomerization domain, Leucine rich Repeat and Pyrin domain containing |
| NMU | Neuromedin U |
| NMUR | Neuromedin U receptor |
| nNOS | Neuronal nitric oxide synthase |
| NO | Nitric Oxide |
| NOD | Nucleotide-binding oligomerization domain |
| NOS | Nitric oxide synthase |
| NPY | Neuropeptide Y |
| NTS | Nucleus Tractus Solitarius |
| ODC1 | Ornithine Decarboxylase 1 |
| $Oligo^{MM12}$ | Oligo-Mouse-Microbiota containing 12 species |
| op/op | Osteopetrotic |
| PAMP | Pathogen-associated molecular pattern |
| PASTAA | Predicting associated transcription factors from annotated affinities |
| PCA | Principal component analysis |
| PCR | Polymerase chain reaction |
| pCREB | Phosphorylated cAMP response element-binding protein |
| PD | Parkinson’s disease |
| Penk | Proenkephalin |
| PI-IBS | Post-infectious irritable bowel syndrome |
| PNS | Peripheral nervous system |
| POI | Post-operative ileus |
| POMC | Pro-opiomelanocortin |
| PP | Peyer’s patch |
| PRR | Pattern recognition receptor |
| PRV | Pseudorabies virus |

| | |
|---|---|
| PVN | Paraventricular nucleus of the hypothalamus |
| PYCARD | PYD and CARD domain containing |
| PYY | Peptide YY |
| RFP | Red fluorescent protein |
| RiboTag | Ribosome-tagging using hemagglutinin epitope insertion |
| RNA | Ribonucleic acid |
| ROS | Reactive oxygen species |
| RPL22 | Ribosomal protein L22 |
| rRNA | Ribosomal ribonucleic acid |
| SCFA | Short-chain fatty acids |
| Seq | Sequencing |
| SFB | Segmented filamentous bacteria |
| SGLT | Sodium-glucose linked transporter |
| Slc17a6 | Solute Carrier Family 17 Member 6 (encoding VGLUT2) |
| Snap25 | Synaptosomal-Associated Protein, 25kDa |
| SNS | Sympathetic nervous system |
| Sox10 | SRY-Box Transcription Factor 10 |
| SPF | Specific pathogen-free |
| *spiB* | *Salmonella* pathogenicity island 2/B |
| Splenda | Sucralose-based artificial sweetener (Splenda ®) |
| Spp | Species |
| SST | Somatostatin |
| SSTR | Somatostatin receptor |
| *SV* | *Strongyloides venezuelensis* |
| *T. cruzi* | *Trypanosoma cruzi* |
| *T. gondii* | *Toxoplasma gondii* |
| Tac1 | Tachykinin Precursor |
| Td | Tandem dimer |
| TED | Transepithelial dendrite |
| TGF-β | Transforming growth factor beta |
| TH | Tyrosine hydroxylase |
| $T_h$ | T helper cell |
| TLR | Toll-like receptor |
| TNF- α | Tumor necrosis factor alpha |
| Tph1 | Tryptophan hydroxylase 1 |
| TRAP | Translating Ribosome Affinity Purification |
| $T_{reg}$ | T regulatory cell |
| TRPV1/4 | Transient receptor potential channels, of the vanilloid subtype 1/4 |
| VGLUT2 | Vesicular glutamate transporter 2 |
| VIP(R) | Vasoactive intestinal peptide |
| Wif1 | WNT Inhibitory Factor 1 |
| WT | Wild-type |
| YP | *Yersinia pseudotuberculosis* |

# CHAPTER 1. INTRODUCTION

## 1.1 Overview of the mammalian digestive system

The digestive system comprises the organs that serve to take in, break down, transport, and assimilate food, i.e., convert it into usable nutrients, and expel waste products in the form of feces. It includes the gastrointestinal (GI) tract from the oral cavity to the anus, and the digestive glands – salivary-, gastric-, intestinal- and pancreatic glands, and the liver (Fig. 1.1)

Histologically, the esophagus, stomach, small and large intestines share a common basic structure consisting of a mucosal layer, with a single-cell epithelial layer and an underlying lamina propria, and submucosal, muscularis, and serosal (intraperitoneal organs) or adventitia (retro-/extraperitoneal organs) layers (Shen, 2009). In the small intestine, the epithelium contains finger-like projections, villi, that extend into the lumen and aid food absorption by increasing surface area. Invaginations between villi,

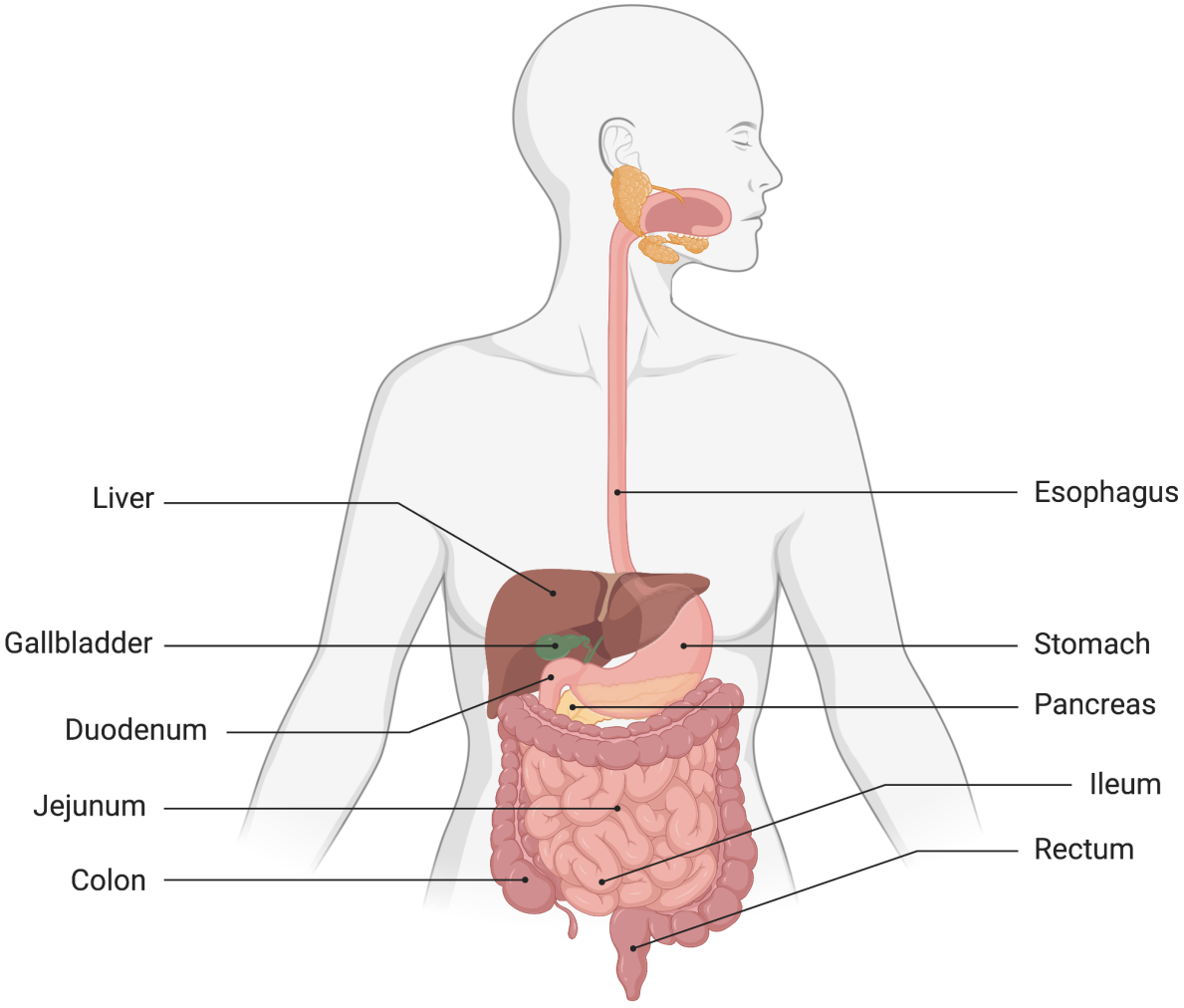


**Fig. 1.1. Anatomy of the human digestive system.** Schematic depicting the tissues involved in digestion and highlighting organs of relevance for this work. Created with Biorender.com

the crypts of Lieberkühn, contain the intestinal epithelial stem cell niche (Peterson and Artis, 2014). Villi decrease in length towards the distal small intestine and are absent in the colon, while crypt depth increases there (Peterson and Artis, 2014).

A rich microbial community colonizes the lumen of the GI tract, which gets denser and more diverse moving from proximal to distal intestine (Martinez-Guryn et al., 2019). The intestinal immune system, which makes up the body's largest immune compartment, as well as a vast neuronal network, the enteric nervous system (ENS), are embedded within the wall of the GI tract (Mowat and Agace, 2014).

### 1.1.1 Digestion and absorption

Food is taken up through the mouth, mechanically disrupted by teeth and tongue, and mixed with saliva, which increases lubricity and adds carbohydrate-degrading amylase. The bolus is then passed through pharynx and esophagus into the stomach, where it is mixed with gastric acids, and enzymatic breakdown continues. The partially digested product, chyme, is released through the pylorus (gastric sphincter muscle) into the duodenum (Kiela and Ghishan, 2016). Luminal contents move along the GI tract through coordinated contractions and relaxations of smooth muscles (peristalsis), while coordinated segmentation ensures sufficient epithelial contact time for absorption (Greenwood-Van Meerveld et al., 2017). Peristalsis is modulated by specialized pacemaker cells, the interstitial cells of Cajal (ICCs), that generate spontaneous electrical waves and are modulated by neurotransmitters (Greenwood-Van Meerveld et al., 2017). In the duodenum, which in humans is the top ~20 cm of the intestine, chyme is mixed with pancreatic juice containing proteolytic enzymes and bile. Pancreatic enzymes break down proteins, and products of enzymatic breakdown are beginning to be absorbed (Kiela and Ghishan, 2016). In the jejunum, the next 2-3 m, a large proportion of nutrients is absorbed. In a physiological setting, the ileum, the distal ~ 3 m of the small intestine, absorbs only a small remaining fraction of nutrients, with the exception of vitamin $B_{12}$ and bile acids (BAs) which are specifically absorbed in the terminal ileum. The large intestine primarily serves for water absorption, movement and temporary storage of indigestible food components, and excretion of fecal matter (Kiela and Ghishan, 2016).

The exocrine pancreas produces proteolytic enzymes and phospholipase A, which are secreted into the duodenum as zymogens (proforms), to prevent pancreatic autodigestion (Leung, 2010). Bile, an alkaline substance containing cholesterol and BAs, is produced in the liver and stored in the gall bladder. BAs, produced by the liver from cholesterol, serve lipid digestion and absorption as micelle-forming surfactants. They are secreted into the intestinal lumen as primary BAs and converted into secondary BAs by anaerobic bacteria including *Clostridia spp.* and *B. fragilis* (Ridlon et al., 2014). Aside from their role in nutrient absorption, they act as ligands for nuclear receptors regulating glucose-, lipid- and hepatic drug metabolism, and reduced levels upon microbial depletion lead to a decrease in serum glucose and triglyceride levels (Kuno et al., 2018; Ridlon et al., 2014).

### 1.1.2 Glucose uptake and its homeostasis through glucoregulatory organs

The majority of dietary carbohydrates come from sugars and starches, the storage form of plant-derived carbohydrates. Sugars include monosaccharides (e.g., glucose, galactose and fructose) and disaccharides (e.g., lactose, sucrose, maltose). Starches are initially digested by salivary and pancreatic enzymes, followed by further breakdown to monosaccharides by mucosal enzymes. Glucose and galactose are absorbed via the glucose transporter sodium-glucose transporter 1 (SGLT1), expressed on the luminal side of absorptive enterocytes (intestinal epithelial cells, IECs), while fructose is taken up via the glucose transporter 5 (GLUT5) by facilitated diffusion. On the basolateral side of IECs, monosaccharides are transported through the glucose transporter 2 (GLUT2) and released into the portal vein system (Kiela and Ghishan, 2016). The portal vein transports nutrients to the liver, where they are either broken down to generate energy, used for synthesis, or stored. Depending on blood glucose, insulin and glucagon levels, the liver synthesizes glucose from amino acids, lactate and glycerol by performing gluconeogenesis, or converts excess glucose into a storage form, glycogen via glycogenesis (Jones, 2016).

The islets of Langerhans of the endocrine pancreas produce the glucoregulatory hormones insulin and glucagon, as well as somatostatin (SST), and pancreatic polypeptide (Roder et al., 2016). The anabolic insulin is produced by pancreatic β-cells. It promotes energy storage by enhancing glucose uptake and utilization by insulin-dependent organs (primarily liver and skeletal muscle), thereby decreasing blood glucose levels, and increasing lipogenesis and protein biosynthesis (Roder et al., 2016). Insulin secretion is stimulated by elevated blood glucose, fatty acids, amino acids, the gut hormones glucagon-like peptide-1 (GLP-1) and gastric inhibitory polypeptide (GIP), increased parasympathetic tone and catecholamines acting on $\beta_2$-adrenergic receptors (ARs). Conversely, insulin secretion is inhibited by increased sympathetic tone, whereby catecholamines act on $\alpha_2$-ARs (Roder et al., 2016; Thorens, 2014). The catabolic glucagon is produced by pancreatic α-cells. As the primary antagonist of insulin, it promotes breakdown of energy stores and increases blood glucose levels, mainly by stimulating glycogenolysis and gluconeogenesis, and inhibiting glycogenesis in the liver (Roder et al., 2016).

## 1.2 The gut microbiota

The mammalian GI tract harbors a complex and diverse ecosystem of trillions of viruses, bacteria, archaea, protozoa and fungi, collectively termed the gut microbiota. It is estimated that as many microbes reside in the human GI tract as there are cells in the body (Sender et al., 2016). Technological advances such as high throughput genomics methods, including bacterial 16S rRNA sequencing, have led to a renaissance of the field over the past 15 years. Yet, the roots of human microbiome research can be traced back to Antonie van Leeuwenhoek, (1632-1723), whose pioneer work in microscopy allowed him to first visualize bacteria, including his own microbial flora (Tropini et al., 2017).

Bacterial density and diversity overall increases moving from proximal to distal GI tract. Chemical gradients, nutrient availability, alterations to the immune cell composition, production of antimicrobials, peristalsis and physical features of the intestine contribute to the changes in microbial composition found in the different anatomical locations. In the stomach, a highly acidic environment, mucosal thickness and strong peristaltic activity allow for relatively few bacterial species to survive (Thursby and Juge, 2017; Donaldson et al., 2016; Metchnikoff, 1901). Similarly, in the proximal small intestine, rapid transit of luminal contents, gastric acids passing through from the stomach, digestive enzymes, oxygen, and antimicrobials secreted from the epithelium impede colonization. By contrast, slower peristalsis, changes to the immune milieu and a largely anaerobe environment enable a richer community of microbes to colonize the distal small and large intestine (Thursby and Juge, 2017). Notably, while novel technologies have allowed us to gain much deeper insight into this microbial biogeography over the past decades, Ellie Metchnikoff, in 1901, already presented a map containing the key features thereof (Metchnikoff, 1901).

Yet, while Metchnikoff was unclear as to any host beneficial effects of this microbial ecosystem (Metchnikoff, 1901), it has now become evident that there are many. Notably, Rockefeller's René Dubos and colleagues, through work on germ-free (GF), mono-, and oligocolonized mice in the 1960s already brought forth the connections between the gut microbiota and host factors such as social behavior, stress, nourishment and immune function (Dubos et al., 1966; Dubos and Schaedler, 1964; Schaedler et al., 1965). Recent research unraveled that the gut microbiota positively influences nutrition (Sonnenburg and Bäckhed, 2016), pathogen resistance (Kim et al., 2017a), bone development (Zaiss et al., 2019) and immune maturation (Al Nabhani and Eberl, 2020; Chung et al., 2012), neurodevelopment (Vuong et al., 2020) and likely host behavior (Mayer et al., 2015; Thursby and Juge, 2017).

A key contribution to host physiology is microbial production and modification of metabolites and small molecules, particularly by colonic carbohydrate-fermenting anaerobe species. These include short-chain fatty acids (SCFAs), amino acids and their derivatives, most notably serotonin (5-hydroxytryptamine, 5-HT), histamine and γ-aminobutyric acid (GABA), BAs, and other signaling molecules including dopamine (Krautkramer et al., 2021; Thursby and Juge, 2017). However, how these microbially derived factors influence host physiology is only beginning to be understood.

Finally, despite its beneficial effects, the presence of the microbiota poses a potential danger to the host, including risk of breaching or outgrowth of certain species in settings of dysbiosis and infection, and thus requires tight regulation, which will be laid out in specific contexts.

## 1.3 Innervation of the intestine

The intestine is a densely innervated organ. Its innervation is comprised of an extrinsic arm, i.e., neurons the cell bodies of which are located in extraintestinal centers and which send axonal projections to the intestine, and an intrinsic one, i.e., gut-resident neurons, the cell bodies of which lie within the wall of the intestine and which form a branch of the autonomous nervous system (Fig. 1.2). Neurons of both compartments work in concert to control essential intestinal functions, such as nutrient absorption, motility, release of gut hormones, and digestion. They interact with the intestinal immune system and epithelial enteroendocrine cells (EECs) and transmit luminal information to extraintestinal centers, including the central nervous system (CNS) (Furness et al., 2014).

While this does not reflect the established nomenclature of the field, in our work studying GI innervation we use the term “enteric-associated neurons (EANs)” to collectively refer to both intrinsic neurons of the ENS located within the intestinal wall (intrinsic enteric-associated neurons, iEANs, i.e., enteric neurons) and extrinsic gut-innervating sensory afferents and sympathetic and parasympathetic efferents (extrinsic enteric-associated neurons, eEANs).

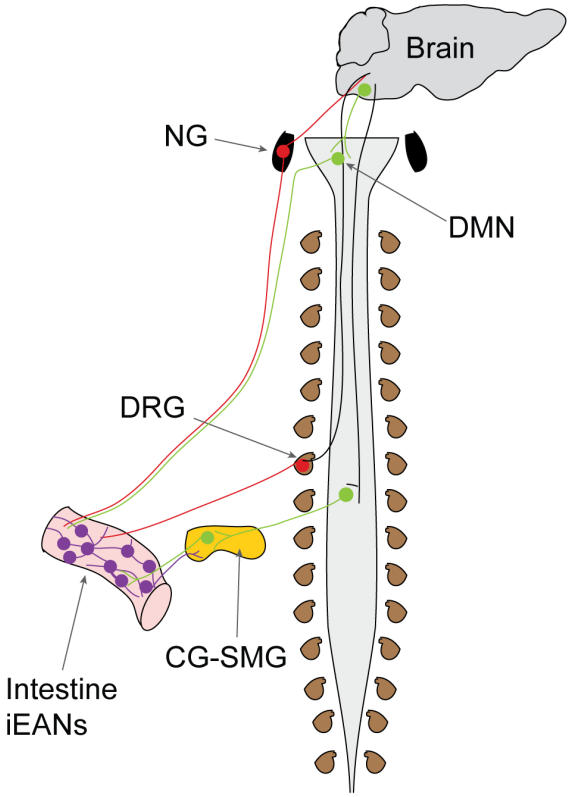


**Fig. 1.2. Innervation of the intestine.** Schematic depicting intrinsic enteric nervous system and extrinsic ganglia containing cell bodies of neurons connecting to the intestine. NG - nodose, DRG - dorsal root, CG-SMG - celiac-superior mesenteric ganglion, DMN - dorsal motor nucleus of the vagus nerve, iEANs - intrinsic enteric-associated neurons (ENS).

### 1.3.1 Intrinsic enteric nervous system

"It is evidently impossible to explain this complicated reaction of the isolated gut to local stimulation on any hypothesis which does not take into account the occurrence of a complicated system of nerve-fibres and ganglion-cells in the wall of the intestine." (Bayliss and Starling, 1899). While it is now well-established that critical neuronal input to enteric function also comes from extraintestinal centers, Bayliss and Starling's conclusions drawn from studies of the contraction patterns of explanted, denervated canine intestines underscore a unique feature of the GI tract – the ability of the ENS to perform essential functions without control from the CNS. It represents the only part of the peripheral nervous system (PNS) that is intrinsically capable of mediating independent reflex activity. Comprising a population of roughly 400-600 million neurons in humans, and around 1 million in mice, the ENS contains about as many neurons as the spinal cord (Furness, 2006).

Contrary to the CNS, which is sheltered from a large fraction of peripheral stimuli, blood-borne pathogens and endogenous and exogenous circulating factors by the blood-brain barrier, there is no such boundary for the ENS (Joly et al., 2020). Embedded in muscle and stromal layers, iEANs are in direct contact with myocytes, stromal and immune cells, and likely IECs, and may easily get exposed to penetrating luminal factors. The ENS consists of small groups of neuronal cell bodies (ganglia), bundles of nerve fibers connecting different ganglia, axonal projections innervating local blood vessels, the circular and longitudinal muscles, the mucosa (including ICCs) and some reaching the epithelial cell layer. A small population of so-called viscerofugal neurons also send projections to extraintestinal regulatory centers (Furness, 2012). Enteric neuronal ganglia

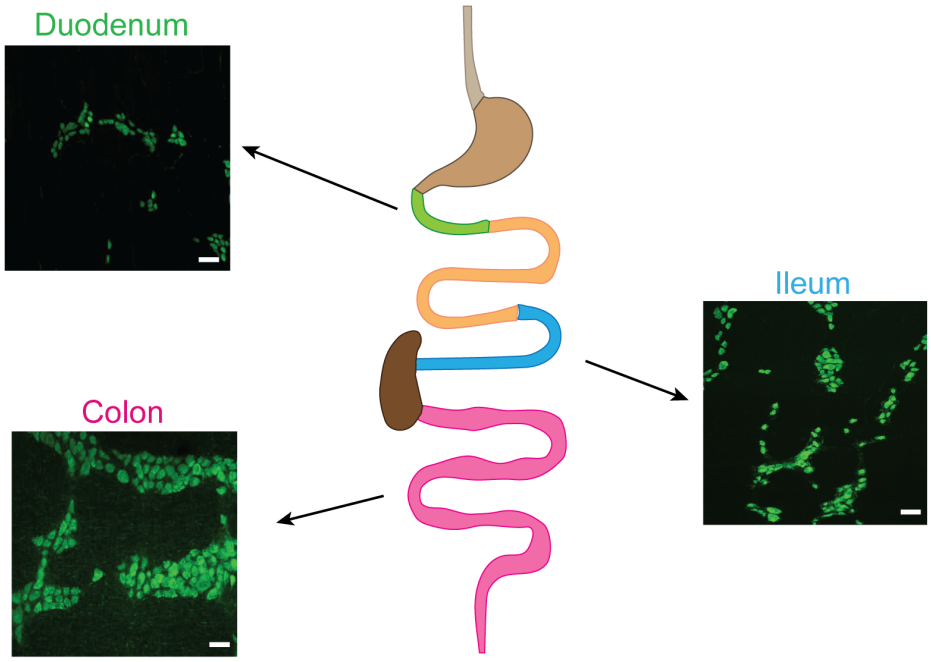


**Fig. 1.3. Distribution of intrinsic enteric neurons along the intestine.** Representative immunofluorescence images of murine duodenum, ileum and colon myenteric plexus regions stained with anti-neuronal nuclear antibody (ANNA-1). Scale bars, 50 µm.

and fibers form two large networks (plexuses) embedded within the intestinal wall: the submucosal or Meissner's plexus, located in the submucosal layer between lamina propria and muscularis propria, and the myenteric or Auerbach's plexus, embedded within the muscularis propria (Furness et al., 2014). The submucosal plexus contains fewer neurons than the myenteric plexus. Further, neuronal numbers increase along the intestine toward the distal end (Fig. 1.3, personal observations).

Enteric glia, a transcriptionally unique, unmyelinated glia population, are also part of the ENS (Rao et al., 2015). They outcompete iEANs in frequency by a factor of 3 to 5 (Veiga-Fernandes and Pachnis, 2017), surround iEAN cell bodies and fibers, and are microbially-regulated (Kabouridis et al., 2015). They are actively involved in processes such as neurotransmission (Boesmans et al., 2019), neuronal protection (Aube et al., 2006; Bush et al., 1998), regulation of peristalsis (Rao et al., 2017) and innate immune regulation (Ibiza et al., 2016).

Unlike the rest of the GI tissue, iEANs and glia are neural crest-derived (Obermayr et al., 2013). A small number of *Sox10*-expressing neural crest cells populates the embryonic foregut, where it undergoes proliferation and differentiation, giving rise to both iEANs and glia (Lasrado et al., 2017; Wang et al., 2011). Initiated *in utero*, ENS development continues postnatally (Foong, 2016). Although discrete adult enteric neurogenesis has been reported upon stimulation (Liu et al., 2009), it is generally thought to cease after weaning (Joseph et al., 2011; Pham et al., 1991; Uesaka et al., 2016). By contrast, a recent study has proposed a continuous turnover of iEANs in which differentiated iEANs die in a caspase-dependent manner, are phagocytosed by surrounding macrophages and replenished from a pool of nestin-expressing neuronal precursors (Kulkarni et al., 2017). In settings of neuronal damage, enteric glia have been suggested to serve as a reservoir for adult neurogenesis, which iEANs replenish from (Laranjeira et al., 2011). By contrast, other work has suggested a role for enteric glia in mediating iEAN death in a model of colitis (Brown et al., 2016). Thus, the effects of enteric glia on iEANs – beneficial or detrimental – may be context-dependent. Further, the mechanism(s) by which iEANs die in physiological and pathological conditions is unclear.

#### 1.3.1.1 iEAN subsets and neurochemical coding

The ENS consists of a variety of different neuron types using multiple different neurotransmitters (denoted in parentheses) to control intrinsic intestinal function. These include cholinergic excitatory muscle motor neurons (acetylcholine, ACh), nitrergic inhibitory muscle motor neurons (nitric oxide, NO), motor neurons to epithelium and arterioles (ACh), interneurons (ACh; NO; ATP), VIP-ergic secretomotor neurons (ACh; vasoactive intestinal peptide, VIP), intrinsic sensory neurons (intrinsic primary afferent neuron, IPAN) (ACh; calcitonin gene-related peptide, CGRP; tachykinin), and intestinofugal neurons to sympathetic ganglia (ACh; VIP; opioid peptides) (Furness, 2012). The dominating neurotransmitters in the ENS are the excitatory ACh, inhibitory NO, and primarily excitatory VIP. Glutamate, the major excitatory neurotransmitter in the CNS, is found in a small population of iEANs, albeit the functions of glutamatergic iEANs remains largely unclear (Liu et al., 1997).

Traditionally, enteric neurons have primarily been classified by morphology and pharmacological and immunohistochemical methods to locate neuropeptides, i.e., the neurochemical code (Furness, 2000). More recently, several studies using single-cell profiling techniques have provided more comprehensive mapping of the ENS, further unraveling iEAN identity and diversity in mice and humans (Drokhlyansky et al., 2020; Zeisel et al., 2018). For example, Regev and colleagues have identified 5, 7 and 3 different types of excitatory and inhibitory motor, and sensory neurons, respectively (Drokhlyansky et al., 2020). However, functional characterizations of these subsets are to date lacking.

Owing to their particular relevance to our studies, a more detailed overview of some iEAN neuropeptides will follow.

#### 1.3.1.2 Neuropeptides in the enteric nervous system

**Somatostatin (SST)**

SST was first isolated from the ovine hypothalamus as a substance inhibiting pituitary growth hormone (somatotropin) secretion (Brazeau et al., 1973). It has broad, mostly inhibitory effects on endocrine and exocrine secretion. SST is widely expressed throughout the CNS and periphery, including by pancreatic δ-cells (Rorsman and Huising, 2018), EECs (Gribble and Reimann, 2016), sensory afferents (Uyama et al., 2004), and the ENS (Furness, 2012; Gonkowski and Rytel, 2019; Portbury et al., 1995; Teitelbaum et al., 1984). Its effects are mediated via G protein-coupled SST receptors, SSTRs 1-5, expressed in a wide range of target tissues (Theodoropoulou and Stalla, 2013).

In the CNS, SST is expressed by a prominent population of hypothalamic neurons, where, aside from its eponymous effects on somatotropin secretion, it also inhibits the release of further hypothalamic and pituitary hormones, including adrenocorticotropic hormone (ACTH), dopamine and norepinephrine (NE) (Ben-Shlomo and Melmed, 2010). It is also found in large population of cortical inhibitory interneurons (Yavorska and Wehr, 2016).

In the digestive system, SST produced by pancreatic δ-cells and EECs inhibits secretion of insulin and glucagon, and enzyme release from the exocrine pancreas. Via inhibition of other GI hormones, it also reduces e.g., gastric acid production and bile secretion (Gribble and Reimann, 2016; Rorsman and Huising, 2018). SST expression by iEANs can be found in both plexuses, including myenteric interneurons and submucosal secretomotor neurons. Enteric SST is mostly thought to inhibit smooth muscle contraction and secretion (Furness, 2012; Gonkowski and Rytel, 2019; Portbury et al., 1995; Teitelbaum et al., 1984), albeit, owing to limited tool availability to study these neurons in a tissue-specific manner, these results are not conclusive.

**Cocaine- and amphetamine-regulated transcript (CART)**

*Cart* was first discovered in the rat brain, through a differential PCR screen aiming to identify transcripts enhanced by psychomotor stimulants (Douglass et al., 1995). It is widely, though discretely, localized throughout CNS areas, most prominently in hypothalamic nuclei and basal ganglia, where it is involved in regulating processes such

as feeding behavior, energy homeostasis, reward, stress, and addiction (Rogge et al., 2008).

Several different biologically active forms of CART peptide exist. These are generated by posttranslational processing of a proform (Dey et al., 2003; Thim et al., 1999; Thim et al., 1998), albeit these are mostly characterized in the CNS and active variants in peripheral tissues likely differ (Ekblad, 2006). Despite significant efforts, a receptor for CART has thus far not been identified, hampering studies of its functions. However, several studies point to a GPCR-mediated mechanism of target cell activation (Jones and Kuhar, 2008; Maletinska et al., 2007; Yermolaieva et al., 2001).

In the CNS, involvement in brain-wired feeding behavior and regulation of body weight was first suggested due to the predominant expression of CART in hypothalamic regions known to be involved in energy homeostasis and regulation of food intake, including the arcuate (ARC) and paraventricular nuclei (PVN) (Koylu et al., 1998; Koylu et al., 1997; Lau and Herzog, 2014). Subsequent studies established its potent anorexigenic effects, demonstrating that during food deprivation, hypothalamic CART levels are markedly decreased (Kristensen et al., 1998), and that central administration of CART peptide decreases, while its sequestration increases food intake (Kristensen et al., 1998; Lambert et al., 1998). Because CART levels in the ARC are regulated by circulating leptin (Lau and Herzog, 2014), and disrupted leptin signaling was associated with nearly undetectable hypothalamic CART levels, it has been suggested that hypothalamic CART-expressing Pro-opiomelanocortin (POMC) neurons mediate the effects of leptin in hypothalamic areas (Elias et al., 2001; Kristensen et al., 1998). More recently, however, these effects were reported to be predominantly mediated by AgRP neurons (Xu et al., 2018), while both AgRP and CART/POMC neurons were shown to regulate peripheral leptin-dependent sympathetic innervation (Wang et al., 2020). The close association of hypothalamic CART+ and NPY+ fibers, which has opposing effects on food intake, further suggests that negative regulatory mechanisms between these two populations exist (Lambert et al., 1998). In support of its anorexigenic role, several human genetic studies have found obese individuals to carry either polymorphisms or missense mutations in the *Cart* gene with reduced serum CART peptide levels (del Giudice et al., 2001; Yamada et al., 2002; Yanik et al., 2006).

CART has also been implicated in the response to systemic stress. It is found at every regulatory level of the hypothalamic-pituitary-adrenal (HPA) axis, and its levels increase in response to systemic stressors such as bacterial lipopolysaccharide (LPS) (Sergeyev et al., 2001) or cold exposure (Kong et al., 2003). Peripheral CART expression has also been found in the pancreas, portal vein, intestine, as well as vagal afferents and autonomic efferents (Rogge et al., 2008). In the pancreas, CART expression is documented in islet cells and in innervating afferent and efferent nerve terminals (Wierup et al., 2004; Wierup et al., 2005). CART-/- mice were shown to have impaired insulin production and glucose intolerance, suggesting a role for CART in regulating endocrine pancreatic function (Wierup et al., 2005).

In the intestine, CART is widely expressed particularly in the myenteric region across different species (Couceyro et al., 1998; Ekblad, 2006; Ekblad et al., 2003; Ellis and Mawe, 2003; Gunnarsdottir et al., 2007; Kuhar and Yoho, 1999; Murphy et al., 2000),

albeit in mice, enteric CART expression is not well documented. However, in recently published single-cell datasets, *Cart* can be found in a proportion of iEANs (Drokhlyansky et al., 2020; Zeisel et al., 2018), where it is co-expressed with NOS and ChAT. Given this overlap with both excitatory and inhibitory neurotransmitters, CART-expressing iEANs may play dual roles depending on the context. However, the functional roles of CART-expressing iEANs and CART peptide in the intestine remain largely unknown.

**Neuropeptide Y**

Neuropeptide Y (NPY), first isolated from the porcine hypothalamus in 1982 (Tatemoto et al., 1982), is the most abundant polypeptide in the mammalian brain (Yi et al., 2018). It exerts its biological functions by binding to G protein-coupled NPY receptors, Y1-5. The highest density of NPY+ neurons in the CNS is found in the hippocampus, while it has been most studied in the hypothalamus. It is also expressed across cortical regions, cerebellum and brainstem (Li et al., 2019). Acting in concert with AgRP, NPY is best known for its involvement in the regulation of food intake and energy homeostasis. The discovery that loss of neurons expressing the two peptides induces hypophagia, weight loss and starvation (Luquet et al., 2005), led to NPY receiving significant attention as a putative target for metabolic disease. Here, the orexigenic effects of hypothalamic NPY+ AgRP+ ARC neurons, functionally antagonize CART+ POMC populations, and are also regulated by circulating leptin (Cowley et al., 2001; Waterson and Horvath, 2015). Most recently, a hypothalamic-thalamic NPY circuit has been implicated in hunger-dependent food odor preference, whereby hypothalamic AgRP neurons projecting to the thalamus trigger thalamic NPY release and an olfactory response circuit enhancing food odor attraction (Horio and Liberles, 2021).

Outside the CNS, NPY expression can be found in postganglionic sympathetic (Holzer and Farzi, 2014; Lundberg et al., 1990), and a small population of dorsal root ganglion (DRG) neurons (Brumovsky et al., 2007). In the ENS, NPY is expressed in both submucosal and myenteric neurons (Holzer et al., 2012), where it has been ascribed inhibitory effects on gastrointestinal motility (Abot et al., 2018; Browning and Lees, 2000; Holzer et al., 1987), and a proinflammatory role in the context of inflammatory bowel disease (IBD) (El-Salhy and Hausken, 2016). However, overall, our understanding of its functions in the ENS is incomplete. As with other enteric neuropeptides, the lack of tools for site-restricted targeting approaches have thus far hampered the ability to study the roles of NPY in the periphery.

**Agouti-gene related peptide**

Agouti gene-related peptide (AgRP) was first described in the murine hypothalamus where it was found to be overexpressed in leptin-deficient mice and implicated in the control of body weight (Ollmann et al., 1997; Shutter et al., 1997). Together with NPY, hypothalamic AgRP has potent orexigenic effects. It acts as an interoceptive sensor that monitors and responds to circulating metabolic signals, most notably leptin (Cowley et al., 2001; Xu et al., 2018) and ghrelin (Betley et al., 2013; van den Top et al., 2004). Optogenetic AgRP neuron activation increases, whereas their inhibition decreases food consumption (Aponte et al., 2011; Krashes et al., 2011; Xu et

al., 2018). More recently, hypothalamic AgRP has further been suggested to also function as a driver for food discovery in fasted animals (Chen et al., 2015b).

The tissue distribution of AgRP is very restricted. Aside from the hypothalamus, it has thus far only been described in chromaffin cells of the adrenal medulla, where it has been implicated in the sympathetic response to fasting (Gupta et al., 2017). While in the hypothalamus it is co-expressed with NPY, which is also found in the intestine, whether AgRP might also be expressed by EANs has thus far not been answered.

#### 1.3.1.3 Microbial modulation of iEANs

In the CNS, the microbiota has been implicated as a critical modulator of normal neuronal development, function, and behavior (Diaz Heijtz et al., 2011; Kim et al., 2017b; Vuong et al., 2020; Vuong et al., 2017). In the intestine, GF mice have been shown to have neuroanatomical abnormalities in the ENS early postnatally, including decreased neuronal numbers and fiber density, as well as altered neurochemical coding in distal small and large intestines, accompanied by dysmotility (Collins et al., 2014). Thus, postnatal development of the ENS is likely influenced by the microbiota. This is further supported by the finding that the ENS in the scarcely colonized proximal small intestine is not altered in GF animals (Collins et al., 2014). Similar changes have been reported for adolescent and adult GF as compared to conventionally housed mice (Anitha et al., 2012; De Vadder et al., 2018; McVey Neufeld et al., 2015). Altered proportions of nitrergic iEANs and changes in neuronal firing patterns reported in GF mice (Collins et al., 2014; McVey Neufeld et al., 2013; McVey Neufeld et al., 2015) further suggest a role for the microbiota in influencing enteric neuronal network maturation. Notably, both structural and functional changes were restored upon conventionalization, i.e., colonization with microbiota of conventionally housed animals, (De Vadder et al., 2018; McVey Neufeld et al., 2015), suggesting a degree of adult ENS plasticity induced by microbial signals. Similarly, antibiotic-mediated microbial depletion of neonatal and juvenile mice resulted in altered neurochemical coding, dysmotility, and changes to iEAN excitability (Caputi et al., 2017; Hung et al., 2019; Hung et al., 2020). Of note, while different studies reported alterations to iEAN subtypes, the subtypes affected varied between reports. Because different antibiotics or combinations thereof were applied, specific bacterial species or their metabolites may distinctly shape neurochemical coding, and depletion or increase in one or another species may thus shift iEAN subtype frequency.

How do gut microbes influence iEANs? One possible route is through neuronal sensing of microbial components via Toll-like receptor (TLR) signaling. TLRs, which detect conserved microbial components known as pathogen-associated molecular patterns (PAMPs), are expressed by a wide range of intestine-resident cells, including IECs, immune cells, neurons and glia (Hyland and Cryan, 2016). TLR2 and TLR4 have been implicated in mediating iEAN survival during intestinal inflammation and microbial depletion, respectively (Anitha et al., 2012; Brun et al., 2013). Additionally, microbial stimulation of TLR2 and neuronal TLR2 signaling was suggested to induce enteric neurogenesis in adult antibiotic-treated mice (Yarandi et al., 2020). However, due the use

of global TLR-/- mice and systemic agonist treatment to determine neuronal TLR activation, bacterial sensing may also involve other intestinal cells.

One microbiota-modulated signal that has been suggested to mediate iEAN maturation is serotonin (5-HT). 95% of the body's 5-HT is produced in the intestine – most notably by enterochromaffin cells (ECs) – where it can act on at least 14 different receptors expressed by IECs, iEANs, and immune cells (Drokhlyansky et al., 2020; Yano et al., 2015; Zeisel et al., 2018), and has been implicated in peristalsis (Mawe and Hoffman, 2013) and intestinal inflammation (Ghia et al., 2009). Further, activation of the 5-HT receptor 5-$HT_4$R has been implicated in adult enteric neuroprotection and neurogenesis during homeostasis and colitis (Liu et al., 2009; Bianco et al., 2016). GF mice have been shown to have reduced levels of circulating, intestinal, and fecal 5-HT, and reduced numbers of ECs (Sjogren et al., 2012; Wikoff et al., 2009; Yano et al., 2015). Further, colonization of GF mice with indigenous spore-forming bacteria, which increased host 5-HT production, led to iEAN activation and rescued alterations in motility (Yano et al., 2015). Upon full conventionalization of GF mice, microbiota-dependent 5-HT release and activation of 5-$HT_4$R, expressed by iEANs (Drokhlyansky et al., 2020; Zeisel et al., 2018), was necessary and sufficient for ENS maturation (De Vadder et al., 2018). However, these studies were conducted using total body knockout mice for *Tph1*, the rate-limiting enzyme for 5-HT production, and systemic 5-$HT_4$ agonist treatment. Hence, while normalization of 5-HT levels by microbial colonization clearly drives iEAN maturation, and iEANs are capable of responding to exogenous 5-HT administration (Bertrand et al., 1997), the underlying mechanisms need further investigation.

The aryl hydrocarbon receptor (AHR), a nuclear receptor regulated by multiple endogenous, microbial and dietary signals has been suggested as another candidate for microbiota-iEAN interactions. *Ahr* expression by myenteric iEANs was shown to allow these neurons to sense microbial cues, and this signaling pathway was required for normal peristaltic activity. In the absence of a microbiota, neuronal *Ahr* expression was dampened, which resulted in abnormal motor output of enteric neuronal circuits and delays in intestinal transit time in GF and antibiotic-treated mice (Obata et al., 2020). Exogenous administration of AHR ligands rescued these changes, rendering AHR a role as a neuronal luminal biosensor, and linking microbial sensing to neuronal activity.

Mono-colonization of GF mice with an abundant gut bacterium, *Bacteroides thetaiotaomicron*, was also shown to increase iEAN and EC numbers and improve motility deficits (Aktar et al., 2020). This confirms the plastic potential of iEANs and suggests that products of single species can be sufficient to drive iEAN maturation. Yet, what specific microbial cues these might be, and how their presence gets sensed by, or information thereof relayed to, iEANs, remains unresolved.

### 1.3.2 Extrinsic innervation of the intestine

The GI tract receives extrinsic innervation from both afferent (sensory) and efferent (effector) populations. The cell bodies of neurons providing extrinsic intestinal innervation are located in 6 major ganglia (Fig. 1.2. above): Thoracic dorsal root ganglia (DRGs) and vagal nodose-jugular ganglia (NG/JG) contain cell bodies of neurons the axonal

projections of which transmit afferent information from the intestine to central centers. The dorsal motor nucleus of the vagus (DMN) and intermediolateral nucleus of the sacral spinal cord (IML) contain cell bodies of parasympathetic efferents. Finally, celiac, superior- and inferior mesenteric ganglia (CG, SMG, and IMG, respectively) contain sympathetic gut-projecting efferents. Of note, in mice, NG and JG (Kaelberer and Jordt, 2016) as well as CG and SMG (Schmidt et al., 2003) are fused and will be referred to as NG and CG-SMG, respectively. Functionally, the roles of the respective neuronal populations can be summed according to the flow of information into gut-to-CNS and CNS-to-gut pathways.

#### 1.3.2.1 Gut-to-CNS pathways

Primary afferent innervation conveys mechanical, chemical and sensory (nociceptive) information from the intestine to CNS centers. Each intestine segment receives dual sensory input, through vagal afferents, with cell bodies in the NG, and spinal afferents, with cell bodies in DRGs. Specifically, the small intestine and proximal colon are innervated by vagal afferents (i.e., left and right vagus nerves) and thoracolumbar spinal afferents (i.e., splanchnic nerves). The distal colon receives afferent innervation from thoracolumbar and lumbosacral spinal afferents (i.e., pelvic and rectal nerves, respectively), while vagal fibers do not reach beyond the proximal colon. Vagal afferents primarily terminate in the nucleus of the solitary tract (NTS) of the brainstem, where they mono- and polysynaptically connect to and modulate *parasympathetic* vagal efferents projecting back to the intestine. By contrast, spinal afferents can modulate *sympathetic* efferents via polysynaptic circuits (Brookes et al., 2013).

Several different types of primary afferent endings within the gut have been described, with distinct properties and anatomical locations, making them responsive to distinct stimuli (Brookes et al., 2013; Williams et al., 2016). They reach all layers of the intestine, and include muscularis ganglia afferents (intraganglionic laminar endings, IGLEs), muscular mucosal, intramuscular and vascular afferents (intramuscular arrays, IMAs), as well as mucosal afferents. Mucosal afferents can reach villus tips, albeit they are thought to not reach beyond the basolateral epithelial side (Berthoud et al., 1995; Janssen and Depoortere, 2013). Instead, they respond to chemicals released from the basolateral side of IECs (Brookes et al., 2013). They have been implicated in detecting mechanical distortion, wall tension and noxious stimuli (Brookes et al., 2013). Via connections to EECs they can respond to nutrients by triggering reflex pathways that control intestinal function, or relay information such as satiety signals to central centers (Bohórquez et al., 2015; Kentish et al., 2013; Steinert and Beglinger, 2011). Notably, transient receptor potential cation channel subfamily V member 1 (TRPV1)-expressing nociceptor neurons have recently been suggested to both sense and respond to enteric *Salmonella* infection to mediate tissue protection (Lai et al., 2020).

Recent work has started to shed more light on the functional significance underlying the anatomical divisions of GI sensory innervation. Using a combinatorial viral and optogenetic approach, de Araujo and colleagues mapped a circuit implicating specifically the *right* vagus nerve in nutrient sensing and gut-induced reward through

nigrostriatal activation. By contrast, gut-innervating *left* vagal fibers terminated in a different brain stem region and induced satiety, but not reward (Han et al., 2018). Because different vagal populations can respond to distinct stimuli (Williams et al., 2016), it is possible that the sensory terminals of right versus left upper GI vagal fibers respond to distinct stimuli, i.e., nutrients (right) versus wall tension (left) (Han et al., 2018). The application of novel tools will likely unravel further such functional subtleties to sensory innervation along the vertical axis and within gut regions.

Finally, while recent advances using single-cell sequencing approaches have started to shed more light on the transcriptional profiles of some of these populations during homeostasis (Drokhlyansky et al., 2020; Zeisel et al., 2018), how sensory afferents respond to luminal perturbations, such as shifts in microbial composition or acute inflammation, is thus far largely unknown.

#### 1.3.2.2 CNS-to-gut pathways

Sympathetic and parasympathetic pathways run together with afferent pathways and transmit efferent top-down information. Sympathetic preganglionic neurons innervating the intestine are located in the thoracolumbar spinal cord, and project to postganglionic sympathetic neurons in prevertebral and pelvic ganglia, i.e., CG-SMG and IMG (also referred to as gut sympathetic ganglia). Broadly, sympathetic effects on the GI tract are inhibitory, including tonic inhibition on musculature (decreased peristalsis), decreasing secretion and reducing blood flow via neurally-regulated vasoconstriction. The primary postganglionic sympathetic neurotransmitter in the GI tract is norepinephrine (NE), which binds to α- and β-ARs expressed by neurons, immune and other cells (Browning and Travagli, 2014; Furness et al., 2014). For the studies presented in this work, the most notable ganglion transmitting postganglionic sympathetic information is the CG-SMG. Its postganglionic sympathetic axons, mostly tyrosine hydroxylase (TH, i.e., the rate-limiting enzyme for catecholamine synthesis)- or NPY-expressing fibers, project to the stomach, liver, gallbladder, spleen, kidney, small intestine, and the ascending and transverse colon (Browning and Travagli, 2014; Kaestner et al., 2019). In addition to preganglionic sympathetic input, the CG-SMG receives input from vagal efferents (Berthoud and Powley, 1993, 1996; Furness and Anderson, 1994), collateral axons from primary afferents of NG and DRG (Kaestner et al., 2019) and enteric neurons (Brookes et al., 2013). The CG-SMG thereby forms a major integrative regulatory command center that coordinates information flow between CNS and multiple visceral organs (Kaestner et al., 2019).

Contrary to their sympathetic counterparts, parasympathetic efferents can have both excitatory and inhibitory effects on gastric tone and intestinal motility, providing more discriminate, fine-tuned influence on GI function, aiding digestion and absorption (Browning and Travagli, 2014, 2019). Gut parasympathetic efferents are preganglionic and cholinergic, and act on nicotinic ACh receptors expressed by target cells such as iEANs and ICCs (Browning and Travagli, 2014). They reach the intestine via vagus and pelvic nerves, where they synapse postganglionic effector neurons located in both plexuses (Furness et al., 2014). In addition to control through higher CNS centers, vagal

efferents also respond to circulating hormones and input from sensory afferents projecting from the intestine to the DMN, forming direct (vago-vagal) reflex loops (Browning and Travagli, 2014; Rogers et al., 1995). Through the cholinergic anti-inflammatory pathway – the efferent arm of the inflammatory reflex – vagal efferents also exert control over intestinal immune function in response to infection, injury and tissue damage (Tracey, 2002) (described in Chapter 1.5.1). Through anatomical tracing studies, parasympathetic input has also been shown to reach the CG-SMG (Berthoud and Powley, 1993), thus some level of parasympathetic control of sympathetic effects on the intestine, similar as has been shown in the case of lymphoid tissues (Rosas-Ballina et al., 2008), is plausible, albeit functionally, this still requires investigation (Kaestner et al., 2019). As with sensory afferents, the effects of luminal stimuli on sympathetic and parasympathetic efferents are not fully elucidated.

### 1.3.3 Viscerofugal neurons

Viscero- or intestinofugal neurons (used interchangeably) are a relatively small population of neurons the cell bodies of which reside within the intestinal wall, and which send axonal projections to extraintestinal sites, predominantly gut sympathetic ganglia. First anatomical evidence of a population of iEANs connecting to prevertebral ganglia was provided by A. Kunz in 1938 (Kuntz, 1938). Szurszewski and colleagues, in intracellular electrical recordings performed on colonic explants, later detected excitatory input from the colon tissue reaching the IMG (Crowcroft et al., 1971). These neurons were shown to exclusively arise from the myenteric plexus, increase in frequency from proximal to distal intestine (Messenger and Furness, 1992), and likely receive some excitatory input from intrinsic ENS pathways (Sharkey et al., 1998). By forming circuits with sympathetic neurons in prevertebral ganglia, they were shown to control intestinal motility (Weems and Szurszewski, 1977) and secretion (Quinson et al., 2001) through intestino-intestinal reflexes. In the colon, viscerofugal neurons have been suggested to be uniformly mechanosensitive (Hibberd et al., 2012). Whether these or small intestinal viscerofugal populations are responsive to stimuli other than mechanical stress, and whether they receive input from intestinal cell populations such as submucosal EAN or EECs, and by extension luminal stimuli, remains unclear. More importantly, functional data on viscerofugal populations is virtually absent.

### 1.3.4 Enteric neuropathies and ENS involvement in systemic diseases

As laid out in the previous sections, the ENS controls and coordinates a wide range of GI functions. It is thus apparent that damage to and dysfunctions of it can have drastic effects on tissue function and host physiology. For example, cholera toxin, secreted by the cholera-causing bacterium *Vibrio cholerae*, can directly act on secretomotor iEANs, leading to their constitutive activation with secretory diarrhea and severe fluid loss (Furness, 2012; Gwynne et al., 2009).

By contrast, the absence of ENS proportions, as seen for example in congenital aganglionic megacolon, or Hirschsprung's disease, in which enteric ganglia in intestine

segments of variable length fail to develop, leads to pseudo-obstruction and, if left untreated, life-threatening complications including bowel perforation, newborn enterocolitis, toxic megacolon and sepsis (Kessmann, 2006). In Chagas disease, infection with the neurotropic protozoan pathogen *Trypanosoma cruzi* causes regional iEAN loss, resulting in severe dysmotility and development of acquired megacolon (Furness, 2012). Similarly, the neurotropic West Nile and Zika viruses, have been reported to induce iEAN death through muscularis-infiltrating antiviral CD8+ T cells, resulting in long-term dysmotility (White et al., 2018). In the neurodegenerative Parkinson's disease (PD), loss of dopaminergic neurons in the CNS results in a progressive movement disorder driven by motor neuron degeneration and eventually lethal loss of muscle function, and their loss in the ENS in chronic constipation. Because PD-associated GI dysfunction often precedes CNS symptoms, biopsy-mediated screening has potential as an early diagnostic tool (Rao and Gershon, 2016). Of note, a recently published single-cell dataset has found iEANs to express risk genes related to PD development, such as *SCN3A* and *DLG2* (Drokhlyansky et al., 2020). Further analysis of their gene products in iEANs may expand our understanding of intestinal PD manifestations.

#### 1.3.4.1 Irritable bowel syndrome and PI-IBS

Along with functional dyspepsia, irritable bowel syndrome (IBS) is currently considered a functional gastrointestinal disorder, as its etiology remains largely unclear (Holland et al., 2021). The most common risk factor for IBS is a preceding GI infection, often with entero-invasive bacteria such as *Salmonella enterica* and *Shigella dysenteriae*. These are thought to pave the way for chronic dysbiosis thereafter (Barbara et al., 2019), resulting in what is referred to as post-infectious IBS (PI-IBS). While evidence for organic causes is now accumulating, IBS is currently a symptoms-based diagnosis (Holland et al., 2021), involving abdominal pain, dysmotility (diarrhea, constipation, or both), nausea and bloating (Ford et al., 2017), hence pointing to ENS involvement. Recently, increased branching of nerve terminals in the gut mucosa of human IBS biopsy specimens (Dothel et al., 2015), increased expression of the capsaicin receptor TRPV1 in sensory afferents (Akbar et al., 2010; Akbar et al., 2008), and a mucosal immune infiltrate accumulating around nerve terminals (Barbara et al., 2004; Wouters et al., 2016) have been reported, pointing to neuro-immune involvement in IBS-associated symptomatology (further detailed in Chapter 1.5.2.1).

### 1.3.5 Enteric chemosensory cells and gut metabolic regulation

#### 1.3.5.1 Enteroendocrine cells and gut hormone distribution

First evidence that cells of the gastrointestinal mucosa could be involved in nutrient sensing and metabolic regulation was provided by Bayliss and Starling in 1902, with their discovery of the first gut hormone, secretin, and its inhibitory effect on insulin secretion following its release in response to gastric acidity (Bayliss and Starling, 1902). Since then,

more than 20 different types of gut hormones have been described (Furness et al., 2013). They are produced by specialized chemosensory epithelial cells, EECs, found in crypts and villi scattered throughout the epithelial layer from stomach to anus. Making up only about 1% of IECs, their sum forms the body's largest endocrine organ (Ahlman and Nilsson, 2001; Janssen and Depoortere, 2013; Worthington et al., 2018). Through hormone secretion in response to luminal signals, with effects on digestion, absorption, motility, appetite and glucoregulatory hormone modulation, they contribute to metabolic regulation. Upon stimulation, hormones are released into the paracellular space, where they either act locally or get taken up into the bloodstream to act on distant target sites (Worthington et al., 2018).

EECs sense luminal signals through diverse signaling cascades, including ion channels, transporters, and GPCRs (Gribble and Reimann, 2016; Worthington et al., 2018). Glucose taken up via SGLUT1 stimulates GLP-1/GIP release (Gorboulev et al., 2012). GPCRs located on the cell surface are used to sense fatty acids (FFAR1) (Lu et al., 2018), BAs (GPBAR1) (Brighton et al., 2015), and amino acids (Diakogiannaki et al., 2013). EECs can also detect microbial stimuli such as hormones and neurotransmitters, SCFAs and secondary BAs generated by commensal bacteria (Cohen et al., 2017; Worthington et al., 2018). Through TLR expression, EECs can also detect bacterial components such as LPS (Bogunovic et al., 2007; Lebrun et al., 2017).

The traditional nomenclature of EEC subtypes is based on the original understanding that one EEC subtype produces one type of gut hormone, although it has become clear that these cells, based on anatomical location, can produce an array of gut hormones (Grunddal et al., 2016; Svendsen et al., 2016; Svendsen et al., 2015). The stomach contains EECs producing 5-HT (enterochromaffin cells, ECs), histamine (enterochromaffin-like cells, ECL cells), gastrin (G-cells), SST (D-cells), ghrelin (X-like-cells) and leptin (P-cells). In the duodenum, a large fraction of EECs produces the incretin glucose-dependent insulinotropic peptide (GIT) (K-cells), as well as CCK (I-cells) and secretin (S-cells). In the distal small and large intestines, L-cells produce GLP-1 and -2, as well as PYY and insulin-like peptide 5 (INSL5), and neurotensin-producing N-cells (Gribble and Reimann, 2016).

**Gut hormones in control of digestion, appetite and metabolism**

Within the GI tract, SST, gastrin and histamine stimulate gastric acid and hormone production. A range of anorexigenic hormones is released primarily in the small intestine in response to food ingestion, which together coordinate digestion, absorption, and extra-intestinal assimilation and nutrient storage. They amplify insulin- and inhibit glucagon secretion in the pancreas (GLP-1, GIP), promote fat storage (GIP), stimulate gall bladder contraction and bile release into the duodenum (CCK), stimulate exocrine pancreas secretion (secretin, CCK), and slow gastric emptying (PYY, GLP-1, CCK). In addition, GLP-1 and PYY act on the area postrema in the CNS to induce nausea, and GLP-1, CCK and PYY induce satiety by acting on hypothalamic nuclei. By contrast, the orexigenic hormones ghrelin and INSL5 are released in anticipation of food intake, and their secretion is inhibited by luminal nutrient increase (Gribble and Reimann, 2016).

#### 1.3.5.2 Neuropods and tuft cells

Sensing of gut hormones released by EECs was generally thought to be a purely passive process, whereby surrounding cells, including sensory afferents take up hormones released by EECs into the basolateral space. However, recent studies uncovered that a subset of EECs, termed neuropod cells, forms basolateral processes extending to the lamina propria. Using viral tracing techniques, work from Bohórquez and others demonstrated that via these processes, EECs are capable of forming synapses with nerve terminals in the intestinal mucosa to directly activate sensory afferents in response to luminal stimuli (Bellono et al., 2017; Bohórquez et al., 2015; Lu et al., 2019). Another study further demonstrated a pathway of direct signal transduction from the gut to brain areas via synaptic release of the neurotransmitter glutamate by neuropod cells, activating adjacent vagal afferents (Kaelberer et al., 2018). Whether these EECs also make direct contact with iEANs, such as intestinofugal neurons, allowing for CNS-independent response circuits, remains to be investigated.

Tuft cells, another type of chemosensory and secretory IECs, are increasingly appreciated for their role in type 2 immune responses. The discovery that intestinal tuft cells, upon sensing luminal helminths and protists, secrete the cytokine IL-25, thereby setting off downstream canonical type 2 immune activation (Gerbe et al., 2016; Howitt et al., 2016; von Moltke et al., 2016), provided a long missing trigger for type 2 immune activation. In addition, tuft cells also produce the neurotransmitter ACh, rendering them a potential means to communicate with EANs (O'Leary et al., 2019). More recently, tuft cells have been shown to also produce cysteinyl leukotrienes (cysLTs) (McGinty et al., 2020), the receptor for which is expressed by some peripheral sensory neuron populations (Voisin et al., 2021), where neuronal $CysLT_2R$ receptor activation has been implicated in inducing itch in a model of atopic dermatitis (Voisin et al., 2021). It may thus be possible that helminth sensing by tuft cells and engagement of sensory afferents induces protective reflexes to mediate worm expulsion. However, whether they, like other chemosensory epithelial cells, form direct cell-cell contacts with sensory or effector neurons in the intestine, and directly activate or get activated by EANs, remains to be addressed.

## 1.4 The intestinal immune system

### 1.4.1 Balancing tolerance and protection: Overview of the largest immune compartment of the body

Under continuous antigenic exposure, both innocuous and pathogenic, the intestinal immune system is tasked with the unique challenge of mediating an intricate balance between efficiently responding to pathogenic insults, while avoiding excessive inflammation and maintaining tissue homeostasis. Coordinated tolerance and resistance mechanisms serve to prevent pathogen dissemination, limit tissue damage, and initiate repair responses induced by pathogenic burden or injury (Medzhitov et al., 2012).

As a first line of defense, the intestinal epithelium provides a physical and biochemical barrier that maintains segregation between luminal contents, including microorganisms, and the epithelial cell lining (Fig. 1.4). While the majority of IECs are absorptive enterocytes, additional specialized secretory epithelial cell types, including the aforementioned chemosensory cells, antimicrobial peptide (AMP)-producing Paneth cells, and mucus-producing goblet cells, provide a potent physical and chemical separation between the environment and underlying tissue (Peterson and Artis, 2014). Along with IECs, a population of antigen-experienced T cells termed intraepithelial lymphocytes (IELs) can be found patrolling the epithelial compartment (Mowat and Agace, 2014). These have been implicated in both pathogen resistance (Hoytema van Konijnenburg et al., 2017; Meresse et al., 2006; Tang et al., 2009) and tissue tolerance mechanisms (Ismail et al., 2011; Sujino et al., 2016), and most recently, in sensing of luminal nutrients (Sullivan et al., 2021). While infrequently found during homeostasis, during active type 2 immune responses, mast cells and eosinophils can drastically expand within the epithelial compartment (unpublished observations).

The underlying lamina propria houses the grand majority of intestinal immune cells, including B cells, T cells and a vast amount of innate immune cells, including macrophages, dendritic cells (DCs), and innate lymphoid cells (Fig. 1.4) (ILCs) (Faria et al., 2017). Stretching from submucosa to the mucosa, the organized lymphoid structures

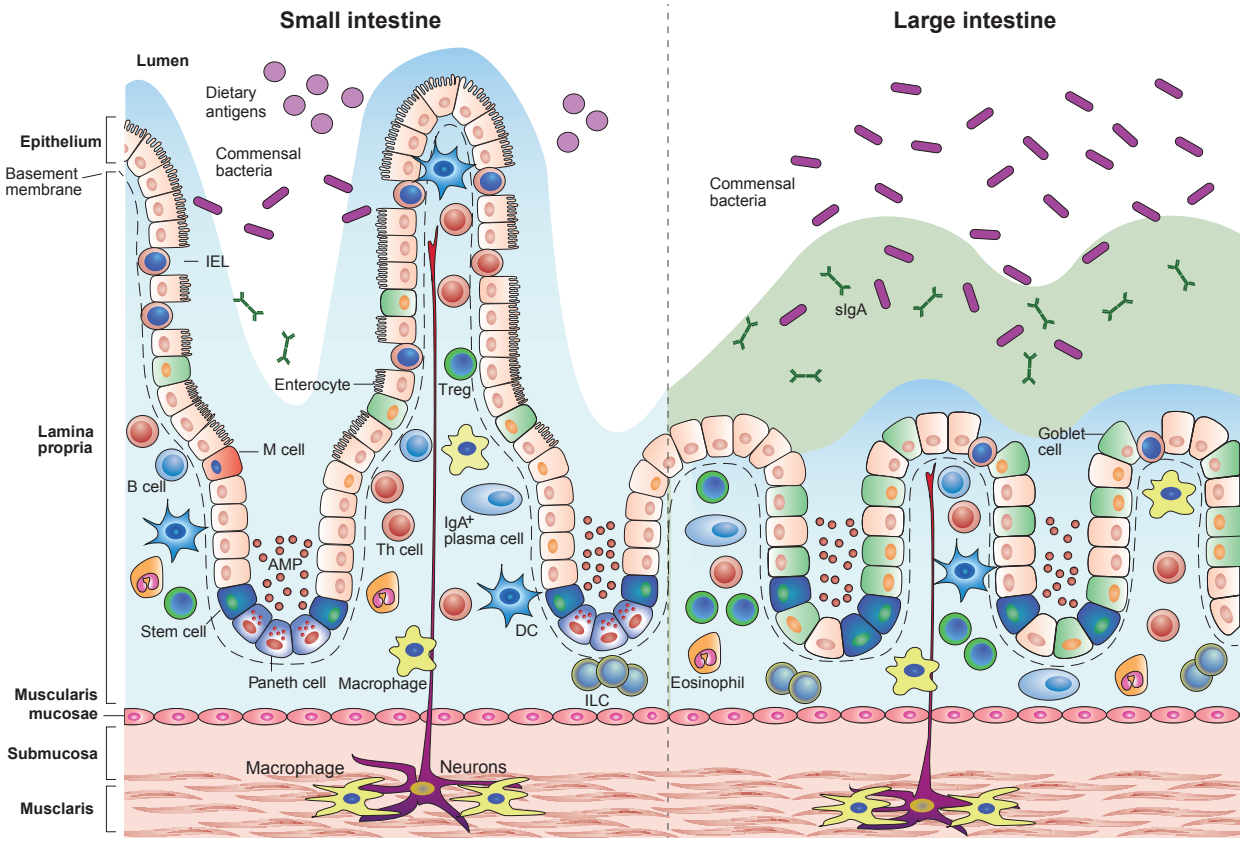


**Fig. 1.4. Diversity of the intestinal immune system.** Schematic depicting the regional organization of the intestinal immune system of the small and large intestines and highlighting major immune cell populations present in each region. DC - dendritic cell, ILC - Innate lymphoid cell, IEL - intraepithelial lymphocitye, AMP - antimicrobial peptide. Adapted with permission from Faria et al., 2017.

of the intestine, the gut-associated lymphoid tissue (GALT), such as the small intestinal Peyer's patches (PPs), are found. Along with gut-draining lymph nodes, these are the major locations of initiation of adaptive immune responses. In PPs, specialized epithelial cells termed microfold (M) cells sample and deliver luminal antigen, and T and B cells get activated upon antigen encounter and priming by DCs and macrophages. They contain numerous B cell follicles in which germinal centers form upon B cell activation, and are the major sites of intestinal immunoglobulin A (IgA) production (Mowat and Agace, 2014).

By contrast, in the further underlying muscularis layer, the grand majority of immune cells are a population of tissue-resident macrophages that surround the neurons of the myenteric plexus (Fig. 1.4) (Veiga-Fernandes and Mucida, 2016). These muscularis macrophages (MMs), contrary to their mucosal counterparts, have a predominantly anti-inflammatory phenotype (Gabanyi et al., 2016). This niche-specific adaptation of one immune cell type within the intestine can be viewed as a mechanism of intestinal immunity to balance pathogen defense and tissue protection.

### 1.4.2 Gut macrophages: key players in intestinal immunity and tissue physiology

The mammalian gastrointestinal tract harbors a large reservoir of tissue macrophages, which, in concert with other immune cells, help to maintain a delicate balance between tolerance to commensal microbes and food antigens, and resistance to potentially harmful microbes or toxins. Macrophages are known to quickly adapt to the tissue environment in which they reside, but initial descriptions of intestinal macrophages were the result of whole tissue preparations where physical, or phenotypical, separation between macrophage populations residing in the different layers of the intestinal wall was not routinely performed. Recent work has shown that within the human and murine intestines, macrophages can be defined by their anatomical location, broadly divided into mucosal or lamina propria macrophages (LpMs) and muscularis macrophages (MMs) (Bujko et al., 2018; De Schepper et al., 2018; Gabanyi et al., 2016; Muller et al., 2014). Further functionally distinct populations likely exist in the epithelium, submucosal and serosal regions (Bujko et al., 2018; De Schepper et al., 2018).

#### 1.4.2.1 Origin and maintenance of intestinal macrophages

Intestinal macrophages, in contrast to other murine tissue-resident macrophages, are thought to be continuously replaced by circulating monocytes through a process known as the "monocyte waterfall", and evidence has recently emerged that this stepwise differentiation is also present in humans (Bain et al., 2014; Bain and Schridde, 2018; Bernardo et al., 2018). As an early population of embryo-derived macrophages are turned over during development, monocytes, defined as $MHC^{hi}$ CD64- $CX_3CR1^{int}$ MHCII- (P1), enter the gut where they begin to transition through three subsequent stages of differentiation, P2-P4, becoming mature CD64+ $CX_3CR1^{hi}$ $MHCII^{hi}$ macrophages (Bain et al., 2014; Bain and Schridde, 2018). While the fractalkine receptor, $CX_3CR1$, is a critical mediator of murine intestinal macrophage function, macrophages in the intestine of humans do not express significant levels during homeostasis (Bernardo et al., 2018).

Notably, recent work by two different groups has challenged the concept of continuous replenishment by identifying a population of early-seeded, long-lived tissue-resident intestinal macrophages not replaced by circulating monocytes (De Schepper et al., 2018; Shaw et al., 2018). Flow cytometric phenotyping and fate mapping experiments in mice indicated the existence of macrophages that were present at birth and displayed little to no turnover as the animals aged (De Schepper et al., 2018; Shaw et al., 2018). Observations from human patients receiving intestinal transplants also identified a population of long-lived macrophages that differ from those readily replaced by circulating monocytes (Bujko et al., 2018). Other departures from the monocyte waterfall can occur in the context of inflammation induced by intestinal manipulation in mice or inflammatory bowel disease in humans, as it was recently suggested that recruited monocytes can directly transition into mature macrophages, effectively bypassing the intermediate stages of differentiation (Bernardo et al., 2018; Desalegn and Pabst, 2019).

Intestinal macrophages express high levels of colony stimulating factor receptor (CSF1R) and targeting of CSF1 or CSF1R by genetic or pharmacologic approaches results in a complete lack of macrophages in the gut (Avetisyan et al., 2018; Cipriani et al., 2018; Muller et al., 2014). Among the sources of CSF1, studies have reported a role for nestin+ stem cells in the bone marrow as systemic sources (Lavin et al., 2015), or non-hematopoietic compartments within the intestine as local sources, including endothelial cells and ICCs in developing mice, or intestinal crypts and enteric neurons in the adult, the latter of which is postulated to be age- and partially microbiota-dependent (Avetisyan et al., 2018; Muller et al., 2014). Additional factors have been reported to play a role for macrophage recruitment and differentiation in different segments of the GI tract, including CD11c+ cell-intrinsic Notch signaling in the small intestine, macrophage-secreted monocyte chemoattractants, and TGF-β signaling in the colon (Ishifune et al., 2014; Schridde et al., 2017). Beyond the role for local growth factors and recruitment cytokines, the presence of the microbiota is a critical mediator of intestinal macrophage recruitment and differentiation. Both monocyte-derived and tissue-resident macrophages are decreased in number in GF or microbiota-depleted mice (Bain et al., 2014; Muller et al., 2014; Shaw et al., 2018).

The basic mechanisms by which LpMs and MMs seed the tissue are likely similar, however there appears to be a clear difference in the balance of macrophage composition, as MMs were recently described to primarily originate from a long-lived subset rather than being monocyte-derived (De Schepper et al., 2018). This, coupled with lamina propria and muscularis comprising very distinct niches, has led to the recent recategorization of intestinal macrophages based upon their location within the tissue.

#### 1.4.2.2 Mucosal macrophages

In the initial description of the intestinal villus as a unit by electron microscopy in 1959, Karlin and colleagues first described the presence of LpMs (Palay and Karlin, 1959). These macrophages line the intestinal epithelium and are thus strategically positioned to sample luminal antigens, phagocytose dead cells, and eliminate pathogens that succeed in crossing the epithelial layer. LpMs are mostly composed of macrophages

derived from the monocyte waterfall, with a smaller contribution of long-lived macrophages compared to deeper layers of the intestine. They are classically defined as CD64+ CD11c+ MHCII$^{hi}$, and in mice are $CX_3CR1^{hi}$. Intravital imaging showed that these sessile macrophages have rapid and dynamic membrane ruffling and pseudopod extensions (Gabanyi et al., 2016). LpM pseudopods can form transepithelial dendrites (TEDs) that efficiently cross the epithelium to sample the intestinal lumen and capture potential pathogens, a process that is dependent on $CX_3CR1$ expression in mice but may also be antigen-dependent (Chieppa et al., 2006; Niess et al., 2005; Vallon-Eberhard et al., 2006). Due to their unique positioning in a tissue continuously exposed to foreign antigen, LpMs possess a more pro-inflammatory transcriptional profile than their muscularis counterparts (Gabanyi et al., 2016). Regardless, LpMs are also precisely equipped to be tolerogenic in nature. While seemingly contradictory, this allows for balancing pathogen clearance, while simultaneously regulating local immune cell populations, and maintaining basic tissue integrity.

#### 1.4.2.2.1 Role of mucosal macrophages in pathogen resistance

Due to the positioning of a large number of LpMs immediately beneath the intestinal epithelium, there is a high probability of them encountering or directly sampling pathogens. These macrophages are programmed such that they can contribute to the immediate antibacterial or -parasitic response. Current work has shown that in addition to TED-mediated sampling of luminal stimuli that may contribute to IL-10 production (Hadis et al., 2011), $CX_3CR1$+ LpMs can extravasate from the lamina propria to the lumen of the intestine during *Salmonella* infection, a process that is also dependent on TLR signaling in IECs (Man et al., 2017). Once in the lumen, they can phagocytose pathogens to prevent entry to the intestine and decrease pathogen load early in infection. While LpMs can play a role in barrier function, it is also clear that they possess an antibacterial machinery to respond to bacterial invasion, which, in some cases, can lead to tissue pathology if left unchecked. In mouse models of *Helicobacter pylori* and *Citrobacter rodentium* infection, LpM-specific epidermal growth factor receptor signaling (EGFR) was found to be responsible for induction of cytokine production and macrophage activation, which directly contributes to tissue inflammation (Hardbower et al., 2016). In another study by the same group using identical infection models, ODC1, the rate-limiting enzyme of polyamine synthesis, and its product putrescine, were described as critical regulators of proinflammatory LpM activation. This was proposed to be mediated via direct alteration of histone modifications of proinflammatory genes such as IL-1β, IL-6 and TNF-α (Hardbower et al., 2017). As was the case with EGFR, LpM-specific loss of ODC1 enhanced antibacterial properties, but at the expense of increased tissue inflammation. In line with polyamine histone modification, a role for the microbial-derived SCFA butyrate as an HDAC inhibitor was recently investigated. Butyrate was shown to induce lasting metabolic and transcriptional changes in colonic macrophages, which led to increased potential to ramp up ROS production as well as upregulation of the AMPs lysozyme and calprotectin. These effects were mediated by inhibition of HDAC3, which led to increased macrophage antimicrobial activity and resistance to enteric pathogens *in vivo* (Schulthess

et al., 2019). The ability of LpMs to properly balance resistance with limiting tissue damage is a key feature of these macrophages, and this tolerogenic programming is reflected in their role in maintaining homeostasis in the inflammatory local environment.

#### 1.4.2.2.2 Mucosal macrophages in tissue tolerance

The intestinal lamina propria, due to constant exposure to luminal commensal bacterial and diet-derived antigens, comprises an inflammatory milieu. Despite this reactive environment, the immune system is tightly regulated to avoid inadvertent harm to self, and LpMs are key mediators in generating a tolerogenic environment (Hine and Loke, 2019). The most studied LpM tolerogenic factor is IL-10, the total lack of which leads to spontaneous enterocolitis (Kuhn et al., 1993). Production of IL-10 by LpMs is important for the balance of T cell populations in the gut (Denning et al., 2007). A recent study identified that epithelial-adherent bacteria were required to induce IL-10 production of $CX_3CR1$+ LpMs, which in turn increased intestinal regulatory T cell ($T_{reg}$) numbers, while dampening the expansion of T helper 1 ($T_h1$) cells. Conversely, during antibiotic-mediated microbiota depletion, LpMs no longer produced IL-10, and instead promoted antigen-specific $T_h1$ cell expansion (Kim et al., 2018). These findings align with previous work showing that the adherent bacterium *Clostridium butyricum* was sufficient to induce IL-10 production by LpMs and suppress an antimicrobial program (Hayashi et al., 2013). Another new study reported that a common bacterial mouse pathobiont, *Helicobacter hepaticus*, induces a tolerogenic response in mucosal macrophages triggered by TLR2 stimulation. This was mediated by *H. hepaticus* secretion of a soluble polysaccharide, SN*Hh*t, and involved MSK/CREB-dependent induction of an anti-inflammatory macrophage profile, including IL-10 production (Danne et al., 2017). Thus, it is becoming evident that interactions with resident microbial species play a key role in balancing proinflammatory and tolerogenic responses in LpMs. Further, while an anti-inflammatory role of IL-10 in LpMs has been established, other work has demonstrated that IL-10Rα signaling in $CX_3CR1^{hi}$ macrophages is crucial for their tolerogenic profile during homeostasis. The failure of macrophages to respond to, rather than produce, IL-10 results in their expression of an array of proinflammatory cytokines driving deleterious T cell responses and the development of spontaneous colitis in mice (Zigmond et al., 2014). Further, IL-23 production from LpM lacking IL10-Rα has been shown to be the primary driver of colitis, leading to IL-22 release from $T_h17$ and ILC3 cells (Bernshtein et al., 2019), suggesting IL-10 sensing as a major LpM-intrinsic tolerogenic axis.

Beyond a role for the microbiota in imprinting an anti-inflammatory program in LpMs, how else do these macrophages maintain homeostasis? LpMs contribute to tissue homeostasis by controlling the maintenance and activation of intestinal ILCs and T, including $T_{reg}$ cells. For example, tissue-resident $CX_3CR1$+ LpMs have been implicated as the main producers of proinflammatory cytokines such as IL-23 and IL-1β in the intestine, thereby increasing IL-22-production by ILC3s (Longman et al., 2014; Zhou et al., 2019). LpM production of IL-23 and IL-1β in turn is kept under control by MHCII modulation of LAG3+ Treg cells (Bauche et al., 2018). Other recent work demonstrated that IL-1β production by LpMs selectively induces ILC3s to produce IL-2, which in turn

was required for $T_{reg}$ maintenance (Zhou et al., 2019). Together, these findings establish a feedback loop in which proinflammatory LpMs induce $T_{reg}$ cells to contribute to a tolerogenic milieu. Other neighboring cell-LpM interactions can contribute to the anti-inflammatory status of LpM. In concert with dendritic cells, two distinct CD11b+ LpM subsets were shown to sample and clear apoptotic IECs via efferocytosis. Uptake of apoptotic IECs induced a cell-type specific transcriptional program associated with dead cell clearance along with immunosuppression, including TLR2-downmodulation. These adaptations may likely be coupled to prevent unwanted inflammatory or autoimmune responses (Cummings et al., 2016).

#### 1.4.2.2.3 Mucosal macrophages in GI physiology and homeostasis

Given the unique challenges of the intestinal environment, the majority of studies on LpM function has focused on their specific roles in inflammatory settings and protection from invading pathogens. Yet, LpMs, like their counterparts in other tissue sites, also exert functions more classically associated with macrophages, including phagocytosis of cell debris, and mechanical support of surrounding tissue.

A study using single-cell RNA sequencing coupled with fate-mapping strategies recently identified a distinct population of tissue-resident $CX_3CR1$+ LpMs associated with the vasculature. Targeted depletion of tissue-resident macrophages led to overt restructuring of blood vessels in the mucosa and submucosa, and functionally, to leaky vasculature as evidenced by increased presence of intravenously delivered microspheres (De Schepper et al., 2018). A role for LpMs has also been described in the maintenance of the intestinal stem cell niche. Here, antibody-mediated depletion of CSF1R-depedent LpMs led to impairment in differentiation of Paneth cells and a reduction in *Lgr5*+ stem cells, which in turn affected the differentiation and replenishment of further IECs, including Goblet and M cells (Sehgal et al., 2018). These findings suggest that a population CSF1R-depedent LpMs is crucial for intestinal crypt homeostasis. Indeed, effects on crypt IEC development may be mediated by long-lived LpMs that appear to associate with Paneth cells (De Schepper et al., 2018). Given the highly heterogenous numbers of cell types and structures in the mucosa and lamina propria that LpMs associate with, it is likely that we have only scratched the surface of their ability to support basic intestinal physiology.

### 1.4.2.3 Muscularis macrophages

Macrophage-like cells were first observed in the muscularis externa of the intestine by Mikkelsen and colleagues in 1982 through analysis of electron microscopy images (Mikkelsen et al., 1985; Rumessen et al., 1982). Following this initial observation, these cells were defined to be macrophages present in the serosal, circular, and longitudinal muscle layers with a significant proportion in the myenteric or Auerbach's plexus containing intrinsic enteric-associated neurons (iEAN). Muscularis macrophages (MMs) display two distinct morphologies, bipolar and stellate, and are intimately associated with cell bodies and processes of both glia and neurons (Gabanyi et al., 2016; Mikkelsen et al., 1985). Phenotypically, they can be defined by their high expression of MHCII, CD163,

and $CX_3CR1$ (Muller et al., 2014). In the steady state, they do not migrate through the tissue and display slow continuous remodeling of their dendritic-like pseudopod processes (Gabanyi et al., 2016). In comparison to LpMs, a large proportion of MMs are composed of early-seeded macrophages of both bone marrow and embryonic origin (De Schepper et al., 2018). MMs are skewed towards an anti-inflammatory profile, suggestive of roles in tissue homeostasis and repair (Gabanyi et al., 2016). Despite their description close to four decades ago, the function of MMs remained relatively unknown until recent work that has established these macrophages as key players in gut function and tissue homeostasis, with a particular emphasis on gut motility, which will be described in more detail in the context of neuronal communication.

### 1.4.3 The inflammasome machinery in the intestine

Because we found an unexpected role for components of an innate immune sensing machinery termed the inflammasome, this section will lay out basic principles of inflammasome signaling and its role in the intestine.

The term inflammasome was brought forth by Tschopp and colleagues who, in 2002, identified a cytoplasmic multi-protein complex capable of inducing caspase 1- and 11- mediated proteolytic maturation of interleukin-1β (IL-1β) and IL-18. These findings provided a missing link between sensing of microbial patterns or cellular stress, and innate immune activation (Martinon et al., 2002).

Inflammasomes are genetically encoded signaling complexes that induce innate immune responses and a lytic form of cell death termed pyroptosis. Several distinct inflammasomes have been characterized, each distinguished by different activating signals (pattern recognition receptor, PRR) in response to pathogen-associated molecular patterns (PAMPs) or danger-associated molecular patterns (DAMPs). Pattern recognition leads to activation of an intracellular sensor of the nucleotide-binding oligomerization domain (NOD) leucin-rich repeat (LRR)-containing protein (NLRP) family, oligomerization and recruitment of an adaptor protein called Apoptosis-associated speck-like protein containing a CARD (ASC, also known as PYCARD) and cleavage of effector caspases 1 and 11, inducing downstream effector responses including IL-1β and IL-18 release, and pyroptosis (Rathinam and Fitzgerald, 2016).

Depending on their routes of activation, inflammasomes can be divided into canonical, or classical, and non-canonical inflammasomes. Canonical inflammasomes are activated upon different bacterial pathogens or signals from damaged or dying cells (PAMPs, DAMPs), and consists of cytosolic sensor (NLRs, absent in melanoma 2 (AIM2) or pyrin), an adaptor protein (ASC), and pro-caspase 1 (von Moltke et al., 2013). The non-canonical inflammasome pathway, on the other hand, involves activation of caspase 11 (caspase 4 in humans), which subsequently cleaves gasdermin D (GSDMD) Activated gasdermin D induces pore formation in the cell membrane, resulting in pyroptosis; simultaneously, active GSDMD can induce non-canonical inflammasome assembly, resulting in interleukin production (Broz and Dixit, 2016). Caspase 11 activation in this setting can be triggered through cytosolic sensing of LPS from Gram-negative bacteria such as *Salmonella enterica* spp., which either directly activate caspase 11 or through

TLR4 activation (McKenzie et al., 2020; Rathinam and Fitzgerald, 2016; Rathinam et al., 2012).

Inflammasomes have been established as critical defense mechanisms during bacterial infections, but their activation requires tight regulation, to avoid tissue damage (von Moltke et al., 2013). Over the past years, their pathological activation has been linked to variety of diseases including autoinflammatory conditions such as multiple sclerosis (MS), and neurodegenerative diseases like Alzheimer's disease (AD) (McKenzie et al., 2020).

#### 1.4.3.1 The NLRP6 inflammasome and its role in intestinal immunity

While the most studied NLR is NLRP3, in the intestine, NLRP6 has also been implicated. NLRP6 is highly expressed in the epithelium of the small and large intestines, where it is thought to be an essential regulator of host-microbe interactions (Levy et al., 2017). Its activity in goblet cells was shown to be critical for mucus production, to strengthen the epithelial lining and prevent bacterial invasion (Wlodarska et al., 2014). Through promoting cellular repair via IL-18 activation in absorptive IECs during intestinal inflammation, it was linked to prevention of tumorigenesis (Chen et al., 2011; Elinav et al., 2011; Huber et al., 2012). By contrast, IL-18 hyperactivity in IECs was shown to enhance dextran sulfate sodium (DSS)-induced colitis and promote goblet cell damage (Nowarski et al., 2015), suggesting that its activity needs to be finely balanced to maintain homeostasis. Its activity in proinflammatory monocytes and macrophages has been associated with dampening of inflammation in DSS-induced colitis (Seregin et al., 2017).

In studies using *Nlrp6-/-* mice, *Nlrp6* deficiency correlated with dysbiosis and intestinal inflammation, and NLRP6 was thus proposed to shape the intestinal microbial composition (Levy et al., 2015). However, the presence of a specific microbial signature in *Nlrp6-/-* mice was recently contradicted by several studies that minimized non-genetic influences on microbial composition (Lemire et al., 2017; Mamantopoulos et al., 2017), albeit it might still influence the microbial composition in a community-dependent manner.

Studies linking NLRP6 activity with downstream caspase cleavage and interleukin production are thus far largely lacking. Similarly, the activators of NLRP6 assembly, are only beginning to be understood. One study integrating metabolomics and metagenomics approaches, showed that NLRP6 can recognize microbial metabolites which, in turn can modulate its activity. The metabolite taurine was found to activate, whereas histamine and spermine dampened NLRP6 signaling, and its downstream effectors IL-1β and IL-18 (Levy et al., 2015), whereby the effects where primarily ascribed to caspase 1. Recently, lipoteichoic acid (LTA) produced by Gram-positive bacteria was suggested to be sensed by cytosolic NLRP6 in infected macrophages, resulting in non-canonical Casp11 and Casp1 activation, effects that were associated with exacerbated infection in a murine model of *Listeria monocytogenes* infection (Hara et al., 2018).

Together, while a significant amount of data demonstrates NLRP6 presence in the intestine, and suggests crosstalk with microbial components, how specifically it gets activated and how NLRP6, in turn, influences downstream caspase activation and cytokine production, is thus far largely unclear.

Of note, while most work on NLRP6 has been focused on the intestine, it is also expressed in other sites including liver, kidney and astrocytes in the CNS (Zhang et al., 2020). However, studies investigating its functional involvement in physiological and pathological processes in these sites are lacking.

## 1.5 Neuro-immune interactions: Crosstalk between the body's main sensory systems

### 1.5.1 Brief historical perspective

While our understanding of neuro-immune crosstalk has certainly drastically expanded over the past decades, the concept *per se* is not a new one. Observations of a tight interconnectedness between nervous and immune functions were already documented in ancient times: In defining the cardinal signs of inflammation, Aulus Celsus, in 25 A.D., already pointed out an intricate link between nociception and inflammatory immune responses (Kockerling et al., 2013). Work in the late 1800s and early 1900s then provided the anatomical basis for these observations, demonstrating peripheral nerve involvement in inflammatory responses (Sousa-Valente and Brain, 2018). Neuronal mediators of inflammation such as calcitonin gene-related peptide (CGRP), substance P and histamine discovered in the 1960s, and their role in causing rash, edema, later provided molecular basis and a causative role for sensory neurons in the pathophysiology of what is commonly referred to as "neurogenic inflammation" (Jacobson et al., 2021; Sousa-Valente and Brain, 2018).

#### 1.5.1.1 The inflammatory reflex

Wexler and colleagues, in the 1950s, first demonstrated that upon systemic LPS treatment, an anti-inflammatory mechanism initiated in CNS led to pituitary-dependent activation of the adrenal medulla – a response now known as the cholinergic anti-inflammatory pathway (Tracey, 2002; Wexler et al., 1957). The circuit was closed 20 years later, when Besedovsky and colleagues showed that inflammation in the periphery can alter neuronal signaling in hypothalamus (Besedovsky et al., 1977). A body of work thereupon established that neuronal and immune cells each express signaling molecules and receptors classically ascribed to the other. For example, and ACh receptors (AChRs) are expressed by T and B cells, as well as APCs (Fujii et al., 2017), and conversely, various neuroactive substances such as histamine, 5-HT and substance P are produced by mast cells and IECs (Forsythe, 2019; Gribble and Reimann, 2016), and TNF-α, IL-1β, and IL-1 receptor (IL-1R) (Breder et al., 1988; Breder et al., 1994; Tracey, 2002) as well as several PRRs by neurons, including iEANs (Barajon et al., 2009; Furness et al., 2013).

In the early 2000s seminal work by Tracey and colleagues demonstrated that the nervous system, in a reflex loop, can sense and adjust inflammatory responses in real time in what is known as the "inflammatory reflex". Here, vagus nerve stimulation dampened the systemic inflammatory response to LPS in a model of sepsis (Borovikova et al., 2000). The afferent arm of this pathway is activated by an inflammatory milieu,

including via direct sensing of cytokines through IL-1R on vagal neurons (Goehler et al., 1997; Tracey, 2002). The efferent arm, also known as the cholinergic anti-inflammatory pathway, subsequently leads to activation of vagal effector fibers and their release of ACh. This activates nicotinic AChRs (nAChRs) on tissue macrophages, resulting in their downmodulation of proinflammatory cytokines such as TNF-α and IL-1β (Tracey, 2002).

Over the past decades, development of novel tools for imaging, transcriptionally profiling, cell-type specific genetic targeting, and mapping of neuronal circuits have led to a drastic expansion of our understanding of how these two systems interact to maintain homeostatic tissue function and respond to disturbances (Veiga-Fernandes and Mucida, 2016).

### 1.5.2 Intestinal neuro-immune interactions

In the intestine, the nervous and immune systems are the main sensory systems that perceive, integrate and respond to luminal stimuli. Critical roles of bidirectional interactions between neurons and a range of different immune cells have been demonstrated in response to nutrients, microbial composition and enteric infection, while they can be altered during a range of intestinal and systemic diseases such as IBS (Holland et al., 2021) and neurodegeneration (Rao and Gershon, 2016).

#### 1.5.2.1 Intestinal neuron-mast cell interactions

Mast cells are an evolutionarily old cell type and arguably the prototype immune cell in mediating neuronal communication. Previous studies have found gut mast cells to be in close proximity to processes of sensory afferents in rodent and human tissues (Stead et al., 1989; Stead et al., 1987). Furthermore, mast cells secrete neurotransmitters such as histamine, 5-HT and dopamine, rendering them the potential of activating closely apposed sensory afferents expressing the corresponding neurotransmitter receptors (Forsythe, 2019). Conversely, mast cells can be activated by the nervous system through their expression of receptors for a range of neurotransmitters, including VIP, substance P and neurokinins (Kleij and Bienenstock, 2005), resulting in their activation and a positive feedback mechanism (van Diest et al., 2012). Although these largely anatomical descriptions highly suggest a reciprocal communication between mast cells and enteric-associated neurons, experimental evidence is incomplete. In a report of immunoglobulin E (IgE)-mediated food allergy, stimulation of the vagus nerve has been shown to dampen mast cell expansion and activation, which correlated with allergy symptom improvement (Bosmans et al., 2019). However, the underlying mechanisms remain to unclear.

In humans, interactions between mucosal mast cells and adjacent sensory nerve terminals are thought to be involved in mediating pain sensation in IBS (Ford et al., 2017). Here, increased mast cell association with mucosal nerve endings in colonic biopsies correlated with the extent of visceral pain in patients (Barbara et al., 2004). While these results were purely correlative, they open up the possibility that mast cell degranulation in response to dietary antigen triggers nociceptor activation and targeting of this cell type may thus be a therapeutic strategy. A recent elegant study performed in mice and humans

now provided experimental evidence and mechanistic insight supporting a causal role for IgE production and mast cell expansion, and abdominal pain in IBS. In this study, Boeckxstaens and colleagues demonstrated that enteric bacterial infection with *C. rodentium* can result in lasting alterations to the local immune environment such that ingestion of certain previously tolerated food components thereupon trigger an aberrant immune response, resulting in activation of sensory nerve terminals and an abdominal pain response in a process dependent on mucosal mast cell degranulation, histamine release and activation of adjacent sensory afferents (Aguilera-Lizarraga et al., 2021). How this process gets initiated, and whether other cellular mediators are involved, is still unclear.

#### 1.5.2.2 Crosstalk between neurons and ILCs in the intestine

A recent body of work has established ILCs as major players in mucosal neuro-immune regulation. An evolutionarily ancient cell type, they are innate counterparts to T cells, that lack a diversifying antigen receptor. They are categorized in 3 major groups, ILC1, ILC2 and ILC3, reflecting their functional association with $T_h1$, $T_h2$ and $T_h17$ cells. ILCs are highly enriched in mucosal surfaces, where they contribute to, coordinate and selectively amplify immune responses (Vivier et al., 2018).

Interactions between neurons and ILC2s have been implicated in both activation and negative regulation of ILC2 activity at mucosal sites. Multiple complementary studies have recently shown that cholinergic neurons act as potent activators of type 2 immune responses, which was mediated via secretion of a neuropeptide, neuromedin U (NMU), that binds to receptors expressed by adjacent ILC2s. Receptor engagement led to their activation and proliferation, in a similar manner as IL-33 and IL-25 from IECs and tuft cells, amplifying their pro-inflammatory responses to helminth infection and allergic airway inflammation (Cardoso et al., 2017; Klose et al., 2017; Wallrapp et al., 2017). Addition of helminth products or the alarmin IL-33 to neuronal organoids resulted in their production of NMU, opening up the possibility that these neurons can directly sense certain pathogens (Cardoso et al., 2017). Because *in vivo*, many enteric helminths indeed penetrate and migrate through the intestinal wall, neuronal fibers likely get exposed to their products in the course of an infection, even in the absence of them extending into the epithelium. It is possible that this and potentially similar circuits may have evolved as a result of frequent enteric helminth infections.

In contrast to this activating NMU-dependent neuron-ILC2 circuit, work from Artis and colleagues described a regulatory circuit between the sympathetic nervous system (SNS) and ILC2s to constrain type 2 inflammation at mucosal sites (Moriyama et al., 2018). Expression of *Adrb2*, the gene encoding the $\beta_2$-adrenergic receptor ($\beta_2$-AR) by ILC2s, and activation of this signaling pathway by systemic treatment with a $\beta_2$-AR agonist led to dampening of their response to anti-helminth immunity during infection with *Nippostrongylus brasiliensis* (Moriyama et al., 2018). These results thus opened up the possibility that sympathetic neurons and adrenergic signaling negatively regulate ILC2 responses. However, due to employment of systemic drug administration, the source of adrenergic signals remains to be addressed. Several studies also implicated the

neuropeptide CGRP, expressed by both sensory afferents and iEANs, in allowing neurons to fine-tune ILC2 responses. CGRP was shown to selectively enhance IL-5- while suppressing IL-13 production by and proliferation of ILC2s, potentially skewing them toward a tissue repair phenotype and providing a negative feedback loop (Nagashima et al., 2019; Wallrapp et al., 2019; Xu et al., 2019).

ILC3s are critical in the response to extracellular bacteria and in keeping luminal commensals on a leash. They integrate microbial and dietary luminal cues and enhance epithelial AMP production and barrier function. Talbot *et al.* recently showed that the axonal projections of VIPergic iEANs projecting to the lamina propria are surrounded by clusters of ILC3s which selectively express the type 2 VIP receptor. In the presence of a normal microbiota, ILC3s produced IL-22, which was dampened by neuronal VIP secretion and VIP-VIPR engagement on ILC3s. Functionally, this regulatory circuit promoted food absorption at transient expense of barrier function and AMP production and increased susceptibility to infection (Talbot et al., 2020).

#### 1.5.2.3 Role of neuronal communication in epithelial immunity

Defense against invasion of pathogens is in part is mediated by forming and maintaining of a mucus layer, and production of AMPs. IL-18 production by enteric neurons has recently been implicated as a critical mediator of host protection against enteric bacterial infection (Jarret et al., 2020). This was driven by IL-18-mediated AMP production in goblet cells and promoting of pathogen killing in a mouse model of acute *Salmonella enterica* infection. Further, during homeostasis, this neuro-epithelial axis appeared to strengthen the inner mucus barrier (Jarret et al., 2020). Interestingly, the same group had previously shown that in a model of colitis, increase of IL-18 produced by IECs and immune cells had opposing effect on goblet cell mucus production (Nowarski et al., 2015). Thus, the effects of IL-18 may be dependent on cellular source and/or the driving stimulus. What drives neuronal IL-18 production, and how it signals to IECs remains to be investigated.

In a complementary study, crosstalk between gut-innervating extrinsic nociceptor neurons, M cells and commensal microbes was implicated in promoting host defense and protection against *Salmonella enterica* infection. (Lai et al., 2020). TRPV1+ nociceptors mediate protection against bacterial pathogens via direct bacterial sensing of and their release of CGRP. This led to a reduced M cell frequency, which are hijacked by invasive bacteria as a port of entry, and mediated microbial homeostasis by maintaining levels of a commensal species during the course of infection, aiding pathogen resistance (Lai et al., 2020). While the mechanism by which nociceptors recognize pathogenic bacteria and how CGRP release from nociceptive endings controls M cell numbers and SFB levels is still unclear, this study shows that sensing of luminal pathogens can activate an eEAN-dependent protective response. Overall, albeit the underlying mechanisms by which products released by intrinsic and extrinsic neurons alter IECs remain to be investigated, neuronal influence on epithelial function and barrier integrity is becoming apparent.

#### 1.5.2.4 Neuron-LpM crosstalk

Aside from aforementioned responsiveness to luminal cues and other immune cells, input may also come from neuronal interactions, as LpMs are in close apposition to nerve fibers in the intestinal villi and mucosa (De Schepper et al., 2018; Palay and Karlin, 1959) and they have been shown to express receptors for neurotransmitters or neuropeptides, such as VIP (Buckinx et al., 2017; Gabanyi et al., 2016). A recent report showed that in the context of experimental food allergy, stimulation of the vagus nerve significantly improved intestinal inflammation, and this was associated with an increase in allergen uptake by $CX_3CR1^{hi}$ LpMs, suggesting a role for a neuron-macrophage axis to dampen tissue damage during food allergy (Bosmans et al., 2019). Despite these descriptions and literature suggesting a role for neuropeptides in general modulation of macrophage inflammatory responses (Carrion et al., 2016; Nijhuis et al., 2010; Ran et al., 2015), a specific function for neuron-LpM interactions is largely lacking in experimental evidence. Recent advances in neuronal mapping within the intestine (Muller et al., 2020a; Zeisel et al., 2018) coupled with high-resolution single cell macrophage sequencing (De Schepper et al., 2018) is likely to uncover the true potential for neuron-LpM crosstalk.

#### 1.5.2.5 Neuron-MM crosstalk

Bauer and colleagues in the late 1990s focused on clinical conditions associated with GI dysmotility, sepsis and post-operative ileus (POI), to better understand possible functions of MMs. The release of LPS in sepsis resulted in MM activation and upregulation of lymphocyte activation marker 1 (LFA-1) and correlated with a profound decrease in intestinal motility (Eskandari et al., 1997). An increase in LFA-1+ MMs was also correlated with POI in humans (Kalff et al., 1998), which is characterized by a large influx of immune cells, predominantly neutrophils (Farro et al., 2017; Pohl et al., 2017). In turn, a recent study suggested that the immune infiltrate in POI is driven by activation of MMs, as depletion of macrophages improve the symptoms in murine models (Farro et al., 2017). However, the resolution of POI has also been attributed to an increase in monocyte-derived macrophages, a process that may be partially driven by the activation of local dendritic cells (Farro et al., 2017; Pohl et al., 2017). Additionally, cholinergic stimulation of macrophages, in part derived from vagal efferent input to enteric neurons, has been described to reduce neutrophil and additional macrophage recruitment, and ameliorate symptoms in POI (Cailotto et al., 2014; de Jonge et al., 2005; Kimura et al., 2019). The understanding of possible effects of MM activation on gut motility is not limited to POI. In the context of diabetes-induced gastroparesis, MM-derived inflammatory cytokines, including IL-6, TNF-α and IL-1β, seem to contribute to the loss of the pacemaker cells (ICCs) in the muscularis (Cipriani et al., 2018). These findings clearly implicate the pro-inflammatory potential of MMs in dictating subsequent inflammation-induced dysmotility.

In contrast to the pro-inflammatory roles for MMs in specific GI disorders, recent studies have also begun to elucidate a possible anti-inflammatory, tissue protective function for these cells. A recent study investigating the distribution of intestinal macrophages in chemical-induced colitis found an increase in mannose receptor

(CD206)+ MMs during the resolution of inflammation, suggesting a potential tissue protective role for MMs (Kodani et al., 2018). During enteric infections, this macrophage population has been shown to be further skewed towards a tissue-protective profile (Gabanyi et al., 2016). Rapid changes in MM gene expression, in particular the gene *Arg1*, were found to be mediated by stimulation of MM $\beta_2$-AR.

The use of anatomical dissection to study layer-specificity in intestinal macrophages revealed that MMs are transcriptionally distinct from their LpM counterparts, with particular enrichment for receptors and molecules that can contribute to neuronal interaction (De Schepper et al., 2018; Gabanyi et al., 2016; Muller et al., 2014). While the original concept of macrophage contribution to GI motility was put forth by groups studying models of sepsis and POI, high resolution light-microscopy at steady state depicted the extent to which MMs are positioned within the smooth muscle and in close apposition to EAN (Phillips and Powley, 2012). Additional studies established that MMs are in close contact with enteric neurons within the myenteric and submucosal plexuses (De Schepper et al., 2018; Gabanyi et al., 2016). A direct role for MMs in steady state peristalsis was demonstrated by an antibody-mediated MM-preferential depletion, which led to significant changes in colonic motility (Muller et al., 2014). Among the most differentially expressed genes, bone morphogenetic protein 2 (BMP2) was found to be one of the main drivers of steady state MM control of GI motility (Muller et al., 2014). BMP2 was shown to impact the generation of colonic migrating motor complexes in the large intestine, an effect that was mediated by BMP2 signaling through intrinsic EANs expressing BMP receptor IIα (BMPRIIα). The role of macrophages in setting GI motility does not seem to be only a result of interactions with neuronal networks. Macrophages in the small and large intestines were found to express transient receptor potential cation channel 4 (TRPV4) (Luo et al., 2018). Specific loss of *Trpv4* in CX3CR1+ macrophages led to deficits in colonic motility, an effect that was attributed to TRPV4-stimulation of prostaglandin E production by MMs, which in turn directly modulates smooth muscle contractility. In conjunction with observations of inflammation-associated dysmotility, these studies establish a role for MMs in the regulation of peristaltic activity.

Macrophage deficiency during development, as observed for instance in *Csf1*$^{op/op}$ mice, leads to an increase in numbers of enteric neurons, possibly due to a reduction in MM-derived BMP2 (Cipriani et al., 2019; Muller et al., 2014). Developmental control of neuronal numbers also appears specific to particular subpopulations of enteric neurons. For example, in the stomach, the number of nNOS-expressing neurons are preferentially controlled by the presence of MMs (Cipriani et al., 2018). Recent work has challenged the idea that enteric neuronal numbers are set developmentally, rather it has now been proposed that they may be continuously turned over during adulthood. MMs were shown to continuously phagocytose dying neurons, a process that may be necessary to maintain appropriate numbers of enteric neurons (Kulkarni et al., 2017). During aging, the neuro-supportive role of MMs switches as they upregulate pro-inflammatory markers. This phenotypic change in MMs during aging was linked to a macrophage-intrinsic decrease in the immune-regulatory forkhead transcription factor FoxO3, resulting in a decline in enteric neural stem cell populations (Becker et al., 2018). While the exact nature of MM contribution to neuronal numbers in the adult remains unclear, ablation of resident

neuron-associated macrophages has been reported to be associated with rapid neuronal degeneration (De Schepper et al., 2018). These findings may be particularly relevant in clinical cases of hypo-, hyper-, or agangliosis, where large changes in enteric neuronal numbers can lead to intestinal pathology, as observed in pseudo-obstruction or even irritable bowel syndrome (Heuckeroth, 2018). Although further work is needed to link the aforementioned studies that span a wide range of experimental contexts, a multifaceted role for MMs in enteric neuronal differentiation and support is becoming evident.

## 1.6 Influence of gut microbes on enteric nervous and immune systems, and tissue physiology

As the site of multi-network communication, the intestine provides an excellent model for understanding how biological systems interface to maintain homeostasis and prevent disease. In the studies presented in this thesis we aimed to elucidate the influence of enteric microbes – commensal and pathogenic – on enteric nervous and immune systems, and interactions between the two. The product of several effective collaborations, this work reveals the impact of the gut-resident microbiome on the function of enteric-associated neurons. We uncovered a gut region-specific and microbiota-dependent adaptation of intrinsic enteric neurons and identified a subset critical for regulating host physiology independently from the central nervous system. We further uncovered that survival of enteric neurons is dependent on a healthy microbiota, where depletion thereof as well and enteric infections result in damage to the enteric nervous system, leading to a novel mechanism of enteric neuronal cell death involving the NLRP6 inflammasome and caspase 11 (**Chapter 2**). Based on these findings, we then sought to determine a role for intestinal immune cells in neuronal damage or protection during enteric infections. We found that a population of intestinal macrophages respond to luminal infection to limit neuronal damage, likely by signaling from the sympathetic nervous system. Intriguingly, these muscularis macrophages remain in a state of alertness thereupon, preventing cumulative neuronal damage during future insults. Aiming to determine the cellular intermediates activating intestinal macrophages during an acute infection, we then sought to better characterize extrinsic, gut-projecting neurons and their response to microbial stimulation. We found that gut-projecting sympathetic neurons are robustly modulated by gut microbes. Finally, we determined that the sympathetic nervous system, activated upon microbial imbalances including enteric infection, mediates the polarization of muscularis macrophages, limiting infection-induced tissue damage (**Chapter 3**). The final chapter will provide a discussion of these studies connect to and potentially expand the current understandings of the field, consider implications of our findings from a clinical standpoint and look ahead to define future directions (**Chapter 4**).

# CHAPTER 2. IMPACT OF GUT MICROBES ON THE ENTERIC NERVOUS SYSTEM AND HOST PHYSIOLOGY

Recent studies have demonstrated that the gut microbiota influences the basal activity of intestine-resident cells, including the excitability of enteric-associated neurons (EAN) and the activation state of immune cells (Furness et al., 2013; Pavlov et al., 2018; Rankin and Artis, 2018; Veiga-Fernandes and Mucida, 2016). These interactions have also been implicated in several disease processes, ranging from irritable bowel syndrome (IBS) to CNS diseases, such as Alzheimer's disease and Parkinson's disease (Fung et al., 2017). Additionally, microbial dysbiosis has a potential role in a host of metabolic disorders including obesity and diabetes (Qin et al., 2012; Ridaura et al., 2013). While these studies highlight the impact of the gut microbiota on EANs and key mammalian physiological processes, the cellular circuits and molecular components that mediate microbe-EAN or gut-brain communication remain poorly understood.

In this chapter, we sought to investigate the influence of gut microbes – commensal and pathogenic ones – on the ENS and its function. We further sought to determine the impact of disturbances of microbial colonization – during microbial depletion and in infections – on iEAN function and GI physiology. Finally, we aimed to functionally characterize iEAN subsets that are modulated by the gut microbiota, to investigate the role of these interactions in host physiology.

## 2.1 Regional characterization of the enteric nervous system

The expression profile of iEANs is only recently beginning to be uncovered by single-cell sequencing, which thus far has lacked spatial resolution and the ability to capture these neurons in their native state. We thus first sought to profile iEANs from different regions of the intestine to better study their role in host physiology.

### 2.1.1 Intrinsic enteric neurons are a unique peripheral neuronal population

To profile iEANs in an untargeted and region-specific manner, we performed translating ribosomal affinity purification (TRAP) (Heiman et al., 2014), a cell type-specific actively translated mRNA profiling approach. We used this method to bypass the need for tissue fixation or single-cell suspension, thereby avoiding possible confounding effects of neuronal dissociation on gene expression. We interbred pan-neuronal *Snap25*$^{Cre}$ with *Rpl22*$^{lsl\text{-}HA}$ (RiboTag) mice (Sanz et al., 2009), which express a hemagglutinin (HA)-tagged ribosomal subunit 22, allowing immunoprecipitation of actively-translated mRNA in a cell type-specific manner. Expression of HA-tagged ribosomes was observed in neurons in the myenteric plexus of the duodenum, ileum, and colon of *Snap25*$^{RiboTag}$ mice (Fig. 2.1 A). We confirmed successful immunoprecipitation (IP) of intact mRNAs bound to HA-tagged ribosomes from myenteric neurons in the intestine muscularis. RNA sequencing of bound transcripts revealed significant enrichment of neuron-specific genes and pathways in *Cre+* animals when compared to *Cre-* controls (Fig. 2.1 B to D).

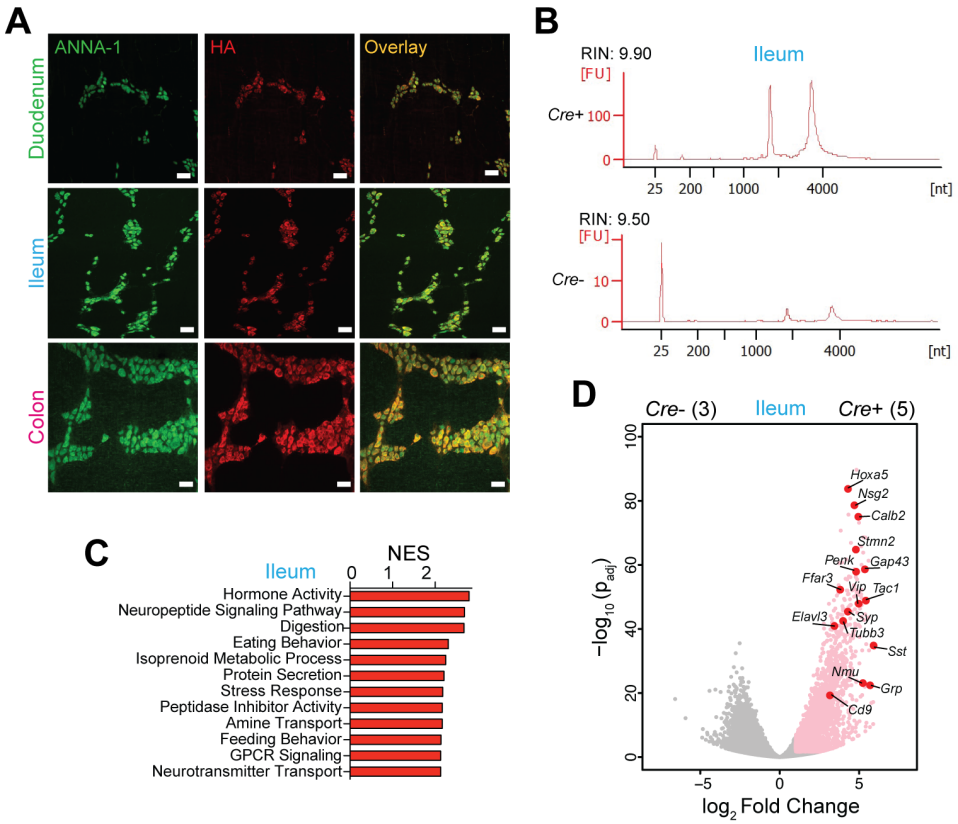


**Fig. 2.1. Specificity of RiboTag sequencing of myenteric intrinsic enteric neurons.** (**A** to **D**) *Snap25*$^{\text{RiboTag}}$ SPF mice were analyzed. (**A**) Whole-mount immunofluorescence (IF) image of duodenum, ileum and colon myenteric plexus using anti-hemagglutinin (HA) and anti-neuronal nuclear (ANNA-1) antibodies. Scale bars, 50 µm. (**B**) Bioanalyzer traces of immunoprecipitated (IP) ribosome-bound mRNA eluted from the ileum muscularis externa of *Snap25*$^{\text{RiboTag}}$ (*Cre+*) and *Snap25*$^{Cre-}$ (*Cre-*) SPF mice. (**C**) Graph of the top 12 gene ontology pathways with a FDR < 25% identified by Gene Set Enrichment Analysis (GSEA) from ileum IP-enriched genes (log2 Fold Change > 1, padj < 0.05). (**D**) Volcano plot of differentially expressed transcripts between the ileum muscularis externa of *Snap25*$^{\text{RiboTag}}$ (*Cre+*) and *Snap25*$^{Cre-}$ (*Cre-*) SPF mice. Pink dots highlight transcripts with a $\log_2$ Fold Change of >1 and padj-value <0.05. Red dots and black labels highlight select IP-enriched transcripts of interest. Number of samples shown in parentheses.NES, normalized enrichment score; FDR, false detection rate.

TRAP RNA-seq (TRAP-seq) analysis of iEANs and extrinsic EANs (nodose, NG; celiac–superior mesenteric, CG-SMG; and dorsal root ganglion, DRG) suggested that iEANs possess a distinct translational profile (Fig. 2.2 A and B). We found that iEANs were primarily defined by enriched transcripts related to neuropeptide signaling as compared to NG/DRG and CG-SMG, which had increased expression of genes involved in sensory processes and catecholamine production, respectively (Fig. 2.2 C to F).

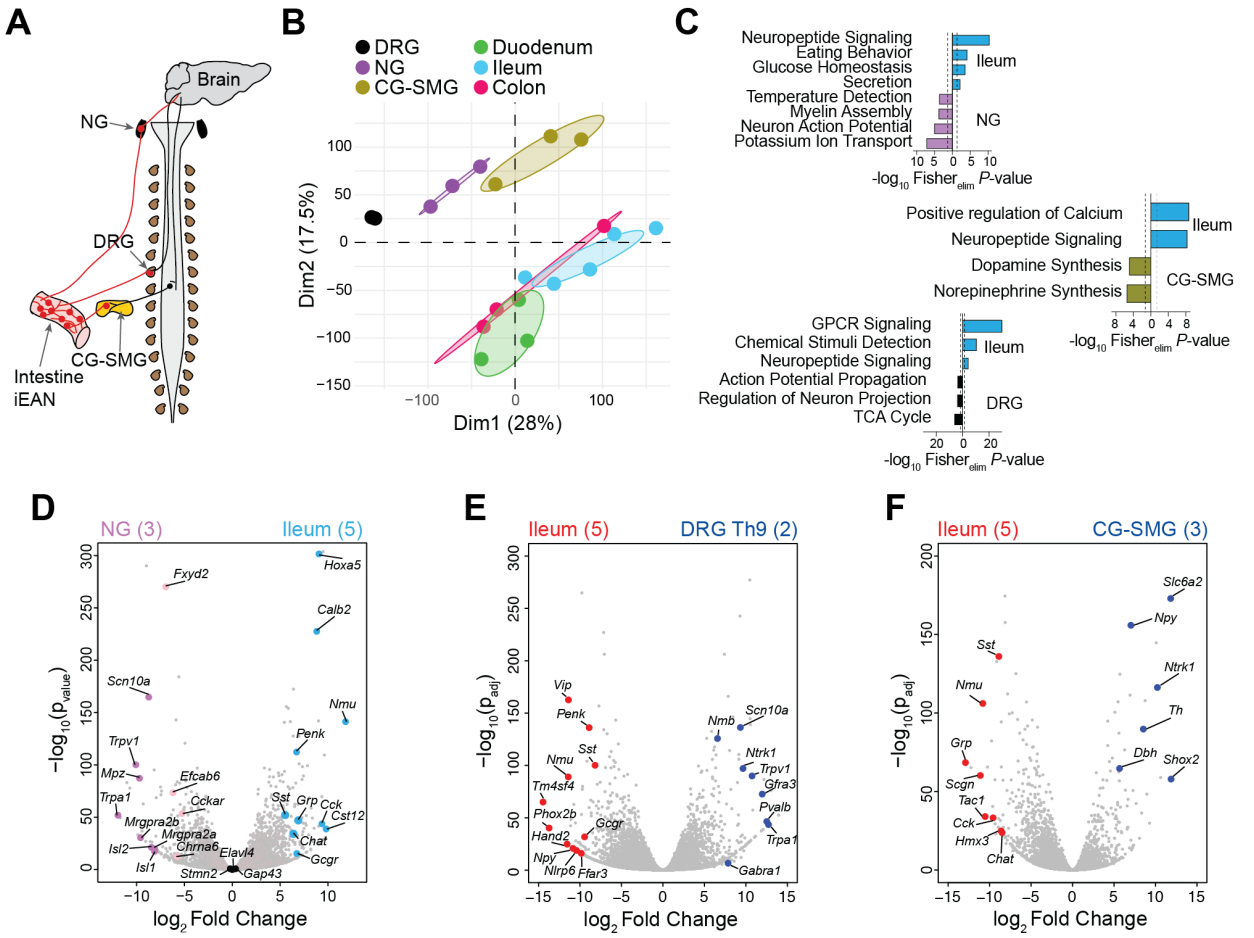


**Fig. 2.2. Intrinsic enteric neurons form a unique neuronal population.** (**A**) Anatomical diagram of intrinsic and extrinsic EANs. Red dots and lines highlight relevant ganglia and fibers. NG = nodose, DRG = dorsal root, CG-SMG = celiac-superior mesenteric ganglion. (**B-E**) *Snap25*$^{RiboTag}$ SPF mice were analyzed. (**B**) Principal Component Analysis (PCA) of neuronal translatomes from NG, CG-SMG, DRG, ganglia, and duodenum, ileum, and colon. (**C**) Gene ontology (GO) pathways of differentially expressed genes (DEGs) ($log_2$ Fold Change (FC) > 1, padj < 0.05) enriched in ileum myenteric iEANs vs indicated ganglia. Colored (**D-F**) Volcano plot of differentially expressed transcripts from the ileum and indicated ganglia. nodose ganglion (NG) and ileum myenteric iEANs of *Snap25*$^{RiboTag}$ SPF mice. Grey dots, all transcripts analyzed by differential expression analysis. Colored dots, DEGs of interest between each tissue pair. Sample numbers indicated in parentheses.

## 2.1.2 Profiling of iEANs reveals anatomical, region-specific differences

Comparison between translational profiles of myenteric neurons isolated from the duodenum, ileum, and colon indicated that iEANs segregate based on their anatomical location (Sang and Young, 1996) (Fig. 2.3 A to D). Compartmentalized translational profiles of myenteric neurons are consistent with the anatomically distinct functions of the corresponding segments of the intestine. The proximal small intestine is highly absorptive, enriched with EEC subsets associated with lipid and nutrient detection (Gribble and Reimann, 2016). We found that duodenal iEANs, in comparison to those of the ileum and colon, express significantly higher levels of transcripts encoding receptors involved in the response to proximal EEC- or iEAN-derived signals, such as cholecystokinin receptor A (*Cckar*), glucagon receptor (*Gcgr*), and tachykinin receptor 3 (*Tacr3*) (Haber et al., 2017)

(Fig. 2.3 B to E). We also found regional differences in neuropeptide transcripts, including neuropeptide Y (*Npy*) enrichment in duodenum iEAN. The terminal ileum and colon iEANs are enriched in neuropeptide transcripts, such as somatostatin (*Sst*), cocaine- and amphetamine-regulated transcript (*Cartpt*), proenkephalin (*Penk*), gastrin releasing peptide (*Grp*), agouti gene-related peptide (*Agrp*), and tachykinin 1 (*Tac1*), all of which, besides *Agrp*, are thought to be involved in the control of intestine motility through the myenteric plexus (Degen et al., 2001; Ekblad et al., 2003; Holzer, 2009; Lecci et al., 2008; Portbury et al., 1995; Teitelbaum et al., 1984) (Fig. 2.3 B to E).

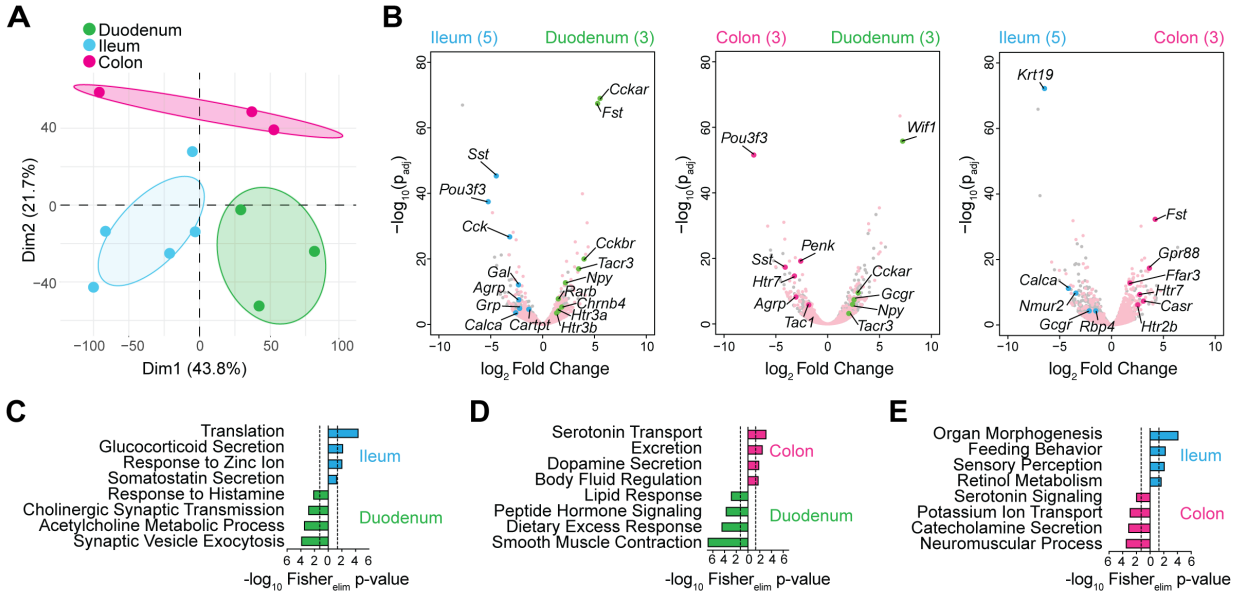


**Fig. 2.3. The enteric neuronal translatome changes along the length of the intestine.** (**A**) PCA of neuronal translatomes from duodenum, ileum, and colon of *Snap25*$^{RiboTag}$ SPF mice. (**B**) Volcano plots of DEGs between indicated intestinal segment of *Snap25*$^{RiboTag}$ SPF mice. Pink dots, all intestine neuronal IP-enriched transcripts. Colored dots, DEGs of interest between each pair of intestine segments. Sample numbers indicated in parentheses. (**C** to **E**) GO pathways identified by TopGO analysis of DEGs ($log_2$ Fold Change > 1, padj < 0.05), enriched in (**C**) ileum vs duodenum, (**D**) colon vs duodenum, and (**E**) ileum vs colon of *Snap25*$^{RiboTag}$ SPF mice. Dashed lines, threshold of significance (1.3) as calculated by Fisher's test with an elimination algorithm.

Immunofluorescence (IF) analysis confirmed a regional compartmentalization of neuropeptides at the protein level and identified regional differences in neuronal number along the intestine (Fig. 2.4 A and B). For instance, NPY, typically involved in intestinal inflammation or inhibition of neurotransmission (Browning and Lees, 2000; Grider, 2003; Holzer et al., 1987), was enriched in duodenum iEANs (Fig. 2.5 A and B). In contrast, the neuropeptide SST, involved in the EEC regulation of several GI hormones (Mace et al.,

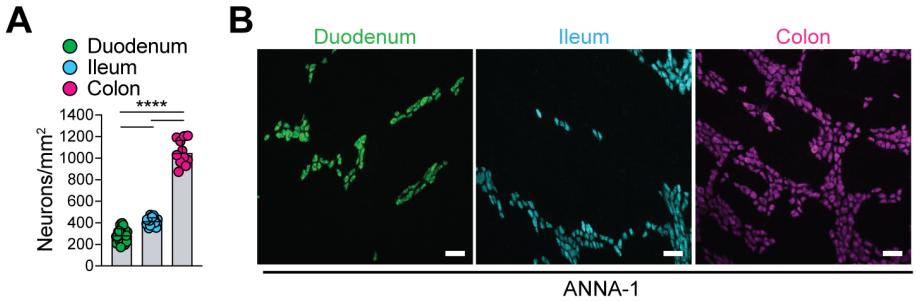


**Fig. 2.4. Regional differences in intrinsic enteric neuronal density along the intestine.** (**A**) Total myenteric iEANs in different gut regions. **** $P < 0.0001$, Brown-Forsythe and Welch ANOVA with Dunnett's T3 multiple comparisons test. (**B**) Whole-mount immunofluorescence images of myenteric iEANs. (stained with anti-ANNA-1) in the duodenum, ileum, and colon of C57BL/6J SPF mice. Scale bars, 50 µm.

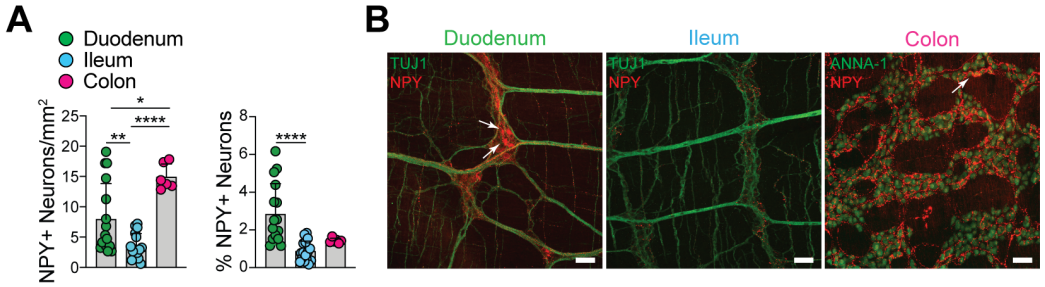


**Fig. 2.5. Regional differences in NPY+ neurons along the intestine.** (**A**) Number and percentage of NPY+ myenteric iEAN in different gut regions. * $P < 0.05$, ** $P < 0.01$, **** $P < 0.0001$, Brown-Forsythe and Welch ANOVA with Dunnett's T3 multiple comparisons test (number), Kruskal-Wallis test with Dunn's multiple comparisons test (percentage). (**B**) Whole-mount IF images of NPY+ (red) myenteric iEANs in the duodenum, ileum, and colon of C57BL/6J SPF mice. White arrows, NPY+ neurons. Scale bars, 50 µm.

2015) and inhibition of smooth muscle contraction through inhibition of neuropeptide-mediated ACh release (Grider, 2003; Portbury et al., 1995; Teitelbaum et al., 1984), is highly expressed in the ileum and colon, but scarcely so in the duodenum (Fig. 2.6 A and B). Further, we observed increased numbers of CART+ neurons, thought to play a role in

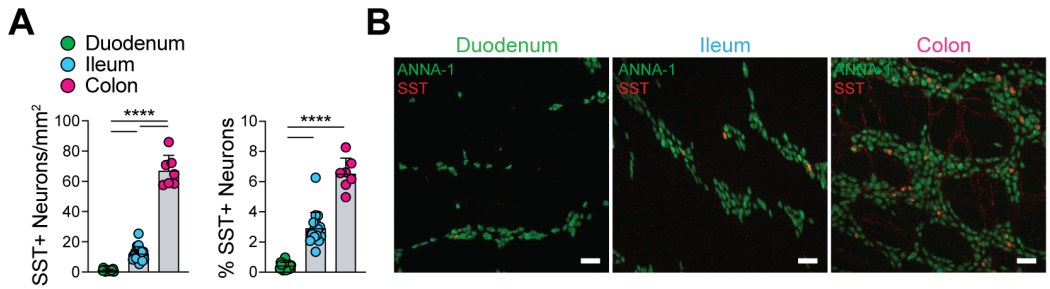


**Fig. 2.6. Regional differences in SST+ neurons along the intestine.** (**A**) Number and percentage of SST+ myenteric iEAN in different gut regions. **** P < 0.0001, Brown-Forsythe and Welch ANOVA with Dunnett's T3 multiple comparisons test (number), Kruskal-Wallis test with Dunn's multiple comparisons test (percentage). (**B**) Whole-mount IF images of SST+ (red) myenteric iEAN in the duodenum, ileum, and colon of C57BL/6J SPF mice. Scale bars, 50 µm.

intestinal NO neurotransmission and neuroprotection (Ekblad, 2006; Ekblad et al., 2003), in the ileum and colon (Fig 2.7 A to D). Finally, we found that the duodenum is particularly enriched in transcripts encoding pleiotropic growth factors previously shown to be expressed in the intestinal epithelium, such as follistatin 1 (*Fst1*) (Sonoyama et al., 2000)

and WNT inhibitory factor 1 (*Wif1*) (Byun et al., 2005) as compared to the ileum or colon, respectively. IF analysis confirmed prominent FST1+ neurons and nerve fibers in the duodenum that were absent in the ileum and sparse within the colon (Fig 2.8 A and B). These data, which add higher resolution findings to prior studies (Sang and Young, 1996), reveal the region-specific gene profiles of iEANs that likely reflect the function of distinct intestinal regions.

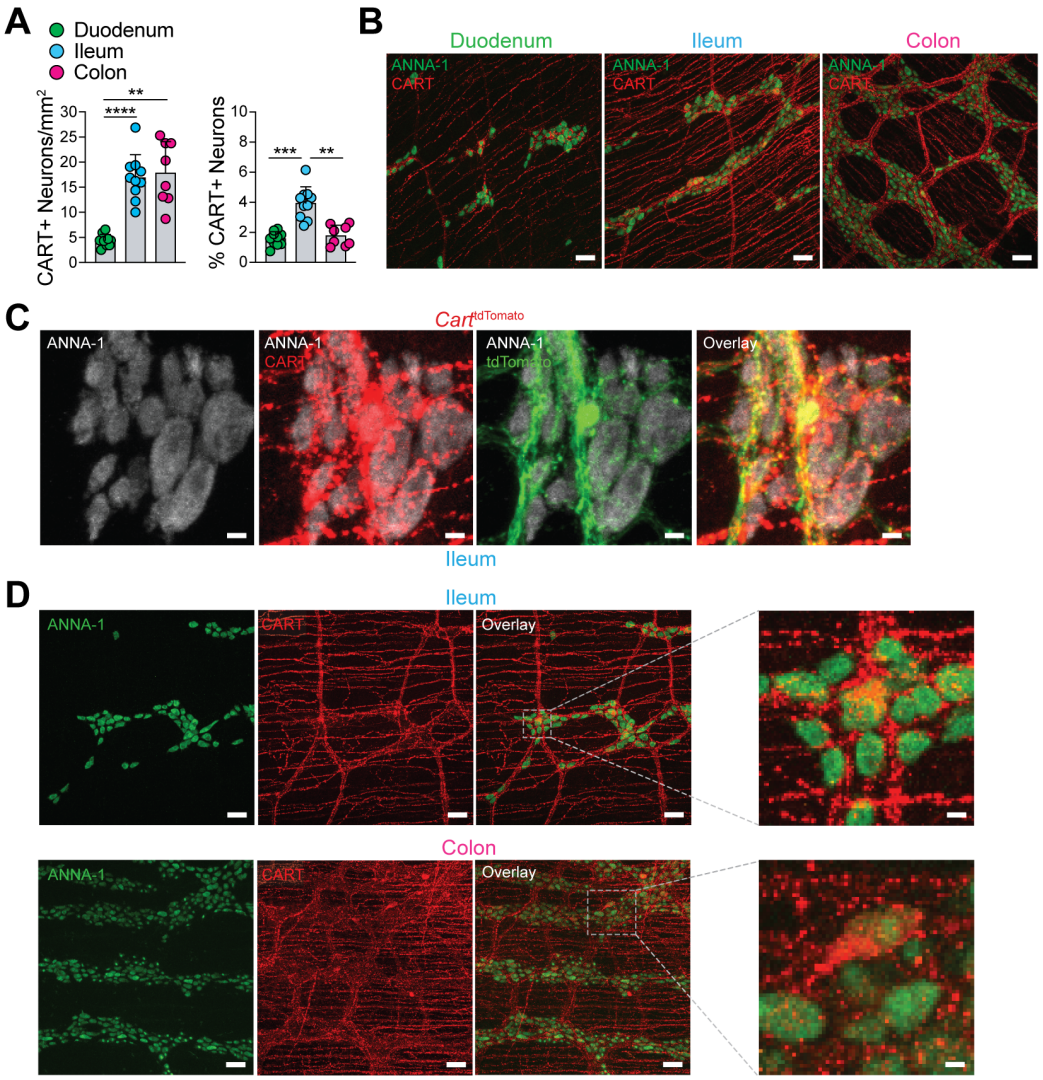


**Fig. 2.7. Regional differences and morphology of CART+ iEANs.** (**A**) Number and percentage of CART+ myenteric iEANs in different gut regions. ** $P < 0.01$, *** $P < 0.001$, **** $P < 0.0001$, Brown-Forsythe and Welch ANOVA with Dunnett's T3 multiple comparisons test (number), Kruskal-Wallis test with Dunn's multiple comparisons test (percentage). (**B** to **D**) Whole-mount IF images of (**B**) CART+ (red) myenteric iEANs in the duodenum, ileum, and colon of C57BL/6J SPF mice. Scale bars, 50 µm, (**C**) CART+ (red, antibody) and tdTomato (green, native fluorescence) myenteric iEANs (grey) in the ileum of *Cart*$^{tdTomato}$ SPF mice. Scale bars (left panel), 50 µm. Scale bars (inset in middle and right panel), 10 µm, (**D**) different types of CART+ (red) myenteric iEANs (grey) in the ileum and colon of C57BL/6J mice. Scale bars, 50 µm. Scale bars of insets on the right, 10 µm.

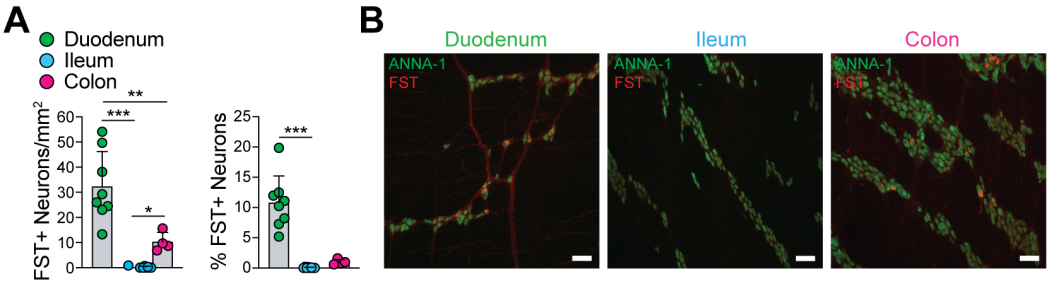


**Fig. 2.8. Regional differences in FST+ iEANs along the intestine.** (**A**) Number and percentage of follistatin (FST)+ myenteric iEAN in different gut regions. **** $P < 0.0001$, Brown-Forsythe and Welch ANOVA with Dunnett's T3 multiple comparisons test (number), Kruskal-Wallis test with Dunn's multiple comparisons test (percentage). (**B**) Whole-mount IF images of FST+ (red) myenteric iEAN in the duodenum, ileum, and colon of C57BL/6J SPF mice. Scale bars, 50 µm.

## 2.2 The gut microbiota affects the enteric nervous system in a compartmentalized manner

Because the density and diversity of the gut microbiota increases from the proximal to distal intestine, we next examined whether the regionally distinct iEAN translational programs are partially influenced by the microbiota (Collins et al., 2014).

### 2.2.1 Distal intestinal iEANs are impacted by the absence of a microbiota from birth

To address the influence of microbial stimuli on iEANs, we first performed AdipoClear (Chi et al., 2018) on whole-mount intestinal tissue followed by light-sheet microscopy, which allows for robust labelling and high-resolution volumetric imaging, of iEANs in the ileum and colon of germ-free (GF) or specific-pathogen free (SPF) mice. In both GF and SPF mice, iEANs were organized into distinct plexuses (Fig. 2.9 A). We also observed vast mucosal innervation in the small and large intestines of both GF and SPF mice that extended into individual villi with fibers adjacent to the epithelium. While colonic morphology and innervation did not reveal gross alterations between mice kept under GF and SPF conditions, we observed that ileum villi are thin and blunted in GF animals, inherently leading to different nerve fiber structure (Fig. 2.9 A).

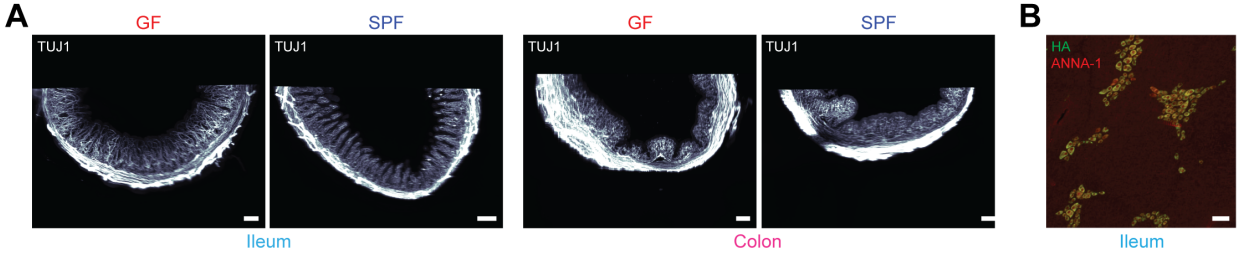


**Fig. 2.9. Gross anatomical differences between SPF and GF ENS.** (**A**) AdipoClear light-sheet images of ileum and colon of GF or SPF C57BL/6J mice using anti-TUJ1 antibody. Scale bars, 200 µm (SPF colon, 100 µm). (**B**) IF staining of the ileum myenteric plexus of *Snap25*$^{\text{RiboTag}}$ GF mice using anti-HA and anti-neuronal nuclear (ANNA-1) antibodies. Scale bar, 50 µm. Image representative of ileum myenteric plexus.

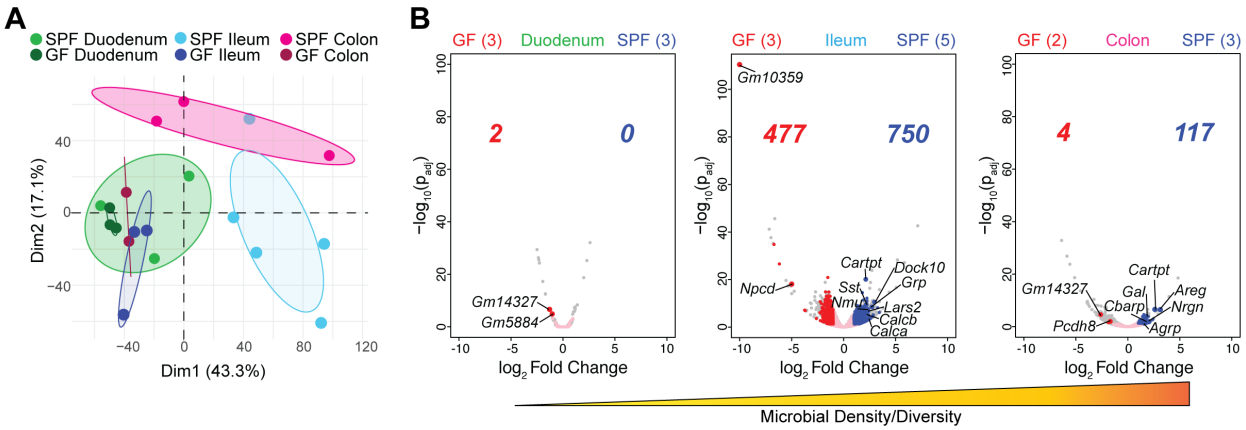


**Fig. 2.10. Microbiota affect the iEAN translatome in a compartmentalized manner.** (**A** and **B**) *Snap25*$^{\text{RiboTag}}$ mice were analyzed. (**A**) PCA of GF and SPF iEANs from duodenum, ileum and colon. (**B**) Volcano plots of duodenum, ileum, and colon iEAN DEGs between GF and SPF. Pink dots, all intestine neuronal IP-enriched transcripts; colored dots and numbers, significantly differentially expressed transcripts ($\log_2$ FC >1 and padj <0.05). Sample numbers indicated in parentheses.

To determine whether the microbiota impacts iEAN gene expression profiles along the intestine, we re-derived *Snap25*$^{\text{RiboTag}}$ mice under GF conditions (Fig. 2.9 B). Analysis of TRAP-seq from duodenum, ileum, and colon myenteric iEANs of GF *Snap25*$^{\text{RiboTag}}$ mice revealed microbiota-dependent transcriptional changes in each region (Fig. 2.10 A and B). While only 4 transcripts were significantly upregulated in SPF compared to GF samples in the duodenum, 709 and 123 transcripts were significantly upregulated in the ileum and colon, respectively (Fig. 2.10 B). The smaller magnitude of microbiota-dependent changes in the duodenum could be related to the lower microbial density and diversity in this region. Furthermore, principal component analysis (PCA) revealed that GF duodenum, ileum, and colon samples all clustered together with duodenum samples of SPF mice (Fig. 2.10 A). To determine whether these distal regions gain a “duodenum-like” gene expression profile, we generated a list of transcripts enriched in SPF duodenum

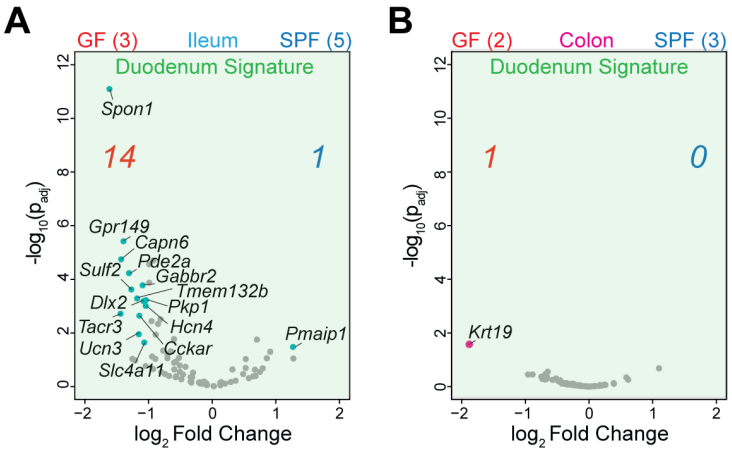


**Fig. 2.11. Shift to a “duodenum-associated” signature in the distal intestine of GF mice.** (**A** and **B**) Volcano plots of differentially expressed “duodenum signature” transcripts in (**A**) ileum and (**B**) colon iEANs of GF and SPF mice. Pink dots, all iEAN IP-enriched transcripts; colored dots and numbers, significantly differentially expressed transcripts ($\log_2$ FC >1 and padj <0.05). Sample numbers indicated in parentheses.

as compared to SPF ileum and colon (Table 1, Appendix 1). A subset of duodenum-enriched transcripts was upregulated in the ileum, but not colon, of GF as compared to SPF animals (Fig. 2.11 A and B). The third principal component also revealed segregation of GF colon from the GF duodenum and ileum samples, which may reflect the presence of iEANs derived from sacral progenitors in the large intestine, or functional differences between segments (Fig. 2.12 A). Direct comparison of GF duodenum, ileum, and colon samples also indicated segregation between regions, suggesting that certain features of region-specific iEAN programming are microbiota-independent (Fig. 2.12 B).

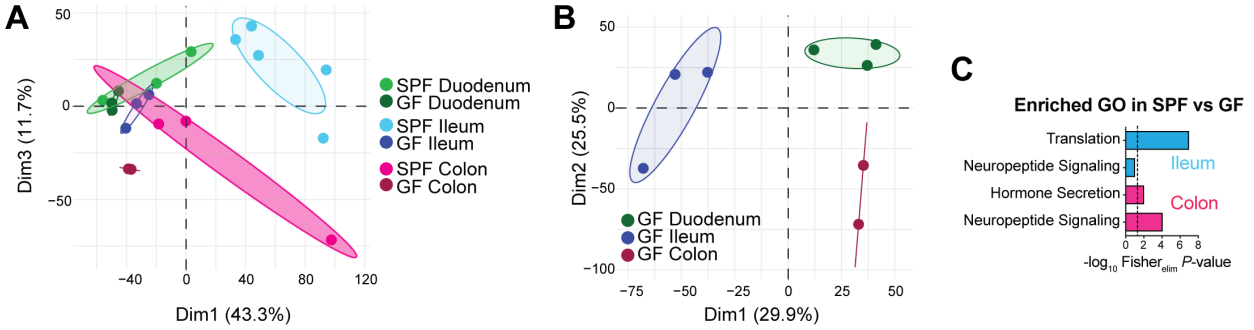


**Fig. 2.12. Compartmentalization of the iEAN translatome is reduced in GF mice.** (**A** and **B**) PCA from (**A**) duodenum, ileum, and colon iEAN of *Snap25*$^{RiboTag}$ GF and SPF mice. (**B**) duodenum, ileum, and colon iEANs of *Snap25*$^{RiboTag}$ GF mice. PCA input was filtered for total iEAN IP-enriched transcripts ($log_2$ Fold Change > 1, padj < 0.05). (**C**) GO pathways of DEGs enriched in SPF versus GF samples.

Microbiota-dependent transcripts in the duodenum included *Nnat* and *Penk*, involved in neuronal development (Ma et al., 2019) and enkephalin production (Lay et al., 2016), respectively. In the ileum and colon, we found microbiota-dependent transcripts encoding neuropeptides associated with neuro-immune crosstalk, such as *Nmu* (Cardoso et al., 2017); EAN physiological function, such as *Sst* and *Cartpt*; and functions outside of the intestine, like *Agrp* (colon only) (Fig. 2.10 B and Fig. 2.12 C). SST and CART protein expression changes were confirmed by quantification of IF images from GF and SPF mice (Fig. 2.13 A to F).

Quantification of iEAN in the myenteric plexus of GF and SPF mice also revealed a significant reduction in iEAN number in the duodenum and ileum, but not colon, of GF mice (Fig. 2.14. A to C). Finally, analysis of GF and SPF datasets using predicting associated transcription factors from annotated affinities (PASTAA) (Roider et al., 2009) identified c-AMP response element binding protein (CREB) amongst the most enriched transcription factors for the ileum and colon in SPF mice (Fig. 2.15 A). Because the level of phosphorylated CREB (pCREB) in neurons is often used as an indirect measure of activation and is a mediator of neuropeptide transcription (Lakhina et al., 2015), we performed IF using CREB phosphorylation at serine 133, a key modification to induce gene transcription. We found a significant reduction of pCREB in the ileum myenteric plexus of GF compared to SPF mice (Fig. 2.15 B and C), demonstrating that iEANs may be hypoexcitable under gnotobiotic conditions, as previously proposed (McVey Neufeld et al., 2015), and providing a possible explanation for the reduction in neuropeptide transcripts observed.

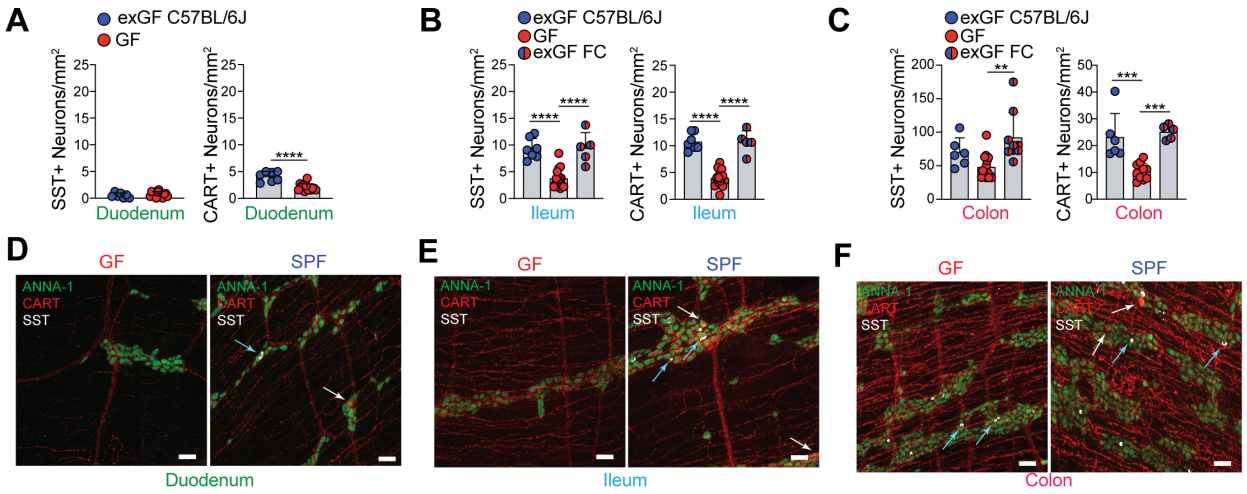


**Fig. 2.13. Alterations to neuropeptide levels in gnotobiotic mice.** (**A** to **C**) Numbers of SST+ and CART iEAN in (**A**) duodenum, (**B**) ileum and (**C**) colon of GF, exGF, and GF colonized with exGF feces (exGF FC). ** $P < 0.01$, *** $P < 0.001$, **** $P < 0.0001$, one-way ANOVA with Tukey's multiple comparisons test (SST) or Brown-Forsythe and Welch ANOVA with Dunnett's T3 multiple comparisons test (CART). (**D** to **F**) Representative whole-mount IF images of SST+ and CART+ myenteric iEAN in the duodenum (**D**), ileum (**E**), and colon (**F**) of (left) GF and (right) SPF mice. Scale bars, 50 µm. Blue arrows, examples of SST+ iEANs; white arrows, examples of CART+ iEANs.

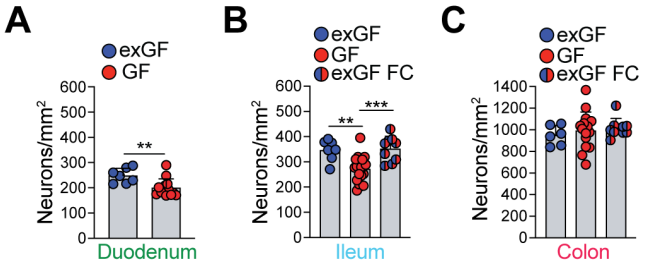


**Fig. 2.14. Alterations to enteric neuron numbers in gnotobiotic mice.** (**A** to **C**) Total iEAN numbers in (**A**) duodenum, (**B**) ileum, and (**C**) colon of GF, exGF, and GF colonized with exGF feces (exGF FC) C57BL/6 mice. ** $P < 0.01$, *** $P < 0.001$, one-way ANOVA with Tukey's multiple comparisons test.

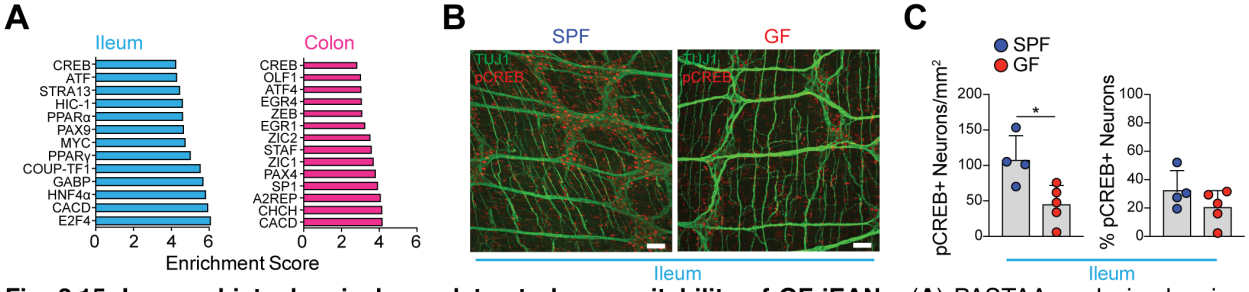


**Fig. 2.15. Immunohistochemical correlates to hypoexcitability of GF iEANs.** (**A**) PASTAA analysis showing enrichment of predicted CREB1 transcription factor binding to the most significant differentially expressed transcripts ($log_2$ Fold Change > 1, padj < 0.05) of the ileum and colon iEAN between *Snap25*$^{RiboTag}$ GF and SPF mice. (**B**) Representative confocal IF image of the ileum myenteric plexus of C57BL/6J (left) GF and (right) SPF mice using anti-pCREB (red) and anti-TUJ1 (green). Scale bars, 50 µm. (**C**) Number and percentage of pCREB+ myenteric iEANs in the ileum of C57BL/6J GF and SPF mice. * $P < 0.05$ as calculated by unpaired t-test.

### 2.2.2 Microbiota-dependent changes to iEANs in gnotobiotic mice can be restored upon colonization during adulthood

To address whether altered neuropeptide levels and iEAN number in gnotobiotic mice are the result of a developmental defect, we provided adult C57BL/6 GF with feces from age- and sex-matched SPF mice maintained on a GF diet (ex-GF mice). Colonization of 8-week-old GF animals with SPF feces was sufficient to increase the number of SST+ and CART+ neurons in the ileum and colon to levels similar to SPF animals after 2 weeks, as well as a notable increase in the density of SST+ and CART+ nerve fibers (Fig. 2.13 B and C and Fig. 2.16 A to D). Total ileal iEAN number decreased in GF mice and was restored by recolonization, whereas total colonic iEAN number was not microbiota-dependent (Fig 2.14 A). Overall, these results establish regional differences and microbial influence on iEAN number and gene expression profiles, particularly on neuropeptidergic coding.

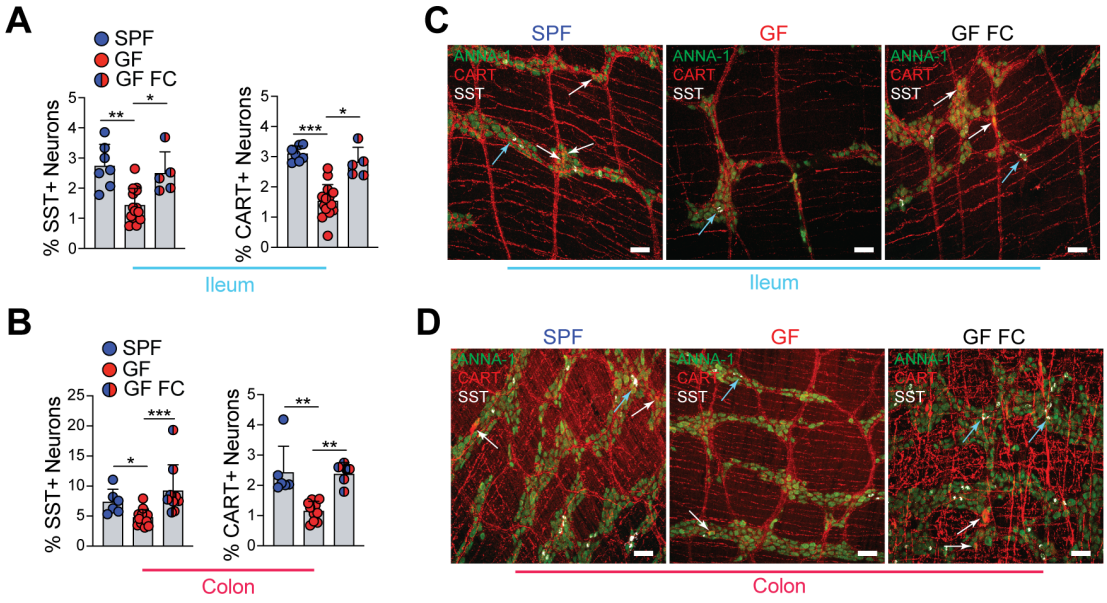


**Fig. 2.16. Enteric neuronal changes in gnotobiotic mice can be restored upon conventionalization.** (**A** and **B**) Percentage of SST+ and CART+ iEAN out of total myenteric iEANs in the (**A**) ileum and (**B**) colon of GF and SPF mice. * $P < 0.05$, ** $P < 0.01$, *** $P < 0.001$ as calculated by Kruskal-Wallis test with Dunn's multiple comparisons test. (**C** and **D**) Representative whole-mount IF images of SST+ (white) and CART+ (red) myenteric iEANs (green) in the (**C**) ileum and (**D**) colon of (left) GF and (right) GF mice colonized with SPF microbiota (fecal colonization, GF FC). Scale bars = 50 µm. Blue and white arrows point to examples of SST+ and CART+ neurons, respectively.

### 2.2.3 Antibiotic-mediated microbial depletion during adulthood impacts iEAN numbers and neuropeptide levels

Since colonization restored total iEAN- as well as CART+ and SST+ neuron numbers in GF mice, we next asked if these microbiota-dependent changes can be observed in SPF mice upon administering broad-spectrum antibiotics, or if a microbiota must be absent from birth. We administered antibiotics (vancomycin, ampicillin,

metronidazole, and neomycin) in the drinking water of SPF mice for 2 weeks and detected a significant decrease in iEAN numbers in the ileum and colon, but not in the duodenum, confirming that the most robust microbiota-dependent changes are consistently observed in the distal intestine (Fig. 2.17 A). Importantly, this neuronal reduction was not

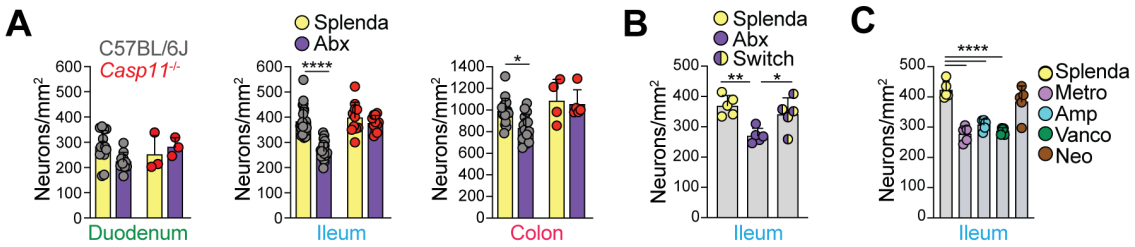


**Fig. 2.17. Microbial depletion leads to iEAN loss in adult wild-type mice.** (**A**) Myenteric iEAN number in duodenum, ileum and colon of C57BL/6J and Casp11–/– mice treated with antibiotics (Abx: vancomycin, ampicillin, metronidazole and neomycin) in drinking water supplemented with sucralose-based artificial sweetener (Splenda®), or Splenda only. (**B**) Ileal myenteric iEAN number of C57BL/6J SPF mice after 4 weeks on Abx or Splenda, or Abx followed by Splenda for 2 weeks each (Switch). (**C**) Ileal myenteric iEAN number of C57BL/6J SPF mice on metronidazole, ampicillin, vancomycin, neomycin or Splenda.

permanent, as antibiotic withdrawal for two weeks resulted in the recovery of neuronal numbers to SPF levels (Fig. 2.17 B). Chronic treatment with vancomycin, ampicillin or metronidazole alone, but not neomycin or a single dose of streptomycin, also induced a reduction in total iEAN numbers, suggesting a possible role for specific bacteria in physiological iEAN maintenance (Fig. 2.17 C). Quantification of microbiota load after oral or intraperitoneal (i.p.) antibiotic administration, and subsequent neuronal quantification, further suggested that neuronal loss was induced by microbial depletion, not by direct antibiotic neurotoxicity or dysbiosis *per se* (2.18 A to D).

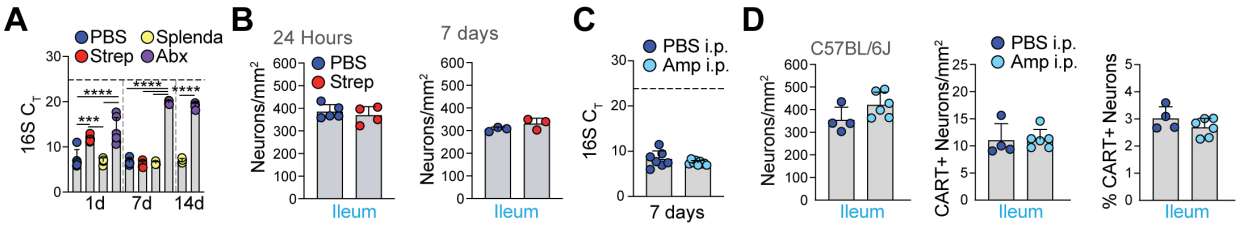


**Fig. 2.18. iEAN loss after microbial depletion is not mediated by antibiotic neurotoxicity.** (**A**) Cycle threshold ($C_T$) values of 16S qPCR from fecal samples of C57BL/6J SPF mice treated with a single oral gavage of streptomycin/PBS or continuously with broad-spectrum antibiotics (Abx)/Splenda in the drinking water. Dotted line, average $C_T$ value of pooled germ-free control samples. *** $P < 0.001$, **** $P < 0.0001$, one-way ANOVA with Tukey's multiple comparisons test. (**B** to **D**) C57BL/6J SPF mice were treated with 1 g/kg ampicillin/PBS or PBS by i.p. injection for 7 days. (**B**) $C_T$ values of 16S qPCR from fecal samples. Dotted line indicates average $C_T$ value of pooled GF control samples; (**C**) Number of (left) myenteric iEANs in the ileum, (middle) CART+ iEANs per mm$^2$ and CART+ iEANs as a percentage of total iEAN. (**D**) Representative confocal IF images of tissue analyzed in (**C**). Scale bars, 50 µm.

We next examined the specific microbiota-modulated neuropeptide pathways that we identified in GF mice and analogously observed a significant decrease in the number and overall percentage of SST+ and CART+ neurons in the ileum and colon, but not duodenum, upon antibiotic treatment (Fig. 2.19 A and B). By contrast, similar to total

neuronal numbers, short-term microbiota depletion by single-dose streptomycin did not

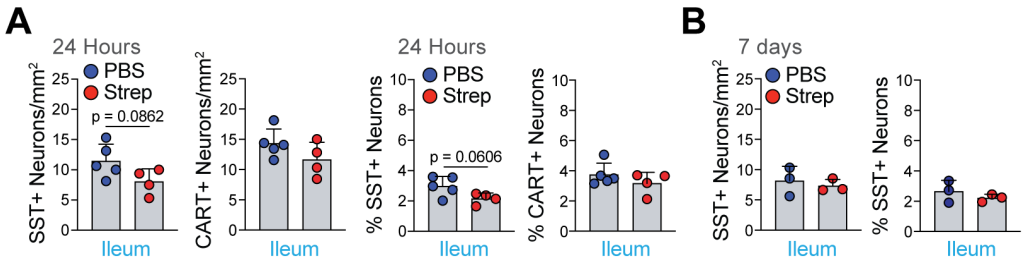


**Fig. 2.19. Alterations to neuropeptide levels in following microbial depletion.** (**A** to **D**) Number (**A** and **B**) and percentage (**C** and **D**) of CART+ (**A** and **C**) and (**B** and **D**) SST+ myenteric iEAN in duodenum, ileum and colon of C57BL/6J and *Casp11*$^{-/-}$ mice on Abx or Splenda. * $P < 0.05$, ** $P < 0.01$, *** $P < 0.001$, **** $P < 0.0001$, (A and B) two-way ANOVA with Tukey's multiple comparisons test or (C, D) Mann-Whitney test.

impact neuropeptide-specific iEAN numbers in the distal intestine (Fig. 2.20 A and B). Given that neuropeptide expression can vary with drastic changes in nutrient availability upon fasting (Fig. 2.21 A to C), we confirmed that antibiotic treatment did not result in body weight change at the time of analysis, indicating that food intake was comparable between groups (Fig. 2.21 D). Together, the above data establish that iEANs, including SST- and CART- expressing subsets, can be tuned by the microbiota.

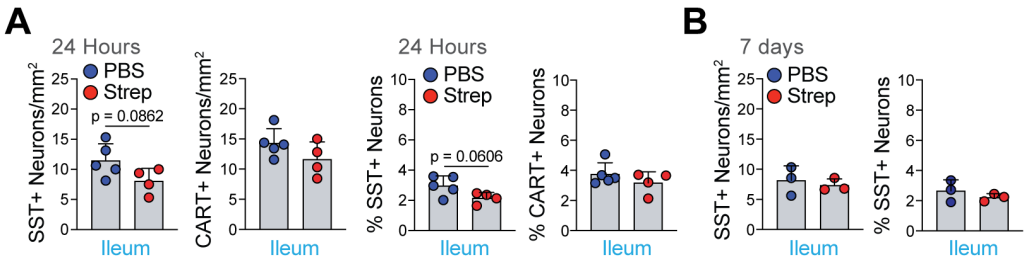


**Fig. 2.20. Acute microbial depletion does not affect SST and CART neuropeptide levels.** (**A** and **B**) Number and percentage of SST+ and CART+ (A only) iEAN of the ileum myenteric plexus of C57BL/6J SPF mice treated with a single oral gavage of PBS or streptomycin and analyzed (A) 24 hours or (B) 7 days post gavage. *P* values determined by unpaired t-test.

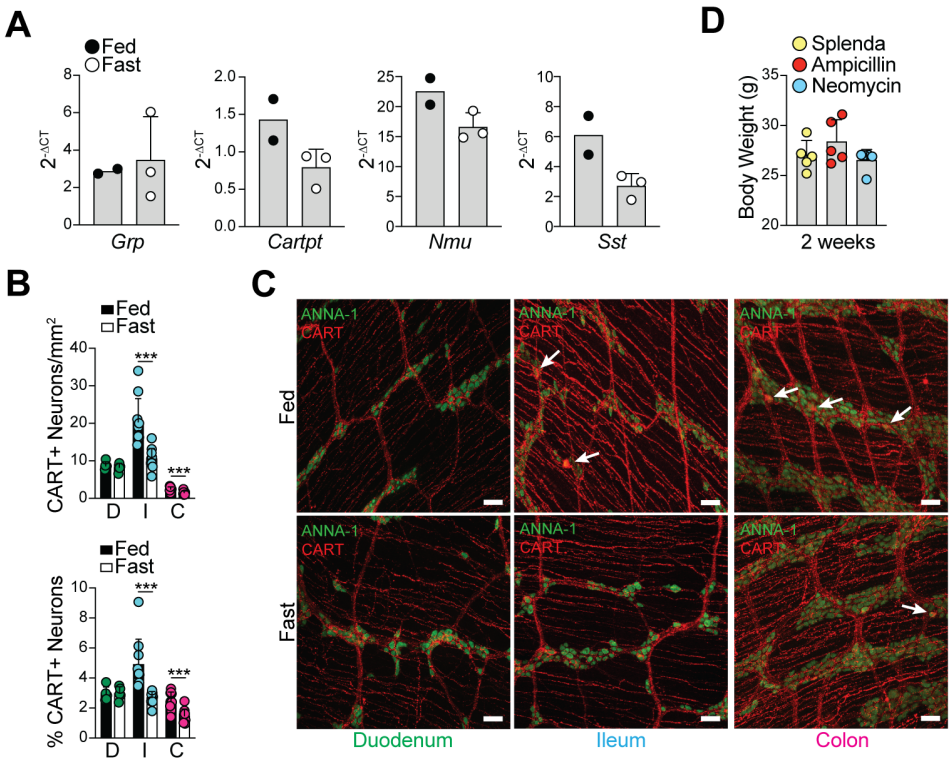


**Fig. 2.21. Effects of fasting on distal intestine iEAN neuropeptide levels.** (**A**) TRAP-qPCR analysis of the indicated neuropeptide genes of the ileum muscularis externa isolated from *Snap25*$^{RiboTag}$ mice with ad libitum food access or following overnight fasting. Data represented as log-transformed expression relative to *Rpl32*. (**B**) Number (top) and percentage (bottom) of CART+ myenteric iEAN in the duodenum (D), ileum (I), and colon (C) of C57BL/6J SPF mice with *ad libitum* food access or following overnight fasting. ** $P < 0.01$, *** $P < 0.001$, **** $P < 0.0001$ as calculated by unpaired t-test (number) or Mann-Whitney test (percentage). (**C**) Representative whole-mount IF images of the myenteric plexus quantified in (**B**). Scale bars, 50 µm. (**D**) Body weights of C57BL/6J SPF mice treated with either ampicillin, neomycin, or Splenda in the drinking water for 2 weeks.

## 2.3 Enteric pathogens cause neuronal damage and impairment in GI physiology

Enteric infections often result in functional GI disorders post-pathogen clearance, and often EANs are targeted (Balemans et al., 2017). Clinical observations indicate that between 6 and 17 % of individuals with IBS develop symptoms after episodes of enteric infections, while around 10 % of people with bacterial gastroenteritis develop IBS (Holschneider et al., 2011; Ohman and Simren, 2010). Further, HSV-1 and flavivirus strains with neuronal tropism, including West Nile and Zika virus, have also been reported to induce long-term intestinal dysmotility (White et al., 2018). The clinical presentation of post-infectious IBS includes unresolved low-grade intestinal inflammation, gastrointestinal motility impairment, and nerve damage (Beatty et al., 2014; Holschneider et al., 2011). However, the underlying mechanisms involved in infection-induced neuronal damage remain poorly understood. We thus next sought to investigate how enteric pathogen-induced inflammation affects iEANs, tissue physiology, and GI function.

### 2.3.1 Enteric infections trigger intrinsic enteric neuronal loss and dysmotility

Acute bacterial infections, including *Salmonella enterica, Shigella dysenteriae,* and *Campylobacter spp*. have previously been linked to long-term GI dysfunction classified as PI-IBS (Ohman and Simren, 2010). To characterize functional outcomes of acute intracellular bacterial infection in mice, we used an attenuated strain of *Salmonella* Typhimurium, *spiB* (Tsolis et al, 1999), which harbors a mutation in the type-III secretion system, impacting its intracellular replication. We chose to use the *spiB* strain due to the fact that wild-type (WT) *Salmonella* Typhimurium rapidly invades and damages the intestinal wall, ultimately resulting in mortality in WT C57BL/6 mice, thus interfering with our goal of studying long-term functional intestinal changes post-pathogen clearance. We observed that orally administered *spiB* was undetected in the feces by 7-10 days post-infection (dpi) (Fig. 2.22 A and B). Infection with *spiB* caused mild intestinal inflammation as evidenced by increased levels of fecal lipocalin-2 (Lcn-2), that peaked at 6 dpi, just before *spiB* clearance, but remained elevated following pathogen clearance (Fig. 2.22 C). This persistent inflammatory response was associated with lasting functional GI changes, including increased ileal ring contractility and a persistent delay in gastrointestinal transit time (GITT) (Fig. 2.22 D and E).

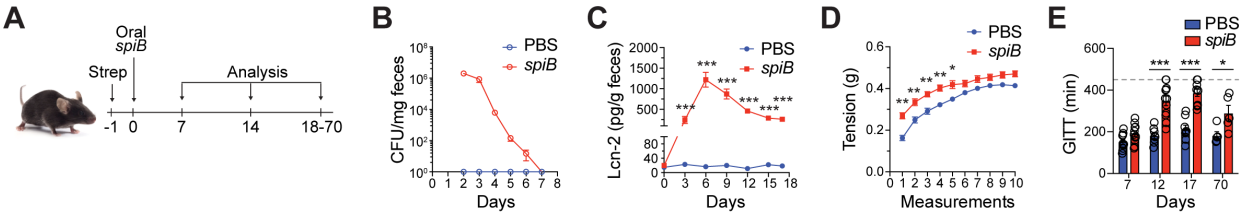


**Fig. 2.22. Enteric bacterial infection leads to intestinal inflammation and dysmotility.** (**A**) Experimental design for (**B** to **E**). (**B** to **E**) C57BL/6J mice were orally gavaged with PBS or $10^9$ colony forming units (CFU) of *Salmonella spiB*. (B) Quantification of fecal CFU. (**C**) Quantification of fecal lipocalin-2 (Lcn-2) levels as assessed by ELISA. (**D**) Ileal ring myography assessed on day 18 post-infection. (**E**) Total gastrointestinal transit time (GITT). Experiments were ended at 450 min (dashed line); * $P < 0.05$, ** $P < 0.01$, *** $P < 0.001$ as calculated by unpaired t-test or one-way ANOVA with Tukey's posthoc test.

Changes in contractility and GITT can be associated with altered neuronal activity and nerve damage (Travagli and Anselmi, 2016). In order to determine the impact of intestinal infection on iEANs, we quantified iEANs along the GI tract, in both the submucosal and myenteric plexuses. Following *spiB* infection, we observed a 20-30% reduction in myenteric neuron numbers as early as 7 dpi in the ileum and colon, both of which are major sites of *Salmonella* colonization and invasion (Fig. 2.23 A); reduced neuronal counts were observed up to 126 dpi (Fig. 2.23 B and C). In contrast, neuronal numbers were preserved in the proximal small intestine, where *Salmonella* invasion normally does not occur (Fig. 2.23 A and D). We did not observe reduction in neuronal numbers in the submucosal plexus from mice infected with *spiB*; additionally, heat-killed *spiB* did not result in neuronal loss in the myenteric plexus (Fig. 2.23 E and F).

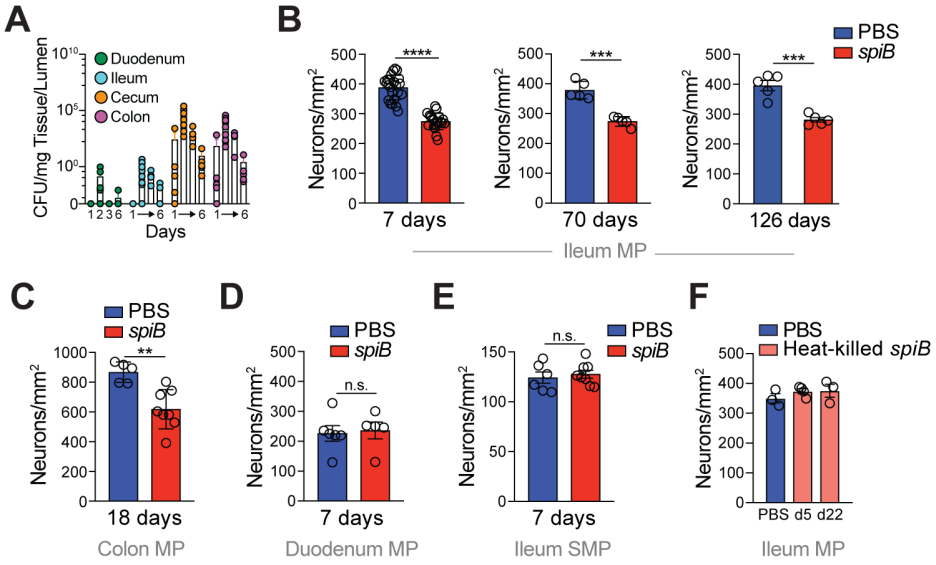


**Fig. 2.23. Enteric *Salmonella* infection leads to distal intestinal neuronal loss.** (**A** to **E**) C57BL/6J mice were orally gavaged with PBS or $10^9$ colony forming units (CFU) of *Salmonella spiB*. (**A**) Number of *spiB* CFU/tissue segment at the indicated timepoints post-gavage. (**B** to **E**) Neuronal quantification as assessed by IF staining (anti-ANNA-1) on the indicated days post-infection in the (*B*) ileum MP (**C**) colon MP, (**D**) duodenum MP, (**E**) ileum SMP. (**F**) Neuronal quantification in the ileum MP post-exposure to $10^9$ CFU of heat-killed *Salmonella spiB*. MP – Myenteric plexus; SMP – Submucosal plexus. n.s. - not significant, ** $P < 0.01$, *** $P < 0.001$, **** $P < 0.0001$ as calculated by unpaired t-test or one-way ANOVA with Tukey's posthoc test.

To determine whether the neuronal damage we found was specifically induced upon *Salmonella* infection, we turned to another bacterial enteric pathogen, *Yersinia pseudotuberculosis (Y. pseudotuberculosis, YP)*. *YP*, like *Salmonella*, is a foodborne Gram-negative bacterium that primarily localizes to the ileum (Fonseca et al., 2015), causing a transient infection undetectable in the feces by 21 dpi (Fig. 24 A). previously reported to cause long-term restructuring of gut lymphatics known as immunological scaring (Fonseca et al., 2015).Though less pronounced than what we observed with *spiB*, *YP infection also led to iEAN loss*, 2 weeks post-infection (Fig. 2.24 B). We further investigated whether we could recapitulate our findings in the context of the clinically relevant protozoan pathogens *Toxoplasma gondii* (*T. gondii*) and *Trypanosoma cruzi* (*T. cruzi*), which are known to induce various GI-related pathologies (Dutra et al., 2009; Wilhelm and Yarovinsky, 2014). These protozoans also induced intestinal inflammation,

increased ileal ring contractility, delayed GITT and significant neuronal loss (Figure 2.24 C to G and *data not shown*). By contrast, infection with the intestinal helminth *Strongyloides venezuelensis*, used as a rodent model for human *Strongyloides* infection that displays distinct duodenal tropism (Esterhazy et al., 2019), did not lead to reduced neuronal numbers in either the duodenum or distal intestine (Fig 2.24 H). These results suggest that parasites co-evolved with mammals do not induce damage in enteric neurons (Maizels et al., 2018). Together, these data indicate that iEAN loss may be a conserved feature of a many, though not all, enteric infections; we chose to continue with *spiB* as an infection model due to the inherent neurotropism of *T. gondii* and *T. cruzi*.

While it is traditionally thought that mammalian enteric neurogenesis ceases postnatally, recent studies suggest continuous turnover of iEANs, for instance by replenishment from Nestin+ stem cells (Kulkarni et al., 2017). However, in the present

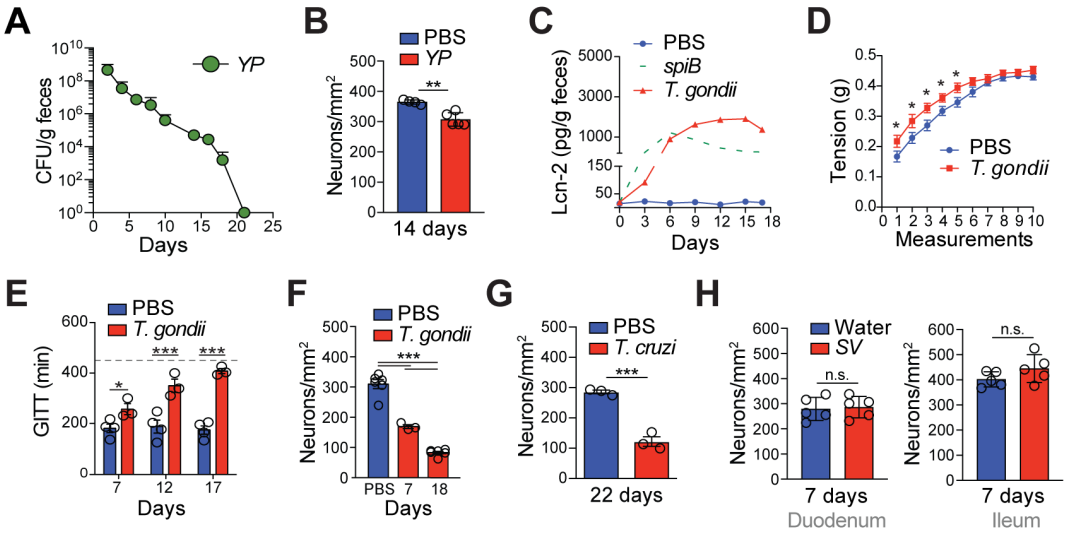


**Fig. 2.24. Infection-induced iEAN damage is pathogen-specific.** (**A** and **B**) C57BL/6J mice were orally gavaged with PBS or $10^8$ CFU of *Y. pseudotuberculosis* (*YP*). (**A**) Quantification of fecal *YP* CFU. (**B**) Neuronal quantification as assessed by IF (anti-ANNA-1) in the ileum myenteric plexus. (**C** to **F**) C57BL/6J mice were orally infected with 5 cysts of *T. gondii*. (**C**) Quantification of fecal Lcn-2 levels; (**D**) Ileal ring myography assessed on day 18 post-infection; (**E**) Total gastrointestinal transit time; experiments were ended at 450 min (dashed line); (**F**) Neuronal quantification (cuprolinic blue staining) in the ileum myenteric plexus. (**G**) Neuronal quantification (cuprolinic blue staining) in the ileum myenteric plexus on the indicated days post-infection of C57BL/6J mice with $10^4$ parasites of *T. cruzi*. (**H**) Neuronal quantification (ANNA-1 staining) in the myenteric plexus of (left) duodenal and (right) ileal segments C57BL/6J mice subcutaneously injected with 700 L3 larvae of *S. venezuelensis* (*S. ven.*). * $P<0.05$, ** $P<0.01$, *** $P<0.001$, **** $P<0.0001$ as calculated by unpaired t-test or one-way ANOVA with Tukey's posthoc test.

study, neither were we able to detect iEAN number recovery up to four months following *spiB* clearance, nor did we observe *Nestin*$^{GFP+}$ cell network changes within the myenteric plexus (Fig. 2.25 A). As an orthogonal approach, we also evaluated whether enteric glia cells or their precursors, which have been shown to replenish iEAN in response to injury (Laranjeira et al., 2011), could be involved in neuronal maintenance after *spiB* infection. Using an inducible *Sox10*$^{RiboTag}$ fate mapping strategy, we found that approximately 10 % of iEANs were HA+ four months following tamoxifen administration to adult *Sox10*$^{RiboTag}$ control mice, suggesting a glial origin of these cells (Belkind-Gerson et al., 2017).

However, we did not observe iEAN recovery nor changes in the frequency of HA+ in the ileum myenteric plexus of *Sox10*$^{RiboTag}$ mice infected with *spiB* in the same period of time (Fig. 2.25 B). These results indicate that without further manipulations, enteric neuronal loss is persistent in this model of infection. Taken together, these results demonstrate that infections with enteric bacterial and protozoan pathogens have the capacity to induce prolonged low-grade inflammation and GI dysmotility, which are associated with a rapid, self-limiting, yet persistent loss of iEANs.

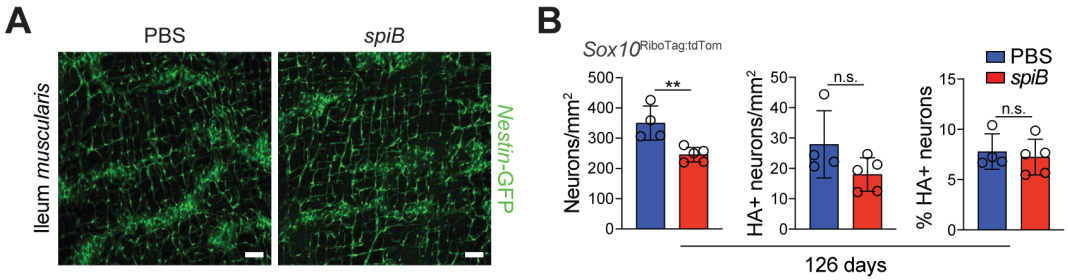


**Fig. 2.25. iEAN precursor populations are unaffected by *Salmonella spiB* infection.** (**A** and **B**) Mice were orally gavaged with PBS or $10^9$ CFU *Salmonella spiB*. (**A**) Representative confocal IF images of ileum muscularis from *Nestin*-GFP mice on day 7 post-infection. Scale bars, 50 $\mu$m. (**B**) Neuronal quantification and reporter overlap as assessed by IF staining (ANNA-1, HA) in the ileum myenteric plexus from tamoxifen-treated *Sox10*$^{RiboTag:tdTomato}$ mice. n.s. - not significant, ** $P < 0.01$ as calculated by unpaired t-test.

### 2.3.2 Re-introduction of a normal microbiota induces neuronal recovery

Human post-infectious IBS generally leads to long-term, yet reversible GI symptoms and neuropathy (Beatty et al., 2014; Ohman and Simren, 2010). However, in the *spiB* model of infection, we did not observe recovery of neurons after a single pathogenic infection. Because of reported effects of the microbiota on the development (Carabotti et al., 2015; Obata and Pachnis, 2016) and maintenance (Chapter 2.2) of enteric neurons, we assessed whether persistent changes in microbial composition (dysbiosis) could explain the lack of recovery of iEANs post-infection. We infected SPF mice with *spiB* and administered a cocktail of broad-spectrum antibiotics after bacterial

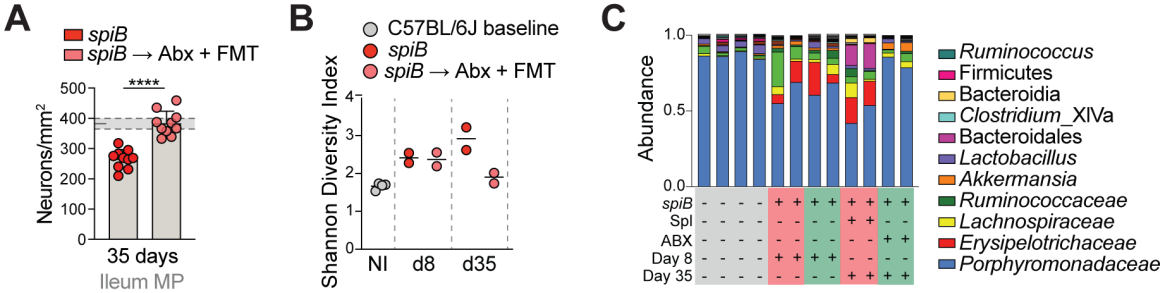


**Fig. 2.26. Re-introduction of a normal microbiota post-infection leads to iEAN recovery.** (**A**) Neuronal quantification in the ileum myenteric plexus of C57BL/6J mice reconstituted with a normal microbiota or not after *spiB* infection. **** $P < 0.0001$ as calculated by unpaired t-test (**B**) Shannon diversity index of 16S sequencing from feces obtained from n=2 mice in representative groups in (**A**). (**C**) Top 11 most abundant genera from 16S sequencing of feces obtained from mice in representative groups in (**A**). Abx, broad-spectrum antibiotics; FMT, fecal microbiota transfer.

clearance, and subsequently re-colonized the animals with “normal” microbiota from naïve SPF mice. This reconstitution of a “normal” or pre-infection microbiota allowed for iEAN recovery (Figure 2.26 A), which correlated with a reduction in a member of the *Erysipelotrichaceae* family and Bacteriodales order when compared to untreated-infected mice (Figure 2.26 B and C). These data point to a role for the gut microbiota in the recovery of iEANs post-in fection.

### 2.3.3 Enteric infection-induced neuronal loss is subtype-specific

iEANs comprise a numerous and heterogeneous population of neurons that monitor and respond to various environmental cues, including mechanical stretch and luminal metabolites (Furness et al., 2013; Mayer, 2011). We first asked whether the observed iEAN loss could be explained by a decrease of ELAVL3/4 protein expression. To address this question, we utilized the RiboTag mouse line, described in Chapter 2.1, in which pan-neuronal Cre (*Snap25*$^{Cre}$) reporter mice express a HA-tagged ribosomal subunit 22. IF analysis of HA+ cells in the myenteric plexus confirmed the significant loss of iEANs as initially determined by pan-neuronal ANNA-1 staining (Fig. 2.27 A and B).

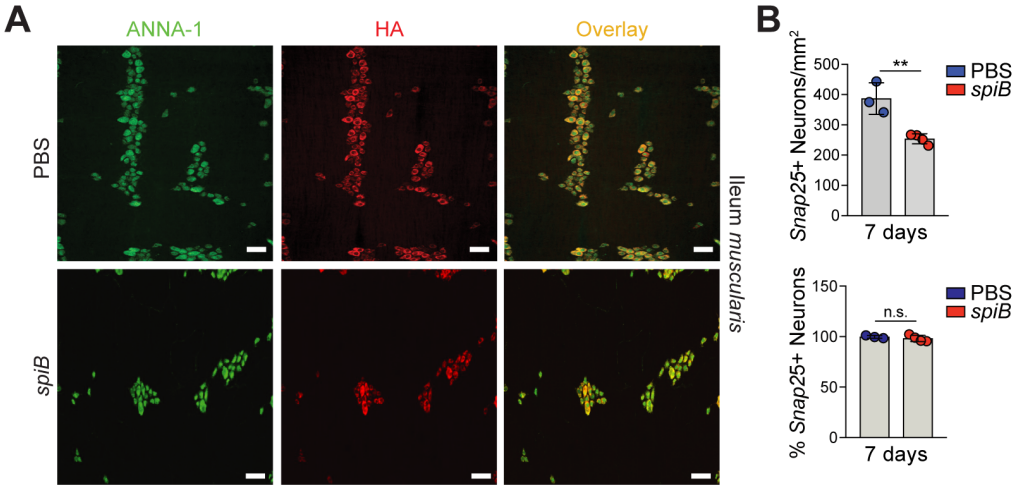


**Fig. 2.27. Reduced iEAN detection post-*spiB* infection is not due to reduction in neuronal-specific protein expression.** (**A** and **B**) *Snap25*$^{RiboTag}$ mice were orally gavaged with PBS or $10^9$ CFU *Salmonella spiB*. (**A**) Representative confocal IF images of the ileum myenteric plexus stained with anti-ANNA-1 (red) and anti-HA (green). Scale bars, 50 $\mu$m. (**B**) Quantification of (top) total number and (bottom) percent HA+ neurons. n.s. - not significant, ** $P < 0.01$ as calculated by unpaired t-test.

It has been reported that in cases of overt intestinal inflammation, such as colitis, there is indiscriminate loss of iEANs (Mawe, 2015). To investigate whether specific neuronal subsets were preferentially lost after enteric infection, we used confocal IF imaging to evaluate the impact on excitatory and inhibitory neuronal cell populations (Zeisel et al., 2018). Imaging of the ileum myenteric plexus from infected and uninfected *Slc17a6*$^{td\text{-}Tomato}$ (VGLUT2) reporter mice revealed a significant reduction in total number and percentage of excitatory VGLUT2+ neurons (Fig. 2.28 A and B).

In contrast, quantification of inhibitory NOS+ and somatostatin (SST)+ iEAN populations revealed no changes (nNOS), and a subtle relative increase (SST) of these

subtypes post infection (Figs. 2.29 and 2.30). These data suggest a preferential loss of excitatory neuronal subsets post-infection, resulting in changes in the neurochemical representation of iEANs, and may provide an explanation for functional changes in GI motility observed after infection.

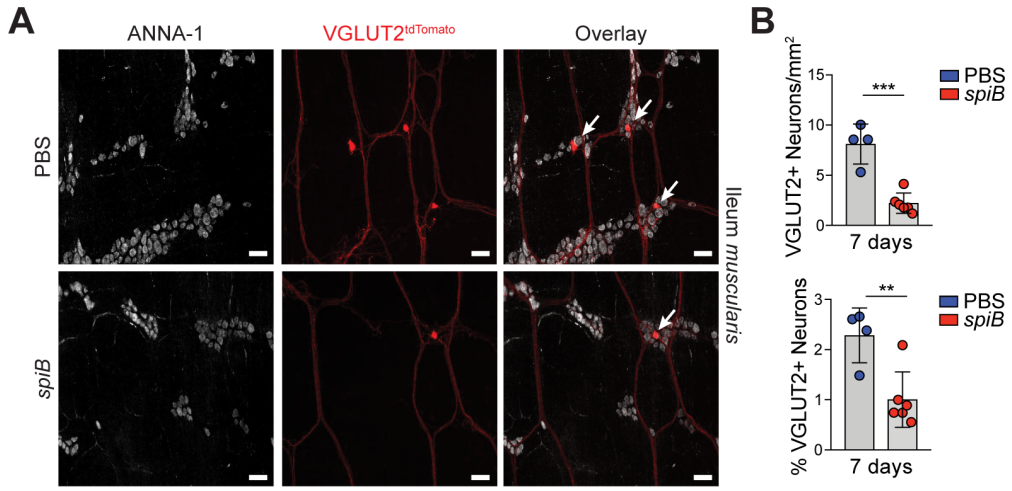


**Fig. 2.28. *Salmonella spiB* infection leads to a loss in excitatory VGLUT2+ iEANs**. (A and B) VGLUT2$^{td\text{-}Tomato}$ mice were orally gavaged with PBS or $10^9$ CFU *Salmonella spiB*. (A) Representative confocal IF images of the ileum myenteric plexus stained with anti-ANNA-1 (grey). Scale bars, 50 $\mu$m. (B) Quantification of the number of VGLUT2+ neurons per mm$^2$ and as a percentage of ANNA-1+ neurons. ** $P < 0.01$, *** $P < 0.001$ as calculated by unpaired t-test.

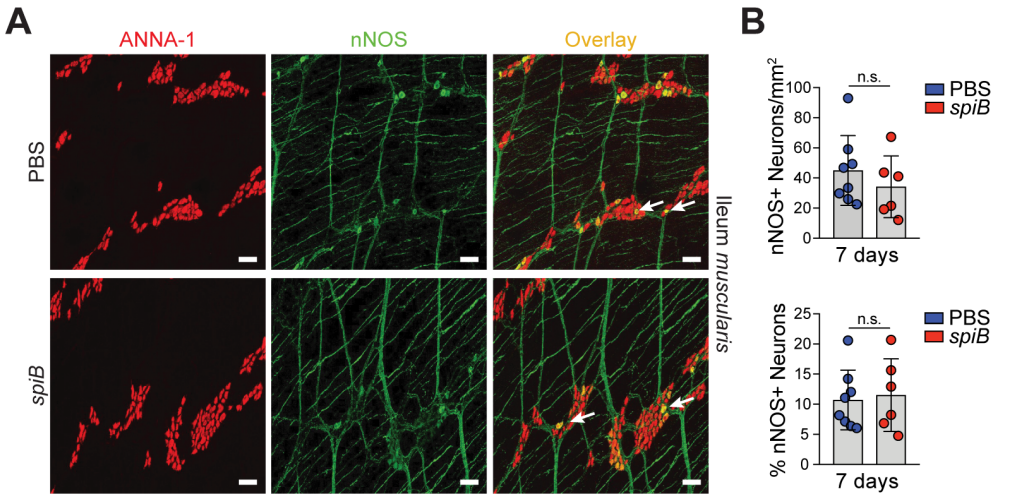


**Fig. 2.29. *Salmonella spiB* infection does not alter nNOS+ iEAN numbers.** (**A** and **B**) C57BL/6J mice were orally gavaged with PBS or $10^9$ CFU *Salmonella spiB*. (**A**) Representative confocal IF images of the ileum myenteric plexus stained with anti-nNOS (green) and anti-ANNA-1 (red). White arrows, examples of nNOS+ neurons. Scale bars, 50 $\mu$m. (**B**) Quantification of the number of nNOS+ neurons per mm$^2$ and as a percentage of ANNA-1+ neurons. n.s. - not significant, as determined by unpaired t-test.

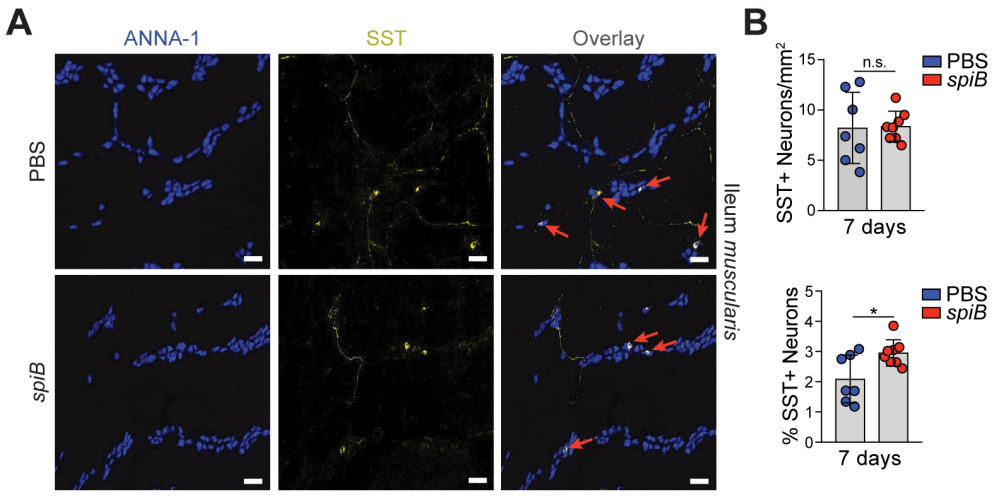


**Fig. 2.30. *Salmonella spiB* infection does not lead to a loss of SST+ iEANs.** (**A** and **B**) C57BL/6J mice were orally gavaged with PBS or $10^9$ CFU *Salmonella spiB*. (**A**) Representative confocal IF images of the ileum myenteric plexus stained with anti-SST (green) and anti-ANNA-1 (red). Red arrows, examples of SST+ neurons. Scale bars, 50 $\mu$m. (**B**) Quantification of the number of SST+ neurons per mm$^2$ and as a percentage of ANNA-1+ neurons. n.s. - not significant, * $P < 0.05$ as determined by unpaired t-test.

## 2.4 Damage to the ENS leads to a novel mechanism of iEAN cell death

Because we found a reduction in intrinsic enteric neurons both in mice devoid of or with a drastically reduced gut microbiota, i.e., in gnotobiotic animals and upon antibiotic-mediated depletion, as well as post-infection, we next aimed to determine the underlying mechanism(s) of enteric neuronal loss in these settings.

### 2.4.1 iEANs possess the machinery to die in an inflammasome-dependent manner

To gain insight into a possible mechanism involved in infection-induced iEAN loss, we first performed translating ribosomal affinity purification (TRAP) using *Snap25*$^{\text{RiboTag}}$ mice, allowing neuronal-specific immunoprecipitation of actively translated mRNA (Chapter 2.1). We compared iEANs with eEANs in the NG of *Snap25*$^{\text{RiboTag}}$ mice; expression of HA-tagged ribosomes was determined in neurons of the myenteric plexus (Fig. 2.27 above) and NG of *Snap25*$^{\text{RiboTag}}$ mice (Fig. 2.31 A). RNA seq analysis of immunoprecipitated intact mRNA bound to HA-tagged ribosomes (TRAP-seq) revealed an iEAN-specific enrichment of genes encoding neuropeptides, such as *Nmu*, as well as components of the inflammasome pathway including *Nlrp6*, *Pycard*, *Casp1*, and *Casp11* (Fig. 2.31 B). These data indicate that iEANs possess the machinery for engaging an inflammasome- and caspase (Casp) 1/11-mediated cell death.

Imaging analyses for the expression of the inflammasome adaptor ASC (PYCARD) using anti-ASC antibody in WT mice or the endogenous fluorescence of *Rosa26*$^{\text{ASC:mCitrine}}$ (ASC$^{\text{mCitrine}}$) mice confirmed the expression of this inflammasome component by iEANs of the ileum of both naïve and *spiB*-infected mice (Fig. 2.31 C and D). To visualize the pattern of *Nlrp6* expression by iEAN, we performed fluorescence *in situ* hybridization (FISH) on ileum and colon sections using RNAscope® probes specific to *Elavl4* (pan-neuronal) and *Nlrp6*. We observed dense localization of *Nlrp6* transcripts in the epithelium of both the ileum and colon, similar to what has previously been reported (Levy et al., 2015). In addition, we visualized *Nlrp6* transcripts in areas of *Elavl4*-expressing cells in the *muscularis* layer, supporting the expression of NLRP6 by myenteric neurons (Fig. 2.31 E). Analysis of data from single-cell transcriptional profiling of iEANs (Zeisel et al., 2018) indicated that *Nlrp6* is highly enriched in excitatory iEANs compared with additional iEAN subsets (Fig. 2.31 F). These results may explain the preferential targeting of excitatory iEAN subsets during enteric infections.

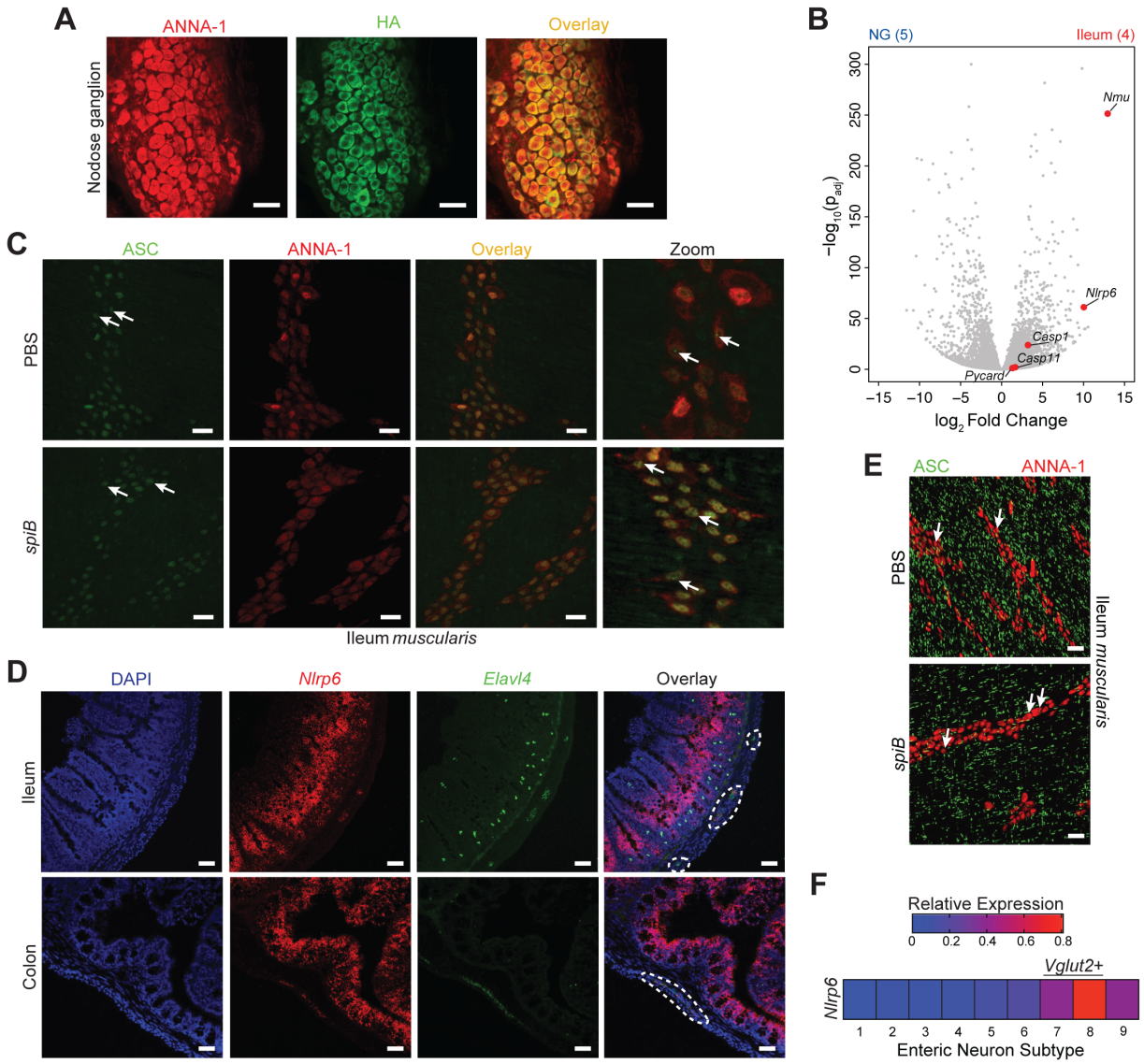


**Fig. 2.31. Translational profiling reveals expression of inflammasome components by iEANs.** (**A**) Representative confocal immunofluorescence (IF) images of nodose ganglia (NG) from *Snap25*$^{RiboTag}$ mice stained with anti-ANNA-1 (red) and anti-HA (green). Scale bars, 50 $\mu$m. (**B**) Volcano plot of differentially-expressed genes (DEGs) of TRAP-seq from NG and ileum myenteric EAN isolated from *Snap25*$^{RiboTag}$ mice. Grey dots, all DEGs; red dots, DEGs of interest significantly differentially expressed in ileum iEAN. Sample numbers indicated in parentheses. (**C**) Representative IF images of the ileum myenteric plexus from C57BL/6J mice using anti-ANNA-1 (red) and anti-PYCARD (ASC, green). Samples obtained 6 hours post-oral gavage of PBS or $10^9$ CFU of *Salmonella spiB*. Arrows indicate ASC "specks". Scale bars, 25 $\mu$m. (**D**) RNAScope® fluorescence in situ hybridization with probes for *Nlrp6* and *Elavl4* (pan-neuronal) in the ileum and colon from C57BL6/J mice. iEAN outlined with dashed line. Scale bars, 50 $\mu$m. (**E**) Representative IF images of ileum myenteric plexus from ASC$^{mCitrine}$ mice using anti-ANNA-1 (red) antibody and native mCitrine fluorescence. Samples obtained 5 days post-oral gavage of PBS or $10^9$ CFU of *Salmonella spiB*. Arrows indicate ASC "specks" within neurons. Scale bars, 50 $\mu$m. (**F**) Heatmap representation of the relative expression of *Nlrp6* in iEAN subsets as defined by single-cell analysis from the published dataset mousebrain.org/genesearch.html (Zeisel et al., 2018). Vglut2+ subsets as defined by the same analysis are highlighted.

### 2.4.2 Infection-induced iEAN loss is dependent on *Nlrp6* and *Caspase 11*

To evaluate the role of caspase-mediated cell death in iEAN loss during infection, we first systemically administered a pan-caspase inhibitor (zVAD-FMK) to mice infected with *spiB*, which reduced infection-induced iEAN loss (Fig. 2.32 A). We directly addressed the role of Casp1 and 11 in infection-induced iEAN loss by infecting *Casp1/11* (ICE)-deficient or haplosufficient ($ICE^{+/-}$) mice (Kuida et al., 1995) with *spiB*. While $ICE^{+/-}$ mice exhibited pronounced iEAN loss in the ileal myenteric plexus 7 dpi, *spiB*-infected $ICE^{-/-}$ mice were completely protected from neuronal loss, despite similar bacterial clearance patterns (Fig. 2.32 B and C, and Appendix 2). Infection with *spiB* also did not result in iEAN loss in single *Casp11*-deficient mice (Fig. 2.32 D). We further dissected the specific role Casp1 and 11 in neuronal cell death by utilizing the 129S1/Sv mouse strain, which carries an inactivating mutation in the *Casp11* locus (human *Casp4*) (Kenneth et al., 2012; Vanden Berghe et al., 2015). 129 mice infected with *spiB* exhibited no loss of colonic iEAN numbers as compared to non-infected controls (Fig. 2.32 E to J). This iEAN protection was independent of the ability of 129 mice to survive WT *Salmonella* infection due to expression of functional *Nramp* (Brown et al., 2013), as we found that CBA/J mice, which also express functional *Nramp*, but do not carry a *Casp11* mutation, exhibited significant neuronal loss when infected with *spiB,* despite similar clearance of the bacteria (Fig. 2.32 E to J, and *data not shown*). These data suggest a Casp11-mediated cell death as a main mechanism involved in iEAN loss following *Salmonella* infection.

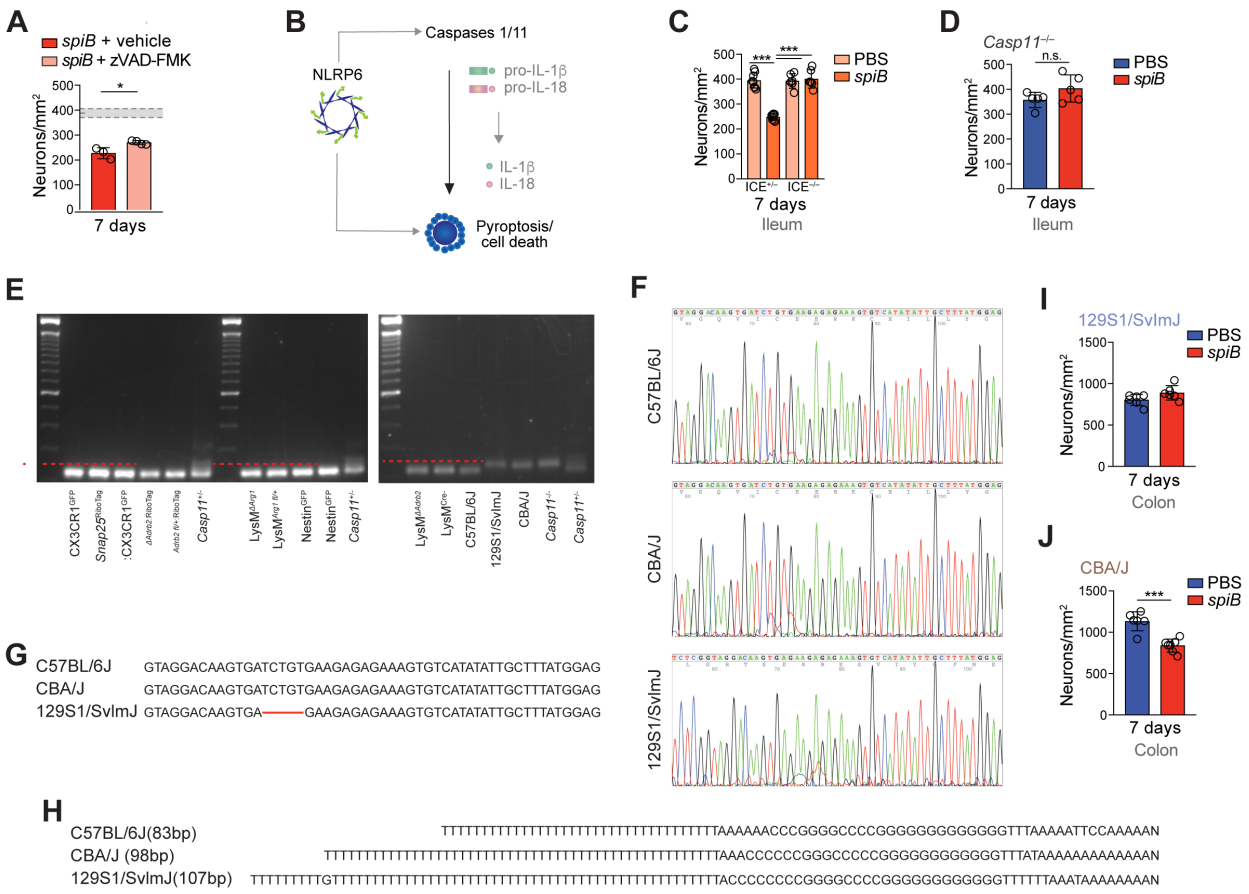


**Fig. 2.32. Components of the inflammasome machinery are necessary for iEAN loss post-infection.** (**A**) Neuronal quantification (ANNA-1 staining) in the ileum myenteric plexus on day 7 post-*spiB* infection of C57BL/6J mice receiving vehicle (dimethyl sulfoxide, DMSO) or zVAD-FMK (150 μg/day) delivered i.p. over the course of infection. Shaded area bounded by dashed lines indicates mean day 7 iEAN numbers +/- SEM of all control C57BL6/J mice analyzed in Fig. 2.23. B. (**B**) Scheme of the NLRP6 inflammasome pathway. (**C** and **D**) Neuronal quantification (ANNA-1) in the ileum myenteric plexus on day 7 post-gavage of PBS or *spiB* of (**C**) *Casp1-/- Casp11-/-* (ICE-/-) mice or controls (ICE+/-) and (**D**) *Casp11-/-* mice. (**E**) 3% agarose gel for *Casp11* 5bp deletion PCR product. Mouse strains used in this work are indicated below each lane. Red dashed line indicates the size at which a potential 5bp deletion PCR product will run; (**F**) Sanger sequencing of *Casp11* 5bp deletion PCR product in C57BL/6J, CBA/J, and 129S1/SvImJ mice; (**G**) Sequence surrounding *Casp11* 5bp deletion region in C57BL/6J, CBA/J, and 129S1/SvImJ mice. Red line indicates 5bp deletion in 129S1/SvImJ mice; (**H**) Comparison of intron sequence lengths obtained from *Casp11* 5bp deletion PCR product in C57BL/6J, CBA/J, and 129S1/SvImJ mice.(**I** and **J**) Neuronal quantification (ANNA-1) in the colon myenteric plexus on day 7 post-*spiB* infection of (**I**) 129S1/SvImJ mice and (**J**) CBA/J mice. * $P < 0.05$, ** $P < 0.01$ as calculated by unpaired t-test.

To define whether the NLRP6 inflammasome and Casp11-mediated mechanisms proposed above were neuron cell-intrinsic, we used two *in vivo* approaches of neuronal-specific gene deletion. Intravenous (i.v.) injection of AAV9 can target peripheral neurons, including iEANs, particularly upon the insertion of the neuronal-specific promoter hSyn (Gombash et al., 2014) (Kugler et al., 2003). Imaging analysis indicated that this strategy led to efficient viral targeting of iEANs (Fig. 2.33 A and B). To remove *Casp11* from iEAN, we i.v.-injected *Casp11*$^{flox/flox}$ mice with AAV9-hSyn-HI-eGFP-Cre-WPRE-SV40, which

results in nuclear eGFP-Cre expression; AAV9-hSyn-eGFP-WPRE-bGH, which leads to eGFP expression mostly in the neuronal processes, was used as a control virus (Fig. 2.33

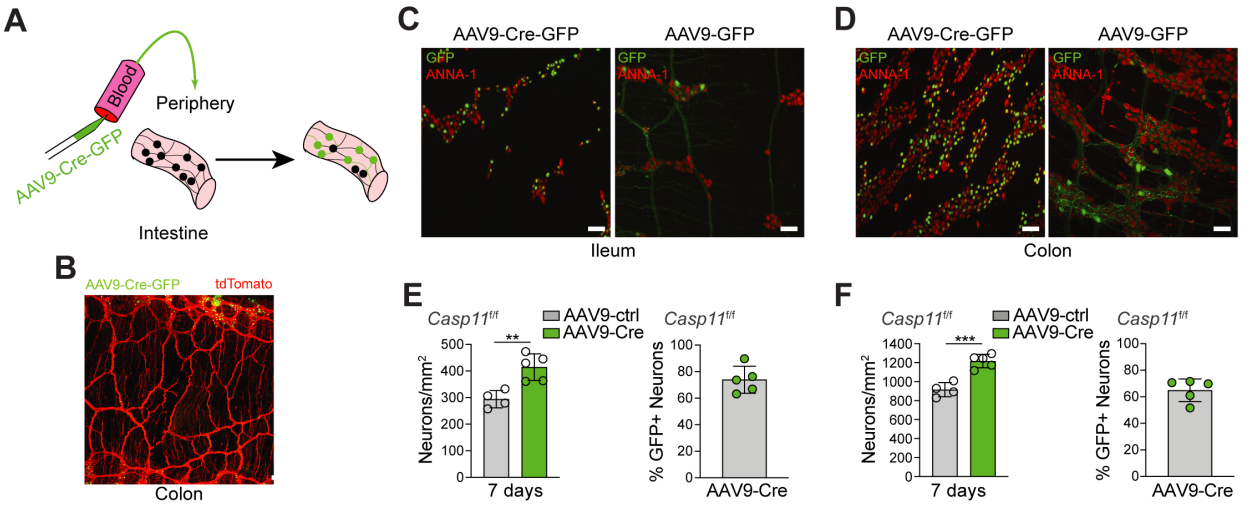


**Fig. 2.33. iEAN loss post-infection is dependent on iEAN-intrinsic *Casp11* expression.** (**A**) Scheme of i.v. AAV9–mediated transduction of peripheral neurons. (**B**) Representative confocal IF image of the colon muscularis of Rosa26lsl-tdTomato mice i.v. injected with AAV9-hSyn-Cre-GFP virus. Scale bar, 50 $\mu$m. (**C** and **D**) Representative confocal IF images of ileum (**C**) and colon (**D**) myenteric plexus of *Casp11*$^{flox/flox}$ mice given i.v. injection of AAV9-hSyn-Cre-GFP or control virus, stained with anti-ANNA-1 (red) antibodies. (**E** and **F**) (left) Neuronal quantification in the ileum (**E**) and colon (**F**) myenteric plexus from iEAN$^{\Delta Casp11}$ or *Casp11*$^{flox/flox}$ mice on day 7 post-spiB infection. (**E** and **F**) (right) Quantification of Cre-GFP transduced cells in the ileum myenteric plexus of iEAN$^{\Delta Casp11}$ mice. ** $P < 0.01$, *** $P < 0.001$ as calculated by unpaired t-test.

A, C and D). We detected Cre-expressing AAV9 in 60-90 % of myenteric iEAN of the ileum and colon (Fig. 3.33 C to F). Upon infection with *spiB,* we observed no neuronal loss in mice injected with Cre-expressing AAV9 as compared to mice injected with control virus (Fig. 2.33 E and F), suggesting that neuronal-intrinsic *Casp11* expression is required for *Salmonella*-induced iEAN loss.

To address whether neuronal-specific *Nlrp6* expression was also involved in post-infectious EAN loss, we crossed pan-neuronal *Snap25*$^{RiboTag}$ mice with a strain carrying a floxed *Nlrp6* locus (*Nlrp6*$^{flox/flox}$) (Fig. 2.34 A). We infected *Snap25*$^{\Delta Nlrp6}$, *Snap25*$^{RiboTag}$x*Nlrp6*$^{flox/+}$ heterozygous and (*Cre*-) *Nlrp6*$^{flox/flox}$ control mice with *spiB* and quantified iEAN numbers post-infection. While both heterozygous and *Cre*- controls

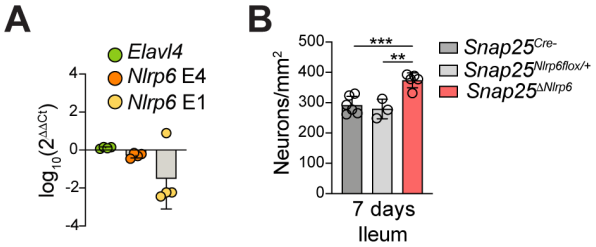


**Fig. 2.34. iEAN loss post-infection is dependent on neuronal-intrinsic *Nlrp6* expression.** (**A**) Log transformed relative expression to *Rpl32* of TRAP-qPCR data of *Elavl4* and *Nlrp6* from *Snap25*$^{\Delta Nlrp6:RiboTag}$ and *Snap25*$^{Nlrp6flox/+:RiboTag}$ mice (**B**) Ileum myenteric iEAN number from *Snap25*$^{Cre-}$, *Snap25*$^{Nlrp6flox/+}$ or *Snap25*$^{\Delta Nlrp6}$ mice on day 7 post-spiB infection. ** $P < 0.01$, *** $P < 0.001$ as calculated by one-way ANOVA with Tukey's posthoc test.

showed reduced iEAN numbers upon *spiB* infection, *Snap25*$^{\Delta Nlrp6}$ did not display EAN loss (Fig. 2.34 B). Together, the above data implicate neuronal-cell intrinsic *Nlrp6* and *Casp11* as main effectors involved in iEAN loss following *Salmonella* infection.

### 2.4.3 Neuronal loss post-microbial depletion is dependent on *Nlrp6* and *Casp11*

To evaluate whether the iEAN reduction we observed post-microbiota depletion (Chapter 2.2.3. above) also engaged neuronal *Nlrp6* and *Casp11*, we first treated *Casp1-/-Casp11-/- (ICE-/-)* and *Casp11-/-* mice with broad-spectrum antibiotics in the drinking water, analogous to C57BL/6 mice (Chapter 2.2.3, Fig. 2.17 A). Quantification of iEANs

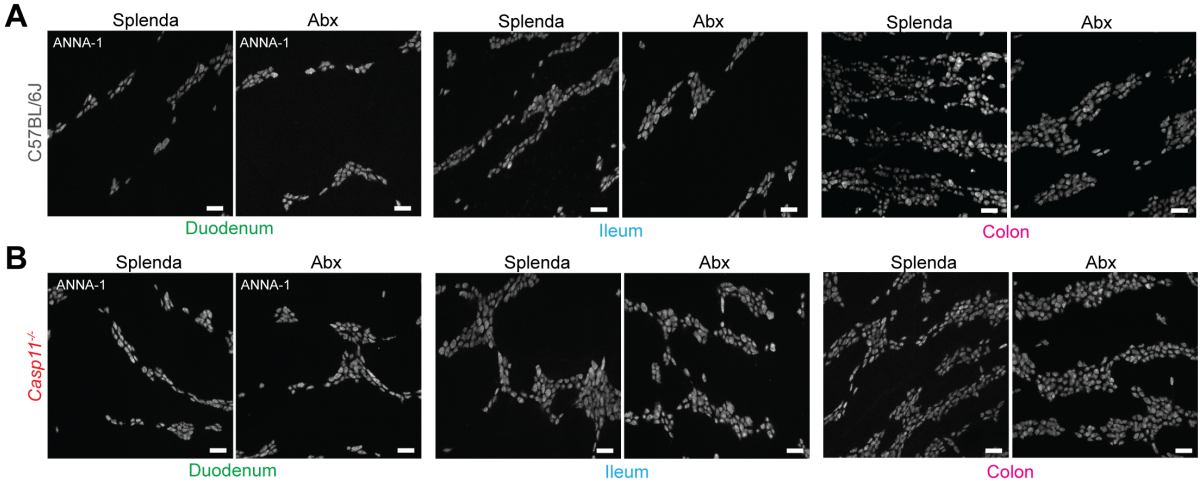


**Fig. 2.35. *Casp11* is necessary for iEAN loss after microbial depletion.** (**A** and **B**) Representative confocal IF images of myenteric iEAN (stained with anti-ANNA-1) in the duodenum, ileum, and colon of (**A**) C57BL/6J and (**B**) *Casp11-/-* mice treated with antibiotics or sucralose-based artificial sweetener (Splenda®) for two weeks. Images representative of n=5 per condition. Scale bars, 50 µm.

in the ileum of antibiotic-treated mice revealed no iEAN loss in *ICE*$^{-/-}$ or *Casp11*$^{-/-}$, mice, suggesting an additional role for Casp11 in the reduction of iEANs during dysbiosis (Figs. 2.17 A and Fig. 2.35 A to B). We confirmed that these changes in neuronal numbers were

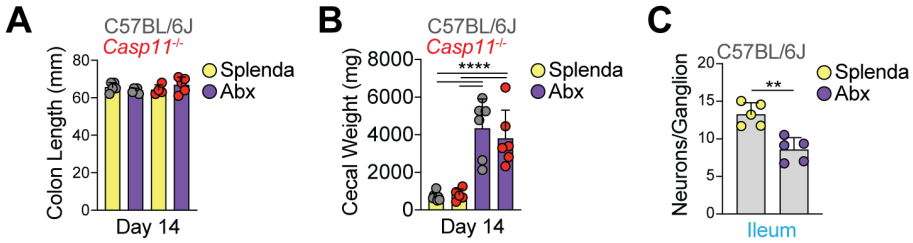


**Fig. 2.36. Reduced iEAN detection post-microbial depletion is not due to tissue distention or edema.** (**A** and **B**) Measurements of (**A**) colonic length and (**B**) cecal weight of C57BL/6J and *Casp11-/-* mice treated with either Splenda or broad-spectrum antibiotics (Abx - vancomycin, ampicillin, metronidazole and neomycin) in the drinking water for 2 weeks. **** $P < 0.0001$ as calculated by two-way ANOVA with Tukey's multiple comparisons test. (**C**) Number of iEAN per ganglion of the ileum myenteric plexus of C57BL/6J SPF mice receiving either antibiotics or Splenda in the drinking water for 2 weeks. ** $P < 0.01$ as calculated by two-tailed unpaired t-test.

not the effect of morphological differences in the intestine induced by antibiotics or genotype (Fig. 2.36 A to C).

Finally, neuronal/neuroendocrine-specific deletion of *Nlpr6* and *Casp11* prevented loss of iEANs otherwise found upon antibiotic administration (Fig 2.37 A and B). Furthermore, continuous broad-spectrum antibiotic-treatment of *ICE*$^{-/-}$, *Casp11*$^{-/-}$,

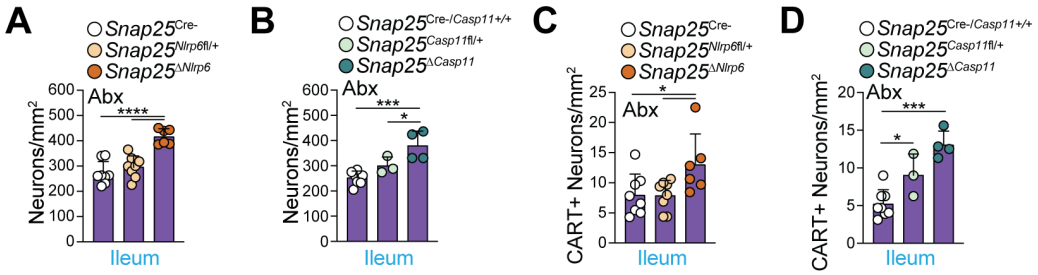


**Fig. 2.37. iEAN loss post-microbial depletion is dependent on neuronal-intrinsic *Nlrp6* and *Casp11*.** (**A** and **B**) Ileal myenteric iEAN number of control or (**A**) *Snap25*$^{\Delta Nlrp6}$ or (B) *Snap25*$^{\Delta Casp11}$ mice on antibiotics (Abx - vancomycin, ampicillin, metronidazole and neomycin). (C, D) CART+ ileal myenteric iEAN numbers of (C) *Snap25*$^{\Delta Nlrp6}$, (D) *Snap25*$^{\Delta Casp11}$ or control mice on Abx. * $P < 0.05$, ** $P < 0.01$, **** $P < 0.0001$, one-way ANOVA with Tukey's multiple comparisons test.

*Snap25*$^{\Delta Nlrp6}$, and *Snap25*$^{\Delta Casp11}$ mice did not impact neuropeptide-specific iEAN numbers in the ileum and colon (Figs. 2.19 A and C, and 2.37 C and D). Together, these analyses define a role for the non-canonical inflammasome sensor, NLRP6, and its downstream effector, Casp11 in microbiota-mediated iEAN regulation.

## 2.5 Microbiota-modulated CART+ enteric neurons autonomously regulate blood glucose metabolism

Our findings described in Chapters 2.1 and 2.2 above established both regional differences in and microbial influence on neuropeptidergic coding of iEANs. However, the functional roles of and microbial influence on different neuropeptide-expressing iEAN subsets are as of yet poorly understood. We thus next aimed to functionally characterize iEAN subsets that express specific neuropeptides and are modulated by the gut microbiota.

### 2.5.1 Microbiota-modulated CART+ intrinsic enteric neurons are viscerofugal and glucoregulatory

To test possible functional roles for microbiota-modulated iEANs in GI physiology, we focused on CART+, NPY+, and AgRP+ neuronal populations because of their distinct features: CART+ iEANs are enriched in the ileum and colon, bidirectionally modulated by the microbiota, and unlike SST, CART is not expressed by EECs in these gut regions (Gunawardene et al., 2011). Meanwhile, AgRP+ iEANs are particularly enriched in the colon and reduced in GF mice, and NPY+ neurons are enriched in the duodenum and not affected by the microbiota. These three neuropeptides are also expressed by neuronal populations in the hypothalamus that work in concert to regulate energy balance (Waterson and Horvath, 2015), and as such, could potentially play a similar role in gut-

specific circuits to influence feeding behavior. Whole-mount analysis of intestinal muscularis externa using RNA *in-situ* hybridization confirmed the expression of *Npy* and *Cartpt* in the ileum and colon, and *Agrp* in the mid-colon (Fig. 2.38 A to C).

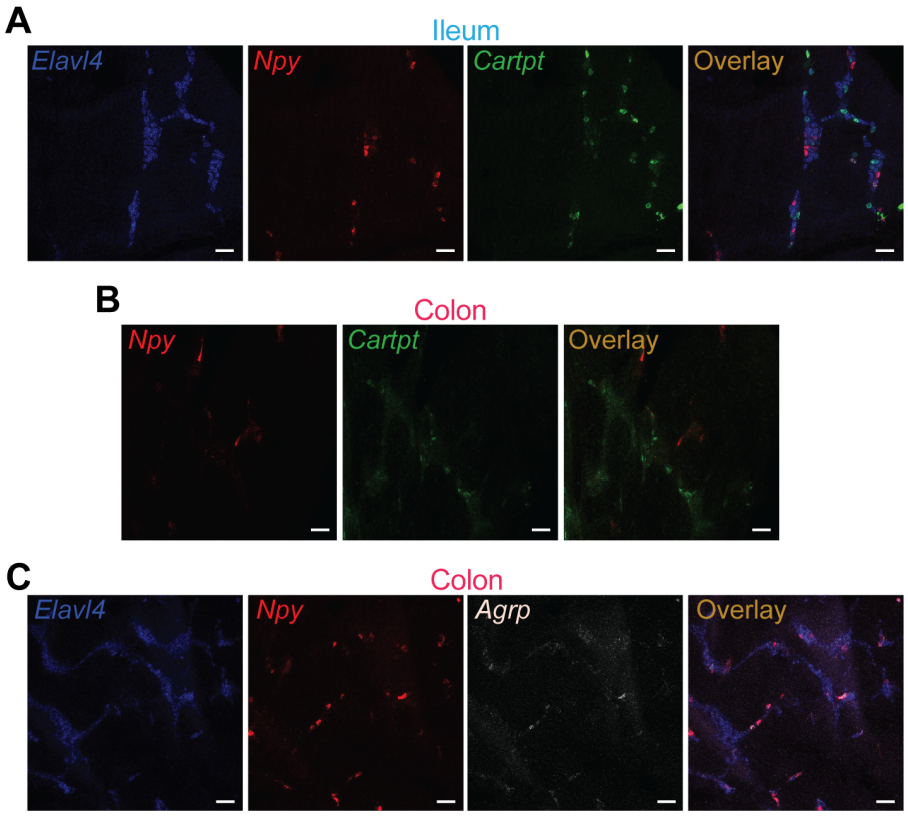


**Fig. 2.38. Characterization of iEAN neuropeptides by *in situ* hybridisation.** (**A** to **C**) RNAscope *in situ* hybridization whole-mount IF images of the indicated intestinal segments from C57BL/6J SPF mice using probes for (**A** and **B**) *Elavl4*, *Npy*, and *Cartpt* in the (**A**) ileum and (**B**) colon or *Elavl4*, *Npy*, and *Agrp* in the colon (C). Scale bars, 50 µm.

We obtained *Cre* lines corresponding to the three neuropeptides and validated *Cre*, *Cartpt, Npy,* and *Agrp* expression in the periphery using *in situ* hybridization (Fig. 2.39 A to D). Because these neuropeptides are known to be expressed both in the periphery (Furlan et al., 2016; Gupta et al., 2017; Shcherbina et al., 2017; Teitelman et al., 1993; Yuan et al., 2016) and CNS (Waterson and Horvath, 2015), we used a local retrograde viral delivery approach (Benskey et al., 2015) into the duodenum, ileum, and colon to guide us on further gut-restricted adeno-associated virus (AAV) approaches (Benskey et al., 2015) and to reveal the morphology of these myenteric neuronal populations. Injection of retrograde AAV (AAVrg)-FLEX-tdTomato (Benskey et al., 2015) into the different gut segments of *Cartpt*$^{Cre}$ (Milstein et al., 2015), *Npy*$^{Cre}$ (Milstein et al., 2015), and *Agrp*$^{Cre}$ (Tong et al., 2008) mice (generating *Cartpt*$^{EAN\text{-}tdTomato}$, *Npy*$^{EAN\text{-}tdTomato}$, and *Agrp*$^{EAN\text{-}tdTomato}$, respectively) revealed a prominent population of tdTomato+ neurons in the duodenum, ileum, and colon myenteric plexus of *Cartpt*$^{EAN\text{-}tdTomato}$ and *Npy*$^{EAN\text{-}tdTomato}$ mice (Fig. 2.40 A and B). *Npy*$^{EAN\text{-}tdTomato}$ and *Cartpt*$^{EAN\text{-}tdTomato}$ neurons displayed considerable innervation

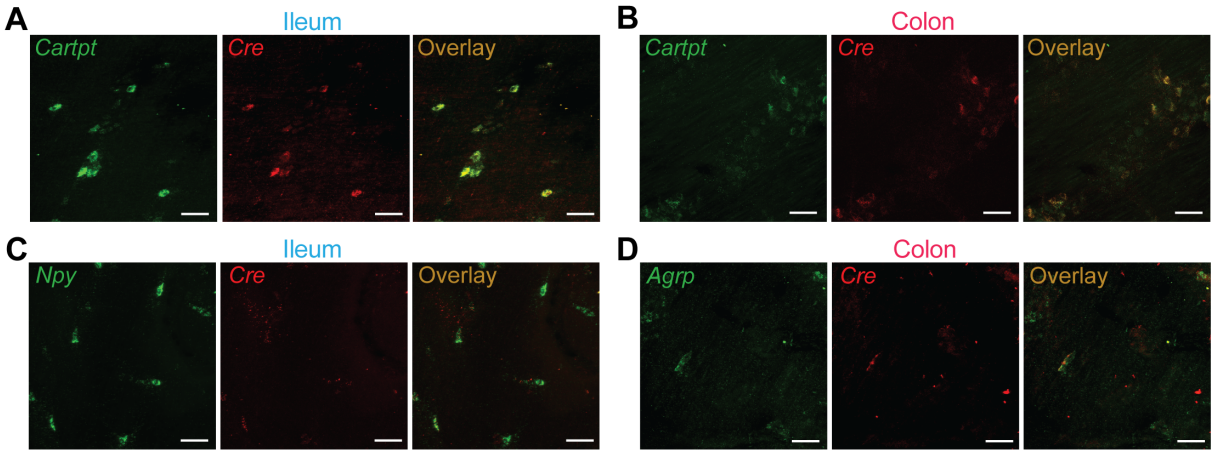


**Fig. 2.39. Validation of *Cre* lines for iEAN neuropeptide targeting.** (**A** to **D**) RNAscope *in situ* hybridization whole-mount IF images of segments from (**A** and **B**) $Cart^{Cre+}$, (**C**) $Npy^{Cre+}$, and (**D**) $Agrp^{Cre+}$ of the (**A** and **C**) ileum and (**B** and **D**) colon using probes for *Cre* and (A, B) *Cartpt*, (C) *Npy* and (D) *Agrp*. Scale bars, 50 µm.

of the circular and longitudinal smooth muscle within these segments of the intestine, with $Cartpt^{EAN\text{-}tdTomato}$ also exhibiting dense inter-ganglionic patterning (Fig. 2.40 A). Similar to the prior *in situ* observations, we found a sparse population of *tdTomato*+ neurons in the mid-colon of $Agrp^{EAN\text{-}tdTomato}$, exhibiting muscular and inter-ganglionic innervation (Fig. 2.40 C). We confirmed a lack of tdTomato expression in the submucosal plexus, NG, DRG, and CG-SMG in $Cartpt^{EAN\text{-}tdTomato}$ and $Agrp^{EAN\text{-}tdTomato}$ mice (*data not shown*). We did find a population of tdTomato+ neurons in the submucosal plexus (*data not shown*) and gut-projecting CG-SMG neurons in $Npy^{EAN\text{-}tdTomato}$ mice (Fig. 3.40 D).

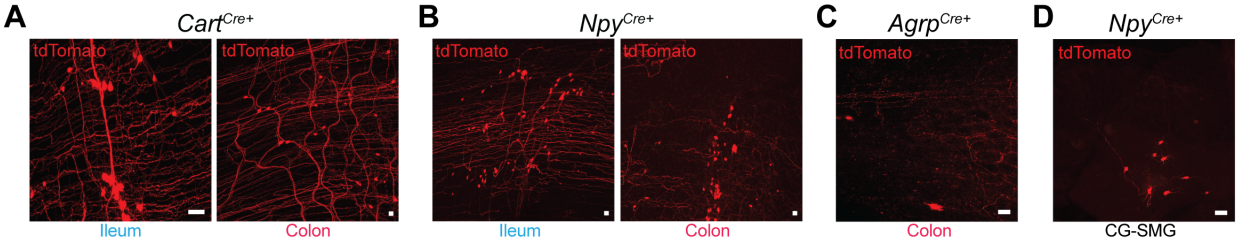


**Fig. 2.40. Gut-restricted adeno-associated virus targeting of neuropeptide+ iEANs.** (**A** to **D**) Whole-mount IF image of (**A**) (left) ileum and (right) colon myenteric plexus injected with AAVrg-FLEX-tdTomato into (left) ileum and (right) duodenum, ileum and colon of $Cart^{Cre+}$ mice; (**B**) the (left) ileum and (right) colon of $Npy^{Cre+}$ mice injected with AAVrg-FLEX-tdTomato into the duodenum, ileum, and colon; (**C**) the colon from $Agrp^{Cre+}$ mice injected with AAVrg-FLEX-tdTomato into the mid-colon; (**D**) the CG-SMG from $Npy^{Cre+}$ mice injected with AAVrg-FLEX-tdTomato into the duodenum, ileum, and colon. Scale bars, 50 µm.

Of note, we also observed a significant number of tdTomato+ fibers in the CG-SMG of $Cartpt^{EAN\text{-}tdTomato}$ mice (Fig. 2.41 A and B), suggesting that a population of CART+ iEANs are viscerofugal. Viscerofugal neurons are defined as iEAN the axons of which project outside of the intestine and have been previously described as mechanosensitive (Hibberd et al., 2012).

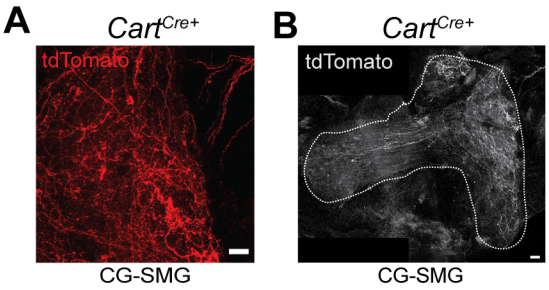


**Fig. 2.41. Fibers of CART+ iEANs reach the CG-SMG.** (**A** and **B**) Whole-mount immunofluorescence image of the CG-SMG of *Cart*$^{Cre+}$ injected with AAVrg-FLEX-tdTomato into duodenum, ileum, and colon. Scale bars = 50 (A) or 100 (B) µm.

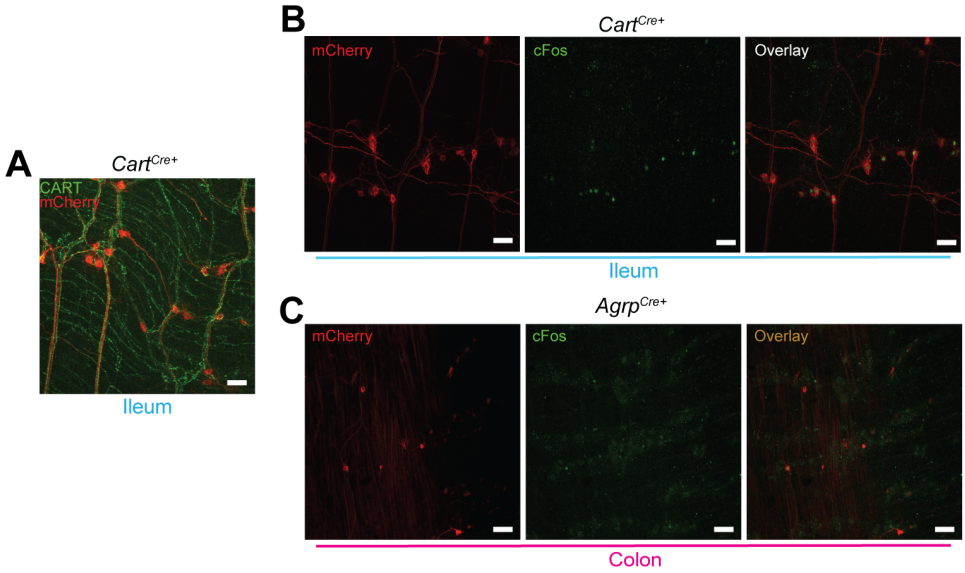


**Fig. 2.42. Chemogenetic targeting of distal intestine neuropeptide+ iEANs.** (**A** and **B**) Whole-mount IF images of the ileum myenteric plexus of *Cart*$^{Cre+}$ mice injected with AAV9-hSyn-DIO-hM3Dq-mCherry into the ileum. (**A**) stained for CART (green) and mCherry (red), and (**B**) 3 h post-C21 administration, stained for cFos (green) and mCherry (red). (**C**) Whole-mount IF images of the colon of *Agrp*$^{Cre+}$ mice injected with AAV9-hSyn-DIO-hM3Dq-mCherry into the mid-colon muscularis, 3 hours post-C21 administration, stained for cFos (green, stained with antibody) and mCherry (red, stained with antibody). Scale bars, 50 µm.

To directly assess the function of intestine-specific neurons within these neuropeptide populations, we decided to specifically modulate their activity using a gut-restricted chemogenetic approach. We injected excitatory designer receptor exclusively activated by designer drugs (DREADD) virus (AAV9-FLEX-Syn-hM3Dq-mCherry) into the distal ileum and proximal-mid colon of *Cartpt*$^{Cre}$ and *Npy*$^{Cre}$ mice or into the mid-colon of *Agrp*$^{Cre}$ mice (Fig. 2.42 A to C).

We first performed an intestinal motility assay following administration of the DREADD ligand, Compound 21 (C21). We found no change in total gastrointestinal transit time (GITT) for any of the three neuropeptide lines tested, although changes in either small or large intestine motility separately cannot be ruled out (Fig. 2.43 A to C). However, we observed a significant decrease in food consumption during daytime feeding at 1 and 2 hours, as well as during nighttime feeding at 2 and 4 hours, post-injection of C21 in *Cartpt*$^{EAN\text{-}hM3Dq}$, but not *Npy*$^{EAN\text{-}hM3Dq}$ or *Agrp*$^{EAN\text{-}hM3Dq}$ mice (Fig. 2.44 A to D).

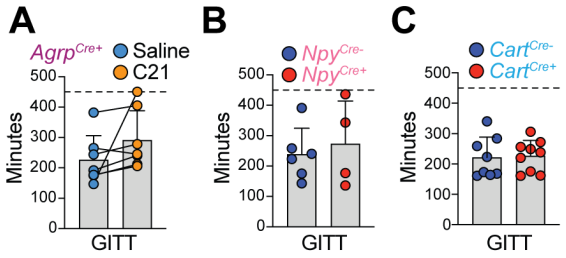


**Fig. 2.43. Gastrointestinal transit time (GITT) post-chemogenetic activation of distal intestine neuropeptide+ iEANs.** (**A** to **C**) GITT of (**A**) *Agrp*$^{Cre+}$, (**B**) *Npy*$^{Cre+}$, and (**C**) *Cart*$^{Cre+}$ mice injected with AAV9-hSyn-DIO-hM3Dq-mCherry into the ileum and colon. Experiments were ended at 450 min (dashed line).

To confirm that viral expression was restricted to CART+ neurons in the intestine, we examined neuronal populations in the NG, DRG, CG-SMG, the dorsal motor nucleus of the vagus (DMN) and duodenal for mCherry expression. We found no clear evidence for hM3Dq expression outside of the distal ileum and proximal colon (*data not shown*), demonstrating that the observed changes in feeding behavior are dependent on iEAN-specific neuronal stimulation. We next evaluated whether the reduction in food consumption was accompanied by acute changes in blood glucose or glucoregulatory hormone levels that can regulate the activity of CNS nuclei controlling feeding behavior (Dunn-Meynell et al., 2009; Gielkens et al., 1998; Havrankova et al., 1978; Woods et al., 1979). We assessed the effects of either excitatory (hM3Dq) or inhibitory (hM4Di) DREADD viruses in *Cartpt*$^{Cre}$ mice, again injected into the distal ileum and proximal colon. Administration of C21 led to significantly higher blood glucose levels in *Cartpt*$^{EAN\text{-}hM3Dq}$ than in control mice, whereas inhibition of these neurons in *Cartpt*$^{EAN\text{-}hM4Di}$ mice did not change blood glucose (Fig. 2.45 A and B). On measurement of canonical glucoregulatory hormones, we found a significant decrease in insulin levels at 30 and 90 minutes post-C21 administration to *Cartpt*$^{EAN\text{-}hM3Dq}$ mice, whereas glucagon levels were not significantly altered (Fig. 2.45 C and D). These data indicate that stimulation of ileum and colon

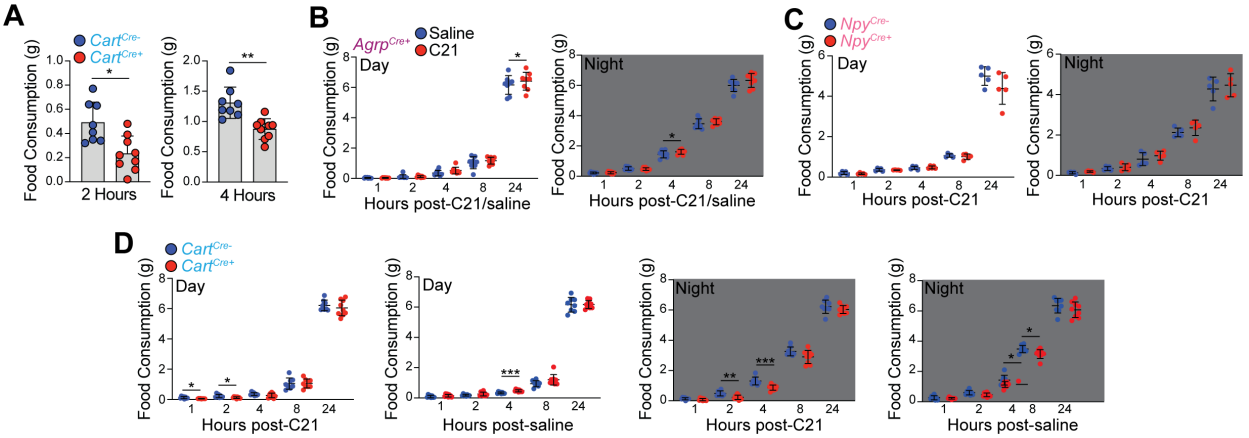


**Fig. 2.44. Food consumption following chemogenetic activation of distal intestine neuropeptide+ iEANs.** (**A**) Food consumption at night 2 (left) and 4 h (right) post-C21 administration in *Cart*$^{Cre+}$ and *Cart*$^{Cre-}$ mice injected with AAV9-hSyn-DIO-hM3Dq-mCherry into the ileum (**B** to **D**) Food consumption (left) during the day or (right) at night post-administration of C21 or saline in (**B**) *Agrp*$^{Cre+}$, (**C**) *Npy*$^{Cre+}$, (**D**) *Cart*$^{Cre+}$ mice injected with AAV9-hSyn-DIO-hM3Dq-mCherry into the ileum and colon. * $P < 0.05$, ** $P < 0.01$, *** $P < 0.001$ as calculated by unpaired t-test.

CART+ neurons results in increased blood glucose and decreased insulin levels, with a subsequent reduction in food consumption.

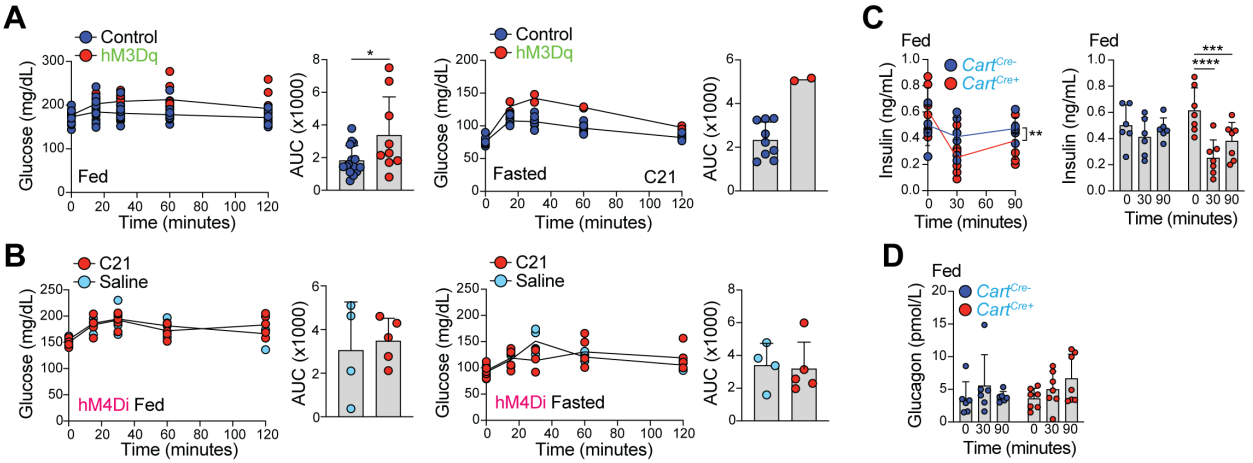


**Fig. 2.45. Changes in levels of blood glucose and glucoregulatory hormones following chemogenetic activation of distal intestine CART+ iEANs.** (**A** and **B**) Blood glucose levels post-C21/saline administration and AUC analysis in (left) fed or (right) overnight fasted *Cart*$^{Cre+}$ and and *Cart*$^{Cre-}$ (control) mice injected with (**A**) AAV9-hSyn-DIO-hM3Dq-mCherry or control AAV9-hSyn-DIO-mCherry into ileum and colon, or (**B**) AAV9-hSyn-DIO-hM4Di-mCherry into the ileum. (**C** and **D**) Plasma (**C**) insulin and (**D**) glucagon levels post-C21 administration in *Cart*$^{Cre+}$ and *Cart*$^{Cre-}$ mice injected with AAV9-hSyn-DIO-hM3Dq-mCherry into ileum and colon. * $P < 0.05$, ** $P < 0.01$, *** $P < 0.001$, **** $P < 0.0001$, (A) unpaired t-test, (C, left) two-way or (C, right) one-way ANOVA with Tukey's multiple comparisons test.

## 2.5.2 Intestinofugal CART+ iEANs are polysynaptically connected to the liver and pancreas through the CG-SMG

We next asked how CART+ iEANs can exert their glucoregulatory function. One possible route could be via direct detection of signals coming from the epithelium. However, imaging analyses confirmed that CART+ neurons are not present in the submucosal plexus, nor do they project to the epithelium (2.46 A and B). We confirmed their viscerofugal nature with viral anatomical and cholera toxin subunit B (CTB) tracing.

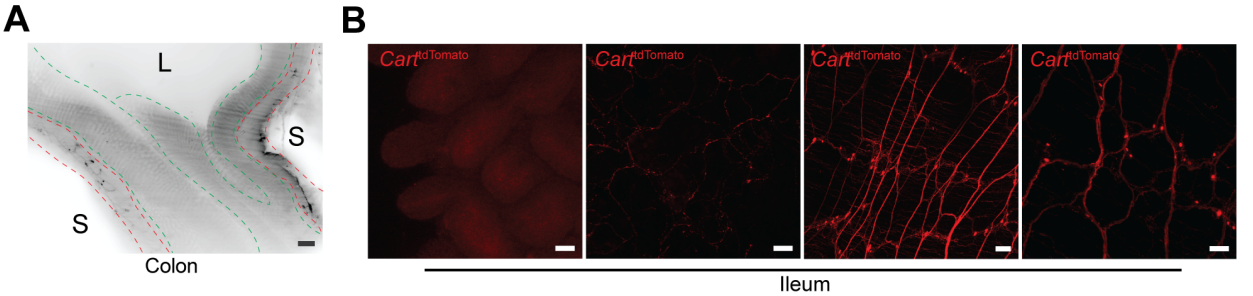


**Fig. 2.46. Expression of CART is restricted to myenteric iEANs.** (**A**) Representative AdipoClear-cleared light-sheet image of the colon of *Cart*$^{Cre+}$ mice injected with AAV9-hSyn-DIO-hM3Dq-mCherry into ileum and colon. Scale bar, 200 µm. L, intestinal lumen; S, serosa. Dotted red line outlines region containing the myenteric plexus. Dotted green line outlines mucosa and epithelium. (**B**) Representative whole-mount native fluorescence images of the intestinal (left) villi, (middle-left) submucosa and (middle- and far-right) ileum muscularis of *Cart*$^{tdTomato}$ mice. Scale bars, 50 µm. Images representative of at least n = 3 mice.

(Fig. 2.47 A and B). We also noted that some CART+ neurons appear to interact directly with viscerofugal neurons (Fig. 2.47 C). These CART+ viscerofugal iEANs send axonal projections to the CG-SMG, which in turn provides sympathetic innervation to a number of visceral organs, including pancreas and liver (Love et al., 2007; Mizuno and Ueno, 2017). Sympathetic innervation of the pancreatic islets can stimulate the release of glucagon and inhibit insulin secretion through adrenergic receptor engagement on α- and

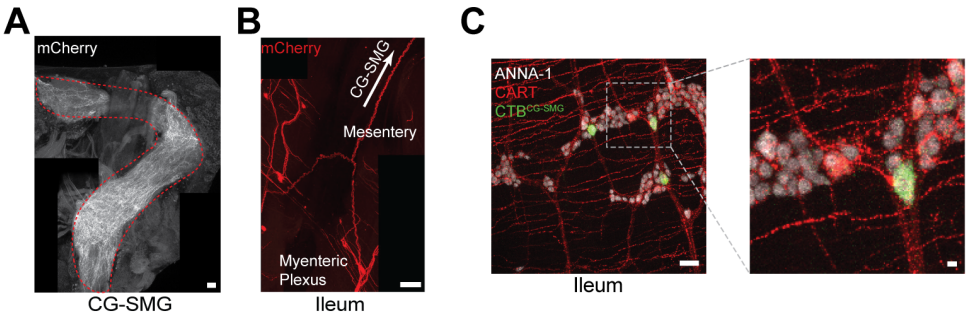


**Fig. 2.47. A population of CART+ iEANs is viscerofugal and projects to the CG-SMG.** (**A** and **B**) Whole-mount immunofluorescence (IF) image of (**A**) CG-SMG and (**B**) ileum myenteric plexus (MP) of *Cart-Cre+* mice injected with AAV9-hSyn-DIO-hM3Dq-mCherry into ileum and colon. Scale bars, 100 µm (**C**) Representative whole-mount IF image of the ileum myenteric plexus highlighting CART+ fiber (red) in close proximity to a viscerofugal neuron (green) from C57BL/6J mice. Scale bar (left) = 50 µm. Scale bar (inset on the right) = 10 µm.

β-cells, respectively (Love et al., 2007; Thorens, 2014). Sympathetic stimulation of the liver can drive gluconeogenesis and glycogenolysis through hepatocyte adrenergic receptor activation (Mizuno and Ueno, 2017).

To determine if a synaptically connected circuit exists between the gut, sympathetic ganglia, and the pancreas or liver, we performed polysynaptic retrograde tracing using pseudo-rabies virus (PRV). We injected enhanced green fluorescent protein (eGFP)-expressing PRV into the pancreas and monomeric red fluorescent protein (RFP)-expressing PRV into the parenchyma of the liver and assessed their synaptic connections to the CG-SMG and the intestine (Fig. 2.48 A). We detected viral spread or CTB labeling from both organs to the CG-SMG as early as one day post-injection (Fig. 2.48 B and C). Upon dissection of intestinal muscularis externa, we observed GFP+ neurons in the

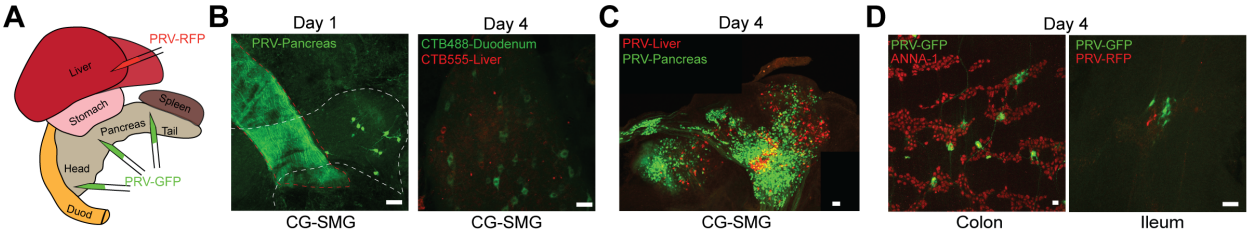


**Fig. 2.48. iEANs are polysynaptically connected to liver and pancreas.** (**A**) Schematic of fluorescent PRV injection into the liver and pancreas. (**B**) Representative whole-mount (native fluorescence) images of the CG-SMG (middle) one day post injection of PRV-GFP into the pancreas and (right) 4 days post injection of CTB488/555 into the duodenum/liver of C57BL/6J SPF mice. (**C**) Whole-mount IF image of the CG-SMG 4 days post injection of PRV-GFP into the pancreas and PRV-RFP into the liver. (**D**) Whole-mount IF image of (left) colon and (right) ileum MP of C57BL/6J SPF mice injected with PRV-GFP (pancreas) and PRV-RFP (liver). Scale bars, (B, D) 50 µm, (C) 100 µm.

myenteric plexuses of the duodenum, ileum, and colon 4 days post-injection, with the highest concentration of neurons in the colon and ileum, while RFP+ neurons were only observed in the ileum (Fig. 2.48 D). We did not observe dual RPF/GFP labeling of ileal viscerofugal neurons, suggesting that the pancreas and liver are connected by two separate circuits. Together, we found that glucoregulatory organs are polysynaptically connected to the gut through viscerofugal neurons.

To investigate whether CART+ viscerofugal iEAN activation could directly modulate sympathetic neuronal activity, we dissected the CG-SMG post-C21 administration and measured cFos expression as an indicator of sympathetic activation (Mei et al., 2001). We observed a significant increase in cFos expression in C21-injected *Cart*$^{\text{EAN-hM3Dq}}$ as compared to control animals (Fig. 2.49 A). Inhibition of catecholamine release by guanethidine prevented the increase in glucose levels in C21-treated *Cart*$^{\text{EAN-hM3Dq}}$ mice, further suggesting the involvement of sympathetic activation. However, guanethidine administration did not prevent the reduction in blood glucose induced by antibiotics (Fig. 2.49 B and C). To determine whether neuropeptide release might impact glucose regulation, we exogenously administered CART peptide in antibiotic or control treated mice and observed no change in blood glucose levels (Fig. 2.49 D). However, we cannot definitively rule out a direct role for CART peptide due to incomplete knowledge of its role in the periphery and lack of identified receptor(s).

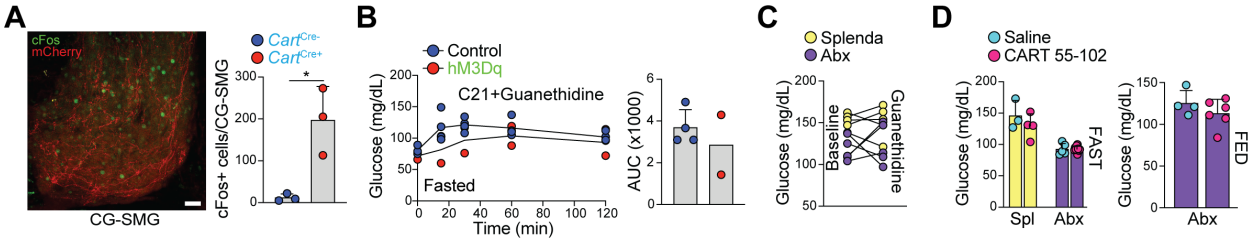


**Fig. 2.49. CART+ iEAN activation leads to increased gut-sympathetic activity.** (**A**) (left) cFos (green) and mCherry (red) expression and (right) number of cFos+ neurons in the CG-SMG of *Cart*$^{Cre+}$ mice injected with AAV9-hSyn-DIO-hM3Dq-mCherry into ileum and colon, 3 h post-C21 injection. * $P < 0.05$, two-tailed unpaired t-test. Scale bar, 50 µm (**B**) (Left) Blood glucose levels and (right) corresponding area under the curve (AUC) calculation of *Cart*$^{Cre+}$ mice fasted overnight, followed by administration of guanethidine and C21, analyzed at the indicated timepoints. Mice were injected with AAV9-hSyn-DIO-hM3Dq-mCherry into the ileum and colon. (**C**) Fasted blood glucose levels of C57BL/6J SPF mice treated with antibiotics for 2 weeks and i.p. injected with guanethidine 1 hour prior to analysis. (**D**) Blood glucose levels 1 hour after i.p. injection of CART 55-102 peptide in fasted (left) or fed (right) C57BL/6J SPF mice treated with antibiotics or sucralose-based artificial sweeteneer (Splenda®).

Next, we investigated whether viscerofugal iEANs would be impacted upon microbial depletion. Indeed, retrograde fluorescent CTB tracing from the CG-SMG revealed a loss of CTB+ iEANs, including CTB+ CART+ iEANs, specifically in the ileum of antibiotic-treated mice (Fig. 2.50 A, B and E), while only a minor reduction was observed in the colon and no changes were found in the sparsely retrograde labeled duodenum (Fig. 2.51 A and B). As expected, antibiotic-treatment to *Casp11*$^{-/-}$ mice did not result in loss of viscerofugal neurons (Figs. 2.50 C, D and H, and 2.51 C and D). We conclude that intestinal CART+ iEANs that can modulate blood glucose levels, are viscerofugal and microbiota-dependent.

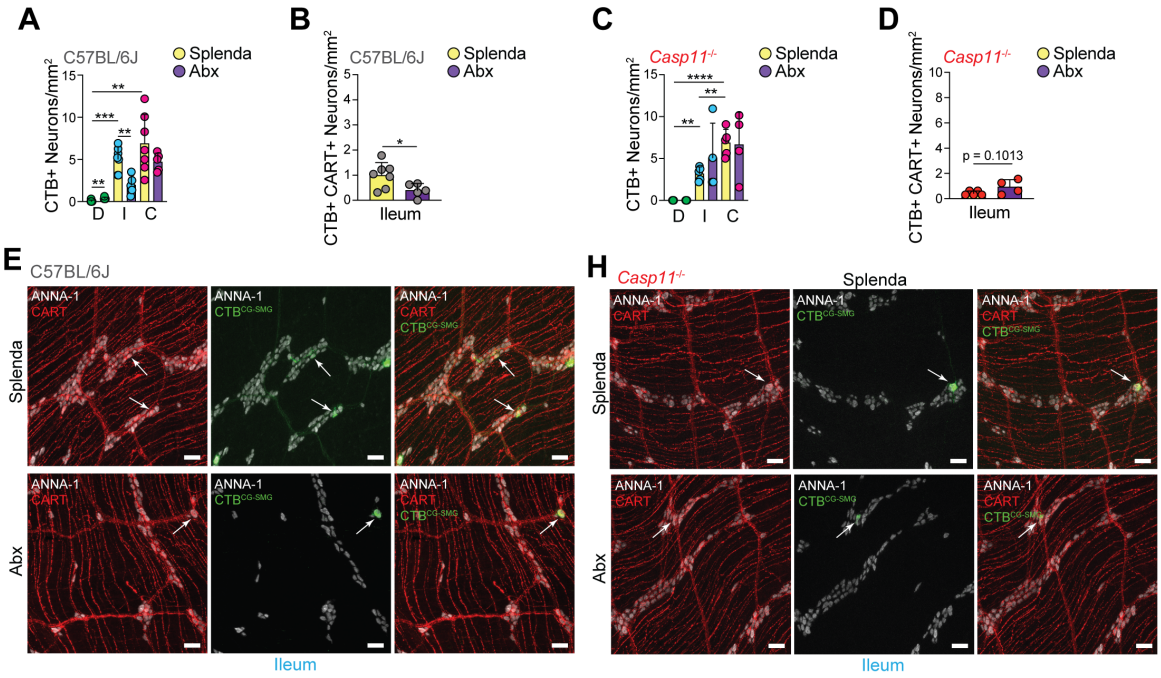


**Fig. 2.50. Loss of CART+ viscerofugal iEANs post-microbial depletion in the ileum.** (**A** and **B**) C57BL/6J or (**C** and **D**) *Casp11-/-* mice treated with Splenda or antibiotics for 2 weeks post-CTB injection into the CG-SMG. (**A** and **C**) CTB-AF647+ neuron numbers in duodenum (D), ileum (I), and colon (C). (**B** and **D**) (left) CTB-AF647+ or (right) CTB-AF647+ CART+ neuron numbers in the ileum. * $P < 0.05$, ** $P < 0.01$, *** $P < 0.001$, **** $P < 0.0001$, (A and C, Abx vs Splenda within region comparisons, (B and D) two-tailed unpaired t-test, one-way ANOVA with Tukey's multiple comparisons test (A and C, Splenda region comparisons). (**E** and **F**) Representative whole-mount IF images of the myenteric plexus quantified in (A to D). White arrows indicate CTB+ CART+ neurons. Scale bars = 50 µm. Images representative of at least n = 5/condition.

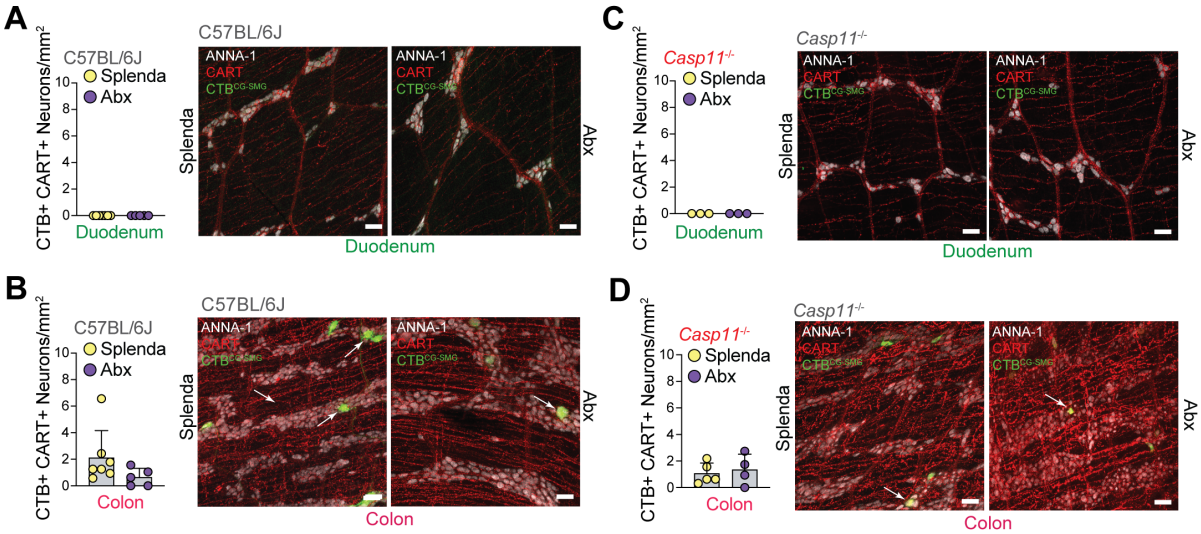


**Fig. 2.51. CART+ viscerofugal iEANs post-microbial depletion in duodenum and colon.** (**A** and **B**) C57BL/6J or (**C** and **D**) *Casp11-/-* mice treated with Splenda or antibiotics for 2 weeks post-CTB injection into the CG-SMG. (Left) CTB-AF647+ CART+ neuron numbers and (right) representative whole-mount IF images of the (A and C) duodenum and (B and D) colon. White arrows, CTB+ CART+ neurons. Scale bars, 50 µm. Images representative of at least n = 5.

### 2.5.3 Modulation of blood glucose levels is dependent on the gut microbiota and CART+ iEANs

To confirm whether microbiota depletion impacts blood glucose regulation, we analyzed antibiotic-treated SPF and GF mice and found a significant reduction in blood glucose, irrespective of diet or feeding state (Fig. 2.52 A to E), corroborating previous studies (Krisko et al., 2020; Martin et al., 2019; Zarrinpar et al., 2018). Consistent with

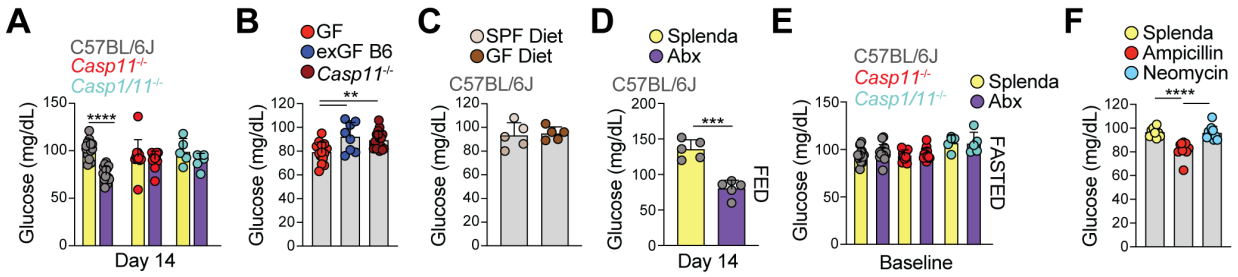


**Fig. 2.52. Control of blood glucose is microbiota-dependent.** (**A** to **F**) Blood glucose levels of fasted (**A**) C57BL/6J, *Casp11-/-* and *Casp1/11-/-* mice treated with Abx or sucralose based-artificial sweetener (Splenda®) (**B**) GF, exGF, and *Casp11-/-* mice, (**C**) C57BL/6J SPF mice receiving regular chow diet or 4 days after switching to autoclaved germ-free diet, (**D**) fed C57BL/6J SPF mice treated with broad-spectrum antibiotics or Splenda for 2 weeks, (**E**) overnight fasted C57BL/6J, *Casp1/11-/-*, and *Casp11-/-* mice treated with Splenda in the drinking water before switching experimental groups on antibiotics (Abx), (**F**) C57BL/6J mice on ampicillin, neomycin, or Splenda. ** $P < 0.01$, *** $P < 0.001$, **** $P < 0.0001$, (B, F) one-way or (A, D) two-way ANOVA with Tukey's multiple comparisons test.

neuronal loss, ampicillin treatment alone specifically led to a reduction in blood glucose levels (Fig. 2.52 F). Fasting blood glucose levels could be rescued upon colonization with the microbiota from SPF animals, irrespective of genetic background (Fig. 2.53 A to D).

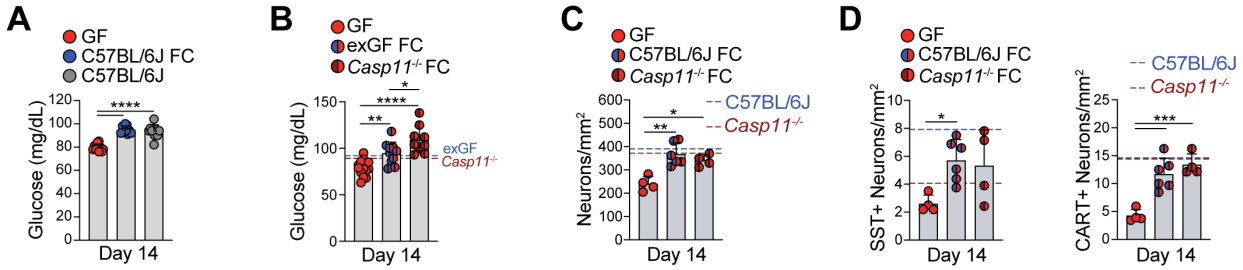


**Fig. 2.53. Changes to blood glucose levels following microbial manipulation can be restored upon colonization.** (**A**) Blood glucose (BG) of overnight-fasted C57BL/6J GF, GF colonized (C57BL/6J microbiota, fecal colonization, FC), and C57BL/6J housed in bioexclusion cages, 2 weeks post colonization. **** $P < 0.0001$, one-way ANOVA with Tukey's multiple comparisons test. (**B** to **D**) C57BL/6J GF mice were colonized with microbiota from C57BL/6J or *Casp11-/-* mice. Dotted blue lines, C57BL/6J (FC donor) baselines. Dotted red lines, *Casp11-/-* (FC donor) baselines. (**B**) Fasted BG levels. Number of (**C**) total neurons, (**D**) (left) SST+ and (right) CART+ myenteric plexus iEAN per $mm^2$. * $P < 0.05$, ** $P < 0.01$, *** $P < 0.001$ as calculated by one-way ANOVA with Tukey's multiple comparisons test.

To determine whether microbiota-mediated changes in glucose levels are associated with loss of iEANs, we measured blood glucose in global or conditional knockout mice targeting the NLRP6 inflammasome and its downstream effector Casp11 because these genotypes did not lose iEANs or CART+ iEANs upon antibiotic treatment. We found blood glucose levels in *Casp1/11*$^{-/-}$, *Casp11*$^{-/-}$, *Snap25*$^{\Delta Nlrp6}$, and *Snap25*$^{\Delta Casp11}$ mice were

higher following antibiotic treatment as compared to WT and heterozygous controls (Figs. 2.52 A, and 2.54 A and B).

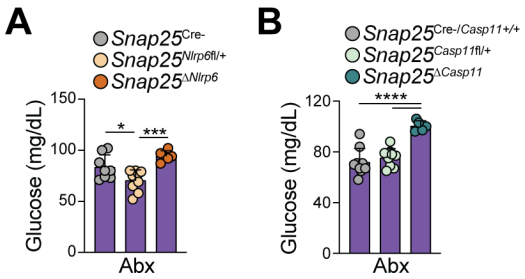


**Fig. 2.54. Changes to blood glucose regulation are dependent on neuronal inflammasome components.** (**A** and **B**) Blood glucose levels of fasted control mice and (**A**) *Snap25*$^{\Delta Nlrp6}$ or (**B**) *Snap25*$^{\Delta Casp11}$ mice on antibiotics (Abx). * $P < 0.05$, **** $P < 0.0001$, **** $P < 0.0001$, one-way ANOVA with Tukey's multiple comparisons test.

We sought to determine which glucose-modulating pathways may be regulated by changes in the microbiota and more specifically, whether the NLRP6-Casp11 inflammasome components were involved. We first confirmed that GLP-1 is elevated in antibiotic-treated mice (Zarrinpar et al., 2018), but found that this elevation was independent on Casp11 (Fig. 2.55 A). Furthermore, administration of a GLP-1R blocking peptide, Exendin-9-39, did not change fasting blood glucose levels of antibiotic-treated WT mice (Fig. 2.55 B). Additionally, insulin levels did not change upon antibiotic treatment in WT, *Casp1/11*$^{-/-}$ and *Casp11*$^{-/-}$ mice (Fig. 2.55 C).

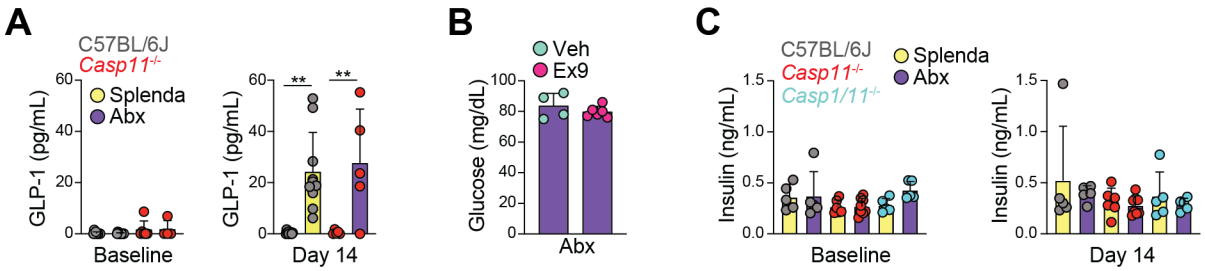


**Fig. 2.55. Insulin and GLP-1 levels are not affected by *Casp11* deletion.** (**A**) Plasma levels of GLP-1 in C57BL/6J and *Casp11-/-* mice at baseline and after treatment with antibiotics or Splenda for 2 weeks. ** $P < 0.01$ as calculated by one-way ANOVA with Tukey's multiple comparisons test. (**B**) Blood glucose levels of C57BL/6J mice previously treated with broad-spectrum antibiotics for 2 weeks, 1-hour post Exendin-9-39 treatment. (**C**) Plasma levels of insulin in C57BL/6J, *Casp1/11-/-*, and *Casp11-/-* mice at baseline and after treatment with antibiotics or Splenda for 2 weeks.

We next investigated whether pyruvate-induced gluconeogenesis (Krisko et al., 2020) was affected by microbial manipulation. We observed significantly blunted temporal changes in blood glucose levels in GF and antibiotic-treated SPF mice compared with control SPF mice after pyruvate administration (Fig. 2.56 A to C). This effect was rescued by microbiota reconstitution in GF mice (Fig. 2.56 B) and global loss of Casp11 in SPF mice (Fig. 2.56 C); additionally, it was partially rescued in SPF mice with neuronal-specific deficits in NLRP6 and Casp11 (Fig. 2.56. D and E). Microbiota normalization between antibiotic-treated WT and *Casp11*$^{-/-}$ mice, which harbored antibiotic resistant bacteria, did not impact blood glucose or pyruvate tolerance deficits, suggesting that the mere presence of any bacteria is not sufficient to reverse effects observed with microbial depletion, but that specific bacterial communities or metabolites are necessary (Fig. 2.57 A to C). These data suggest that iEANs can regulate liver gluconeogenesis independently

from pancreatic insulin production or intestinal GLP-1 release in a microbiota- and inflammasome-dependent manner.

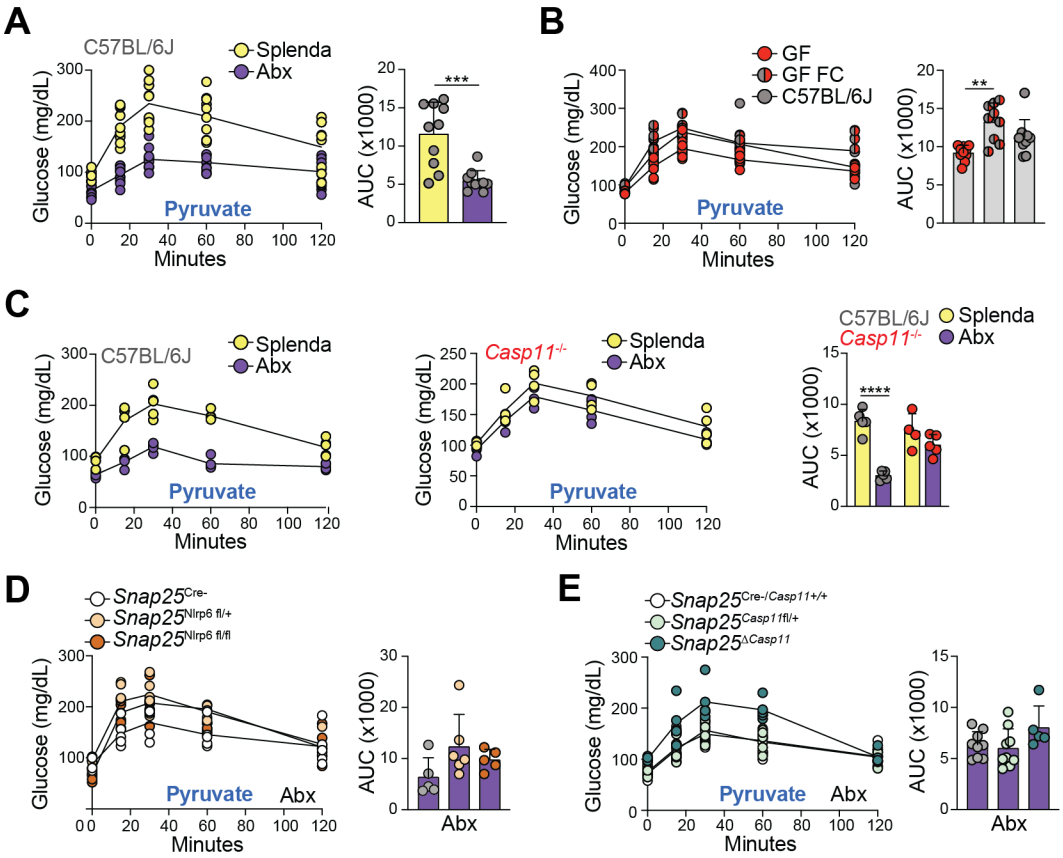


**Fig. 2.56. iEANs can regulate hepatic gluconeogenesis independently of insulin and GLP-1.** (**A** to **E**) Intraperitoneal pyruvate tolerance test (IP-PTT) of fasted (**A**) C57BL/6J mice on Abx or Splenda; (**B**) GF, GF colonized (FC, fecal colonization), and C57BL/6J housed in bioexclusion cages; (**C**) C57BL/6J or *Casp11-/-* mice on Abx or Splenda; (**D**) *Snap25*$^{\Delta Nlrp6}$ and (**E**) *Snap25*$^{\Delta Casp11}$ or control mice on Abx. (Left) BG curves, (right) AUC analyses. ** $P < 0.01$, *** $P < 0.001$ (A) unpaired t-test, (B to E) one-way ANOVA with Tukey's multiple comparisons test.

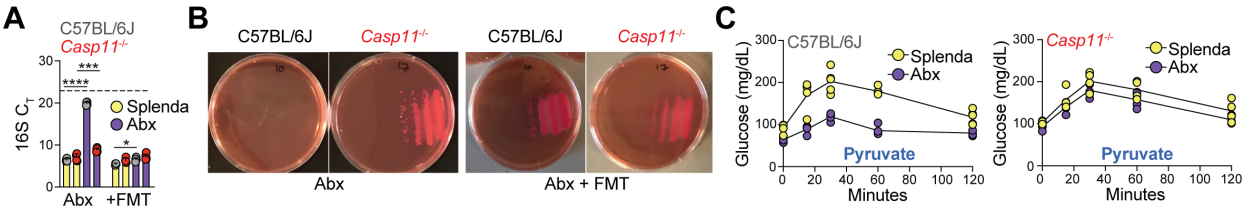


**Fig. 2.57. Colonization with an antibiotic-resistant bacterium during microbial depletion does not restore changes in glucose regulation.** (**A**) $C_T$ values of 16S qPCR from fecal samples of C57BL/6J and *Casp11-/-* mice treated with antibiotics or Splenda for 4 weeks, followed by fecal microbial transfer (FMT) between strains to normalize microbiota. Dotted line, average $C_T$ value of pooled GF controls; * $P < 0.05$, *** $P < 0.001$, **** $P < 0.0001$ as calculated by two-way ANOVA with Tukey's test for multiple comparisons; (**B**) representative agar plates confirming colonization with antibiotic-resistant bacteria. (**C**) Intraperitoneal pyruvate tolerance test (IP-PTT) of fasted C57BL/6J and *Casp11-/-* mice following protocol as in (A).

To directly test the necessity of gut CART+ neurons in blood glucose regulation, we injected AAV5-mCherry-FLEX-DTA into the ileum and colon of *Cartpt*$^{Cre}$ mice to selectively delete CART+ neurons in the intestine (Fig. 2.58 A and B). Two weeks post CART+ neuron ablation, we observed a significant reduction in blood glucose in fasted animals and a significant increase in insulin levels in fasted and fed animals as compared to *Cartpt*$^{Cre}$ mice injected with a control AAV5 virus (Fig. 2.58. C and D). Similar to what was observed in GF and antibiotic-treated mice, we found a trend toward decreased gluconeogenic capacity (Fig. 2.58 E). Thus, loss of CART+ viscerofugal iEANs decreases blood glucose levels, presumably due to the lack of pancreas- and liver-specific sympathetic regulation. Gut CART+ neurons are therefore both sufficient and necessary to modulate blood glucose through glucoregulatory organs.

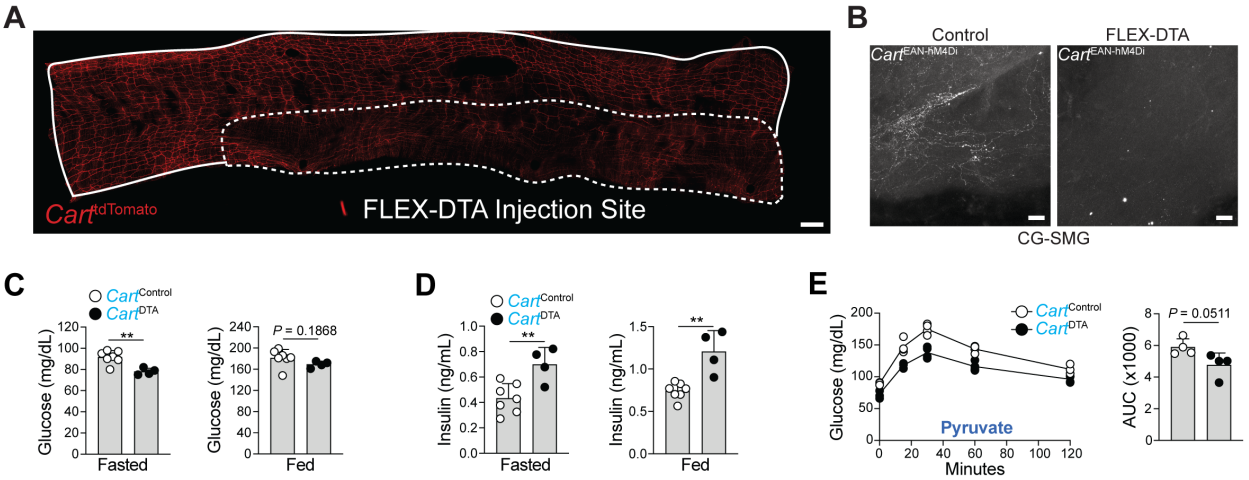


**Fig. 2.58. Ablation of CART+ iEANs affects glucoregulatory processes.** (**A**) Representative whole-mount confocal IF image of the ileum of *Cart*$^{tdTomato}$ mice injected with AAV5-FLEX-DTA or control virus into the ileum. Scale bar, 1 mm. Continuous white line, whole tissue; dotted white, virus injection site. (**B**) Representative whole-mount confocal IF images of the CG-SMG of *Cart*$^{Cre+}$ mice injected with AAV9-DIO-hSyn-hM4Di-mCherry in the ileum and colon (*Cart*$^{EAN\text{-}hM4Di}$) followed by a subsequent injection with control virus or AAV5-FLEX-DTA into the ileum and colon two weeks later. Scale bars, 50 µm. (**C** to **E**) *Cart*$^{Cre+}$ mice were injected with AAV5-DTA into ileum and colon. (**C**) (left) fasted or (right) fed blood glucose levels, (**D**) (left) fasted or (right) fed plasma insulin levels, (**E**) fasted IP-PTT (left) BG curves and (right) AUC analysis. ** $P < 0.01$, unpaired t-test.

Together, these experiments establish a microbiota-sensitive, polysynaptic glucoregulatory circuit connecting the gut, sympathetic ganglia, and the liver and pancreas (Fig. 2.59).

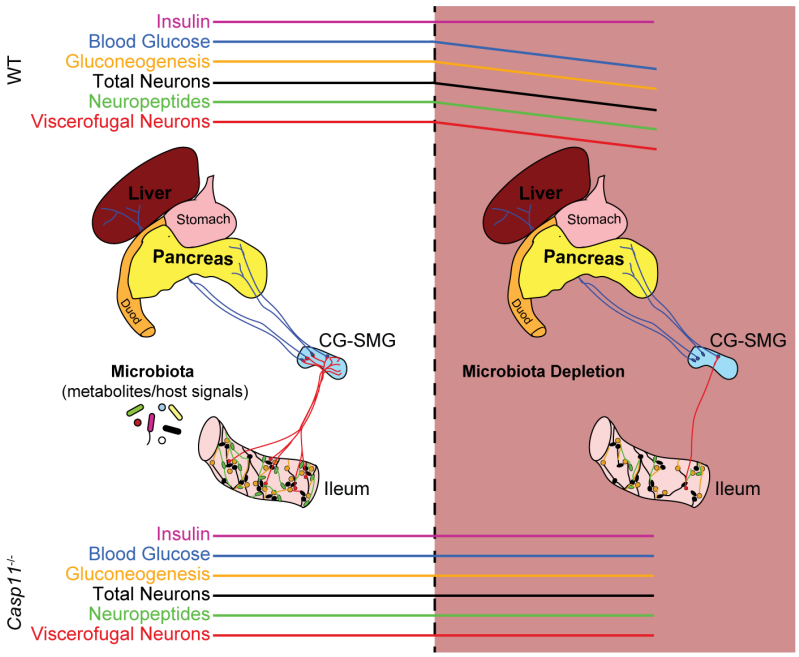


**Fig. 2.59. Schematic of findings in Chapter 2.5.** In the absence of a microbiota there is a significant reduction in gluconeogenesis, coupled to a loss of subset-specific, viscerofugal and total iEANs. CART+ viscerofugal iEANs are capable of modulating blood glucose through sympathetic-mediated effects on the liver (gluconeogenesis) and pancreas (insulin). Loss of gut viscerofugal input to the CG-SMG results in a decreased capacity for sympathetic-mediated gluconeogenesis via a CG-SMG-liver circuit. Rescuing iEAN loss through global or neuronal-specific deletion of *Casp11* prevents changes in glucose levels found upon microbial depletion.

## 2.6 Conclusions

Using cell sorting-independent transcriptomics, confocal microscopy, and microbial manipulation strategies, our data revealed both regional differences and microbial influence on transcriptional profiles, numbers and neurochemical coding of iEANs. We further demonstrated that enteric infections lead to lasting inflammatory changes in the intestine, with concomitant reduction in myenteric neuron numbers and resulting in lasting GI symptoms. Whether and how these inflammatory changes dictate the tissue's response to future insults will be addressed in the following chapter.

Mechanistically, our work uncovered a novel mechanism of enteric neuronal cell death following intestinal infection and microbial depletion, engaging the noncanonical inflammasome components *Nlrp6* and *Casp11*. Functionally, we uncovered a peripheral neuronal circuit encompassing the gut, liver and pancreas, with the capacity to exert metabolic control independently of the CNS. We describe a distinct role for NLRP6 and Casp11 in controlling iEAN number and subsequent glucose regulation in response to commensal microbiota levels. Further studies will be needed to uncover the mechanisms by which intestinal CART+ neurons sense luminal stimuli to exert their glucoregulatory function, and to determine the ligand(s) that activate the non-canonical inflammasome pathway in these contexts.

# CHAPTER 3. CROSSTALK BETWEEN MICROBES, GUT-ASSOCIATED NEURONS AND INTESTINAL IMMUNE CELLS

In concert with the ENS, intestinal immune cell populations are crucial for maintaining GI homeostasis. They sense and integrate luminal cues, and regulate physiological processes, including GI motility, nutrient absorption and secretion. Recent evidence suggests that intestinal-resident macrophage populations play a role in normal functioning of enteric neurons in the absence of infections (De Schepper et al., 2018; Muller et al., 2014). Additionally, work from our laboratory has previously shown that muscularis macrophages (MMs), located within and surrounding the myenteric plexus, displayed a tissue-protective gene expression profile, a signature that was further enhanced following enteric infection (Gabanyi et al., 2016).

In this chapter, we sought to better characterize the role of neuro-immune interactions in the context of enteric pathologies, including GI dysfunction and neuronal damage observed upon enteric infections described in the previous chapter. We further aimed to investigate whether a state of tolerance can be induced after exposure to pathogens, preventing cumulative neuronal loss and functional changes during subsequent infections, and a potential role of innate immune cells therein. Finally, we sought to further characterize extrinsic, gut-projecting neurons to determine their role in sensing of and responding to luminal microbial cues, with the goal of integrating their function in enteric microbe-neuro-immune crosstalk in physiology and during enteric infections.

## 3.1 Adrenergic signaling in muscularis macrophages limits infection-induced neuronal loss

Tissues-resident MMs, the most abundant immune cell population in the myenteric region, are closely juxtaposed to iEANs, and their presence has been linked to normal functioning of these neurons during homeostasis (De Schepper et al., 2018; Gabanyi et al., 2016). Previous work from our group suggested that MMs preferentially express tissue-protective and wound healing genes, such as *Retnla* (encoding Fizz1), *Mrc1*, *Cd163* and *Il10* at steady state. This gene signature was reinforced early (2 h) after enteric infection, with an upregulation of additional tissue-protective genes such as *Arg1* and *Chi3l3* (encoding Ym1) (Gabanyi et al., 2016). We thus sought to determine whether MMs play a role in infection-induced GI symptoms and neuronal damage, or the prevention thereof.

### 3.1.1 Tissue-resident muscularis macrophages respond to luminal infection to limit neuronal damage

To investigate a possible role of MMs in infection-induced iEAN damage, we first depleted MMs using an antibody blocking colony stimulating factor 1 receptor (CSF1R)-signaling, AFS98 (α-CSF1R). We used a dose that preferentially depletes MMs over lamina propria macrophages, due to the fact that MMs express higher levels of CSF1R

(Muller et al., 2014) (Fig. 3.1 A to C). Continuous α-CSF1R-mediated MM depletion did not impact iEAN numbers in naïve mice. However, MM depletion resulted in enhanced iEAN loss in mice infected with *spiB* when compared to mice treated with isotype control antibody, despite similar bacterial load in both conditions (Fig. 3.1 D and Appendix 2). These results indicate that, while short-term depletion of MMs does not impact iEAN survival in the unperturbed state, MMs may play an iEAN-protective role in the context of enteric infection.

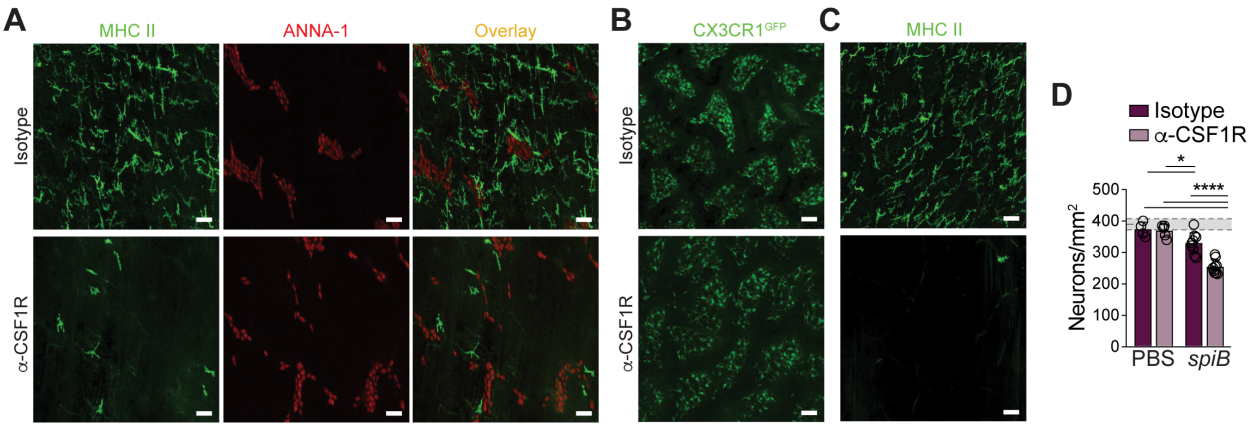


**Fig. 3.1. Antibody-mediated MM depletion exacerbates iEAN loss post-infection.** (**A** to **C**) Mice were injection-habituated, orally gavaged with PBS or *spiB*, and treated with anti-CSF1R or IgG isotype control antibodies. (**A**) Representative confocal IF staining of the ileum myenteric region of C57BL/6J mice stained with anti-MHC-II (green) and anti-ANNA-1 (red). (**B** and **C**) Representative confocal IF image of the ileum (**B**) submucosal layer of *Cx3cr1*$^{GFP}$ mice (green, native fluorescence) and (**C**) myenteric layer of C57BL/6J mice stained with anti-MHC-II (green). (**D**) Number of ileum myenteric iEANs of C57BL/6J mice; Shaded area, mean day 7 iEAN numbers +/- SEM of all control C57BL6/J mice analyzed in Fig 2.23 B. * $P < 0.05$, **** $P < 0.0001$ as calculated by unpaired t-test. Images representative of at least n = 3 mice per condition. Scale bars, 50 $\mu$m.

Because glia cells, both in the CNS and periphery, have been reported to mediate neuronal protection (Brown et al., 2016; Skatchkov et al., 2015), we also tested whether enteric glia are involved in infection-induced iEAN loss or limiting thereof. To target enteric glia, we used mice carrying tamoxifen-inducible *Cre* under the glia-specific *Plp1* promotor (*Plp1*$^{CreER}$) and the *lox*-stop-*lox-DTA* transgene in the *Rosa26* locus (Rao et al., 2017). Depletion of glia in *Plp1*$^{iDTA}$ mice before infection with *spiB* led to a similar loss of iEAN as tamoxifen-treated control animals, indicating that enteric glia do not play either a major neuro-protective, or -detrimental role in this model (Fig. 3.2 A and B).

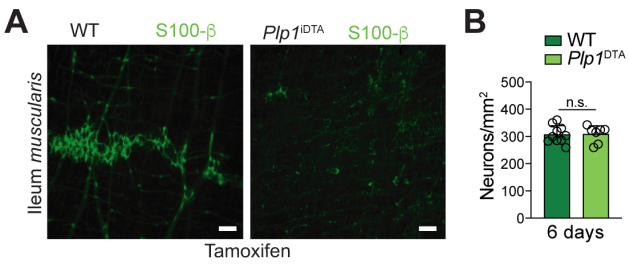


**Fig. 3.2. Enteric glia are not required for iEAN protection post-infection.** (**A** and **B**) *Plp1*$^{iDTA}$ or control mice were treated with tamoxifen 5 days prior to infection with $10^9$ CFU *Salmonella spiB* and analyzed on day 6 post-infection. (**A**) Representative confocal IF images of the ileum myenteric plexus glia using anti-S100-β (green). (**B**) Number of ileum myenteric iEANs.

Next, we used confocal imaging to investigate MM dynamics early upon infection, which revealed a continuing presence and intercalation into ganglia of the myenteric plexus (Fig. 3.3 A and B).

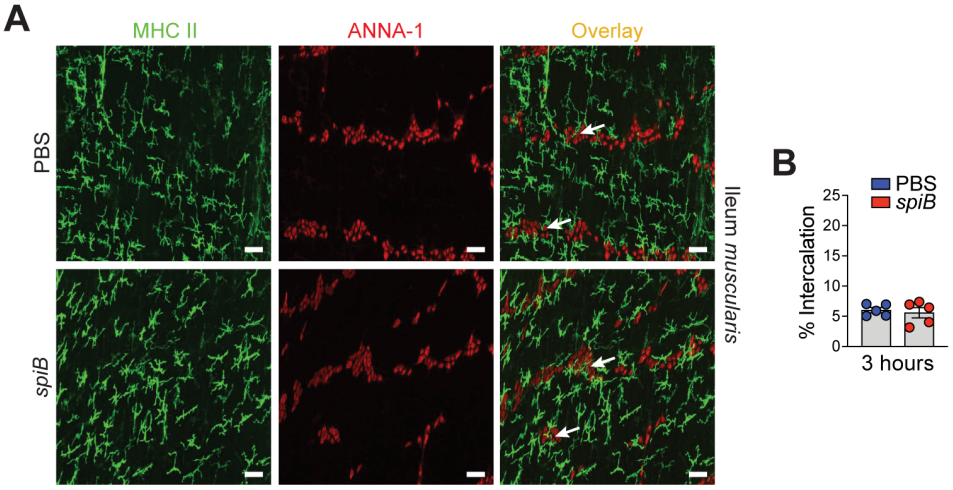


**Fig. 3.3. Interactions between MMs and iEANs do not change early on during *spiB* infection.** (**A** and **B**) C57BL/6J mice were infected with $10^9$ CFU *Salmonella spiB* and analyzed 3 hours post-infection (**A**) Representative confocal IF images from the ileum myenteric plexus using anti-MHC II (green) and anti-ANNA-1 (red). Images representative of n = 5 mice per condition. Scale bars, 50 $\mu$m. (**B**) Quantification of MM intercalation into ileum myenteric plexus ganglia as assessed by confocal IF imaging and calculations based on Imaris software surface functions.

To assess whether inflammatory monocytes recruited from the circulation are involved in infection-induced neuronal damage, we used *Ccr2*$^{-/-}$ mice, which exhibit an impairment in mobilizing inflammatory monocytes into tissues (Boring et al., 1997). *Ccr2*$^{-/-}$ mice failed to clear *spiB* infection, likely reflecting a reduced resistance in the mucosal layer (Dunay et al., 2008), and showed mild acceleration, rather than a delay in GITT 17 days post-infection (Fig. 3.4 A and B). Nonetheless, *Ccr2*$^{-/-}$ mice exhibited similar iEAN loss as WT controls (~25%), suggesting that the persistent luminal pathogen load does not cause an increase in neuronal damage (Fig. 3.4 C). These data also highlight that intestinal macrophages recently differentiated from circulating monocyte precursors may contribute to *spiB* clearance mechanisms but are not required for post-infectious iEAN cell death. The above results suggest a critical response of resident MMs to luminal

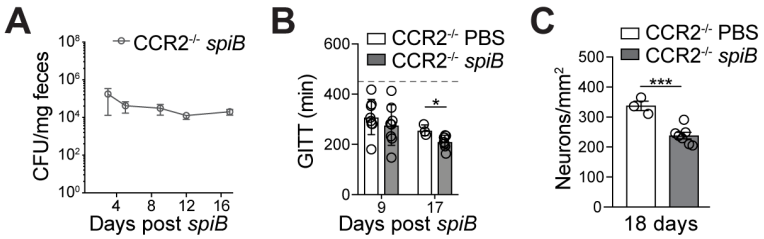


**Fig. 3.4. Inflammatory monocytes do not contribute to iEAN loss post-infection.** (**A** to **C**) CCR2$^{-/-}$ mice were orally infected with *Salmonella spiB* or gavaged with PBS. (**A**) Quantification of fecal CFU; (**B**) Gastrointestinal total intestinal transit time GITT); experiments were ended at 450 min (dashed line); (C) Number of ileum myenteric iEANs. * $P < 0.05$, ** $P < 0.01$, *** $P < 0.001$ as calculated by unpaired t-test.

pathogenic stimulation. While MMs are likely not essential for pathogen resistance mechanisms, they appear to prevent excessive neuronal damage.

### 3.1.2 $\beta_2$-AR signaling in MMs constrains infection-induced inflammation and neuronal death

We previously reported that the tissue-protective gene expression profile of MMs was further enhanced following enteric infection via $\beta_2$-ARs, encoded by *Adrb2* (Gabanyi et al., 2016). We thus next aimed to determine the capacity of $\beta_2$-AR signaling to mediate tissue protection in the context of enteric infections by coupling pharmacological and genetic modulation of this pathway. First, C57BL/6 mice were infected with *spiB* while being treated with a selective $\beta_2$-AR agonist, salbutamol, which was delivered continuously via subcutaneously implanted osmotic pumps for 14 days. We observed no differences in the pathogen load in mice treated with salbutamol (Appendix 2). However, administration of salbutamol protected mice from neuronal loss post-infection (Fig. 3.5 A). To directly assess the role of MMs in the observed salbutamol-mediated protection from neuronal death post-infection, we then depleted MMs using α-CSF1R in mice receiving continuous salbutamol treatment. While we observed a rescue of iEAN death in mice treated with IgG isotype control antibody, MM depletion led to a loss of salbutamol-mediated iEAN protection (Fig. 3.5 B). Taken together, these data suggest that MMs are critical for $\beta_2$-AR-mediated iEAN protection.

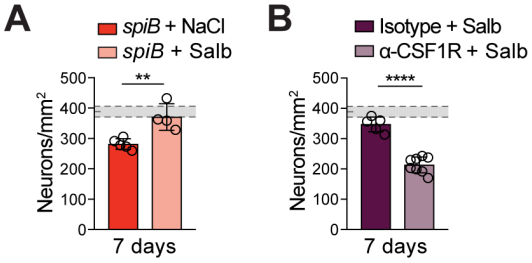


**Fig. 3.5. MMs are critical for $\beta_2$-AR-mediated iEAN protection.** (**A** and **B**) Number of ileum myenteric iEANs of C57BL/6J mice (**A**) continuously receiving NaCl or salbutamol by osmotic pumps for 14 days, and orally gavaged PBS /*spiB* on day 7 of treatment and (**B**) receiving salbutamol as in (**A**), gavaged PBS/*spiB* on day 7 post-pump implantation and receiving anti-CSF1R or control over infection course. Shaded area, mean day 7 iEAN numbers +/- SEM of all control C57BL6/J mice analyzed in Fig. 2.23 B. Samples obtained 7 dpi. ** $P < 0.01$, **** $P < 0.0001$, unpaired t-test.

We complemented these findings using a genetic approach by interbreeding mice carrying *Cre* recombinase under the myeloid *Lyz2* promoter (LysM$^{Cre}$) with *Adrb2*$^{flox/flox}$ mice (LysM$^{\Delta Adrb2}$) (Hinoi et al., 2008). The specificity of *Cre*-targeting of macrophages in the intestinal muscularis was confirmed by immunofluorescence (using HA as a fate-mapping reporter) and TRAP-seq analysis of LysM$^{\Delta Adrb2}$:RiboTag and LysM$^{Adrbfl/}$:RiboTag mice, which demonstrated macrophage-restricted HA expression, enrichment for macrophage-specific genes, and specific loss of *Adrb2* (Fig. 3.6 A to D). Additionally, while we occasionally observed ectopic *Cre* expression in extrinsic ganglia, we were unable to detect iEAN recombination (Fig. 3.6 B). We did not detect infiltrating neutrophils, also targeted by *Lyz2*, in the intestinal *muscularis* at steady state or early post-infection, suggesting that neutrophil-$\beta_2$-AR signaling does not play a major role in this model (*data not shown*). Moreover, we found no differences in GITT or iEAN numbers in LysM$^{\Delta Adrb2}$ as compared to *Cre*- littermate control mice during homeostasis (Fig. 3.7 A and B). Upon *spiB* infection, LysM$^{\Delta Adrb2}$ also exhibited a similar pathogen clearance (Fig. 3.7 C).

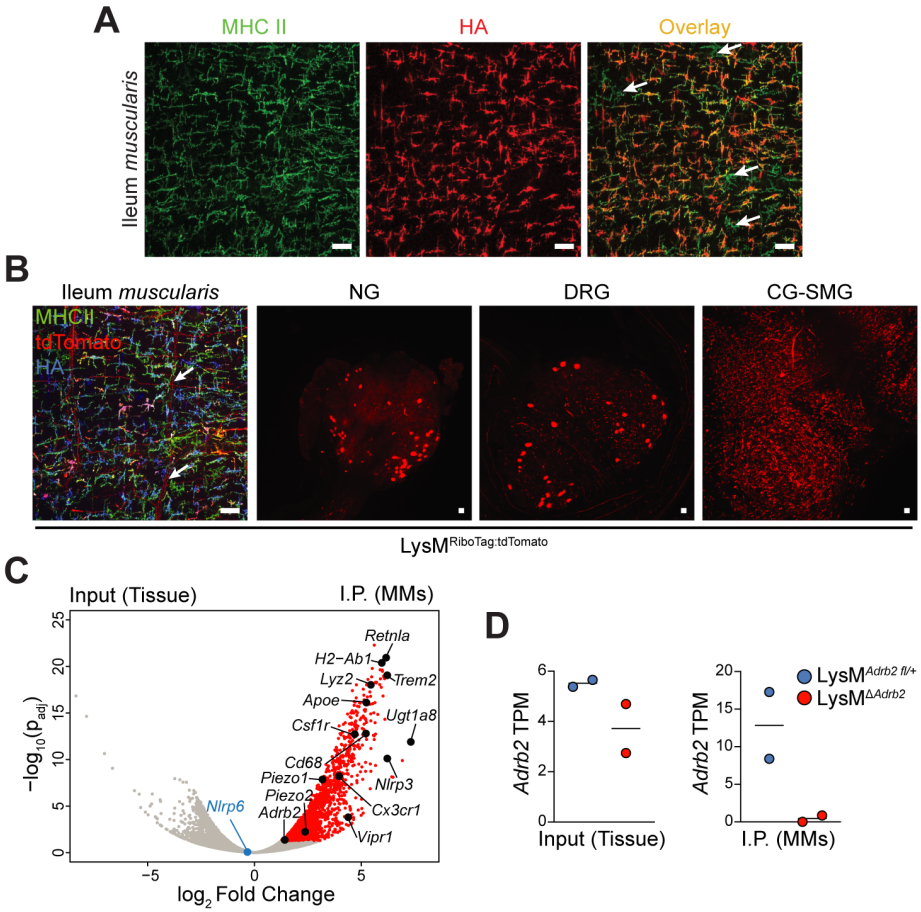


**Fig. 3.6. Specificity of LysM$^{Cre}$ targeting of MMs.** (**A**) IF staining of MMs from the ileum of LysM$^{RiboTag}$ mice using anti-MHC II (green) and anti-hemagglutinin (HA, red) antibodies. White arrows, MHC II+ HA- macrophages. Scale bars, 50 $\mu$m. Images representative of n = 2 mice per group. (**B**) Whole-mount IF images of the ileum myenteric plexus, NG, thoracic DRG, and celiac-superior mesenteric ganglion (CG-SMG) from LysM$^{RiboTag:tdTomato}$ mice, in ileum stained for MHC II (green) and HA (blue). Images representative of n = 4. Scale bars, 50 µm. (**C**) Volcano plot of differential expression analysis (DEseq2) of TRAPseq from LysM$^{Adrb2\text{-}fl/+:RiboTag}$ mice comparing input (ileum tissue) to immunoprecipitated (i.p.) transcripts (red dots). All i.p. samples indicated by red dots are log2 Fold Change > 0.5 and padj > 0.05. Black, relevant macrophage Blue, *Nlrp6* (neuronal specific). (**D**) Transcripts per million (TPM) as calculated by Kallisto alignment of *Adrb2* transcript comparing input (ileum tissue) or i.p. transcripts from LysM$^{Adrb2fl/+:RiboTag}$ and LysM$^{\Delta Adrb2:RiboTag}$ mice.

However, we found that LysM$^{\Delta Adrb2}$ mice had further increased fecal Lcn-2 levels following *spiB* infection as compared to *Cre-* littermates, suggesting a role for myeloid-specific $\beta_2$-AR signaling in the regulation of infection-induced inflammation (Fig. 3.7 D). This enhanced intestinal inflammation was accompanied by further prolonged GITT, which persisted long-term post *spiB* clearance, increased loss of myenteric neurons and enhanced alterations in ileal ring contractility (Fig. 3.7 E to G). To complement these results, and to address whether MMs themselves require intact $\beta_2$-AR signaling to limit neuronal loss, we infected LysM$^{\Delta Adrb2}$ mice and *Cre-* littermates receiving continuous salbutamol treatment. Similar to what we observed in WT C57BL/6 mice, salbutamol treatment in *Cre-* littermate controls carrying an intact $\beta_2$-AR signaling in the myeloid compartment resulted in prevention of infection-induced neuronal loss. By contrast,

salbutamol-treated LysM$^{\Delta Adrb2}$ mice still displayed significant iEAN loss (Fig. 3.7 H). These data establish a role for $\beta_2$-AR signaling in intestinal macrophages that contributes to a neuroprotective program post-enteric infection.

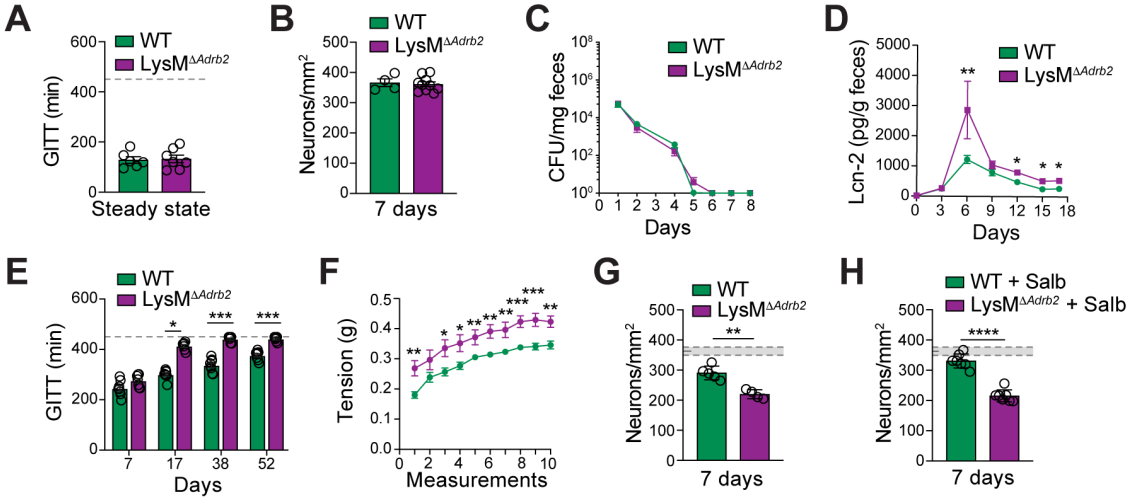


**Fig. 3.7. Loss of $\beta_2$-AR signaling in MMs exacerbates iEAN damage post-infection.** (**A** and **B**) (**A**) Total gastrointestinal transit time (GITT) and (**B**) Number of ileum myenteric iEANs as assessed by IF (ANNA-1) of naïve LysM$^{\Delta Adrb2}$ mice and wild-type (WT) littermates; (**C** to **H**) LysM$^{\Delta Adrb2\ mice}$ and WT littermates were orally infected with *spiB*. (**C**) Fecal colony forming units (CFU), (**D**) Fecal lipocalin-2 (Lcn-2), (**E**) GITT; (**F**) Ileal ring myography assessed on day 53 post-infection (**G** and **H**) Number of ileum myenteric iEANs on day 7 post-*spiB* infection of (G) LysM$^{\Delta Adrb2}$ mice and WT littermates; shaded area indicates mean day 7 iEAN numbers +/- SEM of naïve LysM$^{\Delta Adrb2}$ mice and WT littermates (B); (H) LysM$^{\Delta Adrb2}$ and WT littermates receiving salbutamol via subcutaneous osmotic pumps and infected with *spiB* post-implantation; shaded area indicates mean day 7 iEAN numbers +/- SEM of non-infected LysM$^{\Delta Adrb2}$ and WT littermate mice (A). (A and E) Experiments were ended at 450 min (dashed line). * $P < 0.05$, ** $P < 0.01$, *** $P < 0.001$, **** $P < 0.0001$ as calculated by unpaired t-test or ANOVA with Tukey's posthoc test.

### 3.1.3 An adrenergic-arginase 1-polyamine axis in MMs limits infection-induced neuronal death

To dissect possible mechanisms by which MM $\beta_2$-AR signaling is involved in preventing excessive tissue damage post-infection, we analyzed LysM$^{\Delta Adrb2}$ MM gene expression profiles. MM sorted from *Cre*- littermate controls responded to *spiB* infection by upregulating tissue protective genes upon infection, but we did not observe this upregulation in MMs sorted from infected LysM$^{\Delta Adrb2}$ mice (Fig. 3.8 A and B). Arginase 1

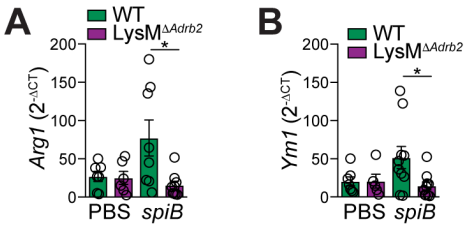


**Fig. 3.8. Loss of tissue-protective gene expression enhancement in LysM$^{\Delta Adrb2}$ mice.** (**A** and **B**) mRNA expression analysis of the indicated genes by quantitative real-time PCR of sorted macrophages isolated from the muscularis of LysM$^{\Delta Adrb2}$ mice and wild-type (WT) littermates 2 hours post-gavage of PBS or -infection with *spiB*. * $P < 0.05$ as calculated by unpaired t-test.

(Arg1) is known to mediate the production of the neuroprotective polyamine spermine (Cai et al., 2002), which in turn was described to suppress NLRP6-Casp1/11 inflammasome activation (Levy et al., 2015). To investigate the participation of

polyamines in iEAN cell death, we supplemented the drinking water of mice infected with *spiB* with spermine or with difluoromethylornithine (DFMO), which inhibits polyamine biosynthesis by selective and irreversible inhibition of ornithine decarboxylase 1 (ODC1), the rate-limiting enzyme of polyamine synthesis (Koomoa et al., 2013). Bacterial load and clearance patterns were similar in either treatment condition. However, mice that received DFMO exhibited enhanced neuronal loss, while those receiving spermine exhibited a significant rescue of neuronal loss post *spiB* infection (Fig. 3.9 A and B, and Appendix 2).

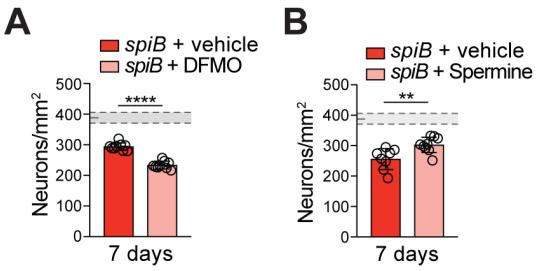


**Fig. 3.9. Polyamines are important for iEAN protection post-infection.** (**A** and **B**) Number of ileum myenteric iEANs on 7 dpi with *spiB* of C57BL/6J mice receiving regular drinking water or water supplemented with (**A**) difluoromethylornithine (DFMO) (**B**) spermine over the course of infection. Shaded area bounded by dashed lines, mean day 7 iEAN numbers +/- SEM of all control C57BL6/J mice Fig 2.23 B; ** $P < 0.01$, **** $P < 0.0001$, unpaired t-test.

Finally, we genetically addressed whether Arg1 activity in MMs was required for their protective role in infection-induced neuronal death in the intestine by interbreeding LysM$^{Cre}$ and *Arg1*$^{flox/flox}$ mice (El Kasmi et al., 2008). Similar to our observations in LysM$^{\Delta Adrb2}$ mice, we did not observe differences in iEAN numbers in LysM$^{\Delta Arg1}$ mice as compared to *Cre*- littermates during homeostasis (Fig. 3.10 A). Upon *spiB* infection, LysM$^{\Delta Arg1}$ animals also exhibited similar pathogen load and clearance patterns, but a trend to increased GITT (Fig. 3.10 B and Appendix 2). However, loss of Arg1 in the myeloid compartment heightened iEAN loss following *spiB* infection (Fig. 3.10 C). Together, these results point to a functional role for $\beta_2$-AR-Arginase 1-polyamine axis in MM-mediated tissue protective program in limiting infection-induced enteric neuronal cell death.

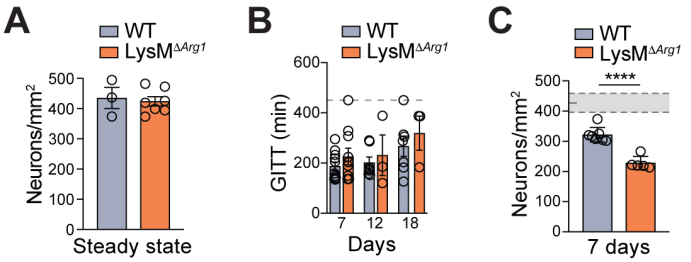


**Fig. 3.10. iEAN protection by MMs is dependent on MM *Arg1*.** (**A** to **C**) LysM$^{\Delta Arg1}$ mice and WT littermates were analyzed. (**A**) Number of ileum myenteric iEANs at steady state, (**B**) total gastrointestinal transit time (GITT) on the indicated days post-*spiB* infection, and (**C**) Number of ileum myenteric iEANs on day 7 post-*spiB* infection; Shaded area indicates mean day 7 iEAN numbers +/- SEM of non-infected LysM$^{\Delta Arg1}$ mice and WT littermates (A); **** $P < 0.0001$ as calculated by unpaired t-test.

## 3.2 Enteric pathogens induce tissue tolerance and prevent neuronal loss from subsequent infections

### 3.2.1 *Y. pseudotuberculosis* infection induces iEAN protection in subsequent infection

Given the significant reduction in ileal and colonic myenteric neurons resulting from a single oral *spiB* infection, we next sought to determine whether subsequent enteric infections would result in exacerbated iEAN loss and functional changes.

Following clearance of *spiB,* we infected mice with WT *Salmonella* Typhimurium, after which we observed no additional loss of iEANs, indicating a possible restructuring or adaptation of tissue cells preventing further damage (Fig. 3.11 A). To exclude the contribution of adaptive immunological memory, since both primary and secondary infections were with strains of *Salmonella* Typhimurium, we next asked whether primary infection with an unrelated bacterial pathogen influences the tissue's response to a subsequent exposure to *Salmonella spiB*. We used *Y. pseudotuberculosis* (*YP*), which, like *spiB*, localizes to the ileum and colon, and also resulted in significant, albeit more subtle, iEAN loss (Chapter 2, Fig 2.24 B) Primary infection with *YP* resulted in iEAN protection against secondary challenge with *spiB*, and conversely, initial iEAN loss with primary *spiB* infection was not enhanced by heterologous *YP* exposure (Fig. 3.11 B). This was not a result of an improved resistance to primary as mice previously infected with *YP* displayed similar pathogen load and clearance pattern to naïve mice (Fig. 3.11 C). This prevention of infection-induced neuronal loss by previous exposure to heterologous pathogens suggests that a form of tissue "trained tolerance" may play a role in limiting enteric neuronal damage.

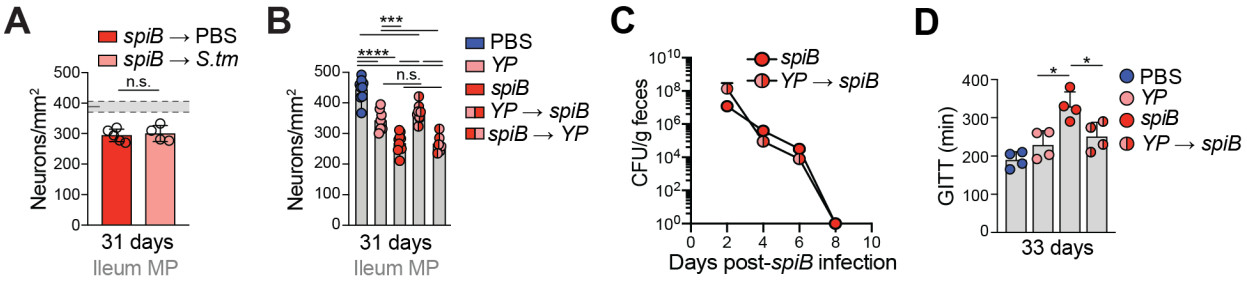


**Fig. 3.11. Enteric bacterial infections induce iEAN protection against secondary ones.** (**A**) Neuronal quantification (ANNA-1 staining) in the ileum myenteric plexus of C57BL/6J mice orally gavaged PBS or wild-type *Salmonella* Typhimurium (S. tm) 21 days post-*spiB* infection and sacrificed on day 10 post-secondary infection. Shaded area indicates mean day 7 iEAN numbers +/- SEM of all control C57BL6/J mice (Fig. 2.23 B). (**B** to **D**) (**B**) Neuronal quantification in the ileum myenteric plexus, (**C**) Quantification of fecal *spiB* CFU and (**D**) Total gastrointestinal transit time of C57BL/6J mice orally gavaged with PBS, *Y. pseudotuberculosis* (*YP*), *spiB*, or *spiB/YP* followed by infection with *YP/spiB*, respectively 21 days later and analysed 10/12 days post-secondary infection. n.s. – not significant, ** $P < 0.01$, *** $P < 0.001$, **** $P < 0.0001$ as calculated by unpaired t-test or one-way ANOVA with Tukey's posthoc test.

Disease tolerance strategies alleviate fitness cost by promoting resilience in the presence of an insult (Ayres, 2020). Because one of the main roles of the ENS in regard to host fitness is the control of intestinal motility, and we demonstrated impairment, i.e.,

prolongation, thereof following infection (Chapter 2.3), we again measured GITT as a functional readout for neuronal loss. While *spiB* infection led to increased GITT, previous *YP* infection preserved gut motility after subsequent *spiB* challenge (Fig. 3.11 D). These results point to development of tissue-, or disease tolerance (Ayres, 2020; Martins et al., 2019) post-bacterial infection, preventing neuronal loss to subsequent infection with a different pathogen.

Since we established a role for MMs in limiting infection-induced neuronal damage via $\beta_2$-AR- and Arg1 signaling (Chapter 3.1), we next sought to test whether *YP*-induced tolerance also relied on this pathway. We first depleted MMs using anti-CSF1R (Fig. 3.1 above). Administration of anti-CSF1R to mice post-*YP* clearance led to a pronounced iEAN loss following challenge with *spiB*, suggesting a requirement for MMs in maintaining *YP*-induced neuronal protection (Fig. 3.12 A). Flow cytometric analysis of the ileum of mice after primary infection revealed that *YP* infection leads to the increased frequency of Arg1-expression by MMs beyond a basal level (Fig. 3.12 B and C). Heightened Arg1 expression by MMs was required for *YP*-induced neuroprotection, as *YP*-mediated neuroprotection was abolished in LysM$^{\Delta Arg1}$ following challenge with *spiB* (Fig. 3.12 D). Moreover, this neuroprotective mechanism also required $\beta_2$-AR expression by MMs, as LysM$^{\Delta Adrb2}$ mice previously infected with *YP* showed significant neuronal loss compared to wild-type littermate control mice upon *spiB* infection, which correlated with decreased

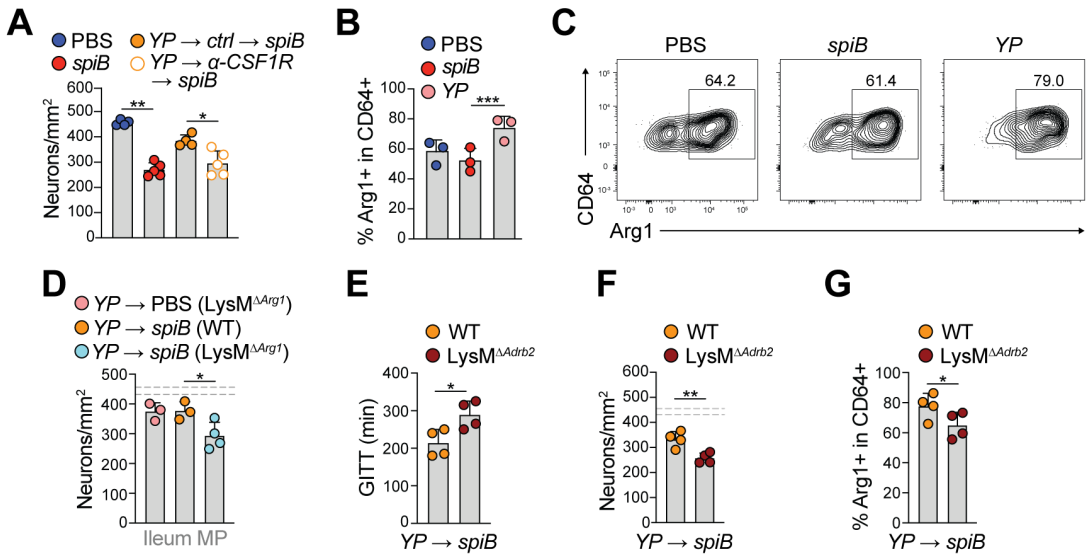


**Fig. 3.12. iEAN protection induced by primary bacterial infection is dependent on MM *Adrb2* and *Arg1*.** (**A**) C57BL/6J mice were orally gavaged with PBS, *spiB* or *YP*. At 20 dpi *YP*-infected mice were treated with anti-CSF1R or IgG isotype control, followed by oral gavage with *spiB*. Ileum myenteric iEANs were quantified on day 7 post-secondary infection. (**B** and **C**) Flow cytometric analysis of Arg1-expressing macrophages isolated from ileum muscularis on day 14 post-infection with *YP* or *spiB*. (**D**) Quantification of ileum myenteric plexus neurons of LysM$^{\Delta Arg1}$ mice and WT littermates orally gavaged with *YP* only or *YP* followed by *spiB* 21 days later. (**E** to **G**) LysM$^{\Delta Adrb2}$ (*Cre+*) mice and WT (*Cre-*) littermates were orally gavaged with *YP* and 21 days later with *spiB*. (**E**) Total gastrointestinal transit time (**F**) Number of ileum myenteric iEANs and (**G**) Arg1 expression by MMs 7 days post-secondary infection as determined by flow cytometry. Areas bounded by dashed lines indicate neuron numbers of range non-infected control LysM$^{\Delta Arg1}$ (D) and (F) LysM$^{\Delta Adrb2}$ mice as defined by mean ± SEM of a large set of control C57BL/6J mice. * $P < 0.05$, ** $P < 0.01$, *** $P < 0.001$, **** $P < 0.0001$ as calculated by unpaired t-test or one-way ANOVA with Tukey's posthoc test.

Arg1 expression by MMs and increased GITT (Fig. 3.12 E to G). These effects were not a result of a failure to clear *spiB*, as bacterial load was not affected by these strategies (*data not shown*). Together, these results indicate that primary bacterial infection results in a state of disease tolerance that mediates neuroprotection to subsequent infections, preserving intestinal motility.

### 3.2.2 *S. venezuelensis* infection induces long-term iEAN protection during subsequent infections

Because helminth infections typically induce a very distinct immune response from that of bacterial pathogens, we next asked whether they too, could prevent infection-induced neuronal loss. We chose to infect mice with *Strongyloides venezuelensis* (*SV*), a parasitic nematode that causes an acute infection, primarily localizes to the duodenum (Esterhazy et al., 2019; Silveira et al., 2002) and did not lead to iEAN loss in the duodenum or ileum (Chapter 2, Fig. 2.24 H). Primary duodenal *SV* infection, which was cleared from the intestine within 12 days, did not alter bacterial clearance in a subsequent *spiB* challenge (Fig. 3.13 A and B). However, it completely prevented ileal iEAN loss and resulted in the maintenance of normal gut motility (Fig. 3.13 C to E).

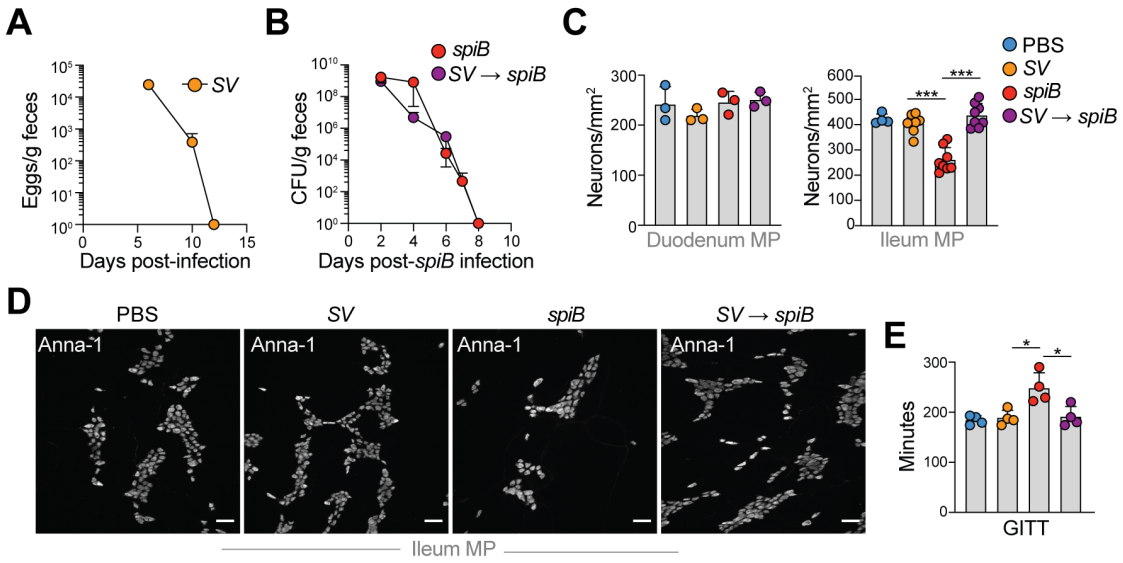


**Fig. 3.13. *S. venezuelensis* infection induces protection against secondary bacterial infection.** (**A** to **E**) C57BL/6J mice were subcutaneously injected with water and then orally gavaged with PBS (non-infected, NI) or infected with $10^9$ colony-forming units (CFU) of *Salmonella spiB*, 700 *SV* larvae only or *SV* and 14 days later with *spiB*. (**A**) Quantification of fecal *SV* eggs (primary infection) (**B**) Quantification of fecal *spiB* CFU post-secondary infection. (**C**) Neuronal quantification in the duodenum or ileum myenteric plexus (MP) assessed by IF staining (ANNA-1) on day 8 post-secondary infection. (**D**) Representative IF images of (C); Scale bars, 50 $\mu$m. (E) Total GI transit time measured on day 7 post-secondary infection. * $P < 0.05$, ** $P < 0.01$, *** $P < 0.001$ as calculated by one-way ANOVA with Tukey's posthoc test.

Like primary bacterial infection, *SV*-induced tolerance depended on MMs, as anti-CSF1R-mediated depletion of MMs post-*SV* clearance abolished the neuroprotection upon *spiB* infection (Fig. 3.14 A). In line with our observations post-primary *YP* infection, following *SV* challenge ~80% of MMs expressed Arg1, compared to ~60% observed after

*spiB* infection (Fig. 3.14 B and C). Of note, MMs in the duodenum expressed heightened Arg1 already at steady state compared to the ileum, which was not further increased following *spiB* or *SV* infection (Fig. 3.14 B).

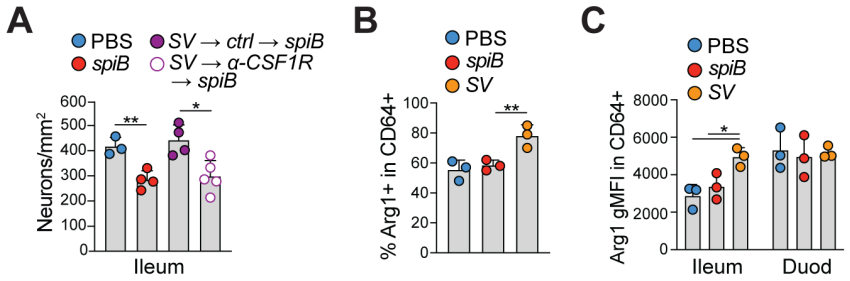


**Fig. 3.14. *S. venezuelensis* induced protection is dependent on MMs.** (**A**) C57BL/6J mice were orally gavaged with PBS or infected with *spiB* or *SV*. At 14 dpi *SV*-infected mice were treated with anti-CSF1R or IgG isotype control, followed by oral gavage with *spiB*. Ileum myenteric plexus neurons were quantified 7 days post-*spiB* infection. (**B** and **C**) Flow cytometric analysis of Arg1-expressing MMs 14 dpi with *SV* or *spiB* isolated from (**B**) ileum (as a percentage of CD64+) and (**C**) duodenum and ileum frequencies (as gMFI of CD64+). * $P < 0.05$, ** $P < 0.01$ as calculated by one-way ANOVA with Tukey's posthoc test. gMFI, geometric mean fluorescence intensity.

LysM$^{\Delta Arg1}$ mice previously infected with *SV* exhibited significant neuronal loss following secondary *spiB* infection, in contrast to wild-type controls (Fig. 3.15 A). However, *SV*-mediated iEAN protection to subsequent *spiB* infection was maintained in LysM$^{\Delta Adrb2}$ mice, which correlated with sustained high frequency of Arg1-expressing MMs,

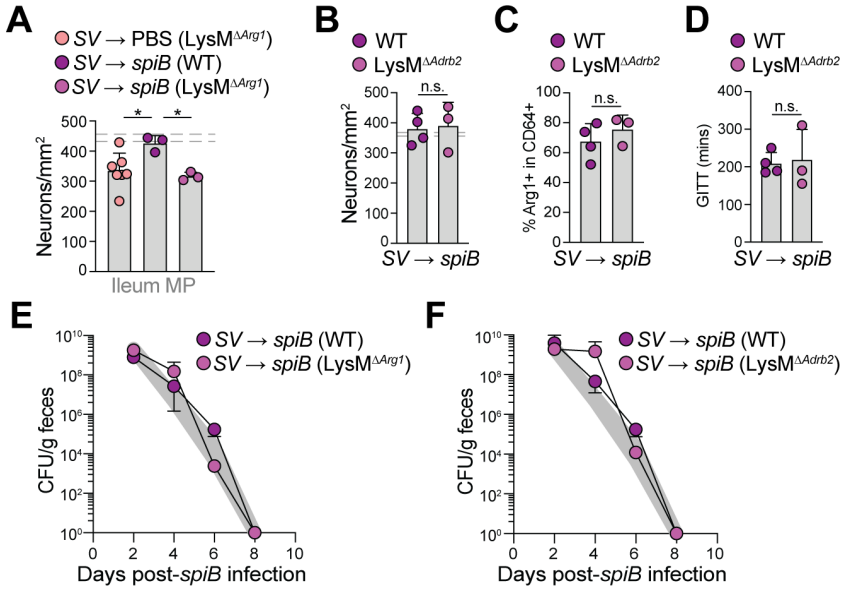


**Fig. 3.15. *SV* induced protection is dependent on MM *Arg1* but not *Adrb2*.** (**A** and **B**) Number of ileum myenteric iEANs of controls or (**A**) LysM$^{\Delta Arg1}$ mice orally gavaged with *SV* only or followed by *spiB* 14 days later, or (**B**) LysM$^{\Delta Adrb2}$ mice orally gavaged with *SV* and 14 days later with *spiB*, and analyzed on day 7 post-spiB infection. (**C** and **D**) Quantification of fecal CFU of controls and (**C**) LysM$^{\Delta Arg1}$ or (**D**) LysM$^{\Delta Adrb2}$ mice infected with *SV* and 14 days later with *spiB*. Shaded area indicates range of *spiB* CFU defined by mean ± SEM of a large set of *spiB*-infected C57BL/6J mice. n.s. – not significant, * $P < 0.05$, ** $P < 0.01$ as calculated by unpaired t-test or one-way ANOVA with Tukey's posthoc test.

and maintenance of a normal GITT (Fig. 3.15 B to D). Moreover, initial infection with *SV* infection did not affect *spiB* load and clearance in LysM$^{\Delta Arg1}$ and LysM$^{\Delta Adrb2}$ mice (Fig. 3.15 E and F). These results indicate that, while converging on neuroprotective MMs, *YP*- and *SV*-induced disease tolerance mechanisms are distinct. Of note *SV*-mediated neuroprotection was fully maintained when challenged with *spiB* up to 12 weeks post-*SV* clearance, and partially up to 24 weeks post-infection, which correlated with sustained high frequency of Arg1-expressing in MMs observed up to 12 weeks post-infection (Fig. 3.16 A and B). These results reveal a long-term neuroprotection in the ileum induced by a single duodenal helminth infection.

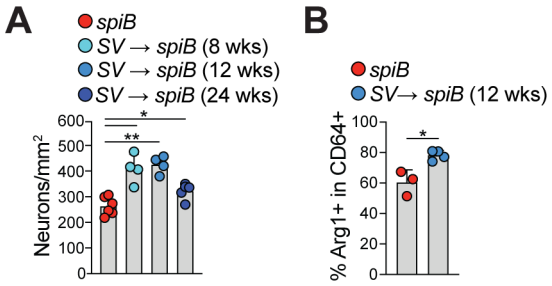


**Fig. 3.16. *SV* induces long-term tissue protection.** (**A** and **B**) C57BL/6J mice were orally gavaged with *spiB* only or *SV* followed by *spiB* on the indicated timepoints post-*SV*. Tissue was analyzed 10 days post-*spiB* infection. (**A**) Neuronal quantification in the ileum myenteric plexus. (**B**) Arg1 expression by MMs in the ileum as determined by flow cytometry.

### 3.2.3 Immune response to helminths is associated with iEAN protection during subsequent infection

To identify a mechanism responsible for the long-term helminth-driven disease tolerance, we next further characterized the immune response to *SV*. Helminths are known to drive a robust type-2 immune response, with accumulation of innate immune cells, including tuft cells, eosinophils, mast cells, group 2 innate lymphoid cells (ILC2), and later CD4$^+$ T helper 2 (T$_h$2) cells (Maizels, 2020; O'Leary et al., 2019; Vivier et al., 2018). We found significantly increased frequencies of mucosal mast cells and eosinophils in the lamina propria (LP) and intraepithelial (IE) compartments of duodenum and ileum upon *SV* infection (Fig. 3.17 A to D).

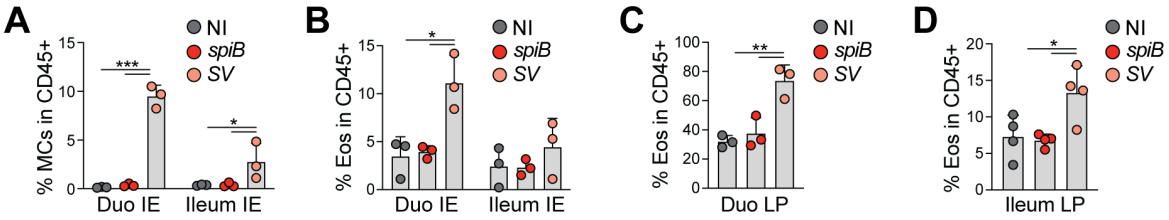


**Fig. 3.17. Innate immune response to helminths is associated with iEAN protection during *SV* infection.** (**A** to **D**) C57BL/6J mice were subcutaneously injected with water (non-infected, NI) or infected with *spiB* or *SV*, and analyzed on day 14 post-infection. (**A**) Frequencies of duodenum IE and LP mast cells. (**B**) Frequencies of duodenum and ileum IE eosinophils. (**C** and **D**) Frequency of (**C**) duodenum and (**D**) ileum LP eosinophils. IE – intraepithelial compartment, LP – lamina propria; * $P < 0.05$, ** $P < 0.01$, *** $P < 0.001$ as calculated by one-way ANOVA with Tukey's posthoc test.

We then assessed whether these two main innate immune cell types that accumulate during helminth infections, play a role in *SV*-induced neuroprotection. To address a possible role for mast cells, which predominantly accumulated in the duodenal

IE compartment (Fig. 3.17 A), we generated a CRISPR-based *knock-in* strain in which human diphtheria toxin receptor (hDTR) and the tdTomato fluorescent protein are expressed under the promoter of *carboxypeptidase A3* (*cpa3*), a gene preferentially active in mast cells (Lilla et al., 2011). Administration of diphtheria toxin (DT) after initial *SV* infection led to a significant reduction in mast cell numbers (Fig. 3.18 A). Consistent with a role for mast cells in resistance to helminths, diphtheria toxin (DT)-treated mice exhibited a significant delay in *SV* clearance (Fig. 3.18 B). However, we found similar iEAN numbers in *SV*-infected DT-treated *cpa3*$^{\text{DTR-tdTomato}}$ and control mice upon subsequent *spiB* challenge, suggesting that mast cells are dispensable for *SV*-induced neuroprotection (Fig. 3.18 C).

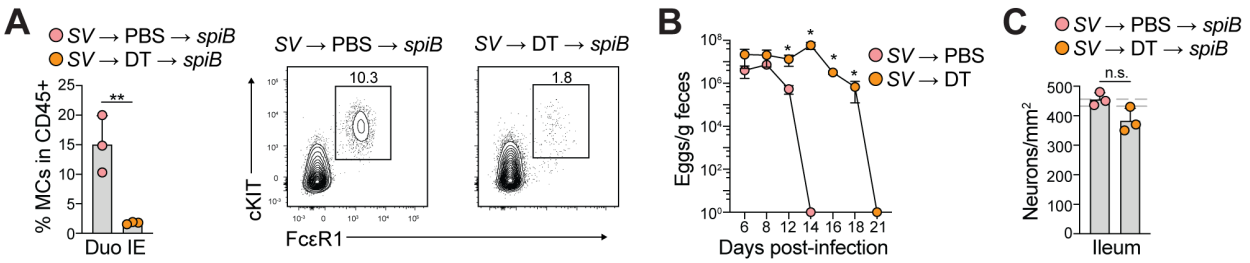


**Fig. 3.18. Mast cells are required for *SV* clearance, but not iEAN protection.** (**A** to **D**) *cpa3*$^{\text{DTR-tdTomato}}$ mice and WT littermates were infected with *SV*, treated with diphtheria toxin (DT) on days 0, 1, 4, 7, 10, 13, 16 and 18 post-infection, and subsequently infected with *spiB* on day 21 post-*SV* infection. (**A**) Left, frequency of duodenum IE mast cells (MCs) on day 7 post-*spiB* as determined by flow cytometry; right, representative flow cytometry plot. (**B**) Fecal *SV* egg load. (**C**) Number of ileum myenteric iEANs on day 7 post-*spiB* infection. IE – intraepithelial compartment, LP – lamina propria; * $P < 0.05$, ** $P < 0.01$ as calculated by unpaired t-test.

Next, to determine a possible iEAN protective role for eosinophils, we used a genetic mouse model in which hDTR is expressed in the eosinophil peroxidase locus (iPHIL) (Jacobsen et al., 2014). DT administration to *SV*-infected iPHIL mice significantly reduced eosinophil numbers in duodenum and ileum LP (Fig. 3.19 A and B). Depletion of eosinophils did not affect *SV* clearance, but abolished *SV*-induced neuroprotection upon *spiB* infection (Fig. 3.19 C and D). This correlated with decreased expression of Arg1 by MMs along with dysmotility (Fig. 3.19 E and F). By contrast, *YP*-induced neuronal protection was not affected by depletion of eosinophils (Fig. 3.20 A and B). Thus, eosinophils are required for enteric neuroprotection induced by primary helminth- but not bacterial infection. We conclude that the intestinal tissue co-opted pathways induced by distinct pathogens into a convergent tissue macrophage phenotype that mediates enteric neuronal protection, aiding host fitness.

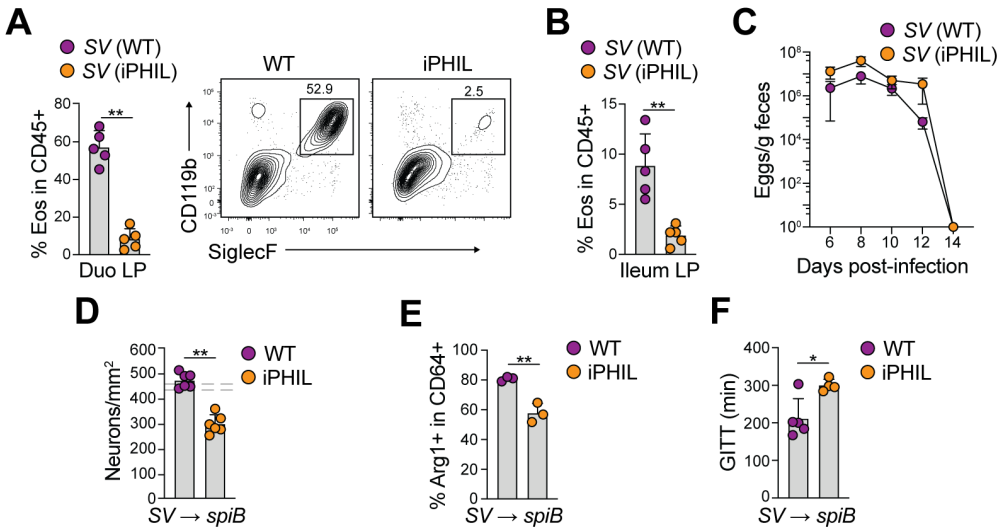


**Fig. 3.19. Eosinophils are required for iEAN protection after *SV* infection.** (**A** to **C**) iPHIL mice and WT littermates were infected with *SV*, treated with diphtheria toxin (DT) on day 0, 1, 4, 6 and 8 post-infection, and analyzed on day 10 post-*SV*. (**A** and **B**) Frequency of (**A**) duodenum and (**B**) ileum LP eosinophils. (**C**) Quantification of fecal *SV* egg load. (**D** to **F**) iPHIL mice and WT littermates were infected with *SV*, treated with diphtheria toxin (DT) on days 0, 1, 4, 7, 10, 13, 16 and 18 post-infection, and subsequently infected with *spiB* on day 14 post-*SV*. (**D**) Number of ileum myenteric iEANs on day 7 post-*spiB*. (**E**) Arg1 expression by ileum MMs on day 7 post-*spiB*. (**F**) Total GI transit time (GITT) measured on day 10 post-*spiB*. IE – intraepithelial compartment, LP – lamina propria; * $P < 0.05$, ** $P < 0.01$ as calculated by unpaired t-test.

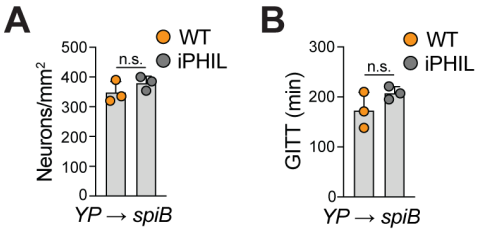


**Fig. 3.20. *YP*-induced iEAN protection is not affected by depletion of eosinophils.** (**A** and **B**) iPHIL mice and WT littermates were infected with *SV*, treated with DT on days 0, 1, 4, 7, 10, 13, 16 and 18 post-infection, and subsequently infected with *spiB* on day 21 post-*SV*. (**A**) Number of ileum myenteric iEANs 7 days post-*spiB* infection. (B) Total GI transit time (GITT) 10 days post-*spiB* infection. n.s. – not significant; * $P > 0.05$ as calculated by unpaired t-test.

## 3.3 Crosstalk between the microbiota, gut-extrinsic sympathetic nervous system and immune cell populations

In addition to the ENS-intrinsic autonomous control of intestinal function, connections between the gut and the brain monitor the intestinal tissue and its microbial and dietary content (Furness et al., 2013), modulating both intestinal physiological functions such as nutrient absorption and motility (Han et al., 2018; Williams et al., 2016), and brain-wired feeding behaviour (Han et al., 2018). Thus, circuits may exist to detect gut microbes – commensal and pathogenic ones – and relay signals to extra-intestinal sites, which, in turn, regulate GI physiology (Fung et al., 2017).

We established above that the neuro-protective effect of MMs during enteric bacterial infections is mediated via sensing of sympathetic signals. Additionally, our laboratory had previously shown that extrinsic, gut-projecting sympathetic neurons (sympathetic eEANs) are activated during acute enteric infections, opening up the possibility that eEANs relay signals to or control the activation of tissue-resident immune cells in this context. However, whether and how eEANs are involved in sensing luminal cues, transmitting information, and mediating top-down effector functions on gut-resident cells is thus far unclear. We thus aimed to further characterize extrinsic, gut-projecting neurons, determine how they are influenced by the gut microbiota, and investigate their role in the response to enteric infections.

### 3.3.1 The intestinal microbiota modulates gut-projecting extrinsic sympathetic neurons

Extrinsic enteric-associated neurons (eEANs), comprised of sensory afferents and autonomic efferents, are equipped to sense multiple areas of the intestine simultaneously, transmit information to other tissues, and complement intrinsic EANs (iEANs) in controlling gut function (Veiga-Fernandes and Mucida, 2016). We first sought to better characterize the connections of eEANs and whether their activity or gene expression is influenced by the gut microbiota.

To identify the location of eEAN cell bodies, we injected a fluorescent retrograde tracer, cholera toxin beta subunit (CTB), into the wall of different intestinal segments, and dissected extrinsic ganglia that project to the gut, specifically the sensory nodose ganglion (NG) and dorsal root ganglia (DRG), and the sympathetic celiac-superior mesenteric (CG-SMG) ganglion (Fig. 3.21 A to D). Individual CTB tracing from intestinal regions highlighted left versus right nodose bias, and an increasing density of sympathetic

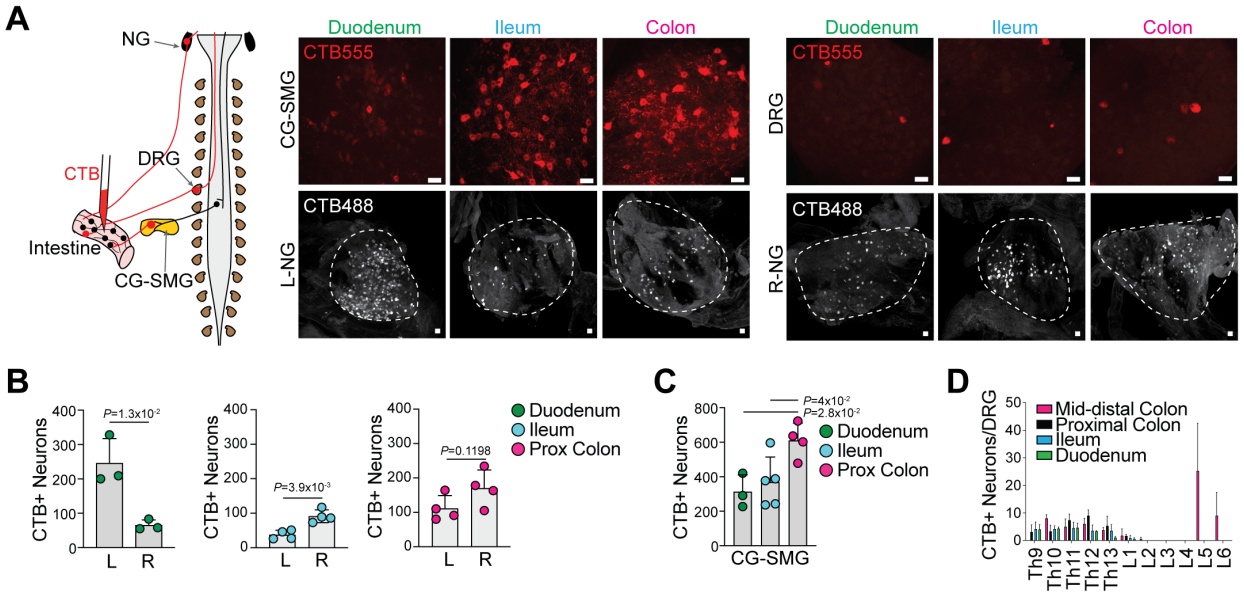


**Fig. 3.21. Distribution of eEAN innervation of the small and large intestines.** (**A**) Left, scheme depicting retrograde CTB555 or CTB488 tracing from intestinal regions to the CG-SMG, left (L) and right (R) NG, and DRG Th10 of C57BL/6J SPF mice. (Right) Representative confocal images of tracing from duodenum, ileum, and colon. (**B** and **C**) Number of CTB+ neurons per (**B**) L-NG and R-NG or (**C**) CG-SMG retrograde labelled from the duodenum, ileum, and proximal colon. (**D**) Distribution of labelled neurons in the averaged pairs of DRGs of mice injected with CTB555 in the indicated intestinal segments.

innervation moving from proximal to distal intestine. Simultaneous CTB tracing from different gut regions illustrated that sensory and sympathetic innervation of these anatomically distinct intestinal regions is mediated by non-overlapping peripheral neuronal cell populations (Fig. 3.22 A and B). These results highlight the compartmentalization of both sensory and effector eEANs projecting to the intestine. We

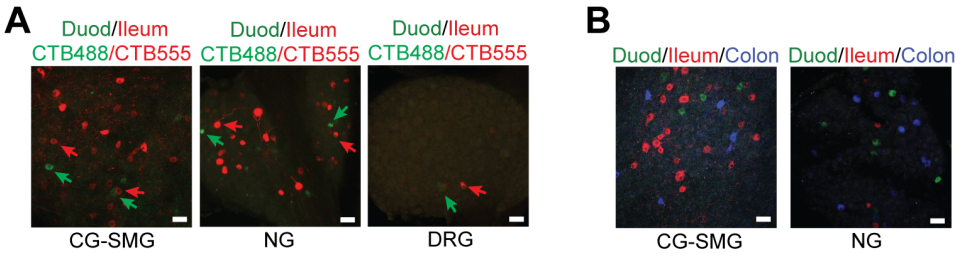


**Fig. 3.22. Compartmentalization of eEANs projecting to the intestine.** (**A**) Dual and (**B**) triple CTB tracing from the indicated intestinal segments into the CG-SMG, NG and DRG with CTB488 (duodenum), CTB555 (ileum), and CTB647 (colon, B) of C57BL6/J SPF mice.

next characterized microbial-mediated changes in eEAN gene expression by transcriptionally profiling ganglia identified by CTB-tracing using translating ribosomal affinity purification (TRAP, Chapter 2.1) (Heiman et al., 2014) of germ-free (GF) and specific pathogen-free (SPF) *Snap25*$^{RiboTag}$ mice. Neuronal HA expression in eEAN ganglia was not altered under gnotobiotic conditions (Fig. 3.23 A and B). We then perfor-

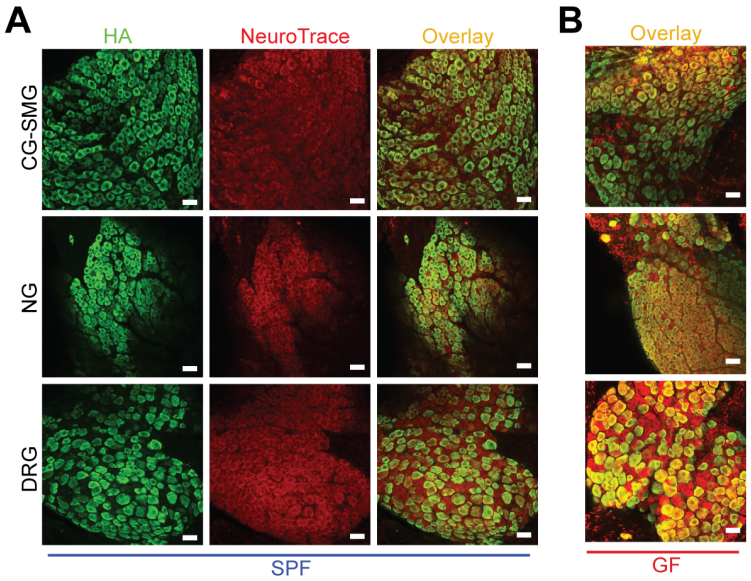


**Fig. 3.23. Neuronal HA expression is not altered in GF mice.** (**A** and **B**) Immunofluorescence images of the nodose ganglion (NG), CG-SMG, and dorsal root ganglion (DRG) Th10 from *Snap25*$^{RiboTag}$ SPF mice using anti-hemagglutinin (HA, in green) antibody and NeuroTrace (red). Scale bars = 50 $\mu$m.

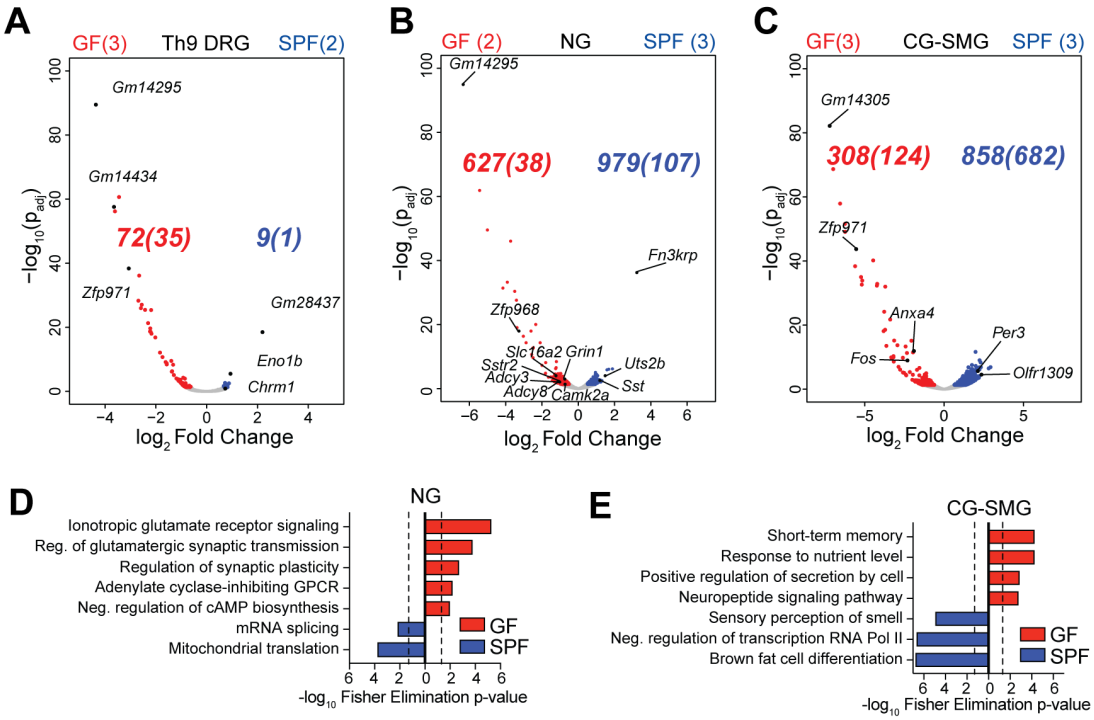


**Fig. 3.24. Gene expression changes in eEAN populations of GF mice.** (**A** to **C**) Volcano plots of differentially expressed genes in the (**A**) Th9 DRG, (**B**) NG and (**C**) CG-SMG of GF and SPF *Snap25*$^{RiboTag}$ mice. (**D** and **E**) Gene ontology pathways, enriched in *Snap25*$^{RiboTag}$ GF vs SPF (**D**) NG or (**E**) CG-SMG. (A to C) Number (n) of independent biological samples analysed are indicated in parentheses. Red/blue dots = $\log_2$ Fold Change > 0.5. Italicized parentheses = $\log_2$ Fold Change > 1. padj = two-tailed Benjamini and Hochberg test p-value of two-tailed Wald test p-value < 0.05. (D and E) padj = two-tailed Benjamini and Hochberg test p-value of two-tailed Wald test p-value < 0.05. Dashed lines represent threshold of significance (1.3) as calculated by one-tailed Fisher's test with an elimination algorithm.

med TRAP-seq of the NG, thoracic 9 DRG, and CG-SMG isolated from and GF and SPF *Snap25*$^{RiboTag}$ mice. We observed no substantial changes in expression of actively-translated genes in the DRG between SPF and GF groups (Fig. 3.24 A). Gene ontology (GO) analysis of the NG suggested an enrichment for genes associated with synaptic signalling and neuronal activation in GF mice (Fig. 3.24 B and D). Additionally, the CG-SMG from GF animals displayed enriched GO pathways for plasticity and signalling, with significantly higher transcript levels of *Fos* (Fig. 3.24 C and E), a neuronal immediate-early gene and indirect marker for neuronal activity (Mei et al., 2001).
IF analysis confirmed that CG-SMGs isolated from GF mice displayed significantly more cFos+ neuronal nuclei than their SPF counterparts (Fig. 3.25 A and B). Of note, low levels of cFos in SPF mice were not driven by facility-specific microbial compositions, as SPF mice obtained from different institutions displayed comparable levels thereof (Fig. 3.25 B) These data indicate that absence of a microbiota results in elevated levels of gut-extrinsic sympathetic activity.

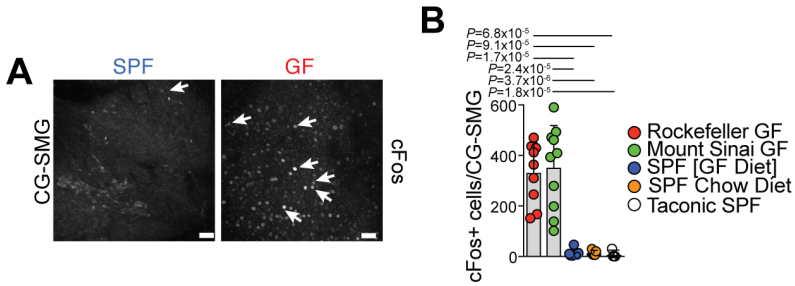


**Fig. 3.25. Increased cFOS levels in gut-sympathetic ganglia of GF mice.** (**A**) IF images of the CG-SMG from C57BL/6J GF and SPF mice using anti-cFos antibody. White arrows, cFos+ nuclei. Images representative of GF and SPF mice on GF diet. Scale bars = 50 $\mu$m. (**B**) Numbers of cFos+ neurons in the CG-SMG of C57BL/6J GF mice from Rockefeller or Mount Sinai animal facilities, compared to SPF mice on GF diet or normal chow, and Taconic SPF mice on normal chow. One-way ANOVA with Tukey multiple comparisons.

### 3.3.2 Dysbiosis triggers gut sympathetic activation

To address whether specific microbes could mediate tonic suppression of CG-SMG neurons, we used multiple microbial manipulation strategies. Fecal transfer from SPF donors into GF mice restored CG-SMG neuronal cFos to levels comparable to SPF conditions, suggesting that the microbiota can suppress gut-extrinsic sympathetic neurons (Fig. 3.26 A). The mere presence of live bacteria was not enough to suppress gut-projecting sympathetic activation, as mono-colonization of GF mice with Segmented Filamentous Bacteria (SFB), *Akkermansia muciniphilia* or *Bacteroides fragilis* did not result in reduced cFos levels in the CG-SMG, while colonization of GF mice with defined bacterial consortia led to SPF levels (Fig. 3.26 B and C). By contrast, microbiota depletion of SPF mice using broad-spectrum antibiotics resulted in increased cFos+ neurons in the CG-SMG (Fig. 3.26 D and E). Treatment with individual antibiotics was sufficient to drive sympathetic cFos, overall suggesting that specific subsets of bacteria are able to suppress cFos activation (Fig. 3.26 F). Additionally, a single oral gavage of streptomycin

resulted in CG-SMG neuronal activation 24h post-gavage, which correlated with shifts in gut microbial composition, and returned to basal levels five days post-treatment (Fig. 3.26 G to I).

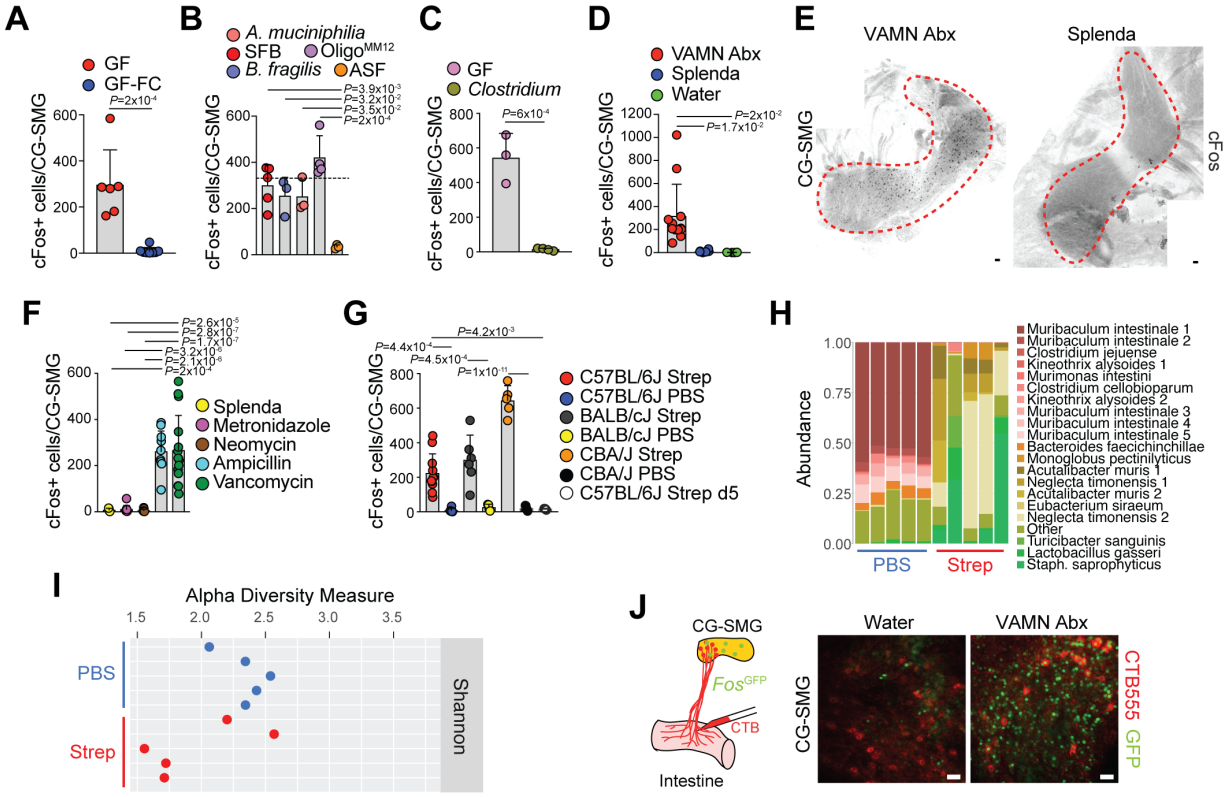


**Fig. 3.26. Sympathetic activation of GF and microbially depleted mice can be suppressed by specific microbes.** (**A** to **D**) Number of cFos+ neurons in the CG-SMG of (**A**) C57BL/6J GF mice and GF mice colonized with feces from SPF (fecal colonization, FC) mice 2 weeks prior to analysis, (**B**) C57BL/6J SFB, *A. muciniphilia*- or *B. fragilis*-mono-colonized mice, and Oligo$^{MM12}$ or ASF consortia-colonized mice, (**C**) C57BL/6J GF mice and GF mice colonized with *Clostridium spp.* consortia from Weill Cornell vivaria, (**D**) C57BL/6J SPF mice treated for 2 weeks with vancomycin, ampicillin, metronidazole, and neomycin (VAMN) in drinking water as compared to Splenda (sucralose-based artificial sweetener)-and water-treated mice. (**E**) Immunofluorescence of the CG-SMG from C57BL/6J SPF mice treated with VAMN or Splenda, using anti-cFos antibody. Images representative of n=6 ganglia. (**F** and **G**) Number of cFos+ neurons in the CG-SMG in (**F**) C57BL/6J SPF mice following 2 weeks of single antibiotic- or Splenda-treatment, (**G**) C57BL/6J SPF mice 24 hours post streptomycin (strep) or PBS, BALBc/J SPF mice 24 hours post-strep or -PBS, CBA/J SPF mice 24 hours post-strep or -PBS, C57BL/6J SPF mice 5 days post strep. (**H** and **I**) (**H**) Most abundant bacterial genera and (**I**) Shannon diversity index in 16S sequencing of cecal samples from 24 hours post PBS- and streptomycin-treated C57BL6/J mice as determined by the phyloseq R package. (**J**) (Left) Scheme for (right) immunofluorescence images of the CG-SMG from *Fos*$^{GFP}$ SPF mice treated with VAMN or water for 2 weeks, with CTB555 injected into the ileum.

To address whether activated sympathetic neurons project to the intestine, we injected fluorescent CTB in the ileum of broad-spectrum antibiotic-treated *Fos*$^{GFP}$ mice. We observed extensive colocalization between CTB+ (red) and cFos+ (green) neurons in the CG-SMG (Fig. 3.26 J), reinforcing the possibility that sympathetic neurons activated upon microbial depletion project to the intestine, while not excluding projections to other visceral tissue connected to the CG-SMG. Finally, we found that pharmacological

blockade of catecholamine release in microbial-depleted mice rescued changes in their gastrointestinal motility, suggesting that increased sympathetic activity is partly responsible for the motility deficits observed in these mice (Fig. 3.27 A to D). The above

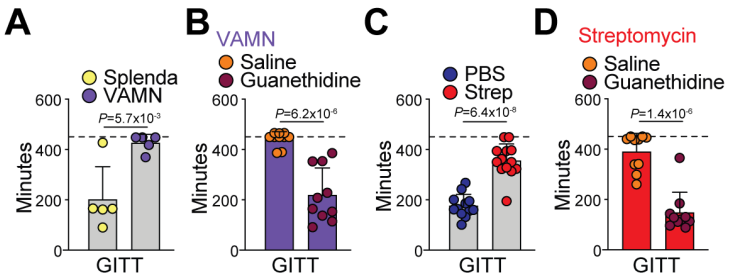


**Fig. 3.27. Blockade of catecholamine release rescues functional changes found upon microbial depletion.** (**A** to **D**) Gastrointestinal transit time (GITT) in C57BL/6J SPF mice treated with (**A**) Sucralose-based artificial sweetener (Splenda®) or antibiotics (VAMN), (**B**) VAMN with saline or guanethidine, (**C**) strep or PBS, (**D**) strep with saline or guanethidine. (**A** to **D**) Two-tailed unpaired t-test. Dashed line indicates maximum time allowed per animal for motility measurement (450 min).

results indicate that specific microbes can suppress cFos expression in gut sympathetic neurons, and that gut-specific sympathetic activity can reflect shifts in the gut microbial community.

### 3.3.3 Effects of luminal metabolites of gut-sympathetic activity

We observed that gnotobiotic manipulations resulted in suppression of CG-SMG neurons when defined microbial consortia, known to restore levels of short-chain fatty acids (SCFAs), were introduced (Atarashi et al., 2013; Biggs et al., 2017). Mass spectrometric quantification of SCFAs in the ceca of mice confirmed that specific antibiotics eliminated, and GF colonization rescued the levels of butyrate, propionate, and acetate to various degrees (Fig. 3.28 A to D).

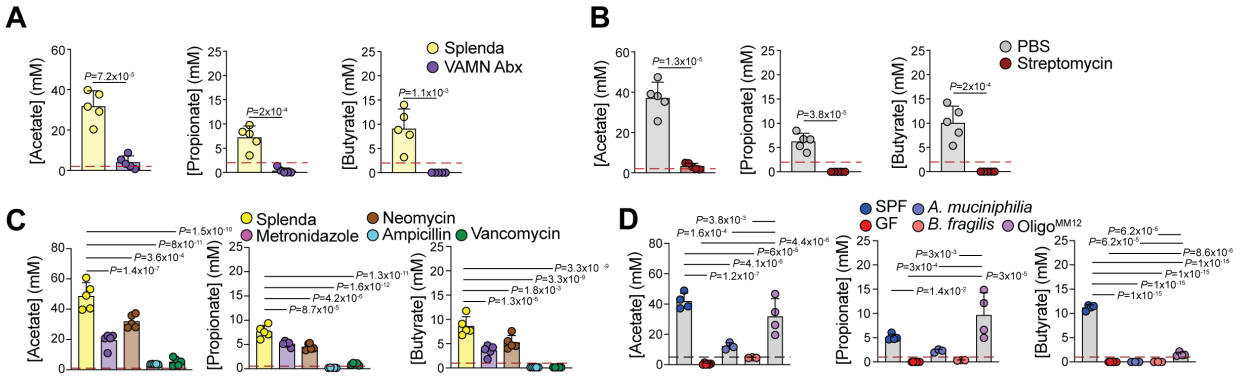


**Fig. 3.28. Microbial depletion results in significant reduction in SCFAs.** (A to D) Quantification of SCFAs in the cecal contents of (**A**) C57BL/6J SPF mice treated for 2 weeks with vancomycin, ampicillin, metronidazole, and neomycin (VAMN) in drinking water supplemented with sucralose-based artificial sweetener (Splenda®) as compared to Splenda-treated mice, (**B**) PBS- and strep-treated C57BL/6J SPF mice, (**C**) single antibiotic- and Splenda- treated C57BL/6J SPF mice, (**D**) C57BL/6J GF, SPF, GF mice colonized with A. muciniphilia, B. fragilis, or OligoMM12 mice. (A and B) Two-tailed unpaired t-test. (C and D) One-way ANOVA with Tukey's multiple comparisons. (A to D) Dashed line indicates lowest limit of detection.

Of note, we found no correlation between enteric infection-induced cFos (Gabanyi et al., 2016) and SCFA levels (Fig. 3.29 A and B). By contrast, in each of the gnotobiotic manipulations above, luminal SCFA levels correlated with the number of cFos+ neurons in the CG-SMG (Fig. 3.26) Thus, we tested whether supplementation of SCFAs in

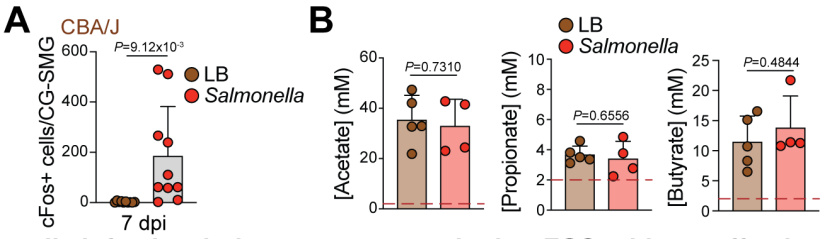


**Fig. 3.29. *Salmonella* infection induces gut-sympathetic cFOS without affecting SCFA levels.** (**A**) Number of cFos+ neurons in the CG-SMG of CBA/J mice orally inoculated with *Salmonella* or given oral gavage of luria broth. Dashed line indicates average number of cFos+ neurons for antibiotic-treated mice (320). (**B**) Quantification of SCFA in the cecal contents of CBA/J mice orally inoculated with Salmonella or given oral gavage of LB. (A and B) Two-tailed unpaired t-test. (B) Dashed line indicates lowest limit of detection.

microbiota-depleted mice restores cFos levels in the CG-SMG. Administration of exogenous butyrate, acetate, and propionate in the drinking water suppressed streptomycin-induced cFos (Fig. 3.30 A). Prior studies suggested that SCFAs can cross the blood-brain barrier (Braniste et al., 2014); however, intra-cerebroventricular infusion of SCFAs did not suppress streptomycin-induced cFos in the CG-SMG (Fig. 3.30 B). Moreover, administration of tributyrin, a butyrate pro-drug (Rivera-Chavez et al., 2016), was sufficient to suppress cFos expression in CG-SMG neurons of both GF mice and SPF mice treated with streptomycin (Fig. 3.30 C). Together, these data indicate that, SCFAs have the ability to suppress sympathetic cFos, and that this is most likely mediated by processes in the periphery.

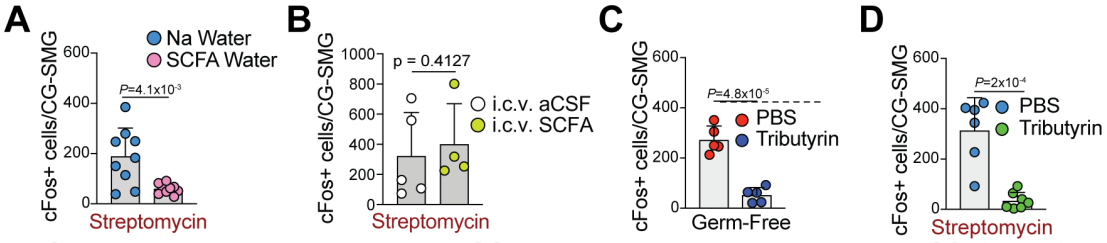


**Fig. 3.30. Supplementation with exogenous SCFAs can suppress sympathetic cFOS.** (**A** to **D**) Number of cFos+ neurons in the CG-SMG of (**A**) C57BL/6J SPF mice 24 hours post oral gavage with strep and treated with SCFA-supplemented or sodium-containing water, (**B**) C57BL/6J SPF mice treated with intracerebroventricular (i.c.v.) artificial cerebrospinal fluid (aCSF) or SCFA in aCSF post-strep treatment, (**C**) C57BL/6J GF mice 24 hours post-treatment with tributyrin or PBS, (**D**) C57BL/6J SPF mice treated with tributyrin or PBS 24 hours post oral gavage of streptomycin. (A to D) Two-tailed unpaired t-test.

SCFAs can modulate target cells via activation of G protein-coupled receptors, including GPR41, 43 or 109A, inhibition of histone deacetylases, or by acting as an energy substrate (Koh et al., 2016). *Gpr41*$^{-/-}$ mice, but not additional SCFA receptor-deficient strains analysed, showed a mild yet significant increase in the number of cFos$^{+}$ neurons in the CG-SMG (Fig. 3.31 A to C), suggesting a potential role for GPR41, expressed by

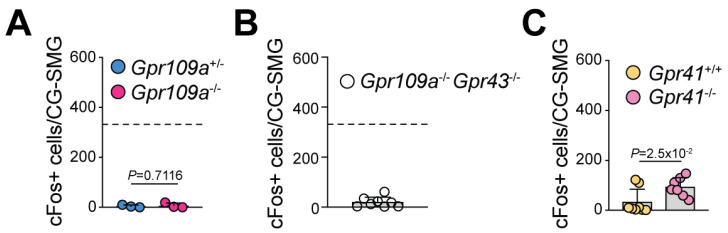


**Fig. 3.31. Gut-sympathetic activation in different SCFA receptor knockout mice.** (**A** to **C**) Number of cFos+ neurons in the CG-SMG of (**A**) Gpr109a$^{-/-}$ and littermate control Gpr109a$^{+/-}$ mice, (**B**) Gpr109a$^{-/-}$Gpr43$^{-/-}$ mice; dashed line indicates average number of cFos+ neurons/CG-SMG for GF mice (334); (**C**) Gpr41$^{-/-}$ and littermate control Gpr41$^{+/+}$ mice. (A to C) Two-tailed unpaired t-test.

IECs, iEANs, and eEANs (Nohr et al., 2015), in modulating gut sympathetic ganglia. In addition to changes in SCFA levels, microbiota-depleted mice have increased intestinal levels of conjugated and decreased levels of unconjugated bile acids (BAs) (Buffie et al., 2015). While a BA sequestrant did not change streptomycin-induced cFos in the CG-SMG, it significantly induced cFos in untreated SPF mice, indicating that other microbiota-modulated metabolites also play a role in sympathetic regulation (Fig. 3.32 A).

We investigated additional microorganism-modulated epithelial cell factors in driving sympathetic activation. Epithelial cell subsets, particularly EECs, are directly exposed to microbial signals and are capable of sensing and transmitting luminal input to EANs (Gribble and Reimann, 2016). Recent evidence pointed to a crucial role for microbial modulation of EECs via three major pathways: upregulation of 5-HT (Hsiao et al., 2013) , downregulation of L cell-derived GLP-1 (Browning and Lees, 2000; Wichmann et al., 2013) , and up- or downregulation of peptide YY (PYY) (Browning and Lees, 2000; Newman et al., 2017). Because secretion of these molecules is particularly enriched in the distal small intestine and colon, locations also enriched for SCFA production, we examined their role in the microbial modulation of sympathetic neurons.

We addressed a possible suppressive role for epithelial-derived serotonin by crossing Tph1fl/fl mice with mice expressing inducible *CreER* under the villin promoter (Villin$^{\Delta Tph1}$). Conditional depletion of the key enzyme for 5-HT production in gut epithelial cells resulted in a 50% reduction in gut-derived 5-HT but did not result in changes in cFos+ neurons in the CG-SMG or intestinal motility (Fig. 3.32 B to D).

In contrast, administration of the GLP-1R agonist Exendin-4 increased cFos+ neurons in the CG-SMG, as well as the total GITT (Fig. 3.32 E and F). The effect of Exendin-4 on motility was likely mediated by sympathetic activation, as catecholamine blockade normalized GITT (Fig. 3.32 G). However, treatment of mice with Exendin-9-39, a GLP-1R antagonist, after administration of streptomycin did not alter CG-SMG cFos levels (Fig. 3.32 H). Treatment of *Glp1r-/-* mice with broad-spectrum antibiotics or Splenda led to similar numbers of cFos+ neurons in the CG-SMG of the antibiotic-treated group as in WT mice, overall indicating that GLP-1 is sufficient to drive sympathetic activity, albeit not required for microbial-dependent modulation of gut sympathetic neurons (Fig. 3.32 I).

Finally, PYY administration did not activate the CG-SMG in SPF animals, but efficiently prevented the increase in cFos+ CG-SMG neurons following treatment with streptomycin (Fig. 3.32 J and K). These data suggest that the neuropeptides GLP-1 and

PYY can modulate activity of gut sympathetic neurons and, in the case of PYY, may contribute to microbial regulation of gut sympathetic activity.

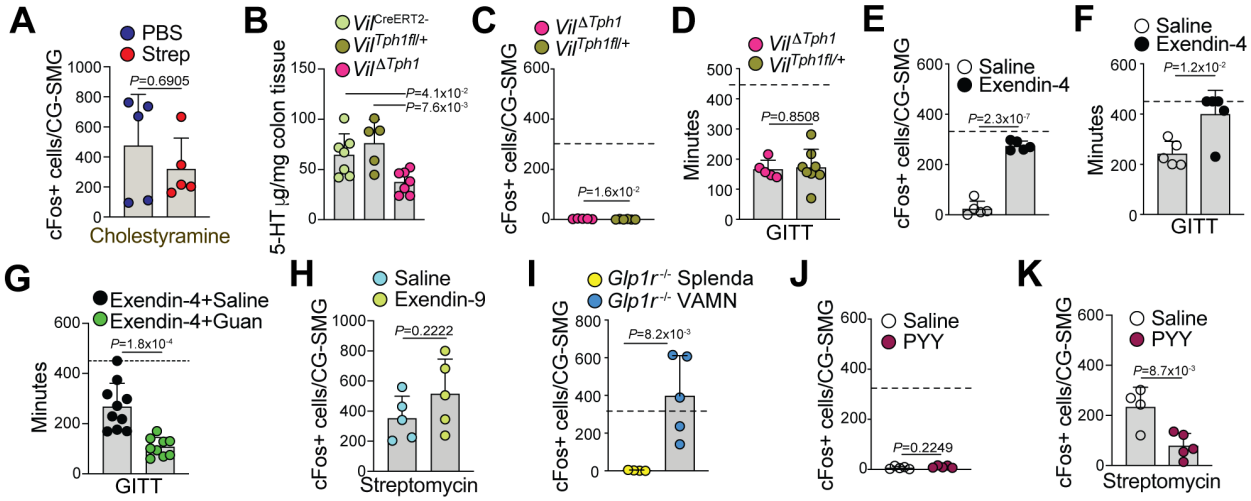


**Fig. 3.32. Effects of gut neurotransmitters and hormones on sympathetic activation and motility.** (**A**) cFos+ neurons in the CG-SMG of C57BL/6J mice treated with cholestyramine after oral gavage of PBS or streptomycin. (**B**) 5-HT concentration in colonic tissues from Vil$^{\Delta Tph}$, Vil$^{Tph1fl/+}$, and Vil$^{CreERT2-}$ mice 2 weeks post-tamoxifen injection. (**C** and **D**) (**C**) Number of cFos+ neurons in the CG-SMG and (**D**) Gastrointestinal transit time of Vil$^{\Delta Tph}$ or control mice two weeks post-tamoxifen injection. (**E** to **G**) (**E**) Number of cFos+ neurons in the CG-SMG, (**G**) colonic motility and (**F** and **G**) gastrointestinal transit time of C57BL/6J mice (**F**) 4 hours post i.p. injection of Exendin-4 or saline or (**G**) 5 minutes post-i.p. injection of Exendin-4 with saline or guanethidine. (**H**) Number of cFos+ neurons in the CG-SMG of C57BL/6J mice 4 hours post i.p. injection of saline or Exendin (9-39) and 24 hours post streptomycin treatment. (**I**) Number of cFos+ neurons in the CG-SMG of Glp1r$^{-/-}$ mice treated for 2 weeks with broad spectrum antibiotics (VAMN) or Splenda in drinking water. (**J** and **K**) Number of cFos+ neurons in the CG-SMG of C57BL6/J mice 4 hours post i.p. injection of saline or PYY in mice (**K**) and treated with saline or streptomycin 24 hours prior. (A, D to K) Two-tailed unpaired t-test. (B) One-way ANOVA with Tukey's multiple comparisons. (D, F, G) Dashed line indicates maximum time allowed per animal for each motility measurement. (C, E, J) Dashed line indicates average number of cFos+ neurons/CG-SMG for antibiotic treated mice (320).

Of note, we did not find any evidence for direct sensing of microbial depletion by sympathetic neurons, or for viscerofugal iEANs in modulating gut sympathetic activity upon microbial depletion (Figs. 3.33 and 3.34).

Together, we find that gut microbes, or their metabolites, either directly, or indirectly via epithelial cells, robustly modulate gut-extrinsic sympathetic activity: Microbiota depletion leads to increased expression of the neuronal transcription factor cFos and colonization of GF mice with bacteria that produce SCFAs suppresses cFos expression in the gut-sympathetic ganglion. We identified different potential microbiota-derived signals that can modulate gut sympathetic activity, which, in turn, can impact gene transcription in a variety of cell targets found in the intestine and elsewhere, including ILCs and gut-resident macrophages (Gabanyi et al., 2016; Moriyama et al., 2018).

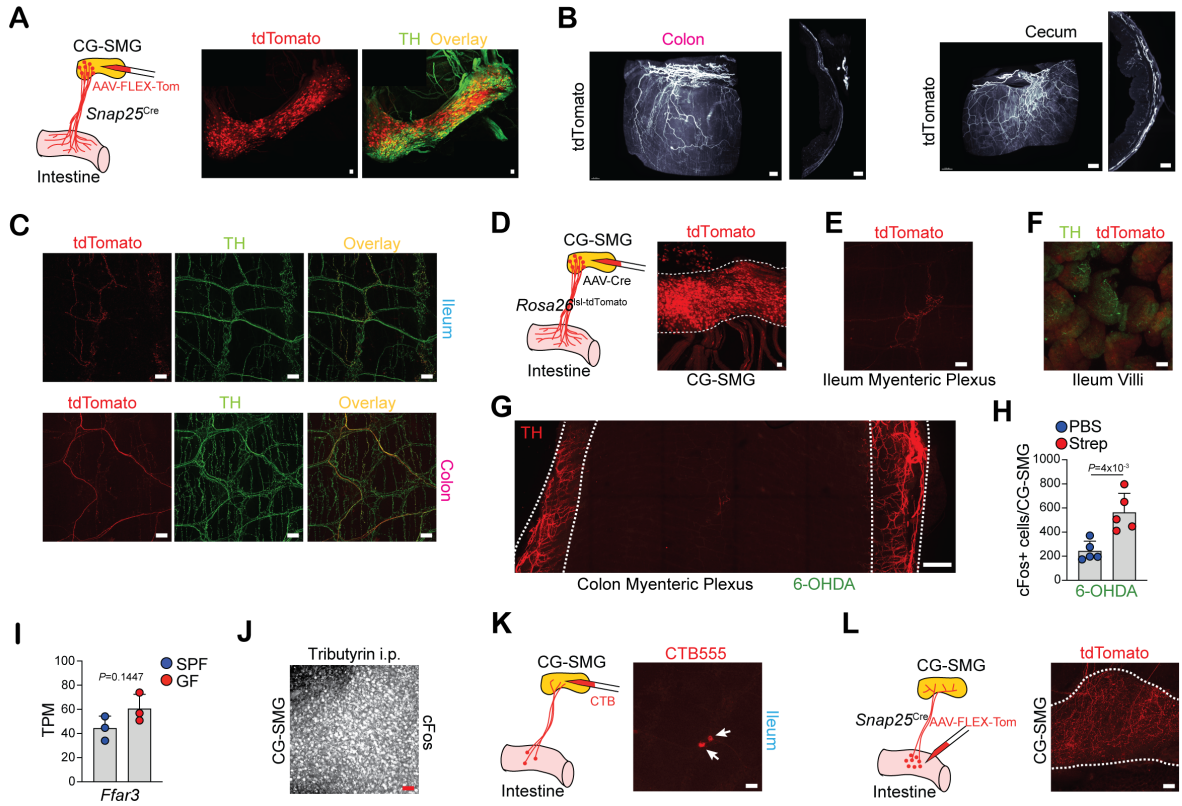


**Fig. 3.33. CG-SMG activation does not require direct sensing of microbes or metabolites.** (**A** to **C**) AAVrg-CAG-FLEX-tdTomato injection into the CG-SMG of *Snap25*$^{Cre}$ mice for tracing of fibres in the intestine. (**A**) (Left) Scheme and (right) IF images of the CG-SMG using anti-TH (green) antibody and native tdTomato fluorescence (red). (**B**) Light-sheet 3D reconstruction and optical section of the (left) colon or (right) cecum. (Left) Scale bars= 300 µm (left image) and 200 µm (right image). (Right) Scale bars = 500 µm (left image) and 200 µm (right image). (**C**) IF images of the (top) ileum and (bottom) colon myenteric plexus using anti-TH (green) antibody and native tdTomato fluorescence (red). (**D** to **F**) AAVrg-hSyn1-Cre injection into the CG-SMG of Rosa26lsl-tdTomato mice for tracing of fibres in the intestine. (**D**) (Left) Scheme and (right) immunofluorescence image of the CG-SMG using native Tomato fluorescence (red). (**E**) IF image of the ileum myenteric plexus using native Tomato fluorescence (red). (**F**) IF image of the ileum villi using anti-TH (green) antibody and native Tomato fluorescence (red). (**G**) IF stitched images of the colon myenteric plexus from C57BL/6J mice treated with 6-OHDA using anti-TH (red) antibody. Dashed lines indicate mesenteric border. Scale bar = 500 µm. (**H**) Number of cFos+ neurons in the CG-SMG of C57BL/6J mice treated with 6-OHDA before PBS or streptomycin treatment. (**I**) Transcripts per million (TPM) as calculated by Kallisto alignment for Ffar3 expression by CG-SMG neurons isolated from SPF and GF *Snap25*$^{RiboTag}$ mice (TRAPseq analyses). (**J**) IF image of the CG-SMG from C57BL/6J mice i.p. injected with Tributyrin using anti-cFos antibody. (**K**) (Left) Scheme representing injection of CT555 into the CG-SMG for visualization of viscerofugal neurons. (Right) IF image of the ileum myenteric plexus using native CTB555 fluorescence. White arrows indicate CTB+ neurons. (**L**) (Left) Scheme representing injection of AAV6-CAG-FLEX-tdTomato into the intestine of *Snap25*$^{Cre}$ mice for tracing of fibres. (Right) IF image of CG-SMG showing tdTomato+ fibres originating, in part, from the intestine. CG-SMG is outlined with dashed lines. (A, C to F, J to L) Scale bars = 50 µm. (H and I) Two-tailed unpaired t-test.

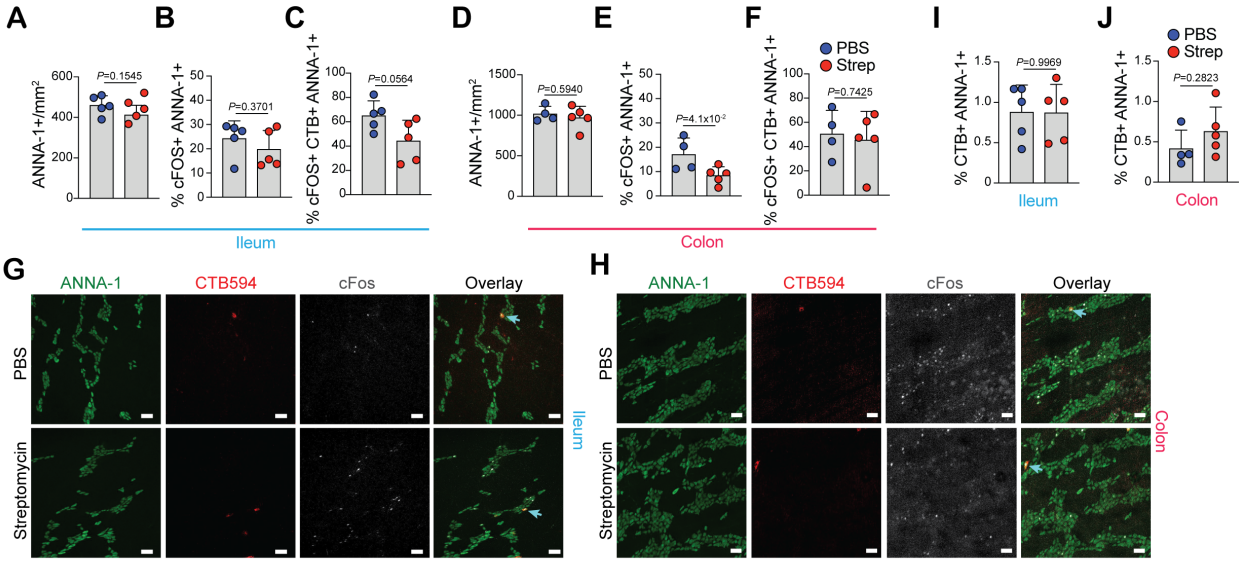


**Fig. 3.34. CG-SMG activation does not require viscerofugal input.** (**A** to **J**) PBS- and streptomycin-treated C57BL/6J mice 24 hours post gavage received retrograde CTB594 injection into the CG-SMG. Analysis of the ileum and colon. (**A** and **D**) Total number of, (**B** and **E**) percentage of cFos+ within, and (**C** and **F**) percentage of cFos+ among CTB+ within, ANNA-1+ neurons. (**G** and **H**) Immunofluorescence staining of myenteric plexus neurons from the (**G**) ileum or (**H**) colon using anti-neuronal nuclear (ANNA-1) (green) and anti-cFos (white) antibodies combined with native CTB594 fluorescence. Arrows indicate CTB+ cFos+ cells. (**I** and **J**) Percent of CTB+ among ANNA-1+ neurons in the(I) ileum or (J) colon. Scale bars = 50 μm. (A to F, I and J) Two-tailed unpaired t-test.

### 3.3.4 Local sympathetic activation mediates neuronal protection during enteric infections

In initial enteric infection experiments performed in this work we found that mice i.p.-injected multiple times with IgG isotype control antibodies (as in MM depletion experiments, Fig. 3.1) or mice anesthetized with isoflurane (as in control salbutamol pump experiments, Fig. 3.5) did not lose usual (~25 %) iEAN numbers post-*spiB* infection, opening up the possibility that *stress-induced* catecholamine release could trigger the same protective pathway in MMs as observed with salbutamol treatment and lost in LysM$^{\Delta Adrb2}$ animals. Indeed, a short pulse of isoflurane anesthesia or i.p. injections of PBS or IgG isotype antibody was sufficient to prevent most iEAN cell death following *spiB* infection, suggesting that stress signals that potentiate $\beta_2$-AR signaling may help in preventing post-infectious iEAN loss (Fig. 3.35 A and B). Similarly, exposing mice to 15

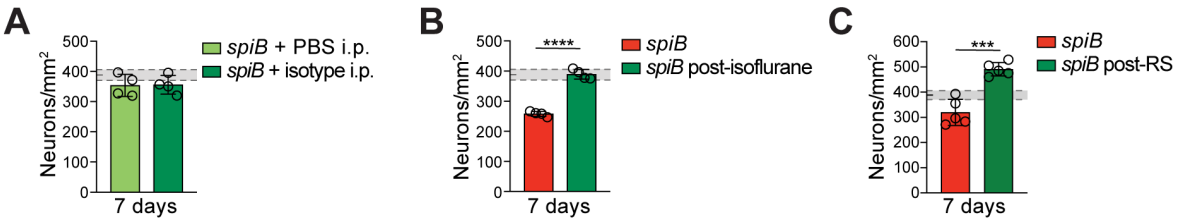


**Fig. 3.35. Systemic stress can prevent iEAN loss following enteric infections.** (**A** to **C**) Neuronal quantification as assessed by IF staining (ANNA-1) in the myenteric plexus of ileal segments on day 7 post-infection of C57BL/6 with *spiB* (A) receiving mock i.p. injections of PBS or IgG isotype control antibody, (**B**) following isoflurane anesthesia for 15 min 1 hour prior to infection or (**C**) following restraint stress (RS) for 15 min 1 hour prior to infection. Shaded area bounded by dashed lines indicates mean day 7 iEAN numbers +/- SEM of all control C57BL6/J mice Fig. 2.23 B. *** $P < 0.001$, **** $P < 0.0001$ as calculated by unpaired t-test.

min of restrain stress 1 hour prior to infection resulted in iEAN protection (Fig. 3.35 C). In light of these findings, we aimed to uncover the source – local or systemic – of catecholamines, i.e., the ligands of adrenoreceptors that initiate the neuroprotective response in MMs. We tested two possible mechanisms: systemic release of catecholamines from the hypothalamic-pituitary-adrenal (HPA) axis, and local release by activated gut-projecting sympathetic fibers (Fig. 3.36 A).

To investigate whether catecholamines systemically released by the adrenal glands could be playing a role in neuronal protection during infection, we performed bilateral adrenalectomy on WT mice. After allowing for a 2-week recovery period, we compared iEAN loss upon *spiB* infection with sham-operated controls. Rather than enhanced iEAN loss post infection, as we observed in LysM$^{\Delta Adrb2}$ mice, adrenalectomized animals exhibited reduced neuronal loss, excluding the possibility that systemic catecholamines were required for iEAN protection, and also suggesting that additional stress hormones produced by the adrenal glands, i.e., corticosteroids, could play a detrimental role in enteric neuronal maintenance during the course of intestinal infections (Fig. 3.36 A to C).

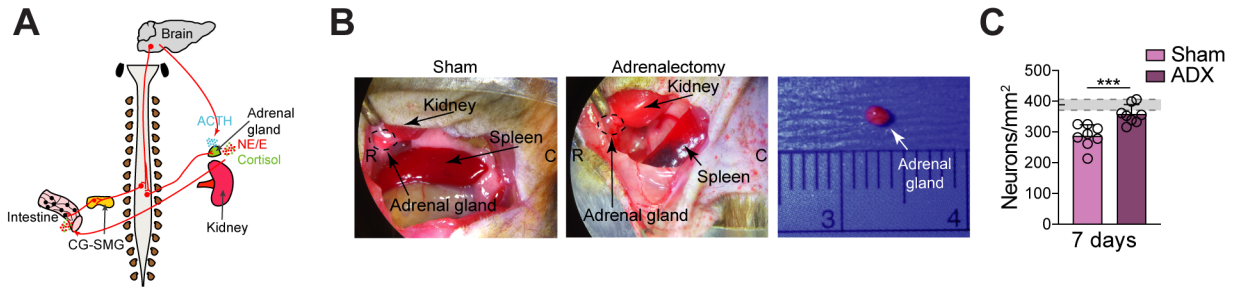


**Fig. 3.36. The HPA axis is not required for iEAN protection following enteric infection.** (**A**) Scheme of hypothalamic-pituitary-adrenal (HPA) axis and local sympathetic innervation of the intestine. NE – noradrenaline, E – epinephrine (adrenaline), CG-SMG – celiac-superior mesenteric ganglion. (**B**) Images demonstrating successful removal of adrenal glands from mice analyzed in (C). (**C**) Neuronal quantification in the ileum myenteric plexus on day 7 post-*spiB* infection of adrenalectomized or sham-operated C57BL/6J mice. *** $P < 0.001$ as calculated by unpaired t-test.

As elaborated above, alterations to the gut microbial composition, both by microbial depletion as well as in the context of *Salmonella* infection lead to a significant increase in the number of recently activated, cFos+ sympathetic neurons in the CG-SMG (Gabanyi et al., 2016). We thus assessed whether stimulation of these neurons, resulting in local intestinal catecholamine release, is sufficient to drive MM-$\beta_2$-AR-mediated tissue protection. We utilized two chemogenetic mouse models, in which administration of the synthetic ligand, C21, to mice carrying an inactivating DREADD driven by promoters active in sensory NG neurons (SNS$^{hM4Di}$ or *Phox2b*$^{hM4Di}$) results in a significant increase in cFos expression by gut-projecting sympathetic neurons (Muller et al., 2020b). We found that DREADD-induced activation of gut-projecting neurons prior to *spiB* infection both in SNS$^{hM4Di}$ and *Phox2b*$^{hM4Di}$ mice significantly rescued iEAN loss (Fig. 3.37 A and B). Finally, we exposed LysM$^{\Delta Arg1}$ and WT (*Cre*-) littermates to restraint stress immediately prior to *spiB* infection. While this prevented iEAN loss in WT mice, we observed no rescue thereof in mice lacking myeloid Arg1 (Fig. 3.37 C). Together, these results further support a role for catecholamines locally released by gut-projecting sympathetic neurons, in triggering activation of a $\beta_2$-AR-arginase 1- polyamine pathway initiated in MMs in limiting of inflammation-induced iEAN loss.

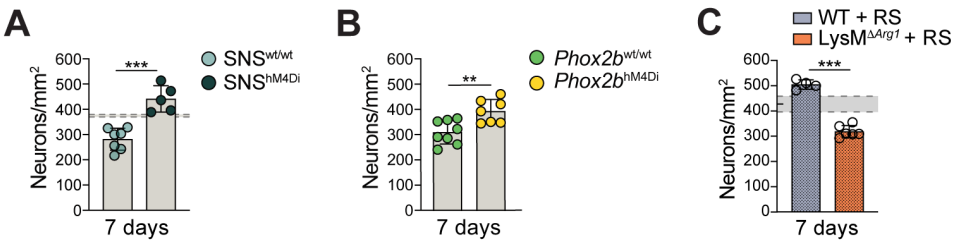


**Fig. 3.37. Chemogenetic activation of gut-sympathetic neurons rescues iEAN loss post-infection.** (**A** to **C**) Neuronal quantification in the ileum myenteric plexus on day 7 post-*spiB* infection of (**A**) SNS$^{hM4Di}$ mice treated with Compound 21 (C21) 24 hours before *spiB* infection, (**B**) *Phox2b*$^{hM4Di}$ mice treated with C21 24 hours before *spiB* infection, or (**C**) LysM$^{\Delta Arg1}$ mice and WT littermates subjected to restraint stress for 15 min 1 hour prior to infection. ** $P < 0.01$, *** $P < 0.001$ as calculated by unpaired t-test.

## 3.4 Conclusions

Using confocal microscopy, cell sorting-independent transcriptomics, pharmacological and genetic gain- and loss-of-function approaches, surgical lesioning, and chemogenetic manipulations, we identified a functional role for a circuit comprising eEANs, MMs and iEANs in limiting ENS damage following enteric infections.

Following a single enteric infection, MMs responded to luminal infection by upregulating a neuroprotective program via $\beta_2$-AR signaling and mediated neuronal preservation through an Arg1-polyamine axis.

Notably, prior infection with an unrelated pathogen prevented infection-induced neuronal loss during exposure to subsequent infection with heterologous pathogens, suggesting that a form of “trained tolerance” plays a role in limiting enteric neuronal damage, and raising the possibility that infections early in life determine the number of enteric neurons in adulthood. This protection was mediated – at least in part – by the same program in MMs, a pathway activated during and sustained following primary infection.

Our data further suggest that during enteric infections, MM activation via $\beta_2$-AR is triggered by local release of catecholamines by extrinsic, gut-projecting sympathetic neurons. These neurons, in turn, are tuned by the microbiota, in that a healthy microbial community suppresses, and dysbiosis and infection enhance their activity. Further studies are warranted to determine how exactly luminal perturbations are sensed in these contexts, to transmit these cues to sympathetic gut-projecting efferents and thereby dictating gut-sympathetic activity.

# CHAPTER 4. DISCUSSION

Overall, the research presented in the previous chapters provides detailed insight into the intricate interplay between gut microbes, enteric-associated neurons and intestinal immune cells. We highlight critical roles of this triangular crosstalk in maintaining the dynamics of the unique environment of the intestine at steady state, and in response to certain perturbations.

We provide high-resolution characterization of intrinsic and gut-projecting extrinsic enteric-associated neurons and demonstrate the influence of gut microbes and their metabolites on these neurons. We found that microbial perturbations lead to a novel form of inflammatory neuronal cell death and uncovered a crucial contribution of intestinal muscularis macrophages in preventing excessive tissue damage, via a process mediated by activation of gut-projecting sympathetic neurons. We further uncovered a microbiota-dependent, central nervous system-independent local neuronal circuit encompassing the gut, liver and pancreas by which a population of viscerofugal neurons influences systemic glucose metabolism.

We demonstrated that disruptions of the crosstalk between the intestinal microbiota, the enteric nervous and immune systems have important medical implications; the absence of commensal microbe-to-neuron communication alters systemic glucose metabolism, and the disruption of communication between nerve-associated muscularis macrophages and enteric neurons aggravates neuronal damage during intestinal infections, leading to long-term GI dysfunction, including intestinal inflammation and dysmotility. By contrast, enhancing gut-sympathetic neuron-to-macrophage crosstalk and thus the tissue-protective potential of muscularis macrophages prevented enteric neuronal damage. Moreover, re-introduction of a healthy microbiota post-infection resulted in neuronal recovery – findings with possible therapeutic potential for both intestinal disorders such as irritable bowel syndrome, as well as systemic diseases with GI manifestations, such as Parkinson's disease and diabetic enteric neuropathy.

## 4.1 Influence of commensal microbes on the ENS

The gut microbiota influences several physiological and pathological processes, including local nutrient absorption and lipid metabolism (Korem et al., 2017; Martin et al., 2019; Ridaura et al., 2013; Zarrinpar et al., 2018), as well as activation of the intestinal and systemic immune systems (Honda and Littman, 2016). Through transcriptional profiling, confocal microscopy and microbial manipulation strategies, our data revealed both regional differences and microbial influence on iEAN numbers, gene expression profiles and particularly neuropeptidergic coding.

Our results are in line with previous reports documenting alterations to iEAN numbers, fiber density and excitability in GF as compared to SPF mice (Anitha et al., 2012; De Vadder et al., 2018; McVey Neufeld et al., 2015). Notably, there are discrepancies in reports regarding iEAN reduction in the large intestine, pointing to the involvement of specific microbial species, differentially present between vivaria, driving

postnatal iEAN maturation. Similarly, treatment with different combinations of antibiotics was shown to alter iEAN numbers, but the specific alterations varied between reports, suggesting that the presence or absence of certain microbial species is capable of influencing different iEAN subsets. This is also reflected in our finding that treatment with ampicillin, vancomycin and metronidazole, but not neomycin drastically affected both iEAN numbers and their neuropeptide expression.

Notably, while the analysis of myenteric iEANs in *humans* is limited to full surgical specimens, a current retrospective study found an increase in IBS diagnoses in a patient cohort who underwent a course of antibiotics as compared to individuals who did not (Ravy Vajravelu, University of Pennsylvania, personal communication). Thus, it is plausible that microbial depletion in humans can also lead to iEAN alterations, and may underlie IBS symptoms in such cases, highlighting the importance of avoiding unnecessary antibiotic exposures.

Postnatal enteric neurogenesis was traditionally thought not to occur. By contrast, conventionalization of GF mice as observed by us and others (De Vadder et al., 2018; McVey Neufeld et al., 2015) as well as re-introduction of a healthy microbiota upon antibiotic-mediated microbial depletion, led to iEAN maturation and recovery, respectively, which demonstrates a degree of iEAN plasticity even during adulthood. This is also reflected in a recent report suggesting continuous turnover of iEANs during adulthood (Kulkarni et al., 2017). Yet, we found that colonization of mice with a single antibiotic-resistant bacterial strain while undergoing broad-spectrum antibiotics treatment did not reverse structural iEAN or functional GI changes, supporting the aforementioned hypothesis that some commensal bacteria and/or their metabolites, but not others, critically affect iEAN maturation and maintenance.

What are potential microbial signals that influence iEAN plasticity? Several studies have suggested detection of microbial components through iEAN-intrinsic TLR signaling (Anitha et al., 2012; Brun et al., 2013; Yarandi et al., 2020). However, the use of global TLR-/- mice in these studies makes these results difficult to interpret, particularly in light of broad expression of TLRs by multiple intestine-resident cell types. Our own TRAP-seq analyses as well as mining of a published single-cell data set (Drokhlyansky et al., 2020) did not reveal significant expression of TLRs by iEANs, suggesting that iEAN-intrinsic TLR signaling is unlikely involved in their microbial modulation.

Several studies have reported a role for 5-HT, levels of which are reduced in GF mice, in iEAN maturation, neuroprotection and adult neurogenesis. Treatment of GF mice with a 5-$HT_4$R agonist, i.e., stimulation of a 5-HT receptor expressed by iEANs, was sufficient to induce iEAN maturation in GF animals (De Vadder et al., 2018). Similar effects were also observed in GF mice following partial and full conventionalization, which correlated with increased 5-HT levels (De Vadder et al., 2018; Liu et al., 2009; Yano et al., 2015), albeit mechanistic data are thus far lacking. How could microbially-driven 5-HT production influence iEAN maturation and survival? While a fraction of iEANs is serotoninergic and could thus contribute to intestinal 5-HT levels, our own analyses along with reports from others (Berthoud et al., 1995; Janssen and Depoortere, 2013) make direct detection of microbes by iEANs appear unlikely in physiological settings with intact epithelial barrier. However, as known sensors of microbes, producers of the majority of

enteric 5-HT, and cellular mediators of neuronal activation (Bellono et al., 2017), enterochromaffin cells (ECs) may induce iEAN maturation through 5-HT production. Whether iEANs directly synapse these ECs, as has been shown for extrinsic vagal afferents (Bellono et al., 2017; Bohórquez et al., 2015; Kaelberer et al., 2018), or whether paracrine mechanisms or extrinsic circuits (such as vagal afferents projecting to sympathetic or parasympathetic efferents, which, in turn, project to intrinsic motor neurons) are involved, remains to be determined. Of note, as for extrinsic EANs, a 50 % reduction in intestinal 5-HT levels through epithelial-specific *Tph1* deletion, mimicking concentrations present in GF mice, did not alter the activity of gut-sympathetic fibers in our studies. This suggests that microbial modulation of *sympathetic* efferents unlikely involves 5-HT signaling during microbial depletion or dysbiosis. Measuring 5-HT levels following acute *Salmonella spiB* infection, and *spiB*-infecting Vilin$^{Tph1}$ mice could further answer whether 5-HT signaling is involved in gut-sympathetic activation post-infection.

Notably, while iEAN maturation continues post-weaning, the majority of its development occurs *in utero*, i.e., in a largely sterile environment (Metchnikoff, 1901; Uesaka et al., 2016). What influences iEAN development during intrauterine development? Intriguingly, in the CNS, signals from the *maternal* microbiota have been shown to impact embryonic neuronal development. For example, 5-HT derived from the placenta can influence embryonic thalamocortical axon guidance (Bonnin and Levitt, 2011). Further, during pregnancy, the maternal gut microbiota was shown to influence fetal brain development through modulation of various metabolites in the offspring (Vuong et al., 2020). In contrast to the CNS, no studies have thus far addressed the intrauterine development of the ENS in GF or microbiota-depleted mice (Joly et al., 2020). However, in light of our own and others' findings of iEAN-microbiota dependence *after* birth and during adulthood, along with drastic alterations therein induced by dysbiosis, microbial modulation of the developing embryonic ENS through placenta-crossing, EAN-modulating factors, including 5-HT and SCFAs, appears highly likely. How might maternal antibiotic use or enteric infections affect the developing ENS?

Bacterial 16S rRNA analyses along with metabolomic and/or metagenomic analyses (Cohen et al., 2017), during different antibiotic courses, or in settings of dysbiosis could aid in identifying further candidates for microbe-to-iEAN signaling. Further, reductionist approaches such as mono-colonizations or colonizations with defined bacterial consortia, such as Oligo$^{MM12}$ or altered Schaedler flora (ASF), could be useful. Finally, mining of published single-cell iEAN atlases could guide in determining possible receptors expressed by iEAN subsets involved in direct or indirect microbial sensing.

## 4.2 CNS-independent regulatory circuitry: Modulation of host physiology by iEANs

### 4.2.1 Regulation of glucose metabolism through a peripherally restricted circuit

Glucose is the central energy substrate of the mammalian body. Tight regulation of its concentration in circulation is fundamental to health as both hypo- and hyperglycemia can have life-threatening effects. As such, several complementary neuronal and endocrine mechanisms exist to ensure glucose homeostasis through controlling its utilization, production and storage (Lin et al., 2021).

Since the first report of a population of enteric neurons reaching extraintestinal regulatory centers, several studies primarily performed in guinea pigs confirmed the existence of these viscerofugal iEANs (Crowcroft et al., 1971; Hibberd et al., 2012). While viscerofugal iEANs have been reported to be mechanosensitive, whether they are responsive to further stimuli has not been documented. Through anatomical tracing experiments coupled with viral intestine-restricted iEAN targeting and chemogenetic manipulations, we identified a population of distal intestinal viscerofugal CART+ iEANs that project to the gut sympathetic ganglion to form the afferent arm of a CNS-independent neuronal circuit connecting the gut, liver and pancreas. This pathway was capable of modulating blood glucose homeostasis in a microbiota-dependent manner. Our anatomical tracing results support a previous study performed in rats, that suggested enteric neuronal input directly reaching the pancreas (Kirchgessner and Gershon, 1990); our manipulation and functional studies reveal physiological significance of such circuitry.

#### 4.2.1.1 Modulation of CART+ (viscerofugal) iEANs by luminal signals

How does this glucoregulatory circuit get activated? We did not find evidence for CART+ neuronal projections to the intestinal epithelium in our image analyses, thus making direct sensing highly unlikely. Yet, these neurons likely receive input from the intestinal lumen, directly or indirectly. It appears plausible that CART+ viscerofugal neurons are functionally connected to potential sensors such as intrinsic primary afferents or EECs, as pointed out in the previous section. Specifically, a recent report demonstrated a pathway of direct signal transduction from the gut to brain areas via synaptic release of the neurotransmitter glutamate by a population of EECs (neuropod cells) directly synapsing and thereby activating adjacent vagal afferent eEANs (Kaelberer et al., 2018). Experiments coupling polysynaptic viral tracing from the CG-SMG with viscerofugal monosynaptic CTB tracing in neuronal CART-reporter animals, to investigate whether viral spread reaches IECs via reporter-positive viscerofugal neurons, may answer this question.

Since viscerofugal iEAN are classically described to be mechanosensitive, and we found that a proportion of CART+ iEANs is also viscerofugal, it is also plausible that these neurons are tuned to mechanical distension (Hibberd et al., 2012). This is further supported by our observation that CART+ iEANs form extensive intramuscular arrays, a feature ascribed to mechanosensitive EANs (Brookes et al., 2013). Yet, in the context of

our described circuit regulating nutrient levels, this potential mechanism of CART+ iEAN activation does not appear very likely. However, one could speculate that because alterations to the luminal microbial composition can have drastic effects on distal intestinal wall tension, as seen in GF and antibiotic-treated mice (i.e., bloating and luminal hypertension), potential CART+ iEAN mechanosensitive capacity may get disrupted in such circumstances, with reduced responsiveness and as a result, loss of CART+ iEAN influence on blood glucose levels as observed in our studies.

Detection of (possibly microbially-modulated) nutrients is another potential route of CART+ iEAN modulation, as we found that fasting mice have lower *Cart* transcript and numbers of CART+ neurons in the ileum. A recent preprint reporting that murine iEANs are capable of differentiating luminal nutrients via signaling initiated in the epithelium, supports this possibility (Fung et al., 2021). While we did not directly address this question in our studies, one could determine CART+ iEAN nutrient responsiveness through gavage of glucose and other nutrients, and/or comparing enteric CART peptide expression of mice maintained on special (e.g., ketogenic) versus regular chow diets.

How does the *microbiota* contribute to CART+ iEAN regulation of metabolic parameters? As mentioned, it is possible that the reduction in CART neuropeptide levels we observed upon microbial depletion may be tied to the loss of microbial metabolites or diet-derived microbially-modulated host factors. However, the change in blood glucose levels we observed appears more likely to be due to the loss of synaptic connections between the gut and the CG-SMG. This is supported by the following observations: (i) Exogenous administration of CART peptide did not restore blood glucose levels in antibiotic-treated mice. Thus, peptide levels *per se* do not appear to be required for CART-iEAN blood glucose regulation. However, we could not rule out that local release of CART peptide into the CG-SMG or an alternatively processed form of CART, which has been reported in the intestine (Ekblad, 2006; Stein et al., 2006), play a role. (ii) When *Cart*$^{\text{EAN-hm3Dq}}$ mice were fasted, chemogenetic CART iEAN activation still increased BG levels. Thus, even with a reduction in CART expression during fasting, the neural connections between gut and CG-SMG very likely remains intact in the absence of microbial depletion. (iii) By contrast, upon antibiotic treatment, we found this neural gut-CG-SMG connection to be partially lost. Modeling this observation by actively depleting viscerofugal connections using *Cart*$^{\text{EAN-DTA}}$ mice resulted in a similar reduction in blood glucose levels. A follow-up experiment coupling microbial depletion with chemogenetic CART iEAN activation would further elucidate whether the loss of connectivity between intestine and gut sympathetic ganglion drives glucose dysregulation in settings of dysbiosis.

How do enteric infections or chronic inflammation with neuronal loss affect CART+ viscerofugal populations, and by extension, blood glucose regulation? And how could this circuit be affected e.g., during metabolic diseases? Several recent studies have revealed considerable plasticity in peripheral autonomic innervation of tissues involved in blood glucose regulation, in particular during metabolic diseases (Blaszkiewicz et al., 2019; Chiu et al., 2012; Lin et al., 2021; Wang et al., 2020). It would be interesting to explore, for example, if in cases of diabetic enteric neuropathy, which results in iEAN dysregulation and loss of some iEAN populations (Chandrasekharan and Srinivasan, 2007), this circuit

is altered, disrupted, or uncoupled, adding to metabolic dysregulation as seen in type 2 diabetes mellitus. Interestingly, in diabetic rats, loss of inhibitory myenteric iEANs along with an increase in excitatory iEANs have been reported (Chandrasekharan and Srinivasan, 2007), which could result in uncoupling (increased activity) of the primarily excitatory CART+ viscerofugal circuit we described. To reiterate the point brought up above, blood glucose levels, central to normal physiology, are regulated by a variety of factors. However, it appears likely that damage caused to these EAN connections during dysbiosis or inflammation could add to the severity of both acute infectious and chronic diseases. Notably, in certain bacterial infections, reduction of blood glucose levels can enhance pathogen resistance. Wang *et al.* demonstrated that administration of glucose to mice systemically infected with *Listeria monocytogenes* was sufficient to cause mortality, while blocking glucose utilization by administering 2-desoxy-glucose (2-DG) effectively protected against fatal sepsis (Wang et al., 2016). By contrast, during viral influenza infections, increase in blood glucose levels *increased* survival. One could speculate whether "shutting off" the connection between CART+ viscerofugal iEANs and the gut sympathetic ganglion, leading to reduced blood glucose levels, can be viewed as a means to prevent fatal outcomes of bacterial GI infections. This hypothesis could be tested by CART+ iEAN depletion prior to infection with a virulent enteric bacterial pathogen, such as wild-type *Salmonella*.

Notably, while we found loss of CART+ iEAN and enteric CART expression to correlate with reduced blood glucose levels, other studies showed *Cart*-deficient mice to have increased blood glucose, reduced insulin, and glucose intolerance. However, the use of global *Cart*-/- animals complicates the interpretation of these results, as these studies also showed altered pancreatic islet structures that are likely due to impaired pancreatic β-cell development (Abels et al., 2016; Wierup et al., 2005). Given that the receptor(s) of CART have not yet been deorphanized, it is possible that CART peptide or CART-expressing neuron activation have differential effects depending on receptor types expressed on target cells. It is also possible that CART peptide *per se* does not, but activation of CART-expressing neurons does, mediate effects e.g., in the CG-SMG, while CART peptide mediates β-cell insulin secretion. Overall, these discrepancies between reports emphasize the value of site-specific targeting approaches to unravel such differential effects.

Prior work has demonstrated that levels of GLP-1, which plays a crucial role in glucose regulation, are significantly increased in GF and antibiotic-treated animals (Wichmann et al., 2013; Zarrinpar et al., 2018). However, our observations do not point to a major, direct role for changes in GLP-1 on glucose levels during microbiota modulation. This is based on our observation that *Casp11*$^{-/-}$ mice still displayed increased levels of GLP-1, but not of blood glucose, upon antibiotic treatment. Additionally, administration of the GLP-1R blocking peptide, exendin 9-39, did not change fasting glucose levels in antibiotic-treated WT animals. It remains possible that other microbiota-modulated host factors, such as 5-HT, do play a role, for instance via maintenance of neuronal populations (De Vadder et al., 2018; Martin et al., 2019).

Together, while nutritional status and the microbiota can impact neuropeptide levels in the gut, our work points to the microbial-mediated maintenance of gut-intrinsic sympathetic control as the key component driving microbiota-induced changes in glucose regulation. In other words, depletion of the gut microbiota led to a significant reduction in viscerofugal connectivity between the gut and the CG-SMG, resulting in changes in metabolic parameters. The upstream sensing mechanisms that mediate these effects still need to be addressed. It also remains to be defined whether CART+ viscerofugal neurons respond to the presence of glucose in the intestinal lumen, release of neuropeptides, or the movement of fecal matter. It will also be important to determine how CART+ viscerofugal neurons are functionally connected to potential sensors such as intrinsic primary afferents, EECs, or mechanosensitive populations and the downstream neuronal populations required to perform glucoregulatory functions (Han et al., 2018; Kaelberer et al., 2018).

### 4.2.2 Exploration of other peripheral-restricted circuits

The ability of viscerofugal neurons in the distal ileum and proximal colon to increase blood glucose levels via a peripheral circuit warrants additional investigations into CNS-independent iEAN circuits. Since we focused on the functional characterization of selected neuropeptides in this study, it will be important to further explore if additional microbiota-modulated and/or microbiota-independent iEAN neuropeptide pathways play complementary or redundant roles in GI physiology, including feeding behavior. This is illustrated by our finding that a degree of overlap between CART+ and viscerofugal iEANs exists, yet a large proportion of viscerofugal iEANs projecting to the intestine was not CART+, raising the question as to what other circuits these neurons could feed into. Anatomical tracing coupled with single-cell profiling of viscerofugal iEANs projecting from different intestinal regions would allow for high resolution insight into the profiles of these small populations. Such experiments would enable selective targeting and functional evaluation using site-specific strategies as the ones employed in this study.

Experiments in rats have shown that some distal intestinal viscerofugal populations can also directly project to DRGs. This suggests that a portion of intestinofugal neurons may have sensory capacity, with potential of direct information transfer to central centers (Doerffler-Melly and Neuhuber, 1988; Neuhuber et al., 1993), albeit functional data is absent. If indeed they have sensing capacity, could these neurons be affected or influence visceral hypersensitivity as seen in chronic inflammatory conditions or IBS? From a translational perspective, targeting peripheral-restricted circuits, such as the one uncovered here, could bypass undesirable CNS effects for the treatment of metabolic disorders, such as type 2 diabetes mellitus.

Finally, it is intriguing to speculate whether intestinofugal iEANs could, in the context of enteric infections, directly activate gut-projecting sympathetic iEANs, thereby sending a “call for help” signal, resulting in adrenergic programming of MMs, ensuring their own protection. Notably, in the skin, such an observation, resulting in enhanced immunity, has indeed been made. TRPV1+ sensory afferents have the capacity to sense extracellular pathogens (Maruyama et al., 2018) and engage in reflex loops to prime the

skin area within and around an infected site. In the immediately affected site, this resulted in enhanced immunity upon secondary exposure, and in non-affected adjacent areas, in "anticipatory immunity" and improved protection during primary exposure of that area (Cohen et al., 2019).

### 4.2.3 Developing strategies to address functional roles of neuropeptide+ iEAN populations

Although they have been subject to investigation for decades, studies on the functional roles of specific neuropeptide-expressing iEAN subtypes are largely lacking. In particular, the fact that the majority of the neuropeptides that were revealed by our TRAP-seq analyses are known to be expressed both in the periphery (Furlan et al., 2016; Gonkowski and Rytel, 2019; Grider, 2003; Gupta et al., 2017; Yuan et al., 2016) and in the CNS (Waterson and Horvath, 2015; Yavorska and Wehr, 2016), creates a significant obstacle in studying their local roles in isolation, and leaves many questions to be addressed. How, for example, are these populations activated? What role does the gut microbial composition play in their activity? Can they sense and/or respond to luminal perturbations, such as dysbiosis or infection? Do they interact with extrinsic populations to transmit information regarding feeding status and microbial composition or perturbations? Using peripherally-, or tissue-restricted cell targeting strategies such as viral approaches with constructs that do not cross the blood-brain barrier, as employed in our studies, is an option. Further, knowledge gained from novel single-cell iEAN atlases (Drokhlyansky et al., 2020; Zeisel et al., 2018) may allow to identify combinations of genes expressed by these populations that may be unique to a specific tissue site, i.e., gut as compared to CNS. Finally, as has recently been demonstrated for immune cell targeting, using multiple Cre lines with non-identical off-target effects may be a possible approach for some questions investigating functional roles of neuropeptide-expressing populations (Silva et al., 2021).

## 4.3 Inflammasome machinery in the ENS

### 4.3.1 Functional significance of iEAN NLRP6/Casp11 signaling

The NLRP6 inflammasome is found in abundance in the small and large intestines, where it has primarily been implicated in influencing barrier integrity, inflammation and possibly microbiome composition through activity in epithelial and myeloid cells (Zheng et al., 2021).

Using neuronal-specific TRAP-seq, *in situ* hybridization and fluorescent reporter animals, we found that components of the inflammasome machinery – canonical as well as non-canonical – are expressed by iEANs. Our functional studies corroborate previous work suggesting a role for inflammasome components in iEAN damage. Gulbransen *et al.* demonstrated that iEAN death following dinitrobenzene sulfonic acid (DNBS)-induced colitis depended on ASC-mediated activation of caspases. However, while this process was independent of *Nlrp3*, it remained unclear as to the trigger(s) of ASC activation

(Gulbransen et al., 2012). Our results derived from neuronal-specific targeting of non-canonical inflammasome components now demonstrate the critical involvement of *Nlrp6* and *Casp11* expression in inflammation-induced iEAN damage. Of note, we did not formally demonstrate requirement for inflammasome *assembly* and *cleavage* of Casp11 *per se*.

What are possible roles of enteric neuronal NLRP6/Casp11 signaling beyond iEAN death? The expression of a functional immune sensing and response machinery by iEANs suggests their capacity to actively engage in immune defense processes, further illustrating the intricate interconnectedness of neuronal and immune sensory compartments at a critical environmental interface. Indeed, recent work by Flavell and colleagues demonstrated that IL-18 secretion by submucosal iEANs enhanced barrier integrity during homeostasis, and pathogen resistance during *Salmonella* infection (Jarret et al., 2020). What triggers led to neuronal IL-18 production in this study remained unclear. However, because we observed that at least myenteric iEANs did not express other known IL-18 triggers, specifically TLRs, it is likely that iEAN IL-18 production is mediated by NLRP6/Casp11, or alternatively, Casp1. In an integrated model, it is possible that NLRP6/Casp11-mediated neuronal production of IL-18 contributes to pathogen resistance, and NLRP6/Casp11-mediated neuronal pyroptosis results in recruitment of further immune effector cells to the site of inflammation. Yet, as suggested by our functional data, hyperactivation of this pathway, resulting in drastic iEAN pyroptosis, can lead to GI dysfunction.

It is also possible that the effects of NLRP6/Casp11 activation in iEANs are anatomically compartmentalized: *Submucosal* iEANs could predominantly produce IL-18 in response to NRLP6/Casp11, to play an active role in pathogen resistance. This is supported by the finding that these iEANs already produce IL-18 at steady state (Jarret et al., 2020) along with our own data showing that submucosal iEANs are less prone to dying upon infection; by contrast, NLRP6 activation in *myenteric* iEANs during infection could kickstart pyroptosis – a model parallel to previous observations from our lab demonstrating the regional, pro- versus anti-inflammatory, specialization of intestinal macrophage populations (Gabanyi et al., 2016). This anatomical compartmentalization between submucosal and myenteric iEANs is further supported by the fact that in our TRAP-seq analyses of *myenteric* iEAN, we failed to detect expression of IL-18 and IL-1 β. In either case, the severity of *Salmonella* infection would likely be altered by NLRP6/Casp11 depletion, with decreased neuronal IL-18 production and collapse of barrier strengthening (i.e., mucus production). Determining barrier integrity, measuring markers of inflammation, and evaluating IL-18 production in the absence of neuronal NLRP6/Casp11 would shed light on this hypothesis. Of note, in our infections with attenuated *Salmonella* the absence of iEAN NLRP6/Casp11 did not have drastic effects on pathogen clearance *per se*, suggesting that *Salmonella* resistance itself is primarily mediated by other known cellular players, including LpMs.

Overall, in conjunction with observations from Flavell and colleagues, our experiments employing neuronal-specific targeting of non-canonical inflammasome components suggest that by engaging NLRP6 and Casp11, iEANs can utilize a novel means to sense and respond to luminal microbial signals, to actively partake in immune

defense (Jarret et al., 2020), albeit activation of this pathway comes at a cost at the individual cell level, and in the case of excessive activation, with consequences for tissue integrity, intestinal function and systemic metabolism. As such, this form of immune engagement is similar to the aforementioned pathogen sensing and response capacity reported for TRPV1+ sensory afferents in the skin promoting enhanced and anticipatory immunity (Cohen et al., 2019; Maruyama et al., 2018).

### 4.3.2 Potential triggers of iEAN NLRP6/Casp11 activation

What signals induce NLRP6/Casp11 activation? At this point, the specific ligand(s) that elicit NLRP6/Casp11 activation in the settings of *Salmonella* infection and microbial depletion we have investigated is unclear. Only lipoteichoic acid (LTA) produced by Gram-positive pathogens has so far been suggested to act as a direct ligand of cytosolic NLRP6 (Hara et al., 2018), thus unlikely a major player in our contexts, as both *Salmonella* and *Yersinia spp*. are Gram-negative pathogens. However, one common feature of enteric infections and antibiotic-mediated microbial depletion is that they both result in a state of dysbiosis. Additionally, our results demonstrate that microbiota normalization, i.e., correcting dysbiosis, leads to neuronal recovery. It is thus plausible that microbial components or their metabolites are involved in activation and/or dampening of NLRP6/Casp11.

One potential route of NLRP6 activation may be via sensing of bile acids (BAs) or their derivatives. BAs are drastically altered in GF, antibiotic-treated and *Salmonella*-infected mice (Claus et al., 2008; Crawford et al., 2012; Sayin et al., 2013; Selwyn et al., 2015; Wostmann, 1973; Zarrinpar et al., 2018), with a specific increase in primary BAs and the BA-conjugate taurine, at the expense of secondary BAs (Sayin et al., 2013; Zarrinpar et al., 2018). BAs and their derivatives on their end can act as triggers of other inflammasome sensors (Alimov et al., 2019; Gong et al., 2016; Zhao et al., 2016). Furthermore, taurine has been reported to promote the assembly of an NLRP6-ASC-Casp1/11 complex (Levy et al., 2015), which may explain the reduced iEAN frequency observed in GF mice in our analyses. This is further supported by the finding that partial correction of the altered BA pool normalized GI functional changes associated with iEAN reduction in GF mice (Yano et al., 2015). Re-derivation of neuronal-specific *Nlrp6/Casp11* KO mice could be used to further explore the role of BAs and BA conjugates in iEAN survival in GF mice. It stands to reason that BA alterations might be similarly involved in settings of dysbiosis: Belkaid and colleagues showed that following an initial infection, commensal bacterial species metabolizing taurine to sulfide enhanced resistance to a subsequent infection by limiting pathogen respiration (Stacy et al., 2021). Thus, accumulating taurine levels in GF or dysbiotic settings may enhance NLRP6 activation, whereas its utilization and further metabolization by commensal species can be protective. In view of above mentioned reported protective effects found for iEAN IL-18 during homeostasis and acute *Salmonella* infection (Jarret et al., 2020), and our own findings of *Salmonella*-induced, NLRP6/Casp11-mediated iEAN death, one possibility is that during homeostasis, low levels of taurine act on submucosal iEAN to promote NLRP6-dependent IL-18 production and barrier integrity. During dysbiosis or in the

absence of a microbiota, significant shifts in the BA pool, with failure to metabolize taurine and accumulation thereof, result in a drastic increase in inflammasome activation and iEAN pyroptosis. Experimentally, this model could be tested using a BA sequestrant during infection or microbial depletion, coupled with bile acid-receptor-deficient (e.g., $FXR^{fl/fl}$, GPBR-1 KO) animals (Poole et al., 2010) and aforementioned GF-rederived neuronal-specific *Nlrp6/Casp11* knockout mice. Re-establishing a balanced BA pool through e.g., targeted colonization or precision microbiome reconstitution (Buffie et al., 2015; Studer et al., 2016), could then be leveraged to restore a normal gut flora and re-establish a balanced BA pool. Finally, the originally developed $Oligo^{MM12}$ consortium does not contain species capable of converting primary to secondary BAs, but addition of one additional strain, *C. scindens*, is sufficient to perform this function without altering other phenotypes associated with $Oligo^{MM12}$ colonization – a model that could thus also be used to study BA effects on iEAN death (Studer et al., 2016).

In cultured macrophages, LPS derived from Gram-negative bacteria, including *Salmonella*, can directly activate Casp11 (Kayagaki et al., 2011; Kayagaki et al., 2013), which, in turn is capable of non-canonically activating NLRP3 (Kayagaki et al., 2011; Yang et al., 2015). It is thus plausible that activated Casp11 mediates neuronal NLRP6 inflammasome assembly in a similar, non-canonical fashion following its cleavage by *Salmonella*-derived LPS.

Microbial sensing by iEANs through immunological means, in particular aforementioned TLRs 2 and 4, has been suggested in the past. Notably, in macrophages, sensing of Gram-negative bacteria through TLR4 was necessary for Casp11 expression and autoactivation through type I IFNs, leading to non-canonical NLRP3 activation (Broz et al., 2012; Rathinam et al., 2012). However, as previously mentioned, we did not find significant iEAN TLR expression in our TRAP-seq analyses or upon mining a published iEAN single-cell dataset by Regev and colleagues (Drokhlyansky et al., 2020), suggesting that in our settings, this pathway does not play a major role.

How do luminal cues get relayed to iEANs to trigger NLRP6/Casp11 activation? As discussed in other contexts, whether direct sensing of luminal stimuli is involved in iEAN activation is unclear altogether. Given our anatomical analyses, it is more likely that information of microbial signals activates e.g., EECs or immune cells, which then act on iEANs. In this context, returning to the hypothesis of BA derivatives as potential triggers, these are known to be sensed by EECs such as L cells, which, in turn can directly and indirectly signal to EANs (Bohórquez et al., 2015; O'Leary et al., 2019).

### 4.3.3 Subtype-specific iEAN targeting

Unlike the indiscriminate iEAN loss previously observed in chemically induced murine colitis models (Mawe, 2015), our studies indicate location- and subset-specific loss of iEANs in settings of both infection and microbial depletion. Importantly, we found excitatory glutamatergic iEANs to be particularly vulnerable during infection, while primarily inhibitory SST+ iEAN were relatively increased, a finding that could be explained by the particularly high *Nlrp6* expression by excitatory iEANs. By contrast, in GF and antibiotic-treated mice, SST+ iEAN were significantly decreased. Importantly, the higher

expression of *Nlrp6* and preferential loss of excitatory iEANs following enteric infection also resulted in GI dysmotility, and may thus directly underlie the GI functional changes we find (i.e., loss of excitatory neurons leading to reduced motility). While we did not investigate *Nlrp6* expression levels of viscerofugal CART+ iEANs, it is likely that these neurons, too, highly express this inflammasome component. This is supported by our functional data showing a rescue of antibiotic-mediated metabolic dysregulation following neuronal specific *Nlrp6* depletion. These subset- and condition-specific discrepancies in iEAN vulnerability warrant further study and additional subset-specific analysis of iEAN in the steady state or under pathological conditions. What accounts for these differences triggered by different insults? What makes a particular iEAN subset particularly prone to damage in one or the other setting? Are different iEAN populations more vulnerable to different inflammatory signals?

### 4.3.4 Potential implications for other intestinal and systemic diseases

Most mechanisms proposed for inflammation-induced neuronal damage thus far are related to CNS neuroinflammation and neurodegeneration. Here, a well-studied example are inflammatory microglia in Alzheimer-s disease, whereby e.g., extracellular protein aggregates activate NLRP3 in microglia, resulting in cytokine release and damage to nearby neurons (Song and Colonna, 2018). In Parkinson's disease (PD), neuronal death has been associated with *neuronal-intrinsic* canonical NLRP3 inflammasome activation in the CNS. By contrast, NLRP6, in the nervous system, has only been reported in myeloid cells, where it was ascribed an anti-inflammatory role in settings of peripheral nerve injury and stroke (Meng et al., 2019; Ydens et al., 2015; Zheng et al., 2021). It would be interesting to evaluate whether enteric neuronal loss observed in PD patients, might engage the NLRP6/Casp11 pathway brought forth here. Our finding of discriminate, subset-specific iEAN targeting could be relevant here, as enteric dopaminergic and other excitatory populations are understood to be preferentially lost and underlying the GI dysfunction associated with PD (Fornai et al., 2016; Rao and Gershon, 2016).

The apparent link observed in our studies, between returning to a "normal" microbiota by correcting dysbiosis, and iEAN recovery offers an interesting direction for studies of further enteric, but also central neuropathies, and a potential therapeutic angle. What are possible microbial signals that allow for maintenance or rescue of neuronal populations? Do specific bacterial species play a beneficial or detrimental role in this process? Detection of signals from commensals by sensory eEANs or viscerofugal iEANs could, for example, induce continuous low-grade catecholamine release during homeostasis, resulting in MM $\beta_2$-AR-Arg 1-polyamine signaling and iEAN inflammasome inhibition. One could also speculate that restoration of pre-infection flora could be employed as a treatment for post-infectious IBS and possibly other diseases involving dysbiosis and GI dysfunction.

## 4.4 Muscularis macrophages as mediators of tissue protection

### 4.4.1 Tissue-protective programming of MMs through neuronal communication

Since the discovery of the cholinergic anti-inflammatory pathway by Tracey and colleagues, the involvement of catecholaminergic neurons in anti-inflammatory responses has been demonstrated in different tissues and is attributed to the broad sympathetic innervation in peripheral tissues associated with expression of $\beta_2$-ARs in immune cells (Pavlov et al., 2018). Catecholamine engagement with adrenergic receptors expressed by both innate and adaptive immune cells is now appreciated as an important regulator of immune responses including modulation of cytokine production and other inflammatory mediators. For example, NE-mediated $\beta_2$-AR activation is crucial for controlling mobilization of hematopoietic cells from the bone marrow and lymphocytes from peripheral lymphoid tissues, whereby $\beta_2$-AR-engagement inhibits e.g., T cell egress from innervated lymph nodes to sites of inflammation. While the effects of the SNS on immune cells is generally thought to be anti-inflammatory, it is receptor-dependent: $\beta_2$-AR signaling predominantly dampens pro-inflammatory cytokine production, while α-AR engagement can also result in heightened cytokine production by e.g., macrophages (Pavlov et al., 2018).

Notably, while the efferent arm of the inflammatory reflex was initially thought to be a purely parasympathetic pathway, it has now become clear that through innervation of sympathetic ganglia, parasympathetic stimulation of sympathetic neurons can indirectly modulate AR-mediated immune function (Rosas-Ballina et al., 2008; Rosas-Ballina et al., 2011). Tracey and colleagues showed that vagal stimulation of sympathetic CG-SMG neurons projecting to the spleen results in their release of NE and $\beta_2$-AR engagement of ACh-producing T cells, which in turn, inhibit cytokine production of nAChR-expressing macrophage (Rosas-Ballina et al., 2008; Rosas-Ballina et al., 2011).

By contrast, the effects of sympathetic NE release in our studies seem to be a result of direct engagement of SNS-released NE and $\beta_2$-AR engagement of MMs. This is supported by our finding that MMs did not express the nAChR, unlike what is reported in other tissue sites and immune cell populations. Additionally, in the myenteric region, MMs far outnumber any other immune cell type. Finally, while effects mediated via glia would be conceivable, our experiments depleting enteric glia did not result in changes to iEAN loss during *Salmonella* infection, suggesting that their presence is not required for MM-mediated tissue protection through $\beta_2$-AR engagement.

$\beta_2$-AR-mediated sympathetic control of intestinal immune responses was also shown to modulate other intestine-resident cells, particularly ILCs. Upon helminth infection, $\beta_2$-AR stimulation of ILC2s residing in close proximity to sympathetic nerve terminals negatively regulated their activity and proliferation following $\beta_2$-AR agonist treatment. By contrast, $\beta_2$-AR-deficient mice exhibited heightened ILC2 responses, resulting in accelerated pathogen clearance (Moriyama et al., 2018). Aside from sympathetic eEANs, activation of VIPergic EANs have been implicated in suppressing IL-22 production by ILC3s during food consumption to enhance nutrient absorption, while transiently rendering mice more susceptible to bacterial infection (Talbot et al., 2020).

Further, the neuropeptide CGRP, expressed by sensory afferents and iEANs, fine-tuned ILC2 activity by selectively enhancing IL-5 secretion (Nagashima et al., 2019; Wallrapp et al., 2019; Xu et al., 2019). Similarly, mucosal glia cells were shown to fine-tune homeostatic ILC3 activity through enhancing their secretion of anti-inflammatory IL-22 via TLR-mediated, Myd88-depedent sensing of commensal microbes, a process partially dependent by glia-LpM crosstalk (Ibiza et al., 2016). An example of *enhanced* immune activity mediated by neuronal communication is the finding that cholinergic EANs, through secretion of NMU and engagement with its receptor expressed by ILC2, can boost their pro-inflammatory activity during helminth infections (Cardoso et al., 2017; Klose et al., 2017; Wallrapp et al., 2017). Can MMs similarly to ILCs engage in other neuro-immune circuits? Our finding that the tissue protective effects in MMs differed in their dependence on eEAN-catecholamine-$\beta_2$-AR signaling between bacterial and helminth infections may be explained by involvement of other eEAN (e.g., vagal)-MM pathways during helminth infections, albeit non-neuronal, i.e., immune or epithelial circuits are also possible. These discrepancies in $\beta_2$-AR dependence also underscore that MM programing is dynamic and context-dependent. Further, while direct evidence for neuronal engagement is lacking, activation of MMs and their production of proinflammatory cytokines was shown to correlate with a loss of ICCs and subsequent dysmotility in cases of diabetes-associated gastroparesis (Cipriani et al., 2018). Similarly, during POI, the characteristic immune infiltrate was shown to be dependent on activation of MMs, while cholinergic stimulation dampened this process (Farro et al., 2017). Thus, MMs appear to have proinflammatory potential, and likely possess further means to communicate with EANs.

Finally, while data for direct neuronal engagement of *mucosal* macrophages (LpMs) is absent, their close approximation to neuronal fibers in the intestinal mucosa is abundant (personal observation). Further, as mentioned above, LpMs have been shown to act as microbial sensors and engage with enteric glia to fine tune ILC3 responses. It thus appears likely that neuronal circuits exist to modulate, enhance or dampen their largely pro-inflammatory activity, or that they modulate further ENS cells. Recent advances in high resolution single-cell sequencing of intestinal macrophages (De Schepper et al., 2018) may help identify further candidates of EAN-MM and EAN-LpM interactions, and explore whether, similar to ILCs, pathways exist to modulate the activity of LpMs, e.g., during acute infections.

### 4.4.2 MM-induced polyamines and neuronal protection

Tissue-resident macrophages are appreciated to prevent inflammation-induced tissue damage and to initiate post-injury repair processes in several contexts. In models of spinal cord injury, for example, incoming monocytes are thought to mediate functional recovery via secretion of anti-inflammatory mediators (Shechter et al., 2009), although an enhancement of macrophage pro-inflammatory markers was also suggested to help CNS axonal regeneration (Gensel et al., 2009). Our data favors a neuronal protective role for muscularis-resident macrophages via upregulation of Arg1 and production of polyamines. This is complementary to previous observations suggesting that “alternatively activated”

("M2 phenotype") macrophages promote axonal growth or regeneration after CNS injury (Cai et al., 2002; Kigerl et al., 2009; Kuo et al., 2011).

Polyamines, naturally occurring aliphatic polycations, are ubiquitously distributed across all cell types and tissues (Handa et al., 2018). Their synthesis consists of conversion of l-arginine to l-ornithine by Arg1, followed by conversion to putrescine by the rate-limiting ornithine decarboxylase (ODC1), and subsequent modifications to spermidine and finally spermine. Polyamines play roles in a vast number of cellular processes, including cell development, differentiation, and proliferation, amino acid and protein biosynthesis, DNA damage, and gene regulation through histone modifications. In the nervous system, polyamines have been implicated in in modulating the activity of glutamate-gated ion channels (Igarashi and Kashiwagi, 2010), as well as in mediating neuronal protection and regeneration in ischemic stroke (Dong et al., 2014; Du et al., 2017; Han et al., 2013). However, their mechanism of action in the neurons is largely unclear.

In the context of innate immunity, polyamines are associated with influencing macrophage polarization. Classical work by Tracey and colleagues showed that spermine inhibits proinflammatory cytokine synthesis of monocytes and macrophages, providing a counterregulatory mechanism that restrains immune responses (Zhang et al., 1999; Zhang et al., 1997; Zhang et al., 2000). Regenerating tissues were shown to contain higher levels of spermine released by injured and dying cells (Zhang et al., 2000). Through epigenetic changes, putrescine is thought to inhibit proinflammatory macrophage gene transcription ("M1 phenotype"). Further, during macrophage activation, spermidine and spermine were shown to regulate the transcription of proinflammatory mediators, whereby spermidine is thought to enhance, and spermine inhibit their transcription (Latour et al., 2020). While some of these effects may also play a role in the MM-neuroprotective effects we observed upon infection, our data primarily suggest a role for these molecules in preventing neuronal cell death via modulation of the inflammasome. This is supported by previous work demonstrating that microbiota-derived spermine regulates NLRP6 inflammasome signaling and IEC secretion of IL-18 (Levy et al., 2015), which could also play tissue protective roles in the enteric infection models described here.

How could MM-released polyamines reach iEANs to act on the inflammasome? While we did not address how specifically these molecules may reach and enter iEANs, we ruled out a glia-mediated process. It is plausible that these molecules get released into the extracellular space and are taken up by nearby iEANs through carrier-mediated processes, as previously suggested (Li et al., 2020; Zhang et al., 2000). This would be in line with previous findings describing that tissue levels of spermine increase in sites of injury, with the potential to influence the inflammatory milieu (Zhang et al., 2000).

How specifically they may act on iEAN inflammasome machinery itself is also unclear, which is further hampered by the fact that the triggers of NLRP6/Casp11 activation are for the most part unclear altogether, as discussed above. However, given that their influence on the inflammatory profile on macrophages is thought to be via modulating the transcription of pro-inflammatory genes (Latour et al., 2020), it is plausible that their influence on inflammasome components occurs in a similar fashion.

In addition to modulating iEAN inflammasome activity, what other functions could MM-induced polyamines have? As mentioned, one main mechanism by which polyamines are thought to act, is through epigenetic modifications and influencing of gene transcription. Similarly, the phenomenon of innate immune memory (discussed below) is thought to be regulated by epigenetic and metabolic modifications that account for the ability of myeloid cells to produce specific inflammatory cytokines (Mulder et al., 2019), albeit the underlying mechanisms driving innate immune memory are not yet fully understood. It would be interesting to investigate whether polyamines, produced by MMs during an ongoing infection, may shape their epigenetic signature, resulting in long-term programming to an anti-inflammatory signature. This could then drive their own enhanced protective signature during a subsequent infection, as we observed in our settings of multiple infections, which did not result in cumulative iEAN damage.

### 4.4.3 MMs as mediators of disease tolerance: potential role of innate immune memory

We found that following enteric infections, MMs acquire a tissue-protective phenotype, preventing exacerbated iEAN damage and protecting from neuronal loss during subsequent heterologous challenges. These results strongly suggest what is now known as innate immune memory, specifically “trained tolerance”.

While immunological memory was traditionally thought to be an exclusive feature of adaptive immune cells, it is increasingly appreciated that innate immune cells can acquire certain adaptive characteristics. Innate immune memory refers to long-lasting cellular reprogramming following an unspecific immune stimulus, which, upon return to steady state, leads to a modified response to a secondary unrelated stimulus (Netea et al., 2011). This can result in either an enhanced (i.e., trained immunity) or a dampened (i.e., trained- or disease tolerance) response during subsequent encounter with an unrelated pathogen (Netea et al., 2020). Our data suggest a third arm: trained tolerance mediated by enhancement of tissue-protective (rather than dampening of pro-inflammatory) activity of MMs.

Trained immunity and tolerance can be viewed as opposite functional outcomes of innate immune memory, where infection-induced enhancement can lead to improved pathogen resistance, while infection-induced dampening/enhanced tissue-protective activity can prevent inflammation-induced tissue damage. Yet, each come at the risk of damaging the host as seen in e.g., certain cases of autoimmunity and chronic inflammation (enhancement), (Arts et al., 2018) or sepsis (tolerance) (Chen et al., 2015a) (Boraschi and Italiani, 2018). Classic examples of trained immunity or tolerance include the observation that infection with an attenuated *Candida albicans* strain protected against subsequent fulminant infection with a virulent strain in a lymphocyte-independent fashion (Bistoni et al., 1986). Similarly, priming with the fungal cell wall component β-glycan rendered mice resistant to sepsis during infection with *Staphylococcus aureus* (Di Luzio and Williams, 1978).

Mechanistically, rather than gene recombination, as is the case for adaptive immune memory, innate immune memory is retained in the form of epigenetic

modifications and in some cases, changes to cellular immunometabolism (Boraschi and Italiani, 2018; Netea et al., 2020). Chromatin immunoprecipitation (ChIP)-seq or assay for transposase-accessible chromatin (ATAC)-seq analyses of MMs before and after primary infection will allow us to determine whether such an epigenetic signature is induced in our heterologous infection settings, and definitely determine involvement of innate immune memory.

In tissue-resident immune cells, innate immune memory is thus far not well studied. Most *in vivo* studies have focused on circulating monocytes during blood-borne infections. While early studies have found LPS priming to dampen monocyte responses to secondary insults, training is largely thought to be beneficial by enhancing pro-inflammatory monocyte activity, resulting in accelerated pathogen clearance (Netea et al., 2020). By contrast, our findings rather suggest enhanced *tolerance* following primary infections with both pathogenic bacteria and parasitic helminths. This resulted in iEAN protection from cumulative damage during subsequent insults.

Our findings of anti-inflammatory training promoting neuronal protection relate to a recent report studying microglia-neuron interactions in the CNS. Wendelin *et al.* described divergent phenotypes of microglia following peripheral LPS priming, resulting in either enhanced or dampened secondary responses, depending on the number of times LPS priming was performed (Wendeln et al., 2018). Molecularly, the altered secondary responses were linked to differential epigenetic modulations in microglia. Functionally, enhanced immunity during secondary challenges exacerbated, while tolerance alleviated CNS neuropathology in mouse models of both stroke and Alzheimer's disease (Wendeln et al., 2018). Given these parallel reports in the CNS and periphery, it would be interesting to explore the memory signatures of macrophages in other neuropathologies, such as diabetic enteric neuropathies, conditions associated with chronic intestinal inflammation, including a pro-inflammatory MM phenotype (Niesler et al., 2021).

Innate immune memory is, with a few exceptions, thought to last for days to months, rather than years or a lifetime; as is the case for adaptive memory, although there are reports of long-term responses in the case of bacillus Calmette-Guérin (BCG) vaccine-induced trained immunity (Netea et al., 2016). By contrast, our results identify two complementary mechanisms that last several months and converge into activation of neuro-protective MMs. Could similarly long durations be observed in other tissue-resident populations, such as microglia in the CNS or non-immune cells? Overall, the duration of innate memory is not well studied and will need to be further defined at the level of bone marrow precursors or long-lived tissue-resident cells. It will also be important to evaluate the duration of these effects in other infections. What are the determinants of waning of trained immunity? Can its duration be extended?

More recently, in addition to innate immune cells, non-immune cells have also been reported to have innate immune memory capacity. In a murine model of imiquimod-induced skin inflammation, Naik and colleagues reported that skin stem cells retained memory of the initial insult through epigenetic modifications. These modifications allowed for continued accessibility of transcription factors to stress response genes. During secondary, unrelated insults, these cells could rapidly respond, resulting in accelerated wound healing (Netea et al., 2020), findings conceptually related to the enhanced MM-

induced iEAN protection we find upon heterologous infection. Is the intestinal epithelial stem cell niche capable of retaining memory in a similar fashion to enable faster tissue recovery following disruption of epithelial integrity? Could other intestine-resident or -projecting cells, such as iEAN, glia or neuronal precursors possess innate immune memory capacity as well?

Further, can innate memory be compartmentalized within a cell type in the intestine? For example, following an insult, do LpMs and MMs get differentially programmed on an epigenetic level? ChIP- or ATAC-seq analyses of the different intestinal macrophage populations following an initial insult would help answer this question. Finally, analyzing these MM populations and iEANs in wild mice, which get repeatedly exposed to pathogens in their natural environment throughout their lifetime, would be of value. Indeed, follow-up studies from our lab revealed that mice obtained from a pet store, i.e., more pathogen-exposed than laboratory animals, albeit likely less so than wild mice, did not lose iEANs following *Salmonella spiB* infection, and exhibited enhanced Arg1 expression in MMs already at a experimentally naïve stage (Ahrends et al., 2021), raising the possibility that infections early in life can determine the number of enteric neurons during adulthood.

### 4.5 Role of local and systemic stress in intestinal inflammation and tissue protection

Stress, a real or perceived threat to homeostasis (Smith and Vale, 2006), is met with a complex array of responses integrating endocrine, neuronal and immune pathways in an attempt to maintain homeostasis in the face of an imminent challenge (Schiller et al., 2021; Smith and Vale, 2006). The classical stress response involves two main pathways: Activation of the HPA axis, resulting in glucocorticoid release, and activation of the sympathetic nervous system, resulting in local, site-specific norepinephrine/epinephrine (NE/E) release. In addition, sympathetic innervation of the adrenal medulla can also stimulate release of adrenal NE/E into the blood stream, leading to their systemic circulation (Schiller et al., 2021). The effects of acute stress are typically thought to be immunosuppressive. However, in the context of cellular damage and death, glucocorticoids can promote pro-inflammatory immune responses, particularly in the CNS (Bellavance and Rivest, 2014; Di Giovangiulio et al., 2015). We found acute whole-body stress in mice to provide significant iEAN protection during enteric infections, an effect that was dependent on MM Arg1 signaling and was lost after specific depletion of Arg1 in myeloid cells.

As mentioned, stress responses can involve both local sympathetic and systemic adrenal release of catecholamines. Hence, the source of catecholamines may be context dependent: Enteric infections may result in the activation of extrinsic sympathetic neurons (Gabanyi et al., 2016). Under conditions of systemic stress, these signals could also originate from the adrenal glands (Kvetnansky et al., 2009). However, our finding that bilateral adrenalectomy followed by infection with attenuated *Salmonella* resulted not in enhanced, but rather reduced neuronal loss, argue against a crucial role for systemic catecholamines in iEAN protection following enteric infections. It further opens up the

possibility that systemically released catecholamines, or, more likely corticosteroids, while essential in disseminated infections, as seen e.g., in adrenalectomized rats succumbing to systemic *Salmonella* challenge, and patients with adrenal insufficiency (Edwards et al., 1991; Sternberg, 2006), could play a detrimental role in iEAN survival during the course of localized intestinal infections. This discrepancy may be related to the aforementioned findings that while primarily immunosuppressive, corticosteroids can also pro-inflammatory effects, observations made predominantly in the CNS (Smith and Vale, 2006). Could stimulation of these local, protective stress pathways in settings of chronic infection or inflammatory diseases alter their course, i.e., induce protection?

How would chronic or repeated systemic stress exposure impact the outcome of an acute GI infection with regard to iEAN survival? Exposing mice to regular stressors, i.e., habituation through mock i.p. injections prior to i.p. interventions, diminished neuro-protective effects previously observed in experiments involving i.p. injections. Thus, our findings suggest a dampening of acute stress responses through repeated exposure to a known stimulus. They further emphasize the importance of controlling for stress as a confounding factor in experimental settings, particularly in the context of inflammation.

### 4.6 Microbial modulation of gut-sympathetic efferents during enteric infections: Sensing and regulation of the catecholamine-$\beta_2$-AR pathway

Upon eliminating a role for circulating catecholamines, our findings established an intricate interplay between iEANs, macrophages and sympathetic eEANs in the response to intestinal infections. The circuitry connecting sensing of luminal pathogens to eEAN activation is, as with other EAN populations, still poorly understood (Muller et al., 2020b; Pruss et al., 2017). Our extensive analyses suggest that direct sensing through sympathetic fibers projecting to the intestine is highly unlikely. Polysynaptic tracing experiments and targeting of sensory channels or receptors on EECs (or more broadly, IECs) or sensory afferents and/or receptors expressed by effector EANs, determined by mining of transcriptional data sets generated by us and others, could determine this missing link to sympathetic activation (Veiga-Fernandes and Mucida, 2016).

Considering that the CG-SMG forms a major integrative regulatory center that coordinates information flow between CNS, and multiple visceral organs (Kaestner et al., 2019), several pathways leading to gut-projecting sympathetic fiber activation during enteric infections are plausible: (i) Sensory afferents (NG/DRG) polysynaptically connected to preganglionic sympathetic neurons in the spinal cord could activate CG-SMG efferents via activation of preganglionic neurons, similar to what we reported for microbial depletion (Muller et al., 2020b) . (ii) Sensory afferents receiving input from IECs/EECs could activate CG-SMG sympathetic efferents through collateral axons innervating the CG-SMG (Kaestner et al., 2019). (iii) Sensory afferents projecting to NG/DRG could activate vagal efferents innervating the CG-SMG, a connection that has anatomically been shown, but has not been functionally characterized. (iv) Viscerofugal iEANs could activate sympathetic efferents through a direct, CNS-independent pathway.

It appears likely, that several – possibly redundant – pathways exist to modulate local sympathetic activity during an acute insult. Exploration of these pathways would

provide insight into sympathetic control of intestinal function during perturbations. For example, one could profile MMs and determine iEAN survival after *Salmonella* infection following vagotomy, i.e., eliminating cholinergic anti-inflammatory input. Reducing viscerofugal input to the CG-SMG through antibiotic pre-treatment would be feasible to determine whether a direct circuit between intestinofugal iEANs and sympathetic efferents may be of relevance during enteric infections.

How is this eEAN control of MMs altered in settings of *chronic* GI inflammation? It is intriguing to speculate on whether eEANs may – like other non-immune cells – have a form of innate memory potential. In such a case, could they get "primed" during an initial infection such that during a subsequent one, their stimulation of MMs to exert their tissue-protective functions is further boosted? In other words, rather than innate memory through epigenetic changes in MMs themselves, or in bone marrow precursors, could sympathetic eEANs retain such memory, and act on MMs with heightened NE release during a subsequent challenge? Evaluating the epigenetic signature of gut-projecting eEANs by ChIP-seq could help answer this question. Information obtained from such experiments could get leveraged to "re-program" MMs or infiltrating proinflammatory monocytes during chronic inflammation, as seen in e.g., diabetic enteric neuropathy. In a non-mutually exclusive scenario, could stimulation by sympathetic eEANs extend the duration MM innate memory?

### 4.7 Concluding remarks

The goal of this work was to elucidate the influence of intestinal microbes – commensal bacteria and pathogens – on enteric nervous and immune systems, and the interactions between them.

Our studies highlighted a critical influence of the gut-resident microbiota on intrinsic and extrinsic enteric-associated neurons. Specifically, gut-intrinsic enteric neurons depend on a normal microbial composition for their survival. We found that during microbial disturbances, such as dysbiosis and enteric infections, enteric neurons die in a unique, inflammatory manner, whereby certain subsets are particularly vulnerable to microbial alterations. We further uncovered a microbiota-dependent subset of enteric neurons critical for regulating systemic metabolic functions independently of the central nervous system. During enteric infections, multi-network communication between gut-extrinsic sympathetic neurons, gut-resident macrophages and intrinsic enteric neurons ensures enteric neuronal protection and intestinal tissue integrity. Conversely, dysregulation of the crosstalk between gut macrophages and enteric-associated neurons during microbial perturbations leads to enhanced alterations to the enteric neuronal network and exacerbated loss of microbiota-dependent subsets, with consequences for local intestinal function and alterations to systemic glucose metabolism. These findings open new doors for understanding how different systems interact, and for developing new treatments for debilitating disorders including metabolic syndrome and irritable bowel syndrome. Looking ahead, it will be exciting to dissect further roles of these dialogues to expand our understanding of host physiology and leverage knowledge gained from such studies for therapeutic purposes.

## MATERIALS AND METHODS

**Mice.** *Wild-type mice used:* C57BL/6J (C57BL/6J, Jackson, 000664 or C57BL/6NTac, Taconic, B6-M/F), CBA/J (Jackson #000656), BALB/cJ (Jackson #000651), CD45.1 B6 (B6.SJL-Ptprc$^{a}$ Pepc$^{b}$/BoyJ).
*Transgenic mice used: Casp1$^{-/-}$Casp11$^{-/-}$*(B6N.129S2-Casp1tm1Flv/J, 016621), CCR2$^{-/-}$ (B6.129S4-*Ccr2$^{tm1Ifc}$*/J, 004999), LysM$^{Cre}$ (B6.129P2-*Lyz2$^{tm1(cre)Ifo}$*/J), *Arg1*$^{flox/flox}$ (C57BL/6-*Arg1$^{tm1Pmu}$*/J), Rosa26$^{tdTomato}$ (B6.Cg-Gt(ROSA)26Sor$^{tm14(CAG-tdTomato)Hze}$/J), VGLUT2$^{Cre}$ (*Slc17a6$^{tm2(cre)Lowl}$*/J), *Rpl22*$^{HA}$ (B6N.129-Rpl22$^{tm1.1Psam}$/J), 129S1(129S1/SvImJ), *Cx3cr1*$^{GFP}$(*Cx3cr1*$^{tm1Litt/LittJ}$), *Phox2b*$^{cre}$ (B6(Cg)-Tg(Phox2b-cre)3Jke/J), *Snap25*$^{Cre}$(*Snap25$^{tm2.1(cre)Hze}$*), NSG (NOD.Cg-*Prkdc$^{scid}$Il2rgtm1$^{Wjl}$*/SzJ), *Casp11$^{-/-}$* (Casp4tm1Yuan/J) , and R26-CAG-ASC-citrine (B6.Cg-Gt(ROSA)26Sortm1.1(CAG-Pycard/mCitrine*,-CD2*)Dtg/J), *Plp1$^{creERT}$* (B6.Cg-Tg(Plp1-cre/ERT)3Pop/J), *Rosa26*$^{lsl-hM4Di}$ (B6N.129-*Gt(ROSA)26Sor$^{tm1(CAG-CHRM4*,-mCitrine)Ute}$*), and ROSA-DTA (B6.129P2-*Gt(ROSA)26Sortm1(DTA)*Lky/J) RiboTag (B6N.129-*Rpl22$^{tm1.1Psam}$*, Jackson, 011029), *Snap25*$^{Cre}$ (B6;129S-*Snap25$^{tm2.1(cre)Hze}$*, Jackson, 023525), *Cart*$^{Cre}$ (B6;129S-Cartpttm1.1(cre)Hze/J, Jackson, 028533), *Npy*$^{Cre}$ (B6.Cg-Npytm1(cre)Zman/J, Jackson, 027851), *Agrp*$^{Cre}$ (Agrptm1(cre)Lowl/J, Jackson, 012899), *Rosa26*$^{lsl-tdTomato}$ (B6.Cg-*Gt(ROSA)26Sor$^{tm14(CAG-tdTomato)Hze}$*, Jackson, 007914), *Casp11$^{-/-}$* (Casp4tm1Yuan/J, Jackson, 024698), Il4;Il13$^{flox/flox}$ (Jackson # 031366, B6.129P2(Cg)-Il4/Il13$^{tm1.Lky}$/J), *Nlrp6*$^{flox/flox}$ by P. Rosenstiel (targeting of Exon 1 of *Nlrp6*, frozen sperm generously provided by T. Kanneganti), and *Casp11*$^{flox/flox}$ by KOMP and A. Wullaert, SNS$^{cre}$ (Tg(*Scn10a*$^{cre}$)1Rkun were a gift of R. Kuhner, Nestin$^{GFP}$ (Tg(Nes-EGFP)33Enik were generously provided by P. Frenette and G. Enikolopov, *Adrb2*$^{flox/flox}$ (Adrb2$^{tm1Kry}$) by G. Karsenty, eoCRE (Epx$^{tm1.1(cre)Jlee}$) and iPHIL (Epx$^{tm2.1(HBEGF)Jlee}$) by E. Jacobsen and *Sox10*$^{CreERT2}$ (Tg(Sox10-icre/ERT2)26Vpa) were generously provided by B. Gulbransen and V. Pachnis. *Fos*$^{GFP}$ (B6.Cg-Tg(Fos/EGFP)1-3Brth, Jackson #014135), *Glp1r*$^{cre}$ (*Glp1r$^{tm1.1(cre)Lbrl}$*/J, Jackson #029283), *Villin*$^{creERT2}$ (Tg(*Vil*-cre/ERT2)23Syr), *Tph1*$^{flox}$ (*Tph1$^{tm1Kry}$,* gift of G. Karsenty), *Htr3a*$^{Cre}$ (Gift of N. Heintz), Glp1r$^{tm1Ddr}$ or *Glp1r$^{-/-}$* (gift of D. Drucker and generously provided by J. Ayala), *Gpr43$^{-/-}$* (Gift of N. Arpaia), *Gpr43$^{-/-}$ /Gpr109a$^{-/-}$* (gift of S. Mehandru), *Gpr41$^{-/-}$* (gift of J. Gordon and M. Yanagisawa, generously provided by J. Pluznick).
*Gnotobiotic mice used:* Germ-Free (GF) C57BL/6J and *Snap25*$^{RiboTag}$. For comparisons to GF mice, respective SPF mice were maintained on sterilized Autoclavable Mouse Breeder Diet (5021, LabDiet, USA) (GF diet), the same used in the gnotobiotic facility. Controls for GF C57BL6/J mice were previously GF and kept on a GF diet under SPF conditions for several generations (exGF). Controls for GF *Snap25*$^{RiboTag}$ mice were *Snap25*$^{RiboTag}$ SPF mice maintained on a GF diet. All other mice used in this study were maintained on a standard Mouse Breeder Diet and we note no difference in fasting blood glucose levels between mice fed a standard diet and those that were switched to a GF diet. ExGF and all other WT or transgenic mice were housed in the same room in our animal facility under SPF conditions. Housing related to GF colonization with bacteria is detailed below. Mice were bred within our facility to obtain strains described and were 7-12 weeks of age for all experiments unless otherwise indicated. Female mice were used

for all sequencing experiments. Male and female mice were used for all other experiments due to multiple genetic models utilized. Estrous cycle was not controlled for in female mice. Animal care and experimentation were consistent with NIH guidelines and approved by the Institutional Animal Care and Use Committee (IACUC) at The Rockefeller University.

**Microorganisms.** *Salmonella enterica* serovar Typhimurium (SL1344) and its mutant *spiB* were used for infection experiments and cultured prior to infection as described below. *Yersinia pseudotuberculosis* (IP32777) was cultured prior to infection as described below. *Strongyloides venezuelensis* was maintained in our facility by periodically infecting NSG mice and culturing larvae as described below. *Toxoplasma gondii* was maintained in our lab by periodically infecting C57BL/6 mice with 5 cysts administrated intraperitoneally (i.p.). Cysts were isolated from brain tissue 30 days after infection. *Trypanosoma cruzi*. The *T. cruzi* Y strain was maintained by serial passage from mouse to mouse.

**Enteric infections.** *Salmonella enterica* Typhimurium. For infections with *Salmonella spiB*, mice were pre-treated with a single dose of Streptomycin (20 mg/mouse dissolved in 100 $\mu$l of DPBS) administered by oral gavage 18-24 hours prior to infection Mice were then orally inoculated with $10^9$ CFU of *spiB*. For *Salmonella* re-infection experiments, mice were subjected to *spiB* infection as described above. 1 week post clearance of *spiB* from the feces, mice were fasted for 4 hours and infected with $10^6$ CFU of wild-type *Salmonella enterica* Typhimurium (SL1344). For all *Salmonella* infections, a single aliquot of either strain of *Salmonella* was grown in 3 ml of LB overnight at 37ºC with agitation. Bacteria were then sub-cultured (1:300) into 3 ml of LB for 3.5 hours at 37ºC with agitation, and diluted to final concentration in 1 ml of DPBS. Bacteria were inoculated by gavage into recipient mice in a total volume of 100 $\mu$l. For experiments using heat-killed *spiB*, samples subjected to heat treatment (95°C for 10 min in water bath), prior to gavage and successful inactivation was confirmed by plating a serial dilution made from the suspension and then 5 $\mu$L onto Salmonella-Shigella plates.

*Yersinia pseudotuberculosis*. *Y. pseudotuberculosis* (strain IP32777) was grown as previously described with some adjustments (Fonseca et al., 2015). Briefly a single aliquot of the strain was grown in 3 ml of 2xYT media overnight at 28°C with vigorous agitation. Mice were fasted for 12 hours prior to infection with $10^8$ CFU by oral gavage.

For heterologous re-infection experiments, mice infected with *Y. pseudotuberculosis* as described above were subjected to $10^9$ CFU of *Salmonella spiB* on day 21 days post *Y. pseudotuberculosis* infection, and sacrificed 10 days post-secondary (*spiB*) infection.

*Strongyloides venezuelensis. S. venezuelensis* was maintained in our facility in NSG mice by subcutaneous infection with 700 larvae, resulting in chronic infection of this strain. For each experiment, feces of infected NSG mice were collected and spread on Whatman paper, which was placed into a beaker with water and incubated at 28 °C. The hatching larvae were collected over 2-3 days. Mice were infected subcutaneously with 700 larvae/100 $\mu$l water per mouse. *S. venezuelensis* was passaged by periodically infecting naïve adult NSG mice.

*Toxoplasma gondii*. *T. gondii* was maintained in the lab by periodically infecting mice administered by intraperitoneal injection of 5 cysts/mouse in a total volume of 100 $\mu$l of DPBS.
*Trypanosoma cruzi* (*T. cruzi, Y strain)*. For each experiment, blood from an infected mouse was collected, parasites were quantified, and naïve recipient mice infected by intraperitoneal injection of $10^4$ parasites. Infected mice were sacrificed for tissue analysis at day 22 post infection, when the parasite load reaches a plateau (Arantes et al., 2004).

**Virus.** The following viruses were used: AAV9-hSyn-HI-eGFP-Cre-WPRE-SV40 (105540-AAV9), AAV9-hSyn-eGFP-WPRE-bGH (Addgene #105539-AAV9), AAV9-hSyn-DIO-hM3D(Gq)-mCherry (Addgene, 44361), AAV9-hSyn-DIO-hM4Di(Gi)-mCherry (Addgene, 44362), AAV9-hSyn-DIO-mCherry (Addgene, 50459), AAVrg-CAG-FLEX-tdTomato (Addgene, 28306), AAV5-mCherry-FLEX-DTA (UNC Vector Core), AAV5-hSyn-hChR2(H134R)-EYFP (UNC Vector Core), and PRV-152/614 (Gift of L. Enquist). Fast Green (Sigma, F7252) was added (0.1%) to virus injected into peripheral tissues.

**Antibodies and flow cytometry.** *Antibodies used for whole-mount immunofluorescence imaging.* The following primary antibodies were used, and unless otherwise indicated concentrations apply to all staining techniques: BIII-Tubulin (1:400, Millipore Sigma, T2200; 1:200, Aves Labs, TUJ), NPY (1:200, Immunostar, 22940), SST (1:400, Millipore Sigma, MAB354), RFP (1:1000, Sicgen, AB8181; 1:1000, Rockland, 600-401-379), pCREB Ser133 (1:200, Cell Signaling Technologies, 9198S), ANNA-1 (1:200,000, Gift of Dr. Vanda A. Lennon), cFos (1:1000, Cell Signaling Technologies, 2250S), HA (1:400, Cell Signaling Technologies, 3724S), CART (1:500, R&D Systems, AF163), CD9 (AF647, 1:200, BD Biosciences, 564233), nNOS (1:200, ABCAM, ab76067), MHC II (1:400, Millipore Sigma, MABF33), S100 beta (1:200, Abcam, ab52642), ASC (1:200, Adipogen, AL177), GFP (1:400, Nacalai, GF090R). Fluorophore-conjugated secondary antibodies were either H&L or Fab (Thermo Fisher Scientific) at a consistent concentration of 1:400 in the following species and colors: goat anti-rabbit (AF488/568/647), goat anti-rat (AF488/647), goat anti-chicken (AF488/568/647), goat anti-human (AF488/568/647), donkey anti-guinea pig (AF488/647), donkey anti-rabbit (AF568/647), donkey anti-goat (AF568/647).
*Antibodies used for cell sorting of intestinal macrophages:* Fluorescent-dye-conjugated antibodies were purchased from BD-Pharmingen (USA) (anti-CD45.2, 104; anti-CD45R, RA3-6B2); eBioscience (USA) (anti-CD103, 2E7; anti-MHC II, M5; anti-F4/80, BM8; anti-CD11b, M1/70; anti-CD11c, N418; anti-Siglec F, E50-2440; anti-CD3e,145-2C11; anti-Ly6G, RB6-8C5) or BioLegend (USA) (anti-CD64 X54-5/7.1). Live/Dead staining was performed using Aqua fixable dead cell stain (Invitrogen). Macrophages were sorted as Aqua-CD45+Lin- (CD3-B220-Siglec F-LY6G-) MHCII+F4/80+CD11B+CD11C+CD103-) using a FACS Aria cell sorter flow cytometer (Becton Dickinson).
*Antibodies used for intestinal macrophage, eosinophil and mast cell flow cytometry and sorting:* CD64-APC (Clone X54-5/7.1, cat. # 13906), CD4-BV605 (Clone RM4-5, cat. # 100548), CD150 (Clone TC15-12F12.2, cat. # 115921), CD48-APC (Clone HM480-1, cat. # 103411), Lineage Cocktail-PB (cat. # 133305) were purchases from BioLegend.

Antibodies against CD11b-APC-eFluor780 (Clone M1/70, cat. # 47-0112-82), FceR1-APC (Clone MAR1, cat. # 17-5898-80), CD45-PE-Cy7 (Clone 30-F11, cat. # 25-0451-82), CD45-AF700 (Clone 30-F11, cat. # 56-0451-82), CD45.1-PE-Cy7 (Clone A20, cat. # 25-0453-82), GATA-3-PE (Clone TWAJ, cat. # 12-9966-42), FOXP3-eFluor450 (Clone FJK-16s, cat. # 48-5773-82), MHC II-AF700 (Clone M5/114.15.2, cat. # 56-5321-82), Ly-6G-eFluor450 (Clone RB6-8C5, cat. # 48-5931-82), CD11c-AF488 (Clone N418, cat. # 53-0114-82), IL-4-APC (Clone 11B11, cat. # 17-7041-82), Arg1-PE-Cy7 (Clone A1exF5, cat. # 25-36-97-82), Ly6A/E(Sca-1)-PE (Clone D7, cat. # 12-5981-82), CD16/CD32-FITC (clone 93, cat. # 11-0161-82) were purchases from Thermo Fisher Scientific. Antibodies against CD11b-FITC (Clone M1/70, cat # 553310), Siglec-F-APC-Cy7 (Clone E50-2440, cat. # 565527), -PE (Clone E50-2440, cat. # 552126) and -BV421 (Clone E50-2440, cat. # 56268), c-kit-PE-Cy7 (Clone 2B8, cat. # 558163), CD45.2-PerCP-Cy5.5 (Clone 104, cat. # 552950), CD45.2-AF700 (Clone 104, cat. # 560693), CD45R-FITC (Clone RA3-6B2, cat. # 553088), CD8a-AF488 (Clone 53-6.7, cat. # 557668), I-A/I-E-FITC (Clone M5/114.15.2, cat. # 553623), CD125-AF488 (Clone T21, cat. # 558533) were purchased from BD. Cell surface and intracellular antibodies were used at 1:200 and 1:100 dilution, respectively.

**Isolation of intraepithelial and lamina propria cells.** Intraepithelial and lamina propria cells were isolated as previously described (Bilate et al., 2016). Briefly, sections of small intestines were harvested and washed in PBS and 1mM dithiothreitol (DTT) followed by 30 mM EDTA. Intraepithelial cells were recovered from the supernatant of DTT and EDTA washes and mononuclear cells were isolated by gradient centrifugation using Percoll ®. Cells from lamina propria were obtained after collagenase digestion of the tissue. Single-cell suspensions were then stained with fluorescently labeled antibodies for 30 min on ice.

**Single Cell Suspension of Intestinal Macrophages.** Mice were euthanized, and the small intestine was carefully removed, cleaned, cut open longitudinally and washed 2X in HBSS $Mg^{2+}Ca^{2}$Gibco) and 1X in HBSS $Mg^{2+}Ca^{2}$ with 1mM DTT (Sigma- Aldrich). The tissue was cut in two and the *muscularis* region was carefully dissected from the underlying mucosa. *Muscularis* tissue was then finely cut and digested in HBSS $Mg^{2+}Ca^{2+}$+ 5% FBS + 1x NaPyr + 25mM HEPES + 50 µg/ml DNase I (Roche) + 400U/ml collagenase D (Roche) + 2.5U/ml dispase (Corning) at 37°C. The *muscularis* was digested for 40 min. The tissue was then homogenized with an 18-gauge needle, filtered through a 70 µm cell strainer and washed with HBSS $Mg^{2+}Ca^{2}$. Cells were incubated with Fc block and antibodies against the indicated cell surface markers in FACS buffer (PBS, 1% BSA, 10 mM EDTA, 0.02% $NaN_3$).

**Intracelluar staining for flow cytometry.** Intranuclear staining for transcription factors was conducted using Foxp3/Transcription Factor Staining Buffer Set according to manufacturer's instructions (eBioscience, USA). Intracellular staining for cytokines was conducted in Perm/Wash buffer after fixation and permeabilization in Fix/Perm buffer (BD Biosciences, USA) according to kit instructions. Flow cytometry data were acquired on an

LSR-II flow cytometer (Becton Dickinson, USA) and analyzed using FlowJo software package (Tri-Star, USA).

**Gating strategies.** For flow cytometric analysis following gating strategy was used to identify macrophages: single, live, myeloid cells (based on FSC, SSC and live/dead fixable dye Aqua stain), CD45+, CD11b+ and CD64+. Eosinophils: single, live, myeloid cells, CD45+, CD11b+ and Siglec-F+. Mast cells: single, live, myeloid cells, CD45+, CD117+ and FcεR1+. For all cell types, B220+ and CD8a+ cells were excluded.

**Tissue dissections.** *Intestine dissection.* Mice were sacrificed and duodenum (6 cm moving distal from the gastroduodenal junction), ileum (6 cm moving proximal from the ileocecal junction), or colon (gap of 1 cm from the cecal-colonic junction, then 6 cm moving distal) was removed. For AdipoClear, fecal contents were flushed from the lumen and left intact. For dissection of the *muscularis externa*, following the above procedures, the intestinal tissue was placed on a chilled aluminum block with the serosa facing up. Curved forceps were then used to carefully remove the *muscularis externa* in one intact sheet (Gabanyi et al., 2016).
*Nodose ganglion dissection.* Mice were sacrificed and the ventral neck surface was cut open. Associated muscle was removed by blunt dissection to expose the trachea and the nodose ganglion (NG) was then located by following the vagus nerve along the carotid artery to the base of the skull. Fine scissors were used to cut the vagus nerve below the NG and superior to the jugular ganglion.
*Celiac-superior mesenteric ganglion dissection.* Mice were sacrificed and a midline incision was made, and the viscera were reflected out of the peritoneal cavity. The intersection of the descending aorta and left renal artery was identified, from which the superior mesenteric artery was located. The CG-SMG is wrapped around the superior mesenteric artery and associated lymphatic vessels. Fine forceps and scissors were used to remove the CG-SMG.
*Dorsal root ganglion dissection.* The spinal column was isolated, cleaned of muscle, and bisected sagitally. The spinal cord was removed leaving the dorsal root ganglion (DRG) held in place by the meninges. The thoracic 13 DRG was identified by its position just caudal to thoracic vertebra. The meninges were cleared and the pair of thoracic 9 DRGs were removed with fine forceps and scissors.

**Viral injections.** Mice were anesthetized with 2% isoflurane with 1% oxygen followed by 1% isoflurane with 1% oxygen to maintain anesthesia. After shaving and sterilization of the abdomen, mice were placed on a sterile surgical pad on top of a heating pad and covered with a sterile surgical drape. Ophthalmic ointment was placed over the eyes to prevent dehydration and the incision site was sterilized. Upon loss of recoil paw compression, a midline incision was made through the abdominal wall exposing the peritoneal cavity. The duodenum, ileum, colon, or CG-SMG were located and exposed for injection. All injections were made with a pulled glass pipette using a Nanoject III. The following volumes were used for each viral injection into a different region of the intestine: AAVrg-CAG-tdTomato (1.25 µL), AAV9-hSyn-DIO-hM3D(Gq)-mCherry (1.25 µL), AAV9-

hSyn-DIO-hM4D(Gi)-mCherry (1.25 µL), AAV9-hSyn-DIO-mCherry (1.25 µL), AAV5-mCherry-FLEX-DTA (2.5 µL), and AAV5-hSyn-hChR2(H134R)-EYFP (2 µL). Following injection, the abdominal wall was closed using absorbable sutures and the skin was closed using surgical staples. Antibiotic ointment was applied to the closed surgical site and mice were given 0.05 $mg^{-kg}$ buprenorphine every 12 h for 2 days. All mice with viral transduction in the intestine (hM3Dq, hM4Di, mCherry, hChR2, and DTA) were analyzed starting at two weeks post-injection.

**Viral strategies.** *AAV9 Transduction of iEAN. Casp11*$^{flox/flox}$ mice were retro-orbitally injected with ~5 x $10^{11}$ GC of AAV9-hSyn-HI-eGFP-Cre-WPRE-SV40 (105540-AAV9) or AAV9-hSyn-eGFP-WPRE-bGH (Addgene #105539-AAV9) diluted in 100 µl of sterile DPBS. Mice were then infected at least 2 weeks post-viral injection.
*Anatomical mapping of Cart*$^{Cre}$*, Agrpt*$^{Cre}$*, Npy*$^{Cre}$ (Benskey et al., 2015). AAVrg-CAG-tdTomato (Benskey et al., 2015) was injected into the duodenum, ileum, and colon of *Cart*$^{Cre+}$*, Agrpt*$^{Cre+}$*, Npy*$^{Cre+}$ mice.
*Cart*$^{Cre}$ *modulation*. hM3Dq: AAV9-hSyn-DIO-hM3Dq-mCherry (Krashes et al., 2011)was injected into the ileum and colon of Cart$^{Cre+}$ mice. Controls were AAV9-hSyn-DIO-hM3Dq-mCherry injected into the ileum and colon of *Cart*$^{Cre-}$ mice or AAV9-hSyn-DIO-mCherry into the ileum and colon of *Cart*$^{Cre+}$ mice. All mice were injected with 1 $mg^{-kg}$ of Compound 21. hM4Di: AAV9-hSyn-DIO-hM4Di-mCherry was injected into the ileum and colon of *Cart*$^{Cre+}$ mice. Mice were injected with 1 $mg^{-kg}$ of Compound 21 or saline (controls).
*Cart*$^{Cre}$ *ablation*. AAV5-mCherry-FLEX-DTA (Wu et al., 2014) was injected into the ileum and colon of Cart$^{Cre+}$ mice. Controls were AAV5-hSyn-hChR2(H134R)-EYFP injected into the ileum and colon of *Cart*$^{Cre+}$ mice.

**Retrograde PRV Tracing.** Mice were anesthetized and operated as described above. PRV Bartha 152 (GFP) (Smith et al., 2000) or 614 (RFP) (Banfield et al., 2003) were a gift of L. Enquist. 3 µL with 0.1% FastGreen was injected with a pulled glass pipette using a Nanoject III into the parenchyma of the right liver lobe or into the head, neck, body, and tail of the pancreas. The intestine *muscularis externa* and CG-SMG were harvested one to four days after injection.

**Celiac ganglion tracing.** Mice were anesthetized and operated on as described above. 1.5 µL of AAVrg-hSyn1-Cre with 0.1% FastGreen was injected into the CG-SMG of *Rosa26*$^{lsl\text{-}tdTomato}$ mice. 1.5 µL of AAV2-CAG-FLEX-tdTomato with 0.1% FastGreen was injected into the CG-SMG of *Snap25*$^{cre}$ mice. Intestine samples were dissected after 2.5 weeks for AdipoClear, RIMS, or Focus Clear analysis.

**Fluorogold Labelling.** A stock solution of 4 mg/mL Fluorogold (Fluorochrome) was made in sterile 0.9% saline and then filter sterilized through a 0.22 µm syringe filter. An i.p. injection of 300 µL of Fluorogold solution was given 3 days before tissue harvesting.

**CTB viscerofugal tracing.** Mice were anesthetized and operated on as described above. 1.5 µL of 1% CTB-488, -555, or -647 (Thermo Fisher Scientific, C34775, C22843 and

C34778) in PBS with 0.1% Fast Green (Sigma, F7252) was injected with a pulled glass pipette using a Nanoject III into the CG-SMG. Relevant tissues were then dissected after a minimum of 2- 4 days post-injection.

**Cholera toxin tracing of gut-projecting eEANs.** Mice were anesthetized and operated on as described above. 1.5 µL of 1% CTB 488, 555, or 647 in PBS with 0.1% FastGreen was injected with a pulled glass pipette using a Nanoject III into the ileum, duodenum, colon and celiac-superior mesenteric ganglion. For triple labelling, 0.5uL of 1% CTB488, 555, or 647 was injected into the duodenum, ileum, and proximal colon of the same mice. The tissue was carefully washed several times with PBS to prevent possible spill over of tracer to other tissues. Relevant tissues were then dissected after a minimum of 2- 4 days post-injection.

**CTB NG and CG-SMG counting.** CTB488 was injected into the duodenum, ileum, and proximal colon. Mice were sacrificed by cervical dislocation and the CG-SMG and NG were harvested and fixed overnight in 4 % PFA. Tissue was then washed four times in DPBS at RT and permeabilized in PTxwH for 4 h at RT. Primary antibody anti-AlexaFluor488 (1:400, Thermo Fisher Scientific, A-11094) was added to the samples in PTxwH and incubated at 4°C for 48 h. Samples were washed four times in PTxwH at RT and then stained with goat-anti rabbit AF555/568/647 at 4°C for 24 h. Samples were washed four times in PTxwH at RT, covered in Fluormount G, and coverslipped for confocal imaging. Each ganglion was captured in full by multiple z-stacks and the total number of CTB+ neurons were counted.

**Drug Administrations.** *Salbutamol.* Salbutamol sulfate (Selleck Chemicals) was dissolved in sterile NaCl to a concentration of 56mg/ml, loaded into osmotic pumps and administered by subcutaneous implantation of the pumps at a final dose of 400*µ*g/day for 14 days.
*Pan caspase inhibition.* zVAD-FMK (Selleck Chemicals) was dissolved in DMSO and administered at a dose of 50 µg/mouse by daily intraperitoneal injections over the course of a 7-day infection starting 1 day prior to infection.
*Polyamine administration*. Spermine (Sigma-Aldrich) was administered at a concentration of 2 % in drinking water. Spermine-substituted drinking water was changed daily and fluid intake was monitored. Treatment was started 3 days prior to infection with *Salmonella spiB* and continued over the course of experiments.
*ODC1 inhibition.* Difluoromethylornithine (DFMO, gift from P. Woster, MSSM) was dissolved in tap water, filter-sterilized, and administered at a concentration of 4% in drinking water. DFMO-substituted water was changed daily and fluid intake was monitored. Treatment was started 4 days prior to infection with *Salmonella spiB* and continued over the course of experiments.
*Guanethidine treatment*. Guanethidine monosulfate (Sigma, 1301801) was given at 30 $mg^{-kg}$. For blood glucose experiments, guanethidine was given in combination with 1 $mg^{-kg}$ C21. Blood glucose was then measured at relevant timepoints. To control for stress caused by injections, mice were habituated to mock i.p. injections for at least 5

consecutive days prior to treatment. For Exendin-4 and DREADD experiments, mice were treated with guanethidine by i.p. injection concomitantly with treatment. For streptomycin experiments mice were treated with guanethidine monosulfate (30mg/kg) by i.p. injection 2 hours before streptomycin treatment (18:00) and 2 hours before GITT (08:00) the following day. For broad spectrum antibiotic experiments mice that were on antibiotics for at least 8 days were treated with guanethidine monosulfate (30mg/kg) the day before the experiment (18:00) and 2 hours before GITT (08:00) the following day.

*CART peptide treatment***.** CART peptide 55-102 (25 $\mu g^{-kg}$, Phoenix Pharmaceuticals, 003-62) was dissolved in sterile 0.9 % sterile saline and aliquots were stored at -20 °C. CART peptide or saline was injected i.p. into mice that were previously treated with broad-spectrum antibiotics for at least 2 weeks. Blood glucose levels were measured 1-hour post-injection. To control for stress caused by injections, mice were habituated to mock i.p. injections for at least 5 consecutive days prior to treatment.

*Exendin-4 treatment.* Exendin-4 (Sigma E7144) was dissolved in sterile 0.9% saline and aliquots were kept at -20°C. 20 $\mu$g/kg Exendin-4 or saline was given by i.p. injection and issue was isolated 4 hours post-injection or motility was measured 5 minutes following injection.

*Exendin-9-39 treatment***.** Exendin-9-39 (GLP-1 receptor blocking peptide, Sigma, E7269) was dissolved in 0.9 % sterile saline and aliquots were stored at -20 °C. Exendin-9-39 (40 $\mu g^{-kg}$) or saline was administered by i.p. injection to mice previously treated with broad-spectrum antibiotics for at least 2 weeks. Blood glucose levels were then measured at indicated timepoints. To control for stress caused by injections, mice were habituated to mock i.p. injections for at least 5 consecutive days prior to treatment.

*Tributyrin treatment.* Tributyrin (Sigma W222305, 3.29M) was filter sterilized through a 0.22 µm (EMD Millipore PES Express) syringe filter prior to oral gavage or i.p. injection. 200 µL of tributyrin was given by oral gavage. Two oral gavages were given over a period of 24 h, the first after giving streptomycin/PBS and the second dose given 8 h before sacrifice.

*PYY treatment.* PYY (Sigma P1306) was dissolved in sterile 0.9% saline and aliquots were kept at -20°C. 50 µg/kg PYY or saline was given by i.p. injection. Tissue was isolated 4 hours post-injection.

*Cholestyramine treatment.* Mice were given an oral gavage of 100 µL of cholestyramine (200mg/mL). Two oral gavages were given over a period of 24 h, the first after giving streptomycin/PBS and the second dose given 8 h before sacrifice.

*6-OHDA treatment.* 6-hydroxydopamine (6-OHDA; Sigma) was dissolved in 0.1% L-ascorbic acid (Sigma) in sterile saline. This solution was injected i.p. at a concentration of 80 mg/kg body weight on three consecutive days 7 days before an oral gavage of PBS or streptomycin. Denervation was confirmed by immunofluorescence whole mount of tyrosine hydroxylase in the colon.

**Antibiotic treatments.** *Chronic combined broad-spectrum antibiotic treatment* (designated “Abx” in figure legends)*.* For chronic microbial depletion, 0.25 g vancomycin (Sigma, V2002), 0.25 g metronidazole (Sigma, M3761), 0.5 g ampicillin (Sigma, A0166) and 0.5 g neomycin (Sigma, N6386) were dissolved in 500 mL of filtered water

supplemented with 5 g Splenda® to control for the bitter taste of the antibiotic solution. Splenda controls were given filtered drinking water supplemented with 10 $g^{-L}$ of Splenda. Body weight was monitored in all mice and analysis was performed at a minimum of 1 week after starting treatment, and only if weights were comparable between relevant groups. All solutions were passed through a SteriCup 0.22 µm filter prior to administration.
*Chronic individual antibiotic treatment.* Individual antibiotics (0.25 g vancomycin, 0.25 g metronidazole, 0.5g ampicillin or 0.5 g neomycin) were dissolved in 500 mL of filtered water supplemented with 5 g Splenda. Controls were given filtered drinking water supplemented with 10 $g^{-L}$ of Splenda.
*Acute single antibiotic treatment.* For acute microbial depletion, streptomycin (MP Biomedicals, S9137) was prepared in sterile DPBS at a concentration of 200 $mg^{-mL}$ and then filtered with a 0.22 µm (EMD Millipore PES Express) syringe filter. A dose of 20 mg was administered as an oral gavage of 100 µL of this stock solution. Controls received a single gavage of 100 µL sterile DPBS. Mice were analyzed 24 hours or 7 days following this single treatment. *Intraperitoneal antibiotic treatment.* Ampicillin was prepared in sterile DPBS and then filtered with a 0.22 *µ*m (EMD Millipore PES Express) syringe filter. Mice were injected i.p. with either 1 $g^{-kg}$ of Ampicillin or sterile DPBS for 7 days. To control for the stress caused by injections, mice were habituated by mock i.p. injections for at least 5 consecutive days prior to treatment.
*Antibiotic/FMT-mediated neuronal recovery post-spiB infection***.** 7 days post oral gavage with *spiB* mice were given drinking water supplemented with 10g/L Splenda (artificial sweetener, control), or broad-spectrum antibiotics (1 g/L ampicillin, 0.5 g/L vancomycin, 1g/L neomycin, 0.5 g/L metronidazole) in the drinking water supplemented with 10 g/L Splenda ® for 2 weeks. Mice on antibiotics were then put onto Splenda-containing water and all mice were given feces from an uninfected cage of age-matched C57BL/6J mice. All tissues were then harvested 2 weeks after recolonization.

**Intracerebroventricular (i.c.v.) delivery of SCFA.** Mice were anaesthetized under isofluorane and positioned in a stereotaxic frame (Kopf Instruments). The skull was exposed and a 26-gauge stainless steel guide cannula (PlasticsOne) was implanted into the lateral ventricle (midline -0.2 mm, 1.0 mm posterior from bregma, depth 2.3 mm from skull surface). The cannula was secured to the skull with dental cement and temporarily occluded with a dummy cannula (PlasticsOne). After surgery, the mice were singly-housed and given at least 1 week to recover. Prior to the study, cannula placement was verified by a positive dipsogenic response to angiotensin II (1 nmol in 1 µl; Sigma-Aldrich). I.c.v. injections were performed using a 30-gauge needle that extended 0.5 mm below the guide cannula (PlasticsOne), connected by cannula connector to a 5 µl Hamilton syringe and infused over 1 min using a microinfusion pump (Harvard Apparatus). Mice were habituated to i.c.v. infusions for at least 5 days prior to the experiment. An oral gavage of streptomycin (20mg at 200mg/mL) was given and then later artificial cerebrospinal fluid (aCSF) or SCFA (100 µM sodium acetate, 10 µM sodium propionate, and 10 µm sodium butyrate) dissolved in aCSF were delivered through the cannula. 16 hours later another i.c.v infusion of aCSF or SCFA was given and the CG-SMG was dissected 8 hours after the second infusion.

**Colonization of germ-free mice.** For exGF and *Casp11*$^{-/-}$ colonization experiments measuring fasting blood glucose and intestinal tissue analysis only, GF mice were moved into an SPF room and were housed in a cage with age and sex-matched feces from either exGF or *Casp11*$^{-/-}$ mice kept on an autoclaved germ-free diet. Fasting blood glucose levels from exGF or *Casp11*$^{-/-}$ donor mice were measured to provide a reference point for potential rescue of GF mice. For C57BL/6J colonization experiments measuring fasting blood glucose and gluconeogenesis, male and female GF mice were moved into Tecniplast isolator cages (ISOcages) in a separate room. Age-matched male and female C57BL/6J mice purchased from Jackson Laboratories were also housed in ISOcages in the same room. Following one week of acclimatization, half of the GF mice were then given age and sex-matched feces from C57BL/6J mice. All mice were maintained on autoclaved water and GF diet. All analyses were performed a minimum of two weeks post-conventionalization.

**SFB colonization.** Mice mono-colonized with segmented filamentous bacteria (SFB) were kept in GF isolators and originally colonized by gavage with faecal extract from SFB mono-colonized mice kept at NYU (Littman lab). SFB colonization was verified by real time PCR using SFB-specific 16S primers; GF feces served as a negative control, Taconic Farms C57BL/6 faeces as a positive control.

***Akkermansia muciniphilia* colonization.** 7 week old GF C57BL/6 mice were mono-colonized with a culture of *A. muciniphila* YL44. *A. muciniphila* was BHI (Becton Dickinson) with hemin (5 µg/ml, Sigma), vitamin K1 (5 µg/ml, Sigma0, and 10 g/L porcine mucin type 3 (Sigma) and grown in an anaerobic atmosphere of 5 % hydrogen, 10% carbon dioxide, and 85 % nitrogen. Colonized mice were then kept in sterile isocages for 6 weeks.

***Bacteroides fragilis* colonization.** 7-week-old GF C57BL/6 mice were mono-colonized with a culture of *B. fragilis* NCTC9343. *B. fragilis* was cultured in BHI (Becton Dickinson) with hemin (5 µg/ml, Sigma) and vitamin K1 (5 µg/ml, Sigma) and grown in an anaerobic atmosphere of 5 % hydrogen, 10 % carbon dioxide, and 85 % nitrogen. Colonized mice were then kept in sterile isocages for 6 weeks.

***Clostridium* spp. colonization.** Mice were colonized with *Clostridium spp.* in the Cornell Weill gnotobiotic facility.

**Altered Schaedler Flora colonization.** C57BL/6 mice were maintained in germ-free conditions in ISOcage biocontainment isolator cages (Tecniplast, PA, USA) in the gnotobiotic facility at Rockefeller University. ASF colonization was achieved by inoculating germ-free mice with cecal contents of ASF donor mice stably colonized by vertical transmission (kindly provided by Amanda Ramer-Tait, University of Nebraska-Lincoln). Ceca were prepared by homogenization through a 100 µm filter in sterile phosphate-buffered saline (PBS) at a ratio of one cecum per 1 ml of PBS. Mice received

200 µl of ASF inoculum via oral gavage twice, one week apart. The presence of members of the ASF microbial community was confirmed by a real-time PCR-based. All mice were analysed at least four weeks post colonization, with colonization further confirmed by 16s RNA sequencing of both faeces and ceca of analysed mice. We could detect RNA of at least 6 species by qPCR and 16s RNA sequencing after colonization.

**Oligo$^{MM12}$ colonization.** The Oligo-MM12 consortium was a kind gift from K. McCoy (U. Calgary). Oligo$^{MM12}$ Ceca were prepared by homogenization through a 100 µm filter in sterile phosphate-buffered saline (PBS) at a ratio of one cecum per 1 ml of PBS. We colonized GF C57BL6/J breeders with a single gavage of Oligo$^{MM12}$ and monitored colonization by 16S sequencing, including the presence of the entire consortium in successive generations. Fully colonized mice were maintained and bred in germ free isolators. Vertically colonized C57BL6/J Oligo$^{MM12}$ mice were used for all experiments.

**Colonization with antibiotic-resistant flora.** During the course of chronic antibiotic treatment, antibiotic-resistant bacteria were detected in the feces of *Casp11*$^{-/-}$ but not C57BL/6J mice. To normalize the microbiota, cages and bedding of the respective experimental groups were regularly switched over the course of antibiotic treatment prior to analysis. Successful colonization with antibiotic-resistant bacteria was determined by bacterial 16S rRNA qPCR of fecal samples and by plating fecal samples on agar plates containing antibiotics. To ensure stable colonization and exclude any effects of the detected antibiotic-resistant bacteria, metabolic and intestinal tissue analyses were performed at least one week after successful colonization was determined.

**Chemogenetics.** Water soluble Compound 21 (C21, HelloBio, HB6124) was dissolved in sterile 0.9% saline. Mice were given an intraperitoneal injection at a dose of 1 mg$^{-kg}$. *Chemogenetics for enteric infections.* In the context of enteric infections, mice expressing hM4Di in relevant neuronal populations were injected with C21 24 hours prior to oral gavage with *spiB*. *Chemogenetics of CG-SMG neurons.* 1 µL of AAV2-hSyn-hM3Dq-mCherry or AAV2-hSyn-hM4Di-mCherry (Addgene) was injected into the CG-SMG of C57BL/6J mice. Mice were then sutured, and staples were applied. Antibiotic ointment was applied to the closed surgical site and mice were given 0.05 mg/kg buprenorphine every 12 h for 2 days. After 2 weeks mice were habituated to i.p. injections for 5 days before administration of 1 mg/kg or 10 mg/kg Compound 21.

**Immunocytochemistry.** Cuprolinic blue staining for visualization of enteric neurons was performed as previously described (Holst and Powley, 1995). The method was utilized for quantification of enteric neurons in *T. gondii* and *T. cruzi* infection experiments.

**Confocal imaging.** Whole-mount intestine, NG, DRG, and CG-SMG samples were imaged on an inverted LSM 880 NLO laser scanning confocal and multiphoton microscope (Zeiss) and on an inverted TCS SP8 laser scanning confocal microscope (Leica).

**Whole-mount intestine immunofluorescence.** Following intestine dissection, *muscularis externa* tissue was pinned down on a plate coated with Sylgard, followed by overnight fixation in PBS/4% PFA at 4° C. After washing in DPBS, samples were then permeabilized first in PBS with 0.5% Triton X-100/0.05 % Tween-20/(4 $\mu g^{-\mu L}$) heparin (PTxwH) for 2 hours at room temperature (RT) with gentle agitation. Samples were then blocked for 2 hours in blocking buffer (PTxwH with 5 % donkey or goat serum) for 2 hours at RT with gentle agitation. Primary antibodies were added to blocking buffer at appropriate concentrations and incubated for 2-3 days at 4°C. After primary incubation samples were washed in PTxwH, followed by incubation with secondary antibody in PTxwH at appropriate concentrations for 2 hours at RT. Samples were again washed in PTxwH, and then mounted with Fluoromount G on slides with 1 ½ coverslips. Slides were kept in the dark at 4 °C until they were imaged.

**Intestine neuronal quantification: total numbers.** A minimum of 10 images were randomly acquired across a piece of whole-mount intestine *muscularis externa*. These images were then opened in ImageJ, and the cell counter feature was used to count the number of ANNA-1+ cells in each field. This number was then multiplied by a factor of 2.95 (20x objective) or 3.125 (25x objective), to calculate the number of counted neurons per square millimeter ($mm^2$). The average of 10 (or more) images was then calculated and plotted. Thus, every point on a given graph corresponds to a single animal. For determining iEAN subtype changes, the number of nNOS-, SST-, VGLUT2 (tdTomato)-, CART-, neuropeptide Y (NPY)- and follistatin (FST)-positive neurons were also counted. These numbers were then reported as both number per $mm^2$ and as a percentage of ANNA-1+ neurons.

**Intestine neuronal quantification: neurons per ganglion.** A myenteric ganglion was defined as a continuous group of ANNA-1+ cells that are separated by less than 15 µm in distance. Only complete ganglia were counted per field of view. Thus, the following ganglia were excluded: 1. Ganglia that were truncated; 2. No clear separation (>15 µm) was noted between the last ANNA-1+ cell and the edge of the field of view. In the case of single ANNA-1+ cells that are separated by 15 mm on all sides, this was considered extraganglionic. The number of quantifiable ganglia was averaged across a minimum of 10 images per gut segment per animal.

**Quantification of CG-SMG cFos.** Mice were sacrificed by cervical dislocation and CG-SMG were harvested and fixed overnight in 4 % PFA. CG-SMG were then washed four times in DPBS at RT and permeabilized in PTxwH at 4°C for at least 5 days. Primary antibody cFos (1:1000, Cell Signaling Technologies, 2250S) was added to the samples in PTxwH and incubated at 4°C for 3 days. Samples were washed four times in PTxwH at RT and then stained with goat-anti rabbit AF555/568/647 at 4°C for 3 days. Samples were washed four times in PTxwH at RT, covered in Fluormount G, and coverslipped for confocal imaging. We first established criteria for identifying neuronal cFos+ nuclei by staining CG-SMG from restraint-stressed mice, a condition known to activate the sympathetic nervous system. FluoroGold was used to identify sympathetic neurons and

cFos+ nuclei were defined as morphologically circular with a diameter of 8-14um. These criteria were sufficient to distinguish between small intensely fluorescent cells and possibly macrophages that also have cFos expression. We captured all sympathetic neurons within the CG-SMG, as defined by tyrosine hydroxylase staining, FluoroGold fluorescence, tdTomato fluorescence, or autofluorescence (experiment dependent), with multiple z-stack images. All images were analyzed in Image-J. Total cFos+ nuclei were counted using the Cell Counter plugin for Image-J, and data were not normalized to area or volume. Each data point represents the number of cFos+ cells per CG-SMG.

**Brain immunofluorescence.** Mice were sacrificed and transcardially perfused with cold PBS with heparin followed by cold 4% PFA (Electron Microscopy Sciences). The intact brain was separated carefully from the skull and placed in 4 % PFA, and then rotated for 48 h at 4°C. Whole brains were washed with PBS/0.03%Azide and sectioned at 50 µm on a Leica vibratome for immunofluorescence. Samples were then permeabilized in 0.5% Triton/0.05 % Tween-20 in PBS (PTx) followed by blocking in 5 % goat serum in PTxwH each for 2 h at room temperature. Primary antibody was added to the blocking buffer and samples were incubated with constant rotation at 4°C overnight. Four 15-minute washes were done in PTxwH at RT after which samples were moved to blocking buffer with secondary antibody. Slices were incubated in secondary antibody for 2 hours at room temperature followed by four 15-minute washes in PTxwH at room temperature. Samples were then placed on microscope slides, covered in Fluoromount G, and coverslipped.

**AdipoClear.** AdipoClear whole tissue clearing was adapted from AdipoClear protocol (Chi et al., 2018). Mice were sacrificed and intestinal sections were removed followed by overnight fixation in 4 % PFA. Tissues were washed in PBS then dehydrated in 20/40/60/80/100% Methanol in B1N followed by dichloromethane. Tissues were then rehydrated in 100/80/60/40/20 % methanol in B1N. Subsequently, samples were washed in 0.5 % Triton X-100/0.05 % Tween-20/(4 µg/µL) heparin (PTxwH) and then incubated in primary antibody dilutions in PTxwH for 7 Days. Samples were washed in PTxwH then incubated in secondary antibody at 1:400 in PTxwH for 7 days. Samples were again washed in PTxwH followed by PBS then dehydrated in 20/40/60/80/100 % methanol followed by dichloromethane and finally cleared in dibenzyl ether.

**Light-sheet microscopy and 3D reconstruction.** Whole-tissue cleared samples were imaged submerged in DBE on a LaVision Biotech Ultramicroscope II with 488 nm, 561 nm or 647 nm light-sheet illumination using a 1.3x or 4x objective with 2.5 µm Z-slices. Images were adjusted post hoc using Imaris x64 software (version 9.1 Bitplane) and 3D reconstructions were recorded as mp4 video files. Optical slices were taken using the orthoslicer or oblique slicer tool.

**Colony forming unit counting.** Fecal pellets from *Salmonella spiB* or *Yersinia pseudotuberculosis*-infected mice were weighed and then disrupted in 400 µL of DPBS. Serial dilutions were made from the original suspension and then 5 µL of each dilution was plated onto Salmonella-Shigella plates. The plates were then incubated overnight,

and the number of black colonies were counted for the serial dilution with the clearest delineation of single units. This number was then multiplied by the dilution factor and by 80 to give the number of colony-forming units (CFU) in the original suspension. CFU numbers were then divided by the original fecal pellet weight to give the number of CFU per mg of feces.

**Quantification of *SV* eggs in feces.** Fecal pellets from *Sv*-infected mice were weighed and then disrupted in 400 µl of DPBS. 100 µl of iodine solution was added to increase the visibility of fecal eggs. Eggs in small portions of each sample were counted under a microscope, and the number of eggs per gram of feces was determined for each sample.

**Intestine motility measurements.** For measurement of total intestinal transit time, non-fasted mice were given an oral gavage of 6 % carmine red (Sigma, C1022) dissolved in 0.5 % methylcellulose (made with sterile 0.9 % saline). Total gastrointestinal transit time (GITT) was measured as the time from oral gavage it took for mice to pass a fecal pellet that contained carmine. For DREADD experiments, mice were injected 2 minutes before starting with i.p. Compound 21 (1 $mg^{-kg}$).

**Ileal smooth muscle contractility.** Ileal ring tension was assessed by organ bath (Radnoti) myography as previously described (Muller et al., 2014). Briefly, distal ileal rings were mounted and equilibrated for one hour and were distended to 0.5 g followed by 10 minutes of relaxation. The data was acquired using the PowerLab acquisition system and analyzed using LabChart Software (AD Instruments).

**Feeding assay.** Mice were singly housed for at least 5 days prior to beginning the experiment. Before testing mice with Compound 21 (C21), feeding behavior was first assessed with saline injection during the light cycle (starting at 7:00 AM) and dark cycle (starting at 19:00 PM). Food intake assays were performed in the home cage. Mice were given ad libitum access to food prior to, during, and after the assay. Measurement of food intake (weighing of remaining food at each timepoint) was made at 1, 2, 4, 8, and 24 hours post i.p. injection of C21.

**Fasting experiments.** Unless specified otherwise in figure legends, mice were fasted overnight for 16 hours.

**Controlling for stress.** Due to the sensitivity of the sympathetic nervous system to stress, the following steps were taken eliminate this potential confounding factor. Experiments were not performed on days when cage changing took place. Mice were transported to the lab and sacrificed immediately, and all experiments with injections were done after a minimum of 5 days of i.p./handling habituation.

**Blood glucose measurement.** Mice were fed ad libitum or fasted overnight for 16 hours (indicated in the figure legends) prior to analysis. Mouse tails were cut at the very tip and the first drop of blood was discarded. A single drop of blood was applied to a Breeze2

(Bayer) blood glucose test strip loaded into a Breeze2 blood glucose monitoring system (Bayer). All samples were obtained at the same time of day during the light cycle (10:00-10:30AM).

**Intraperitoneal pyruvate tolerance test.** Mice were fasted overnight for 16 hours prior to analysis. Mouse tails were cut at the very tip and the first drop of blood was discarded. A single drop of blood was applied to a Breeze2 (Bayer) blood glucose test strip loaded into a Breeze2 blood glucose monitoring system (Bayer). After collecting basal blood glucose, mice were injected at a dose of $1g^{-kg}$ of sodium pyruvate (Sigma, P3662) dissolved in 0.9 % in NaCl. Glucose levels were measured after injection at 15, 30, 60, and 120 minutes post-injection to evaluate gluconeogenesis. All samples were obtained at the same time of day during the light cycle (9:00-11 AM).

**Blood- and plasma collection.** Mice were fed ad libitum or fasted overnight for 16 hours (indicated in the figure legends) prior to analysis. Mouse tails were cut at the very tip and the first drop of blood was discarded. At least 100 µL of blood was then collected in a Microvette (Sarstedt Inc., CB300) coated with potassium/EDTA. Tubes were then centrifuged at 3600 RPM for 20 min at 4 °C. Plasma was then collected and frozen at -20°C until analysis. All samples were obtained at the same time of day during the light cycle (10:00-10:30 AM).

**Insulin ELISA.** Insulin levels in plasma samples were measured using an Ultrasensitive Mouse Insulin ELISA kit (Crystal Chem, 90080) according to the manufacturer's instructions.

**Glucagon ELISA.** Plasma glucagon concentrations were determined using a Mouse Glucagon ELISA kit (Mercodia, #10-1281-01) according to the manufacturer's protocol.

**Lipocalin ELISA**. Lipocalin-2 levels in fecal samples were quantified using a Mouse Lipocalin-2 ELISA kit (R&D Systems) according to manufacturer's instructions.

**Serotonin (5-HT) ELISA.** 1 cm of proximal colon, 1 cm distal to the ceco-colonic junction, was dissected and then homogenized in a bead tube with 1 mL of 0.1 % ascorbic acid in PBS. The tubes were spun down and the supernatant was diluted 1/1000 in the same buffer and frozen at -80°C. The samples were then run in a Serotonin Ultrasensitive ELISA Kit (Eagle Biosciences, SEU39-K01) according to the manufacturer's instructions.

**Isoflurane induction.** A plexiglass induction chamber was placed on a heating pad set to 37°C. Isoflurane was set at 1 % with an oxygen flow of 1 liter/minute. Mice were placed in the induction chamber and monitored for loss of movement, after which a period of 15 minutes was elapsed. Respiration was monitored continuously during this period. Following isoflurane treatment, mice were returned to their home cage for a period of 1 hour prior to receiving Streptomycin pre-treatment, followed by *spiB* infection as described above.

**Sham intraperitoneal injections.** Sham intraperitoneal injections of DPBS or IgG (isotype control from MM depletion experiments, see below) were performed by mimicking the anti-CSF1R MM depletion protocol, by intraperitoneal injection of 200 µl of DPBS or IgG/ mouse (100 µl/flank). Injections were performed 12 hours prior to *spiB* infection, and an additional injection was performed at day 3.5 post infection. Mice were sacrificed and tissue was analyzed at 7 days post infection.

**Subcutaneous pump implantation.** Mice were anesthetized using isoflurane and, under sterile conditions, a small incision was made on the dorsal side of the neck. An Alzet pump (Model 1002) filled with Salbutamol sulfate prepared as described above was placed under the skin and moved back towards the right flank. The incision was then closed with surgical wound clips (Kent Scientific). Mice were then left to rest for 7 days before infection with *spiB*.

**Adrenalectomy.** Mice were anesthetized using isoflurane and, under sterile conditions, bilateral incisions were made dorsally just below the rib cage. The adrenal glands were then grasped by forceps from the suprarenal blood vessels and extracted from the surrounding tissue. Care was taken to minimize any bleeding before the muscle incision was closed with absorbable sutures. Surgical wound clips were then used to close the skin. Mice were then kept on 0.9 % saline drinking water for 9 days prior to infection with *spiB*.

**Generation of *Nlrp6*$^{flox/flox}$ mice.** The *Nlrp6*$^{flox/flox}$ strain was generated by Flp-Neo-mediated insertion of loxP sites flanking exon 1 of the *Nlrp6* locus. ES cells were used to generate the conditional knockout allele. The strain was generated in collaboration with genoWay (Lyon, France).

**Generation of cpa3$^{DTR\text{-}tdTomato}$ mice.** cpa3$^{DTR\text{-}tdTomato}$ knock-in mice were generated using CRISPR/Cas9 technology directly in C57BL/6 mice. Briefly, two guide RNA (gRNA) targeting exon 11 in the 3' UTR of the cpa3 locus were designed using the online CRISPR Design Tool. These gRNAs were cloned into a plasmid (Addgene) containing Cas9n. The plasmid was then co-injected into the pronucleus with a repair template plasmid (i.e., targeting vector, Addgene) containing an IRES-DTR-tdTomato fusion cassette. WT and knock-in genotypes were confirmed by PCR. DTR and IRES expression were confirmed using the repair template plasmid as a positive control. Insertion of the cassette into the correct locus was verified by using primers located inside the cassette and outside of the 3' and 5' homology regions, respectively.

**Fecal DNA extraction.** Fecal samples were collected, put on ice following collection and stored at -20 °C until processing. DNA from fecal samples was extracted using a fecal DNA MiniPrep Kit (Zymo Research, D6010) according to the manufacturer's protocol.

**Bacterial 16S rRNA qPCR.** To monitor germ-free status and luminal bacterial load during antibiotic-mediated microbial depletion and GF colonization experiments, q-RT-PCR was performed on DNA extracted from fecal samples using SYBR green PCR master mix (Applied Biosystems, 43-687-02). The following primers were used to amplify the conserved v3 region of bacterial 16S rRNA: 16S forward 5' – ACTCCTACGGGAGGCAGCAGT– 3' 16S reverse 5' – ATTACCGCGGCTGCTGGC – 3'.

**Bacterial 16S sample processing for bacterial rRNA sequencing.** 16S samples were processed utilizing a Promega Maxwell® RSC 48 Instrument. Following RNA extraction from all samples, samples were quantified using a ThermoFisher Quant-It dsDNA High-Sensitivity Kit on a microplate reader.

**Bacterial 16S rRNA sequencing.** 16S rRNA sequencing was performed on either the Illumina HiSeq 2500 or the Illumina MiSeq depending on project-specific needs. Raw paired-end fastq files containing sequence reads were merged at the overlapping region to produce a single 16S contig. All merged sequences having more than 1 expected error per read were filtered. Operational taxonomic units (OTUs) were generated by clustering sequences with a 99 % correspondence and chimera sequences were removed using usearch (Edgar, 2010) (v11).

**Cecal short chain fatty acid measurements.** Concentrations of acetate, propionate, and butyrate were measured as previously described (Zarrinpar et al., 2018). Briefly murine cecal content samples were collected directly into Bead-Ruptor tubes with 2.8-mm ceramic beads (OMNI International) and immediately frozen on dry ice. After thawing, samples were extracted with 80% methanol containing internal standards of deuterated SCFA (d-3 acetate, d-5 propionate, and d-7 butyrate; Cambridge Isotope Laboratories). Pellets were resuspended at a ratio of 100 mg/ml and homogenized. Homogenized samples were centrifuged at 20,000 *g* for 15 min at 4°C. The supernatant was derivatized for 60 min at 65°C with one volume of 50 mM, pH 11.0 borate buffer, and four volumes of 100 mM pentafluorobenzyl bromide (Thermo Scientific) in acetone (Fisher Scientific). The SCFA were extracted in n-hexane and then further diluted 1:10 in n-hexane. Extracted SCFA were quantified by GCMS (Agilent 7890A GC System; Agilent 5975C MS detector) operating in negative chemical ionization mode with methane as the reagent gas. MassHunter software was used for data analysis (B07.0; Agilent Technologies).

**Anti-CSF1R (ASF98) antibody production.** Anti-CSF1R was produced by suspension culture of the ASF98 hybridoma cell line (gift from Miriam Merad). Cells were thawed and passaged twice (1:10) in PFHM-II (Thermo Fisher) media supplemented with P/S (Thermo Fisher). Cells were then seeded at $5x10^6$ in 15 mL of PFHM-II in the cellular compartment of a 1000 mL bioreactor (Wheaton) and allowed to grow for 7-10 days. The cell compartment was then harvested, spun down and the supernatant collected. Supernatant was filtered and antibody was purified from the supernatant by affinity purification using protein G sepharose (GE Healthcare) in a gravity column (Bio-Rad). Briefly, the protein G was equilibrated with 100 mL binding buffer (Thermo Fisher

Scientific) and supernatant was loaded onto and run through the column. The column was then washed with 200 mL of binding buffer and eluted with 10 mL elution buffer (Thermo Fisher Scientific). Antibody was eluted in fractions directly into 100 µl 1 M Tris-HCL pH 8 (Invitrogen) and the concentrations were measured on a Nanodrop 2000 spectrophotometer (Thermo Fisher Scientific). Fractions were combined and dialyzed in 2 L DPBS for 2 days at 4°C using 14,000 MWCO dialysis tubing (Spectrum Labs) changing once. The antibody was then concentrated using centrifugal filters (30,000 MW, Amicon) and stored at 4°C until use.

**MM depletion using anti-CSF1R.** Anti-CSF1R was diluted in sterile DPBS to a final concentration of 6.25 mg/ml and 50 mg/kg of anti-CSF1R or isotype control (IgG from rat serum, Sigma-Aldrich) were administered by i.p. injections. Mice were previously habituated to i.p. injections for at least 5 days prior to the start of depletion and *spiB* infection. For all experiments, depletion was performed twice over the course of 7 days (day 0 and day 3.5). For infection experiments, depletion was performed 12 hours prior to infection. Animals were then subjected to the *Salmonella spiB* infection protocol as described above, and received and additional dose of either anti-CSF1R or isotype control 3.5 days after the initial dose. Animals were sacrificed at 7 dpi and intestinal tissue dissected for analysis.

**RiboTag.** Heterozygous or homozygous *Snap25*$^{\text{RiboTag}}$ and *Snap25*$^{\Delta Nlrp6\text{:RiboTag}}$ mice were used for TRAP-seq analysis as no differences were found between either genotype (Heiman et al., 2014; Sanz et al., 2009). For intestine immunoprecipitation (IP), mice were sacrificed, and tissue removed and divided as above. Samples were washed of fecal contents in PBS with cycloheximide (0.2 mg$^{\text{-mL}}$) (PBS/CHX). Mesenteric fat was removed, the *muscularis externa* was separated from the mucosa as described above and samples were washed 5 times in PBS/CHX. Fresh tissue was used for immunoprecipitation. For *Snap25*$^{\Delta Nlrp6\text{:RiboTag}}$ animals, ileum muscularis was prepared as above, but flash frozen in liquid nitrogen prior to immunoprecipitation. For nodose and CG-SMG IP, tissues were isolated as described above. The RiboTag IP protocol was then followed (http://depts.washington.edu/mcklab/RiboTagIPprotocol2014.pdf) with the following modifications: All samples were homogenized by hand with a dounce homogenizer in 2.5 mL supplemented homogenization buffer (changes per 2.5 mL: 50 µL Protease Inhibitor, 75 µL heparin (100 mg$^{\text{-mL}}$ stock), 25 µL SUPERase• In RNase Inhibitor). Samples were then centrifuged for 10 minutes at 10,000 G, after which 800 µL of supernatant was removed and 5 µL of anti-HA antibody (Abcam, ab9110) was added. Samples were kept rotating at 4°C with antibody for 1 hour. 200 µL of Thermo Protein magnetic A/G beads were washed with homogenization buffer, added to the sample, and kept rotating for 30 minutes at 4°C. The beads were washed four times with high-salt buffer and samples were eluted with 100 µL of PicoPure lysis buffer. RNA was extracted using the Arcturus PicoPure RNA isolation kit (Applied Biosystems) according to the manufacturer's instructions.

**Ribotag RNA-sequencing and differential expression analysis.** SMARTer Ultra Low Input RNA (Takara). cDNA libraries were prepared using Nextera XT DNA library preparation kit (Illumina) and sequenced using 75 base-pair single end reads on a NextSeq 500 instrument (Illumina). Reads were aligned using Kallisto to Mouse Ensembl v91 (Bray et al., 2016). Transcript abundance files were imported into RStudio (version 1.3.1; running R version 4.0.2), and DESeq2 (version 1.28.1) (Love et al., 2014) was used for all downstream differential expression analysis and generation of volcano plots. For intestine samples, Cre+ samples were compared with Cre- samples to generate a list of immunoprecipitated (IP) enriched transcripts (log2FC > 1 and padj < 0.05). For ileum *muscularis* versus nodose ganglion neuronal profiling, differentially expressed genes between samples were then compared with a cutoff of $\log_2$ Fold Change > 1. For regional iEAN GF versus SPF comparisons, a list of total iEAN IP-enriched transcripts was then generated by combining all neuronally-enriched transcripts from duodenum, ileum, and colon of GF and SPF mice ($\log_2$ Fold Change (FC) > 1, padj < 0.05) and was used to perform downstream analyses. All differentially expressed transcripts between samples (gray dots in volcano plots) were then filtered for those contained within the total IP-enriched list (pink dots in volcano plots). Significantly differentially expressed transcripts from each tissue comparison met a cutoff of $\log_2$ FC > 1, padj < 0.05. PCA plots were generated from log transformed DESeq2 data with the FactoMineR R package (version 2.3). GSEA pre-ranked analysis was performed with desktop software and the C5 gene ontology database using 1000 permutations. Gene ontology enrichment analysis was performed with differentially expressed transcripts ($\log_2$ FC > 1, padj < 0.05) using the TopGO R package (version 2.40.0) and a Fisher test with an elimination algorithm was used to calculate significance (dashed lines in figures = threshold of significance at 1.3). Duodenum-enriched transcripts were defined as transcripts contained within the total IP enriched list and significantly enriched in the SPF duodenum ($\log_2$ FC > 1 and padj < 0.05) as compared to both SPF ileum and SPF colon (table S1). We then filtered DESeq2 results for these 86 transcripts in the GF ileum vs SPF ileum and GF colon vs SPF colon comparisons. A duodenum-enriched transcript was considered upregulated in GF tissues if a transcript was significantly enriched ($\log_2$ FC >1 and padj < 0.05) in the GF sample as compared to the SPF sample.

**TRAP-quantitative real-time PCR**. For TRAP-q-RT-PCR, RiboTag-purified mRNA was reverse transcribed using an iScript cDNA Synthesis Kit (BioRad, 1708891) and q-RT-PCR was performed using SYBR green (Bio-Rad Laboratories). The following primers were used:
*Rpl32* forward 5'-ACAATGTCAAGGAGCTGGAG-3'
*Rpl32* rerverse 5'-TTGGGATTGGTGACTCTGATG-3'
*Nlrp6* exon 4 forward 5'-CAGACGCTGTGGACCTTGT-3'
*Nlrp6* exon 4 reverse 5'-ACGTGCTCGCGGTACTTCTT-3'
*Nlrp6* exon 1 forward 5'-TTGACTGTCAGCAAGAGTCC-3'
*Nlrp6* exon 1 reverse 5'-GGTGATCCTTTCTGGGCTAAA-3'
*Elavl4* forward 5'-GATCAGGGATGCTAACCTGTATG-3'
*Elavl4* reverse 5'-GGTGATGATGCGACCGTATT-3'

*Cartpt* forward 5'-TCTACTCTGCCGTGGATGAT-3'
*Cartpt* reverse 5'-CTCTTGAGCTTCTTCAGGACTTC-3'
*Sst* forward 5'-CTGCATCGTCCTGGCTTT-3'
*Sst* reverse 5'-GTACTTGGCCAGTTCCTGTT-3
*Grp* forward 5'-TCTCAGTCTCCAGCCTACTT-3
*Grp* reverse 5'-GCAGAGAGTCTACCAACTTAGC-3
*Nmu* forward 5'-AACGGGAAGAGGTCAACAAG-3
*Nmu* reverse 5'-AGGAGGGATCATTTGTGAGAAC-3
Data were normalized to *Rpl32* (housekeeping gene) and represented as log-transformed expression relative to *Rpl32*. To calculate a fold change, the final qPCR cycle of 45 was chosen in cases in which there was no amplification. This was comparable to water, which was used as a control and did not amplify.

***Tph1*-flox recombination PCR.** DNA was extracted from the epithelial fraction of cells made by Percoll gradient of homogenized colon from Villin$^{\Delta Tph1}$ mice two weeks following tamoxifen administration using Quick Extract (Lucigen) DNA extraction buffer. Target sequences were amplified using the following primers: *Tph1*-forward 5'-GGATCCTAACCGAGTGTTCC-3' *Thp1*-reverse-flox: 5'-GCACACCACCAACTCTTTCC-3' *Tph1*-reverse-recombined: 5'-CTTGGAAGGTTTTGTATCACC-3' PCR products were run on a 2% agarose gel and bands were analysed for the presence of the recombined band.

**PASTAA analysis.** Differentially expressed Ensembl gene ID lists ($log_2$ FC > 1, padj < 0.05) from ileum and colon samples (SPF enriched vs GF) were used in the Predicting Associated Transcription factors from Annotated Affinities (PASTAA) web tool (http://trap.molgen.mpg.de/PASTAA.htm) using default analysis settings and mouse Ensembl 46. Significant (p-value < 0.05) association scores for transcription factors were plotted.

**Mining of published iEAN scRNA-seq.** The published single-cell analysis of the mouse nervous system at mousebrain.org/genesearch.html (Zeisel et al., 2018) was searched for *Nrlp6* and filtered for clusters that express the gene at a trinarization score >= 0.95. Relative expression was then plotted as a heatmap in Prism 8. *Vglut2*+ subsets were defined based on the same single-cell analysis.

**Cryosectioning of fresh-frozen tissue.** Mice were given a lethal dose of isoflurane and then perfused with 30 ml ice cold DPBS. The ileum and colon were removed and flushed of luminal contents. The tissue was then transferred to OCT, positioned, flash frozen, moved to -20° for 2 hours, and finally moved to -80° for long term storage. Prior to cryosectioning, OCT blocks were equilibrated in the cryostat for 20 minutes. Sections were cut at 15 µm, put onto SuperfrostPlus slides, and left to dry for 10-15 minutes. Slides were then transferred to dry ice and finally to -80°C before RNAscope® processing.

**RNA fluorescence *in situ* hybridization (FISH) using RNAscope® technology.** *RNAscope® in situ hybridization on fresh-frozen tissue sections*. RNAscope® was performed using probes against *Nlrp6* and *Elavl4* on 15 *μ*m sections of fresh frozen ileum or colon tissue isolated from C57BL/6J mice according to the manufacturer's instruction with the following modification, tissue was pretreated with Protease IV for 20 min at RT. Samples were then mounted in Fluoromount-G with DAPI and 1 ½ coverslips were applied.
*RNAscope® in situ hybridization on whole-mount intestine.* C57BL/6J, *Cartpt*$^{Cre}$, *Agrp*$^{Cre}$ or *Npy*$^{Cre}$ mice were sacrificed, and the duodenum, ileum and colon removed and dissected as described above. Pieces of *muscularis externa* were pinned on Sylgard-coated plates and fixed in 4 % PFA at room temperature for 3 hours. Samples were removed from the Sylgard plates and washed in PBS twice for 10 minutes. Samples were further washed twice more in PBS or PBS with 0.1% Tween-20 (PBST) for 10 minutes depending on the origin of the tissue. After washing, pieces of *muscularis externa* were pinned again to Sylgard plates and dehydrated along a gradient of 25/50/75/100/100 % ethanol in PBS or PBST for 10 minutes at each step. 5 mm x 5 mm sections were cut from the tissue and mounted on slides and left to dry (~2 minutes). Samples were digested with 50 µL of protease III digestion solution (ACDbio) at room temperature for between 30 and 45 minutes. After digestion, tissue was removed from slides using forceps and washed three times in PBS for 5 minutes each. Tissue was then hybridized overnight at 40 °C in a humidified oven (ACDbio) using relevant probe targets. Tissue was next amplified and stained according to the RNAScope protocol for whole tissue staining with the following modifications: each amplification step was extended by 5 minutes and following the final amplification samples were washed three times for 10 minutes each. Tissue samples were mounted in Prolong gold antifade with DAPI (Thermo Fisher Scientific) on slides with 1 ½ coverslips. Images were acquired within 24 hours on an inverted LSM 880 NLO laser scanning confocal and multiphoton microscope (Zeiss) and processed using Image J.

**Macrophage intercalation calculation**. Raw data as imported from the microscope was used for all cell identification and subsequent analyses. Some post-analysis pseudo-color adjustment was performed for individual images to account for differences in auto-fluorescence and labeling. *Imaris* (Bitplane AG) software was used for cell identification, using the "*Surfaces*" algorithm as described by the manufacturer. A surface was created based on anti-ANNA-1 (neuron) staining to define neuronal ganglia. A masked channel was then created to capture fluorescence in other channels within the neuronal ganglia volume. A second surface was created based on anti-MHCII (macrophage) staining only within the masked channel. Volume statistics on both neuron (total) and macrophage (neuronal ganglia masked) surfaces were then exported. Percent macrophage intercalation per image was calculated as:

$$Macrophage\ Intercalation = \frac{(\Sigma(Macrophage\ surface\ volumes) + \Sigma(Neuronal\ ganglia\ surface\ volumes)}{\Sigma(Neuronal\ ganglia\ surface\ volumes)} \times 100$$

The average of at least 10 random macrophage intercalation percentages was used to determine the percentage for each individual animal.

**3D image reconstruction for MM ganglionic intercalation calculations.** Images were adjusted post hoc using Imaris x64 software (version 9.1 Bitplane) and 3D reconstructions were recorded as mp4 video files. Optical slices were taken using the orthoslicer or oblique slicer tools.

**Determination of caspase 11 mutation status by PCR and Sanger Sequencing.** DNA was extracted from earpieces of mice using QuickExtract™ DNA Extraction Solution (Lucigen). Target sequences were amplified using the following primers: Forward 5'-AGGCATATCTATAATCCCTTCACTG-3'; Reverse 5'-GAATATATCAAAGAGATGACAAGAGC- 3'. The following PCR conditions were used: 4 min 94°C, 1 min 94°C, 0.5 min 58°C, 1 min 72°C, 7 min 72°C, and end at 12°C. Samples were loaded on 3% agarose gels, and bands from all strains were compared to samples from C57BL/6J and 129S mice. The 5 bp deletion in *Casp11* described in the 129S1 strain fragment runs slightly higher than the wild-type fragment at a height of approximately 220 bp (Vanden Berghe et al., 2015). *Casp11* mutation status was further confirmed in C57BL/6J, CBA/J and 129S1 mice by Sanger sequencing of a gel-purified PCR product using primers 5′-CAGTATTATTATTGGTGATGCAAATG-3′ and 5′-GGAATATATCAAAGAGATGACAAGAGC-3′. *Casp11* mutation status was also confirmed in further relevant mouse strains utilized in this study.

**Quantitative PCR of sorted macrophages**. Total RNA was isolated using TRIzol™ (Invitrogen), from which cDNA libraries were reverse transcribed using Superscript II (Invitrogen) and random primers following the instructions provided by the manufacturer. Quantitative PCR (qPCR) was performed using SYBR green (Bio-Rad Laboratories). Data were collected and analyzed on a QuantStudio 3 (Thermo Scientific). The *Rpl32* housekeeping gene was used to normalize samples. The following primers were used: *Rpl32* forward 5'-ACAATGTCAAGGAGCTGGAG-3', *Rpl32* reverse 5'-TTGGGATTGGTGACTCTGATG-3', *Arg1* forward 5'-CTCCAAGCCAAAGTCCTTAGAG-3', *Arg1* reverse 5'-AGGAGCTGTCATTAGGGACATC-3', *Ym1* forward 5'-AGACTTGCGTGACTATGAAGCATT-3', *Ym1* reverse 5'-GCAGGTCCAAACTTCCATCCTC- 3'. To calculate a fold change, the final qPCR cycle of 45 was chosen in cases in which there was no amplification. This was comparable to water, which was used as a control and did not amplify.

**Induction of glia depletion.** *Plp1*$^{CreERT2}$;Rosa26$^{DTA}$ ( *Plp1*$^{iDTA}$, *Cre+*) and Rosa26$^{DTA}$ mice (*Cre-*) received a single oral gavage of 8 mg tamoxifen (Sigma) solubilized in 250 µl sterile corn oil (Sigma) at 6-7 weeks of age. Mice were infected with *Salmonella spiB* 5 days post tamoxifen administration and sacrificed at day 6 post infection (day 11 post tamoxifen).

**Data replication.** All experiments were repeated a minimum of two times. Data points in all graphs are representative of biological replicates.

**Data and Software Availability.** Data generated by RNA sequencing are deposited in the NCBI Gene Expression Omnibus (GEO) database. Specifically, ileum and nodose ganglion *Snap25*$^{\text{RiboTag}}$ TRAP-seq data as well as LysM$^{Adrb2flox/flox}$:RiboTag or LysM$^{Adrb2flox/plus}$:RiboTag is accessible under GEO: GSE140309. GF and SPF duodenum, ileum, and colon *Snap25*$^{\text{RiboTag}}$ TRAP-seq data generated in this work is deposited on the GEO database with accession number GSE156142. GF and SPF *Snap25*$^{\text{RiboTag}}$ eEAN TRAP-seq and 16S rRNA-seq data is deposited on the GEO database with accession number GSE145986.
All software used is available online, either freely or from a commercial supplier. Algorithms described above are purely mathematical calculations and can be performed using any software.

**Statistical analysis.** Significance levels indicated are as follows: * $P < 0.05$, ** $P < 0.01$, *** $P < 0.001$ and **** $P < 0.0001$. All data are presented as mean SD or mean ± SEM. All statistical tests used were two-tailed. Experiments were not randomized, and no statistical methods were used to predetermine sample size. Investigators were not blinded during experiments or outcome analysis. Multivariate data was analyzed by one-way ANOVA with Tukey's multiple comparisons test, two-way ANOVA with Tukey's multiple comparisons test, or Brown-Forsythe and Welch ANOVA with Dunnett's T3 multiple comparisons test. Comparisons between two conditions were analyzed by unpaired Student's t-test. GraphPad PRISM version 8.2.0 and R 3.4.3 was used for generation of graphs and statistics. For pyruvate tolerance test and Compound 21 treatment, area under the curve (AUC) was measured for each animal with time 0 blood glucose levels set as the baseline. AUC measurements were then compared by two-tailed unpaired t-test.

# APPENDIX 1. List of genes of duodenum TRAP signature

| external_gene_name | ensembl_gene_id | description |
|---|---|---|
| Wif1 | ENSMUSG00000020218 | Wnt inhibitory factor 1 [Source:MGI Symbol;Acc:MGI:1344332] |
| Krt19 | ENSMUSG00000020911 | keratin 19 [Source:MGI Symbol;Acc:MGI:96693] |
| Otof | ENSMUSG00000062372 | otoferlin [Source:MGI Symbol;Acc:MGI:1891247] |
| Ucn3 | ENSMUSG00000044988 | urocortin 3 [Source:MGI Symbol;Acc:MGI:1932970] |
| Pnoc | ENSMUSG00000045731 | preprononociceptin [Source:MGI Symbol;Acc:MGI:105308] |
| Esr1 | ENSMUSG00000019768 | estrogen receptor 1 (alpha) [Source:MGI Symbol;Acc:MGI:1352467] |
| Ndufa4l2 | ENSMUSG00000040280 | NADH dehydrogenase (ubiquinone) 1 alpha subcomplex, 4-like 2 [Source:MGI Symbol;Acc:MGI:3039567] |
| Uts2b | ENSMUSG00000056423 | urotensin 2B [Source:MGI Symbol;Acc:MGI:2677064] |
| Dlx5 | ENSMUSG00000029755 | distal-less homeobox 5 [Source:MGI Symbol;Acc:MGI:101926] |
| Grin2c | ENSMUSG00000020734 | glutamate receptor, ionotropic, NMDA2C (epsilon 3) [Source:MGI Symbol;Acc:MGI:95822] |
| Gabra3 | ENSMUSG00000031343 | gamma-aminobutyric acid (GABA) A receptor, subunit alpha 3 [Source:MGI Symbol;Acc:MGI:95615] |
| Ecel1 | ENSMUSG00000026247 | endothelin converting enzyme-like 1 [Source:MGI Symbol;Acc:MGI:1343461] |
| Pmaip1 | ENSMUSG00000024521 | phorbol-12-myristate-13-acetate-induced protein 1 [Source:MGI Symbol;Acc:MGI:1930146] |
| Necab1 | ENSMUSG00000040536 | N-terminal EF-hand calcium binding protein 1 [Source:MGI Symbol;Acc:MGI:1916602] |
| Cckar | ENSMUSG00000029193 | cholecystokinin A receptor [Source:MGI Symbol;Acc:MGI:99478] |
| Rasgrp3 | ENSMUSG00000071042 | RAS, guanyl releasing protein 3 [Source:MGI Symbol;Acc:MGI:3028579] |
| Rnf128 | ENSMUSG00000031438 | ring finger protein 128 [Source:MGI Symbol;Acc:MGI:1914139] |
| Eya1 | ENSMUSG00000025932 | EYA transcriptional coactivator and phosphatase 1 [Source:MGI Symbol;Acc:MGI:109344] |
| Gbx1 | ENSMUSG00000067724 | gastrulation brain homeobox 1 [Source:MGI Symbol;Acc:MGI:95667] |
| Pgf | ENSMUSG00000004791 | placental growth factor [Source:MGI Symbol;Acc:MGI:105095] |
| Rxfp1 | ENSMUSG00000034009 | relaxin/insulin-like family peptide receptor 1 [Source:MGI Symbol;Acc:MGI:2682211] |
| Trpv1 | ENSMUSG00000005952 | transient receptor potential cation channel, subfamily V, member 1 [Source:MGI Symbol;Acc:MGI:1341787] |
| Fam19a4 | ENSMUSG00000046500 | family with sequence similarity 19, member A4 [Source:MGI Symbol;Acc:MGI:2444563] |
| Adamts14 | ENSMUSG00000059901 | a disintegrin-like and metallopeptidase (reprolysin type) with thrombospondin type 1 motif, 14 [Source:MGI Symbol;Acc:MGI:2179942] |
| Kcnj14 | ENSMUSG00000058743 | potassium inwardly-rectifying channel, subfamily J, member 14 [Source:MGI Symbol;Acc:MGI:2384820] |
| Foxs1 | ENSMUSG00000074676 | forkhead box S1 [Source:MGI Symbol;Acc:MGI:95546] |
| Npy | ENSMUSG00000029819 | neuropeptide Y [Source:MGI Symbol;Acc:MGI:97374] |
| Ptgdr | ENSMUSG00000071489 | prostaglandin D receptor [Source:MGI Symbol;Acc:MGI:102966] |
| Sp5 | ENSMUSG00000075304 | trans-acting transcription factor 5 [Source:MGI Symbol;Acc:MGI:1927715] |
| Ntrk1 | ENSMUSG00000028072 | neurotrophic tyrosine kinase, receptor, type 1 [Source:MGI Symbol;Acc:MGI:97383] |
| Adra1b | ENSMUSG00000050541 | adrenergic receptor, alpha 1b [Source:MGI Symbol;Acc:MGI:104774] |
| Gabbr2 | ENSMUSG00000039809 | gamma-aminobutyric acid (GABA) B receptor, 2 [Source:MGI Symbol;Acc:MGI:2386030] |
| Gprin3 | ENSMUSG00000045441 | GPRIN family member 3 [Source:MGI Symbol;Acc:MGI:1924785] |
| Nkain3 | ENSMUSG00000055761 | Na+/K+ transporting ATPase interacting 3 [Source:MGI Symbol;Acc:MGI:2444830] |
| Fam20a | ENSMUSG00000020614 | family with sequence similarity 20, member A [Source:MGI Symbol;Acc:MGI:2388266] |
| Aard | ENSMUSG00000068522 | alanine and arginine rich domain containing protein [Source:MGI Symbol;Acc:MGI:2181621] |
| Tmem132b | ENSMUSG00000070498 | transmembrane protein 132B [Source:MGI Symbol;Acc:MGI:3609245] |
| Nt5dc2 | ENSMUSG00000071547 | 5'-nucleotidase domain containing 2 [Source:MGI Symbol;Acc:MGI:1917271] |
| Hcn4 | ENSMUSG00000032338 | hyperpolarization-activated, cyclic nucleotide-gated K+ 4 [Source:MGI Symbol;Acc:MGI:1298209] |
| Gja3 | ENSMUSG00000048582 | gap junction protein, alpha 3 [Source:MGI Symbol;Acc:MGI:95714] |
| Ghsr | ENSMUSG00000051136 | growth hormone secretagogue receptor [Source:MGI Symbol;Acc:MGI:2441906] |
| Npas1 | ENSMUSG00000001988 | neuronal PAS domain protein 1 [Source:MGI Symbol;Acc:MGI:109205] |
| Tacr3 | ENSMUSG00000028172 | tachykinin receptor 3 [Source:MGI Symbol;Acc:MGI:892968] |
| Bmper | ENSMUSG00000031963 | BMP-binding endothelial regulator [Source:MGI Symbol;Acc:MGI:1920480] |
| Kcnj16 | ENSMUSG00000051497 | potassium inwardly-rectifying channel, subfamily J, member 16 [Source:MGI Symbol;Acc:MGI:1314842] |
| Crhbp | ENSMUSG00000021680 | corticotropin releasing hormone binding protein [Source:MGI Symbol;Acc:MGI:88497] |
| Gpr6 | ENSMUSG00000046922 | G protein-coupled receptor 6 [Source:MGI Symbol;Acc:MGI:2155249] |
| Dclk3 | ENSMUSG00000032500 | doublecortin-like kinase 3 [Source:MGI Symbol;Acc:MGI:3039580] |
| Arg2 | ENSMUSG00000021125 | arginase type II [Source:MGI Symbol;Acc:MGI:1330806] |
| Slc4a11 | ENSMUSG00000074796 | solute carrier family 4, sodium bicarbonate transporter-like, member 11 [Source:MGI Symbol;Acc:MGI:2138987] |
| Asb4 | ENSMUSG00000042607 | ankyrin repeat and SOCS box-containing 4 [Source:MGI Symbol;Acc:MGI:1929751] |
| A930017K11Rik | ENSMUSG00000025727 | RIKEN cDNA A930017K11 gene [Source:MGI Symbol;Acc:MGI:2442713] |
| Maob | ENSMUSG00000040147 | monoamine oxidase B [Source:MGI Symbol;Acc:MGI:96916] |
| Maoa | ENSMUSG00000025037 | monoamine oxidase A [Source:MGI Symbol;Acc:MGI:96915] |
| Emilin2 | ENSMUSG00000024053 | elastin microfibril interfacer 2 [Source:MGI Symbol;Acc:MGI:2389136] |
| Lmo2 | ENSMUSG00000032698 | LIM domain only 2 [Source:MGI Symbol;Acc:MGI:102811] |
| Atm | ENSMUSG00000034218 | ataxia telangiectasia mutated [Source:MGI Symbol;Acc:MGI:107202] |
| Pik3c2g | ENSMUSG00000030228 | phosphatidylinositol-4-phosphate 3-kinase catalytic subunit type 2 gamma [Source:MGI Symbol;Acc:MGI:1203730] |
| Bcat1 | ENSMUSG00000030268 | branched chain aminotransferase 1, cytosolic [Source:MGI Symbol;Acc:MGI:104861] |
| Myh1 | ENSMUSG00000056328 | myosin, heavy polypeptide 1, skeletal muscle, adult [Source:MGI Symbol;Acc:MGI:1339711] |
| Brinp1 | ENSMUSG00000028351 | bone morphogenic protein/retinoic acid inducible neural specific 1 [Source:MGI Symbol;Acc:MGI:1928478] |
| Cnih3 | ENSMUSG00000026514 | cornichon family AMPA receptor auxiliary protein 3 [Source:MGI Symbol;Acc:MGI:1920228] |
| Slc35f4 | ENSMUSG00000021852 | solute carrier family 35, member F4 [Source:MGI Symbol;Acc:MGI:1922538] |
| Pde2a | ENSMUSG00000110195 | phosphodiesterase 2A, cGMP-stimulated [Source:MGI Symbol;Acc:MGI:2446107] |
| C1ql2 | ENSMUSG00000036907 | complement component 1, q subcomponent-like 2 [Source:MGI Symbol;Acc:MGI:3032521] |
| Mrap2 | ENSMUSG00000042761 | melanocortin 2 receptor accessory protein 2 [Source:MGI Symbol;Acc:MGI:3609239] |
| Vmn2r29 | ENSMUSG00000095730 | vomeronasal 2, receptor 29 [Source:MGI Symbol;Acc:MGI:1923479] |
| Serpinf1 | ENSMUSG00000000753 | serine (or cysteine) peptidase inhibitor, clade F, member 1 [Source:MGI Symbol;Acc:MGI:108080] |
| Pkp1 | ENSMUSG00000026413 | plakophilin 1 [Source:MGI Symbol;Acc:MGI:1328359] |
| Slc35f3 | ENSMUSG00000057060 | solute carrier family 35, member F3 [Source:MGI Symbol;Acc:MGI:2444426] |
| Gck | ENSMUSG00000041798 | glucokinase [Source:MGI Symbol;Acc:MGI:1270854] |
| Rasgrf1 | ENSMUSG00000032356 | RAS protein-specific guanine nucleotide-releasing factor 1 [Source:MGI Symbol;Acc:MGI:99694] |
| Mmd2 | ENSMUSG00000039533 | monocyte to macrophage differentiation-associated 2 [Source:MGI Symbol;Acc:MGI:1922354] |
| Capn6 | ENSMUSG00000067276 | calpain 6 [Source:MGI Symbol;Acc:MGI:1100850] |
| Sulf2 | ENSMUSG00000006800 | sulfatase 2 [Source:MGI Symbol;Acc:MGI:1919293] |
| Gpr149 | ENSMUSG00000043441 | G protein-coupled receptor 149 [Source:MGI Symbol;Acc:MGI:2443628] |
| Ackr3 | ENSMUSG00000044337 | atypical chemokine receptor 3 [Source:MGI Symbol;Acc:MGI:109562] |
| Atoh8 | ENSMUSG00000037621 | atonal bHLH transcription factor 8 [Source:MGI Symbol;Acc:MGI:1918343] |
| Moxd1 | ENSMUSG00000020000 | monooxygenase, DBH-like 1 [Source:MGI Symbol;Acc:MGI:1921582] |
| Dlx2 | ENSMUSG00000023391 | distal-less homeobox 2 [Source:MGI Symbol;Acc:MGI:94902] |
| Dync1i1 | ENSMUSG00000029757 | dynein cytoplasmic 1 intermediate chain 1 [Source:MGI Symbol;Acc:MGI:107743] |
| Inhbb | ENSMUSG00000037035 | inhibin beta-B [Source:MGI Symbol;Acc:MGI:96571] |
| Gpr68 | ENSMUSG00000047415 | G protein-coupled receptor 68 [Source:MGI Symbol;Acc:MGI:2441763] |
| 4930550C14Rik | ENSMUSG00000005131 | RIKEN cDNA 4930550C14 gene [Source:MGI Symbol;Acc:MGI:1922561] |
| Stac | ENSMUSG00000032502 | src homology three (SH3) and cysteine rich domain [Source:MGI Symbol;Acc:MGI:1201400] |
| Slc6a4 | ENSMUSG00000020838 | solute carrier family 6 (neurotransmitter transporter, serotonin), member 4 [Source:MGI Symbol;Acc:MGI:96285] |
| Spon1 | ENSMUSG00000038156 | spondin 1, (f-spondin) extracellular matrix protein [Source:MGI Symbol;Acc:MGI:2385287] |
| Bcas1 | ENSMUSG00000013523 | breast carcinoma amplified sequence 1 [Source:MGI Symbol;Acc:MGI:1924210] |
| Vsir | ENSMUSG00000020101 | V-set immunoregulatory receptor [Source:MGI Symbol;Acc:MGI:1921298] |
| Plscr4 | ENSMUSG00000032377 | phospholipid scramblase 4 [Source:MGI Symbol;Acc:MGI:2143267] |
| Fst | ENSMUSG00000021765 | follistatin [Source:MGI Symbol;Acc:MGI:95586] |
| Tnr | ENSMUSG00000015829 | tenascin R [Source:MGI Symbol;Acc:MGI:99516] |
| Rftn1 | ENSMUSG00000039316 | raftlin lipid raft linker 1 [Source:MGI Symbol;Acc:MGI:1923688] |

**Table 1. Duodenum TRAP signature.** Table of genes that are significantly enriched in the duodenum of *Snap25*$^{\text{RiboTag}}$ mice as compared to both the ileum and colon. Used as a filter to generate the volcano plots in Figure 2.11.

# APPENDIX 2. Infection kinetics *of Salmonella spiB*

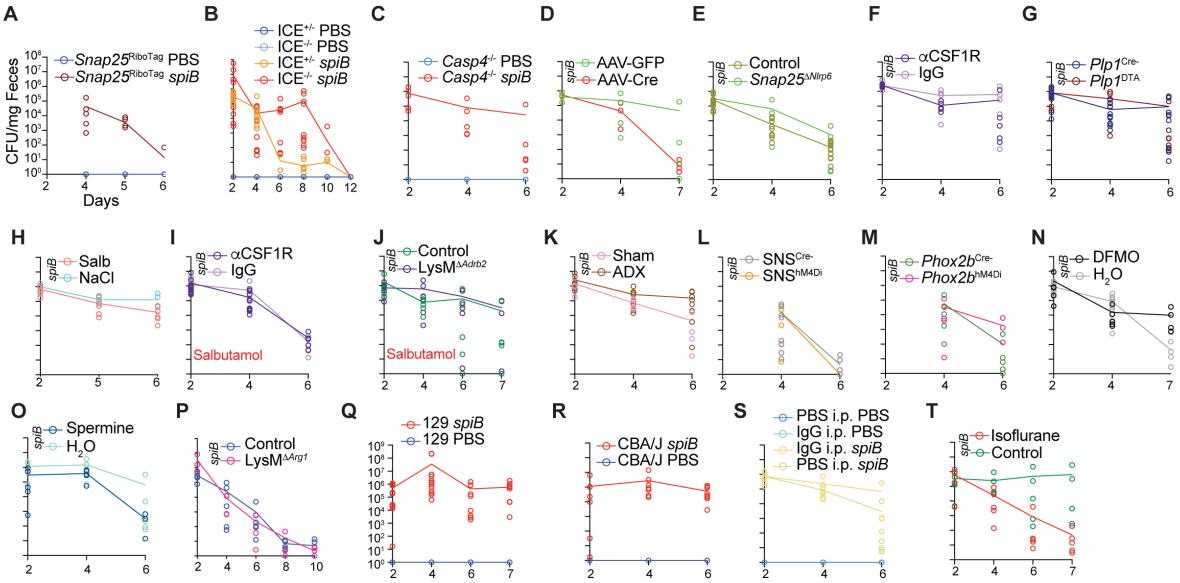


**Infection kinetics of *Salmonella spiB* for experiments in chapters 2 and 3.** (A to T) Quantification of fecal *Salmonella spiB* CFU on the indicated days post infection of the experiment displayed in (A) Figure 2.27; (B) Figure 2.32; (C) Figure 2.32; (D) 2.33; (E) Figure 2.34; (F) Figure 3.1; (G) Figure 3.2; (H) Figure 3.5; (I) Figure 3.5; (J) 3.7; (K) Figure 3.36; (L) Figure 3.37; (M) Figure 3.37; (N) Figure 3.9; (O) 3.9; (P) Figure 3.10; (Q) Figure 2.32; (R) Figure 2.32; (S) Figure 3.35; (T) Figure 3.35. Data are represented as mean (line), and individual values, with each point on a graph representing the value obtained from an individual animal.

## BIBLIOGRAPHY


Abels, M., Riva, M., Bennet, H., Ahlqvist, E., Dyachok, O., Nagaraj, V., Shcherbina, L., Fred, R.G., Poon, W., Sorhede-Winzell, M.*, et al.* (2016). CART is overexpressed in human type 2 diabetic islets and inhibits glucagon secretion and increases insulin secretion. Diabetologia *59*, 1928-1937.

Abot, A., Cani, P.D., and Knauf, C. (2018). Impact of Intestinal Peptides on the Enteric Nervous System: Novel Approaches to Control Glucose Metabolism and Food Intake. Front Endocrinol (Lausanne) *9*, 328.

Aguilera-Lizarraga, J., Florens, M.V., Viola, M.F., Jain, P., Decraecker, L., Appeltans, I., Cuende-Estevez, M., Fabre, N., Van Beek, K., Perna, E.*, et al.* (2021). Local immune response to food antigens drives meal-induced abdominal pain. Nature *590*, 151-156.

Ahlman, H., and Nilsson (2001). The gut as the largest endocrine organ in the body. Ann Oncol *12 Suppl 2*, S63-68.

Ahrends, T., Aydin, B., Matheis, F., Classon, C., Furtado, G.C., Lira, S.A., and Mucida, D. (2021). Enteric pathogens induce tissue tolerance and prevent neuronal loss from subsequent infections. bioRxiv, 2021.2004.2009.439221.

Akbar, A., Yiangou, Y., Facer, P., Brydon, W.G., Walters, J.R., Anand, P., and Ghosh, S. (2010). Expression of the TRPV1 receptor differs in quiescent inflammatory bowel disease with or without abdominal pain. Gut *59*, 767-774.

Akbar, A., Yiangou, Y., Facer, P., Walters, J.R., Anand, P., and Ghosh, S. (2008). Increased capsaicin receptor TRPV1-expressing sensory fibres in irritable bowel syndrome and their correlation with abdominal pain. Gut *57*, 923-929.

Aktar, R., Parkar, N., Stentz, R., Baumard, L., Parker, A., Goldson, A., Brion, A., Carding, S., Blackshaw, A., and Peiris, M. (2020). Human resident gut microbe Bacteroides thetaiotaomicron regulates colonic neuronal innervation and neurogenic function. Gut Microbes *11*, 1745-1757.

Al Nabhani, Z., and Eberl, G. (2020). Imprinting of the immune system by the microbiota early in life. Mucosal Immunol *13*, 183-189.

Alimov, I., Menon, S., Cochran, N., Maher, R., Wang, Q., Alford, J., Concannon, J.B., Yang, Z., Harrington, E., Llamas, L.*, et al.* (2019). Bile acid analogues are activators of pyrin inflammasome. J Biol Chem *294*, 3359-3366.

Anitha, M., Vijay-Kumar, M., Sitaraman, S.V., Gewirtz, A.T., and Srinivasan, S. (2012). Gut microbial products regulate murine gastrointestinal motility via Toll-like receptor 4 signaling. Gastroenterology *143*, 1006-1016 e1004.

Aponte, Y., Atasoy, D., and Sternson, S.M. (2011). AGRP neurons are sufficient to orchestrate feeding behavior rapidly and without training. Nat Neurosci *14*, 351-355.

Arantes, R.M., Marche, H.H., Bahia, M.T., Cunha, F.Q., Rossi, M.A., and Silva, J.S. (2004). Interferon-gamma-induced nitric oxide causes intrinsic intestinal denervation in Trypanosoma cruzi-infected mice. Am J Pathol *164*, 1361-1368.

Arts, R.J.W., Joosten, L.A.B., and Netea, M.G. (2018). The Potential Role of Trained Immunity in Autoimmune and Autoinflammatory Disorders. Front Immunol *9*, 298.

Atarashi, K., Tanoue, T., Oshima, K., Suda, W., Nagano, Y., Nishikawa, H., Fukuda, S., Saito, T., Narushima, S., Hase, K.*, et al.* (2013). Treg induction by a rationally selected mixture of Clostridia strains from the human microbiota. Nature *500*, 232-236.

Aube, A.C., Cabarrocas, J., Bauer, J., Philippe, D., Aubert, P., Doulay, F., Liblau, R., Galmiche, J.P., and Neunlist, M. (2006). Changes in enteric neurone phenotype and intestinal functions in a transgenic mouse model of enteric glia disruption. Gut *55*, 630-637.

Avetisyan, M., Rood, J.E., Huerta Lopez, S., Sengupta, R., Wright-Jin, E., Dougherty, J.D., Behrens, E.M., and Heuckeroth, R.O. (2018). Muscularis macrophage development in the absence of an enteric nervous system. Proc Natl Acad Sci U S A *115*, 4696-4701.

Ayres, J.S. (2020). The Biology of Physiological Health. Cell *181*, 250-269.

Bain, C.C., Bravo-Blas, A., Scott, C.L., Perdiguero, E.G., Geissmann, F., Henri, S., Malissen, B., Osborne, L.C., Artis, D., and Mowat, A.M. (2014). Constant replenishment from circulating monocytes maintains the macrophage pool in the intestine of adult mice. Nat Immunol *15*, 929-937.

Bain, C.C., and Schridde, A. (2018). Origin, Differentiation, and Function of Intestinal Macrophages. Front Immunol *9*, 2733.

Balemans, D., Mondelaers, S.U., Cibert-Goton, V., Stakenborg, N., Aguilera-Lizarraga, J., Dooley, J., Liston, A., Bulmer, D.C., Vanden Berghe, P., Boeckxstaens, G.E.*, et al.* (2017). Evidence for long-term sensitization of the bowel in patients with post-infectious-IBS. Sci Rep *7*, 13606.

Banfield, B.W., Kaufman, J.D., Randall, J.A., and Pickard, G.E. (2003). Development of pseudorabies virus strains expressing red fluorescent proteins: new tools for multisynaptic labeling applications. J Virol *77*, 10106-10112.

Barajon, I., Serrao, G., Arnaboldi, F., Opizzi, E., Ripamonti, G., Balsari, A., and Rumio, C. (2009). Toll-like receptors 3, 4, and 7 are expressed in the enteric nervous system and dorsal root ganglia. J Histochem Cytochem *57*, 1013-1023.

Barbara, G., Grover, M., Bercik, P., Corsetti, M., Ghoshal, U.C., Ohman, L., and Rajilic-Stojanovic, M. (2019). Rome Foundation Working Team Report on Post-Infection Irritable Bowel Syndrome. Gastroenterology *156*, 46-58 e47.

Barbara, G., Stanghellini, V., De Giorgio, R., Cremon, C., Cottrell, G.S., Santini, D., Pasquinelli, G., Morselli-Labate, A.M., Grady, E.F., Bunnett, N.W.*, et al.* (2004). Activated mast cells in proximity to colonic nerves correlate with abdominal pain in irritable bowel syndrome. Gastroenterology *126*, 693-702.

Bauche, D., Joyce-Shaikh, B., Jain, R., Grein, J., Ku, K.S., Blumenschein, W.M., Ganal-Vonarburg, S.C., Wilson, D.C., McClanahan, T.K., Malefyt, R.W.*, et al.* (2018). LAG3(+) Regulatory T Cells Restrain Interleukin-23-Producing CX3CR1(+) Gut-Resident Macrophages during Group 3 Innate Lymphoid Cell-Driven Colitis. Immunity *49*, 342-352 e345.

Bayliss, W.M., and Starling, E.H. (1899). The movements and innervation of the small intestine. J Physiol *24*, 99-143.

Bayliss, W.M., and Starling, E.H. (1902). The mechanism of pancreatic secretion. J Physiol *28*, 325-353.

Beatty, J.K., Bhargava, A., and Buret, A.G. (2014). Post-infectious irritable bowel syndrome: mechanistic insights into chronic disturbances following enteric infection. World J Gastroenterol *20*, 3976-3985.

Becker, L., Nguyen, L., Gill, J., Kulkarni, S., Pasricha, P.J., and Habtezion, A. (2018). Age-dependent shift in macrophage polarisation causes inflammation-mediated degeneration of enteric nervous system. Gut *67*, 827-836.

Belkind-Gerson, J., Graham, H.K., Reynolds, J., Hotta, R., Nagy, N., Cheng, L., Kamionek, M., Shi, H.N., Aherne, C.M., and Goldstein, A.M. (2017). Colitis promotes neuronal differentiation of Sox2+ and PLP1+ enteric cells. Scientific reports *7*, 2525.

Bellavance, M.A., and Rivest, S. (2014). The HPA - Immune Axis and the Immunomodulatory Actions of Glucocorticoids in the Brain. Front Immunol *5*, 136.

Bellono, N.W., Bayrer, J.R., Leitch, D.B., Castro, J., Zhang, C., O'Donnell, T.A., Brierley, S.M., Ingraham, H.A., and Julius, D. (2017). Enterochromaffin Cells Are Gut Chemosensors that Couple to Sensory Neural Pathways. Cell *170*, 185-198 e116.

Ben-Shlomo, A., and Melmed, S. (2010). Pituitary somatostatin receptor signaling. Trends Endocrinol Metab *21*, 123-133.

Benskey, M.J., Kuhn, N.C., Galligan, J.J., Garcia, J., Boye, S.E., Hauswirth, W.W., Mueller, C., Boye, S.L., and Manfredsson, F.P. (2015). Targeted gene delivery to the

enteric nervous system using AAV: a comparison across serotypes and capsid mutants. Mol Ther *23*, 488-500.

Bernardo, D., Marin, A.C., Fernandez-Tome, S., Montalban-Arques, A., Carrasco, A., Tristan, E., Ortega-Moreno, L., Mora-Gutierrez, I., Diaz-Guerra, A., Caminero-Fernandez, R.*, et al.* (2018). Human intestinal pro-inflammatory CD11c(high)CCR2(+)CX3CR1(+) macrophages, but not their tolerogenic CD11c(-)CCR2(-)CX3CR1(-) counterparts, are expanded in inflammatory bowel disease. Mucosal Immunol *11*, 1114-1126.

Bernshtein, B., Curato, C., Ioannou, M., Thaiss, C.A., Gross-Vered, M., Kolesnikov, M., Wang, Q., David, E., Chappell-Maor, L., Harmelin, A.*, et al.* (2019). IL-23-producing IL-10Ralpha-deficient gut macrophages elicit an IL-22-driven proinflammatory epithelial cell response. Sci Immunol *4*.

Berthoud, H.R., Kressel, M., Raybould, H.E., and Neuhuber, W.L. (1995). Vagal sensors in the rat duodenal mucosa: distribution and structure as revealed by in vivo DiI-tracing. Anat Embryol (Berl) *191*, 203-212.

Berthoud, H.R., and Powley, T.L. (1993). Characterization of vagal innervation to the rat celiac, suprarenal and mesenteric ganglia. J Auton Nerv Syst *42*, 153-169.

Berthoud, H.R., and Powley, T.L. (1996). Interaction between parasympathetic and sympathetic nerves in prevertebral ganglia: morphological evidence for vagal efferent innervation of ganglion cells in the rat. Microsc Res Tech *35*, 80-86.

Bertrand, P.P., Kunze, W.A., Bornstein, J.C., Furness, J.B., and Smith, M.L. (1997). Analysis of the responses of myenteric neurons in the small intestine to chemical stimulation of the mucosa. Am J Physiol *273*, G422-435.

Besedovsky, H., Sorkin, E., Felix, D., and Haas, H. (1977). Hypothalamic changes during the immune response. Eur J Immunol *7*, 323-325.

Betley, J.N., Cao, Z.F., Ritola, K.D., and Sternson, S.M. (2013). Parallel, redundant circuit organization for homeostatic control of feeding behavior. Cell *155*, 1337-1350.

Bianco, F., Bonora, E., Natarajan, D., Vargiolu, M., Thapar, N., Torresan, F., Giancola, F., Boschetti, E., Volta, U., Bazzoli, F.*, et al.* (2016). Prucalopride exerts neuroprotection in human enteric neurons. Am J Physiol Gastrointest Liver Physiol *310*, G768-775.

Biggs, M.B., Medlock, G.L., Moutinho, T.J., Lees, H.J., Swann, J.R., Kolling, G.L., and Papin, J.A. (2017). Systems-level metabolism of the altered Schaedler flora, a complete gut microbiota. ISME J *11*, 426-438.

Bilate, A.M., Bousbaine, D., Mesin, L., Agudelo, M., Leube, J., Kratzert, A., Dougan, S.K., Victora, G.D., and Ploegh, H.L. (2016). Tissue-specific emergence of regulatory and intraepithelial T cells from a clonal T cell precursor. Sci Immunol *1*, eaaf7471.

Bistoni, F., Vecchiarelli, A., Cenci, E., Puccetti, P., Marconi, P., and Cassone, A. (1986). Evidence for macrophage-mediated protection against lethal Candida albicans infection. Infect Immun *51*, 668-674.

Blaszkiewicz, M., Willows, J.W., Dubois, A.L., Waible, S., DiBello, K., Lyons, L.L., Johnson, C.P., Paradie, E., Banks, N., Motyl, K.*, et al.* (2019). Neuropathy and neural plasticity in the subcutaneous white adipose depot. PLoS One *14*, e0221766.

Boesmans, W., Hao, M.M., Fung, C., Li, Z., Van den Haute, C., Tack, J., Pachnis, V., and Vanden Berghe, P. (2019). Structurally defined signaling in neuro-glia units in the enteric nervous system. Glia *67*, 1167-1178.

Bogunovic, M., Dave, S.H., Tilstra, J.S., Chang, D.T., Harpaz, N., Xiong, H., Mayer, L.F., and Plevy, S.E. (2007). Enteroendocrine cells express functional Toll-like receptors. Am J Physiol Gastrointest Liver Physiol *292*, G1770-1783.

Bohórquez, D.V., Shahid, R.A., Erdmann, A., Kreger, A.M., Wang, Y., Calakos, N., Wang, F., and Liddle, R.A. (2015). Neuroepithelial circuit formed by innervation of sensory enteroendocrine cells. J Clin Invest *125*, 782-786.

Bonnin, A., and Levitt, P. (2011). Fetal, maternal, and placental sources of serotonin and new implications for developmental programming of the brain. Neuroscience *197*, 1-7.

Boraschi, D., and Italiani, P. (2018). Innate Immune Memory: Time for Adopting a Correct Terminology. Front Immunol *9*, 799.

Boring, L., Gosling, J., Chensue, S.W., Kunkel, S.L., Farese, R.V., Jr., Broxmeyer, H.E., and Charo, I.F. (1997). Impaired monocyte migration and reduced type 1 (Th1) cytokine responses in C-C chemokine receptor 2 knockout mice. J Clin Invest *100*, 2552-2561.

Borovikova, L.V., Ivanova, S., Zhang, M., Yang, H., Botchkina, G.I., Watkins, L.R., Wang, H., Abumrad, N., Eaton, J.W., and Tracey, K.J. (2000). Vagus nerve stimulation attenuates the systemic inflammatory response to endotoxin. Nature *405*, 458-462.

Bosmans, G., Appeltans, I., Stakenborg, N., Gomez-Pinilla, P.J., Florens, M.V., Aguilera-Lizarraga, J., Matteoli, G., and Boeckxstaens, G.E. (2019). Vagus nerve stimulation dampens intestinal inflammation in a murine model of experimental food allergy. Allergy *74*, 1748-1759.

Braniste, V., Al-Asmakh, M., Kowal, C., Anuar, F., Abbaspour, A., Toth, M., Korecka, A., Bakocevic, N., Ng, L.G., Kundu, P.*, et al.* (2014). The gut microbiota influences blood-brain barrier permeability in mice. Sci Transl Med *6*, 263ra158.

Bray, N.L., Pimentel, H., Melsted, P., and Pachter, L. (2016). Near-optimal probabilistic RNA-seq quantification. Nat Biotechnol *34*, 525-527.

Brazeau, P., Vale, W., Burgus, R., Ling, N., Butcher, M., Rivier, J., and Guillemin, R. (1973). Hypothalamic polypeptide that inhibits the secretion of immunoreactive pituitary growth hormone. Science *179*, 77-79.

Breder, C.D., Dinarello, C.A., and Saper, C.B. (1988). Interleukin-1 immunoreactive innervation of the human hypothalamus. Science *240*, 321-324.

Breder, C.D., Hazuka, C., Ghayur, T., Klug, C., Huginin, M., Yasuda, K., Teng, M., and Saper, C.B. (1994). Regional induction of tumor necrosis factor alpha expression in the mouse brain after systemic lipopolysaccharide administration. Proc Natl Acad Sci U S A *91*, 11393-11397.

Brighton, C.A., Rievaj, J., Kuhre, R.E., Glass, L.L., Schoonjans, K., Holst, J.J., Gribble, F.M., and Reimann, F. (2015). Bile Acids Trigger GLP-1 Release Predominantly by Accessing Basolaterally Located G Protein-Coupled Bile Acid Receptors. Endocrinology *156*, 3961-3970.

Brookes, S.J., Spencer, N.J., Costa, M., and Zagorodnyuk, V.P. (2013). Extrinsic primary afferent signalling in the gut. Nat Rev Gastroenterol Hepatol *10*, 286-296.

Brown, D.E., Libby, S.J., Moreland, S.M., McCoy, M.W., Brabb, T., Stepanek, A., Fang, F.C., and Detweiler, C.S. (2013). Salmonella enterica causes more severe inflammatory disease in C57/BL6 Nramp1G169 mice than Sv129S6 mice. Vet Pathol *50*, 867-876.

Brown, I.A., McClain, J.L., Watson, R.E., Patel, B.A., and Gulbransen, B.D. (2016). Enteric glia mediate neuron death in colitis through purinergic pathways that require connexin-43 and nitric oxide. Cell Mol Gastroenterol Hepatol *2*, 77-91.

Browning, K.N., and Lees, G.M. (2000). Inhibitory effects of NPY on ganglionic transmission in myenteric neurones of the guinea-pig descending colon. Neurogastroenterol Motil *12*, 33-41.

Browning, K.N., and Travagli, R.A. (2014). Central nervous system control of gastrointestinal motility and secretion and modulation of gastrointestinal functions. Compr Physiol *4*, 1339-1368.

Browning, K.N., and Travagli, R.A. (2019). Central control of gastrointestinal motility. Curr Opin Endocrinol Diabetes Obes *26*, 11-16.

Broz, P., and Dixit, V.M. (2016). Inflammasomes: mechanism of assembly, regulation and signalling. Nat Rev Immunol *16*, 407-420.

Broz, P., Ruby, T., Belhocine, K., Bouley, D.M., Kayagaki, N., Dixit, V.M., and Monack, D.M. (2012). Caspase-11 increases susceptibility to Salmonella infection in the absence of caspase-1. Nature *490*, 288-291.

Brumovsky, P., Shi, T.S., Landry, M., Villar, M.J., and Hokfelt, T. (2007). Neuropeptide tyrosine and pain. Trends Pharmacol Sci *28*, 93-102.

Brun, P., Giron, M.C., Qesari, M., Porzionato, A., Caputi, V., Zoppellaro, C., Banzato, S., Grillo, A.R., Spagnol, L., De Caro, R.*, et al.* (2013). Toll-like receptor 2 regulates intestinal inflammation by controlling integrity of the enteric nervous system. Gastroenterology *145*, 1323-1333.

Buckinx, R., Alpaerts, K., Pintelon, I., Cools, N., Van Nassauw, L., Adriaensen, D., and Timmermans, J.P. (2017). In situ proximity of CX3CR1-positive mononuclear phagocytes and VIP-ergic nerve fibers suggests VIP-ergic immunomodulation in the mouse ileum. Cell Tissue Res *368*, 459-467.

Buffie, C.G., Bucci, V., Stein, R.R., McKenney, P.T., Ling, L., Gobourne, A., No, D., Liu, H., Kinnebrew, M., Viale, A.*, et al.* (2015). Precision microbiome reconstitution restores bile acid mediated resistance to Clostridium difficile. Nature *517*, 205-208.

Bujko, A., Atlasy, N., Landsverk, O.J.B., Richter, L., Yaqub, S., Horneland, R., Oyen, O., Aandahl, E.M., Aabakken, L., Stunnenberg, H.G.*, et al.* (2018). Transcriptional and functional profiling defines human small intestinal macrophage subsets. J Exp Med *215*, 441-458.

Bush, T.G., Savidge, T.C., Freeman, T.C., Cox, H.J., Campbell, E.A., Mucke, L., Johnson, M.H., and Sofroniew, M.V. (1998). Fulminant jejuno-ileitis following ablation of enteric glia in adult transgenic mice. Cell *93*, 189-201.

Byun, T., Karimi, M., Marsh, J.L., Milovanovic, T., Lin, F., and Holcombe, R.F. (2005). Expression of secreted Wnt antagonists in gastrointestinal tissues: potential role in stem cell homeostasis. J Clin Pathol *58*, 515-519.

Cai, D., Deng, K., Mellado, W., Lee, J., Ratan, R.R., and Filbin, M.T. (2002). Arginase I and polyamines act downstream from cyclic AMP in overcoming inhibition of axonal growth MAG and myelin in vitro. Neuron *35*, 711-719.

Cailotto, C., Gomez-Pinilla, P.J., Costes, L.M., van der Vliet, J., Di Giovangiulio, M., Nemethova, A., Matteoli, G., and Boeckxstaens, G.E. (2014). Neuro-anatomical evidence indicating indirect modulation of macrophages by vagal efferents in the intestine but not in the spleen. PLoS One *9*, e87785.

Caputi, V., Marsilio, I., Filpa, V., Cerantola, S., Orso, G., Bistoletti, M., Paccagnella, N., De Martin, S., Montopoli, M., Dall'Acqua, S.*, et al.* (2017). Antibiotic-induced dysbiosis of the microbiota impairs gut neuromuscular function in juvenile mice. Br J Pharmacol *174*, 3623-3639.

Carabotti, M., Scirocco, A., Maselli, M.A., and Severi, C. (2015). The gut-brain axis: interactions between enteric microbiota, central and enteric nervous systems. Ann Gastroenterol *28*, 203-209.

Cardoso, V., Chesne, J., Ribeiro, H., Garcia-Cassani, B., Carvalho, T., Bouchery, T., Shah, K., Barbosa-Morais, N.L., Harris, N., and Veiga-Fernandes, H. (2017). Neuronal regulation of type 2 innate lymphoid cells via neuromedin U. Nature *549*, 277-281.

Carrion, M., Perez-Garcia, S., Martinez, C., Juarranz, Y., Estrada-Capetillo, L., Puig-Kroger, A., Gomariz, R.P., and Gutierrez-Canas, I. (2016). VIP impairs acquisition of the macrophage proinflammatory polarization profile. J Leukoc Biol *100*, 1385-1393.

Chandrasekharan, B., and Srinivasan, S. (2007). Diabetes and the enteric nervous system. Neurogastroenterol Motil *19*, 951-960.

Chen, G.Y., Liu, M., Wang, F., Bertin, J., and Nunez, G. (2011). A functional role for Nlrp6 in intestinal inflammation and tumorigenesis. J Immunol *186*, 7187-7194.

Chen, K., Geng, S., Yuan, R., Diao, N., Upchurch, Z., and Li, L. (2015a). Super-low dose endotoxin pre-conditioning exacerbates sepsis mortality. EBioMedicine *2*, 324-333.

Chen, Y., Lin, Y.C., Kuo, T.W., and Knight, Z.A. (2015b). Sensory detection of food rapidly modulates arcuate feeding circuits. Cell *160*, 829-841.

Chi, J., Wu, Z., Choi, C.H.J., Nguyen, L., Tegegne, S., Ackerman, S.E., Crane, A., Marchildon, F., Tessier-Lavigne, M., and Cohen, P. (2018). Three-Dimensional Adipose Tissue Imaging Reveals Regional Variation in Beige Fat Biogenesis and PRDM16-Dependent Sympathetic Neurite Density. Cell Metab *27*, 226-236 e223.

Chieppa, M., Rescigno, M., Huang, A.Y., and Germain, R.N. (2006). Dynamic imaging of dendritic cell extension into the small bowel lumen in response to epithelial cell TLR engagement. J Exp Med *203*, 2841-2852.

Chiu, Y.C., Hua, T.E., Fu, Y.Y., Pasricha, P.J., and Tang, S.C. (2012). 3-D imaging and illustration of the perfusive mouse islet sympathetic innervation and its remodelling in injury. Diabetologia *55*, 3252-3261.

Chung, H., Pamp, S.J., Hill, J.A., Surana, N.K., Edelman, S.M., Troy, E.B., Reading, N.C., Villablanca, E.J., Wang, S., Mora, J.R.*, et al.* (2012). Gut immune maturation depends on colonization with a host-specific microbiota. Cell *149*, 1578-1593.

Cipriani, G., Gibbons, S.J., Miller, K.E., Yang, D.S., Terhaar, M.L., Eisenman, S.T., Ordog, T., Linden, D.R., Gajdos, G.B., Szurszewski, J.H.*, et al.* (2018). Change in Populations of Macrophages Promotes Development of Delayed Gastric Emptying in Mice. Gastroenterology *154*, 2122-2136 e2112.

Cipriani, G., Terhaar, M.L., Eisenman, S.T., Ji, S., Linden, D.R., Wright, A.M., Sha, L., Ordog, T., Szurszewski, J.H., Gibbons, S.J.*, et al.* (2019). Muscularis Propria Macrophages Alter the Proportion of Nitrergic but Not Cholinergic Gastric Myenteric Neurons. Cell Mol Gastroenterol Hepatol *7*, 689-691 e684.

Claus, S.P., Tsang, T.M., Wang, Y., Cloarec, O., Skordi, E., Martin, F.P., Rezzi, S., Ross, A., Kochhar, S., Holmes, E.*, et al.* (2008). Systemic multicompartmental effects of the gut microbiome on mouse metabolic phenotypes. Mol Syst Biol *4*, 219.

Cohen, J.A., Edwards, T.N., Liu, A.W., Hirai, T., Jones, M.R., Wu, J., Li, Y., Zhang, S., Ho, J., Davis, B.M.*, et al.* (2019). Cutaneous TRPV1(+) Neurons Trigger Protective Innate Type 17 Anticipatory Immunity. Cell *178*, 919-932 e914.

Cohen, L.J., Esterhazy, D., Kim, S.H., Lemetre, C., Aguilar, R.R., Gordon, E.A., Pickard, A.J., Cross, J.R., Emiliano, A.B., Han, S.M.*, et al.* (2017). Commensal bacteria make GPCR ligands that mimic human signalling molecules. Nature *549*, 48-53.

Collins, J., Borojevic, R., Verdu, E.F., Huizinga, J.D., and Ratcliffe, E.M. (2014). Intestinal microbiota influence the early postnatal development of the enteric nervous system. Neurogastroenterol Motil *26*, 98-107.

Couceyro, P., Paquet, M., Koylu, E., Kuhar, M.J., and Smith, Y. (1998). Cocaine- and amphetamine-regulated transcript (CART) peptide immunoreactivity in myenteric plexus neurons of the rat ileum and co-localization with choline acetyltransferase. Synapse *30*, 1-8.

Cowley, M.A., Smart, J.L., Rubinstein, M., Cerdan, M.G., Diano, S., Horvath, T.L., Cone, R.D., and Low, M.J. (2001). Leptin activates anorexigenic POMC neurons through a neural network in the arcuate nucleus. Nature *411*, 480-484.

Crawford, R.W., Keestra, A.M., Winter, S.E., Xavier, M.N., Tsolis, R.M., Tolstikov, V., and Baumler, A.J. (2012). Very long O-antigen chains enhance fitness during Salmonella-induced colitis by increasing bile resistance. PLoS Pathog *8*, e1002918.

Crowcroft, P.J., Holman, M.E., and Szurszewski, J.H. (1971). Excitatory input from the distal colon to the inferior mesenteric ganglion in the guinea-pig. J Physiol *219*, 443-461.

Cummings, R.J., Barbet, G., Bongers, G., Hartmann, B.M., Gettler, K., Muniz, L., Furtado, G.C., Cho, J., Lira, S.A., and Blander, J.M. (2016). Different tissue phagocytes sample apoptotic cells to direct distinct homeostasis programs. Nature *539*, 565-569.

Danne, C., Ryzhakov, G., Martinez-Lopez, M., Ilott, N.E., Franchini, F., Cuskin, F., Lowe, E.C., Bullers, S.J., Arthur, J.S.C., and Powrie, F. (2017). A Large Polysaccharide Produced by Helicobacter hepaticus Induces an Anti-inflammatory Gene Signature in Macrophages. Cell Host Microbe *22*, 733-745 e735.

de Jonge, W.J., van der Zanden, E.P., The, F.O., Bijlsma, M.F., van Westerloo, D.J., Bennink, R.J., Berthoud, H.R., Uematsu, S., Akira, S., van den Wijngaard, R.M.*, et al.* (2005). Stimulation of the vagus nerve attenuates macrophage activation by activating the Jak2-STAT3 signaling pathway. Nat Immunol *6*, 844-851.

De Schepper, S., Verheijden, S., Aguilera-Lizarraga, J., Viola, M.F., Boesmans, W., Stakenborg, N., Voytyuk, I., Schmidt, I., Boeckx, B., Dierckx de Casterle, I.*, et al.* (2018). Self-Maintaining Gut Macrophages Are Essential for Intestinal Homeostasis. Cell *175*, 400-415 e413.

De Vadder, F., Grasset, E., Manneras Holm, L., Karsenty, G., Macpherson, A.J., Olofsson, L.E., and Backhed, F. (2018). Gut microbiota regulates maturation of the adult enteric nervous system via enteric serotonin networks. Proc Natl Acad Sci U S A *115*, 6458-6463.

Degen, L.P., Peng, F., Collet, A., Rossi, L., Ketterer, S., Serrano, Y., Larsen, F., Beglinger, C., and Hildebrand, P. (2001). Blockade of GRP receptors inhibits gastric emptying and gallbladder contraction but accelerates small intestinal transit. Gastroenterology *120*, 361-368.

del Giudice, E.M., Santoro, N., Cirillo, G., D'Urso, L., Di Toro, R., and Perrone, L. (2001). Mutational screening of the CART gene in obese children: identifying a mutation (Leu34Phe) associated with reduced resting energy expenditure and cosegregating with obesity phenotype in a large family. Diabetes *50*, 2157-2160.

Denning, T.L., Wang, Y.C., Patel, S.R., Williams, I.R., and Pulendran, B. (2007). Lamina propria macrophages and dendritic cells differentially induce regulatory and interleukin 17-producing T cell responses. Nat Immunol *8*, 1086-1094.

Desalegn, G., and Pabst, O. (2019). Inflammation triggers immediate rather than progressive changes in monocyte differentiation in the small intestine. Nat Commun *10*, 3229.

Dey, A., Xhu, X., Carroll, R., Turck, C.W., Stein, J., and Steiner, D.F. (2003). Biological processing of the cocaine and amphetamine-regulated transcript precursors by prohormone convertases, PC2 and PC1/3. J Biol Chem *278*, 15007-15014.

Di Giovangiulio, M., Verheijden, S., Bosmans, G., Stakenborg, N., Boeckxstaens, G.E., and Matteoli, G. (2015). The Neuromodulation of the Intestinal Immune System and Its Relevance in Inflammatory Bowel Disease. Front Immunol *6*, 590.

Di Luzio, N.R., and Williams, D.L. (1978). Protective effect of glucan against systemic Staphylococcus aureus septicemia in normal and leukemic mice. Infect Immun *20*, 804-810.

Diakogiannaki, E., Pais, R., Tolhurst, G., Parker, H.E., Horscroft, J., Rauscher, B., Zietek, T., Daniel, H., Gribble, F.M., and Reimann, F. (2013). Oligopeptides stimulate glucagon-like peptide-1 secretion in mice through proton-coupled uptake and the calcium-sensing receptor. Diabetologia *56*, 2688-2696.

Diaz Heijtz, R., Wang, S., Anuar, F., Qian, Y., Bjorkholm, B., Samuelsson, A., Hibberd, M.L., Forssberg, H., and Pettersson, S. (2011). Normal gut microbiota modulates brain development and behavior. Proc Natl Acad Sci U S A *108*, 3047-3052.

Doerffler-Melly, J., and Neuhuber, W.L. (1988). Rectospinal neurons: evidence for a direct projection from the enteric to the central nervous system in the rat. Neurosci Lett *92*, 121-125.

Donaldson, G.P., Lee, S.M., and Mazmanian, S.K. (2016). Gut biogeography of the bacterial microbiota. Nat Rev Microbiol *14*, 20-32.

Dong, H., Wang, S., Zhang, Z., Yu, A., and Liu, Z. (2014). The effect of mitochondrial calcium uniporter opener spermine on diazoxide against focal cerebral ischemia--reperfusion injury in rats. J Stroke Cerebrovasc Dis *23*, 303-309.

Dothel, G., Barbaro, M.R., Boudin, H., Vasina, V., Cremon, C., Gargano, L., Bellacosa, L., De Giorgio, R., Le Berre-Scoul, C., Aubert, P.*, et al.* (2015). Nerve fiber outgrowth is increased in the intestinal mucosa of patients with irritable bowel syndrome. Gastroenterology *148*, 1002-1011 e1004.

Douglass, J., McKinzie, A.A., and Couceyro, P. (1995). PCR differential display identifies a rat brain mRNA that is transcriptionally regulated by cocaine and amphetamine. J Neurosci *15*, 2471-2481.

Drokhlyansky, E., Smillie, C.S., Van Wittenberghe, N., Ericsson, M., Griffin, G.K., Eraslan, G., Dionne, D., Cuoco, M.S., Goder-Reiser, M.N., Sharova, T.*, et al.* (2020). The Human and Mouse Enteric Nervous System at Single-Cell Resolution. Cell *182*, 1606-1622 e1623.

Du, H., Ming, X., and Zhou, S. (2017). Pre-treatment with spermine for acute cerebral ischemia/reperfusion injuries. Exp Ther Med *14*, 169-172.

Dubos, R., Savage, D., and Schaedler, R. (1966). Biological Freudianism. Lasting effects of early environmental influences. Pediatrics *38*, 789-800.

Dubos, R., and Schaedler, R.W. (1964). The Digestive Tract as an Ecosystem. Trans Assoc Am Physicians *77*, 110-117.

Dunay, I.R., Damatta, R.A., Fux, B., Presti, R., Greco, S., Colonna, M., and Sibley, L.D. (2008). Gr1(+) inflammatory monocytes are required for mucosal resistance to the pathogen Toxoplasma gondii. Immunity *29*, 306-317.

Dunn-Meynell, A.A., Sanders, N.M., Compton, D., Becker, T.C., Eiki, J., Zhang, B.B., and Levin, B.E. (2009). Relationship among brain and blood glucose levels and spontaneous and glucoprivic feeding. J Neurosci *29*, 7015-7022.

Dutra, W.O., Menezes, C.A., Villani, F.N., da Costa, G.C., da Silveira, A.B., Reis, D., and Gollob, K.J. (2009). Cellular and genetic mechanisms involved in the generation of protective and pathogenic immune responses in human Chagas disease. Mem Inst Oswaldo Cruz *104 Suppl 1*, 208-218.

Edgar, R.C. (2010). Search and clustering orders of magnitude faster than BLAST. Bioinformatics *26*, 2460-2461.

Edwards, C.K., 3rd, Yunger, L.M., Lorence, R.M., Dantzer, R., and Kelley, K.W. (1991). The pituitary gland is required for protection against lethal effects of Salmonella typhimurium. Proc Natl Acad Sci U S A *88*, 2274-2277.

Ekblad, E. (2006). CART in the enteric nervous system. Peptides *27*, 2024-2030.

Ekblad, E., Kuhar, M., Wierup, N., and Sundler, F. (2003). Cocaine- and amphetamine-regulated transcript: distribution and function in rat gastrointestinal tract. Neurogastroenterol Motil *15*, 545-557.

El Kasmi, K.C., Qualls, J.E., Pesce, J.T., Smith, A.M., Thompson, R.W., Henao-Tamayo, M., Basaraba, R.J., Konig, T., Schleicher, U., Koo, M.S.*, et al.* (2008). Toll-like receptor-induced arginase 1 in macrophages thwarts effective immunity against intracellular pathogens. Nat Immunol *9*, 1399-1406.

El-Salhy, M., and Hausken, T. (2016). The role of the neuropeptide Y (NPY) family in the pathophysiology of inflammatory bowel disease (IBD). Neuropeptides *55*, 137-144.

Elias, C.F., Lee, C.E., Kelly, J.F., Ahima, R.S., Kuhar, M., Saper, C.B., and Elmquist, J.K. (2001). Characterization of CART neurons in the rat and human hypothalamus. J Comp Neurol *432*, 1-19.

Elinav, E., Strowig, T., Kau, A.L., Henao-Mejia, J., Thaiss, C.A., Booth, C.J., Peaper, D.R., Bertin, J., Eisenbarth, S.C., Gordon, J.I.*, et al.* (2011). NLRP6 inflammasome regulates colonic microbial ecology and risk for colitis. Cell *145*, 745-757.

Ellis, L.M., and Mawe, G.M. (2003). Distribution and chemical coding of cocaine- and amphetamine-regulated transcript peptide (CART)-immunoreactive neurons in the guinea pig bowel. Cell Tissue Res *312*, 265-274.

Eskandari, M.K., Kalff, J.C., Billiar, T.R., Lee, K.K., and Bauer, A.J. (1997). Lipopolysaccharide activates the muscularis macrophage network and suppresses circular smooth muscle activity. Am J Physiol *273*, G727-734.

Esterhazy, D., Canesso, M.C.C., Mesin, L., Muller, P.A., de Castro, T.B.R., Lockhart, A., ElJalby, M., Faria, A.M.C., and Mucida, D. (2019). Compartmentalized gut lymph node drainage dictates adaptive immune responses. Nature *569*, 126-130.

Faria, A.M.C., Reis, B.S., and Mucida, D. (2017). Tissue adaptation: Implications for gut immunity and tolerance. J Exp Med *214*, 1211-1226.

Farro, G., Stakenborg, M., Gomez-Pinilla, P.J., Labeeuw, E., Goverse, G., Di Giovangiulio, M., Stakenborg, N., Meroni, E., D'Errico, F., Elkrim, Y.*, et al.* (2017). CCR2-dependent monocyte-derived macrophages resolve inflammation and restore gut motility in postoperative ileus. Gut *66*, 2098-2109.

Fonseca, D.M., Hand, T.W., Han, S.J., Gerner, M.Y., Glatman Zaretsky, A., Byrd, A.L., Harrison, O.J., Ortiz, A.M., Quinones, M., Trinchieri, G.*, et al.* (2015). Microbiota-Dependent Sequelae of Acute Infection Compromise Tissue-Specific Immunity. Cell *163*, 354-366.

Foong, J.P. (2016). Postnatal Development of the Mouse Enteric Nervous System. Adv Exp Med Biol *891*, 135-143.

Ford, A.C., Lacy, B.E., and Talley, N.J. (2017). Irritable Bowel Syndrome. N Engl J Med *376*, 2566-2578.

Fornai, M., Pellegrini, C., Antonioli, L., Segnani, C., Ippolito, C., Barocelli, E., Ballabeni, V., Vegezzi, G., Al Harraq, Z., Blandini, F.*, et al.* (2016). Enteric Dysfunctions in Experimental Parkinson's Disease: Alterations of Excitatory Cholinergic Neurotransmission Regulating Colonic Motility in Rats. J Pharmacol Exp Ther *356*, 434-444.

Forsythe, P. (2019). Mast Cells in Neuroimmune Interactions. Trends Neurosci *42*, 43-55.

Fujii, T., Mashimo, M., Moriwaki, Y., Misawa, H., Ono, S., Horiguchi, K., and Kawashima, K. (2017). Physiological functions of the cholinergic system in immune cells. J Pharmacol Sci *134*, 1-21.

Fung, C., Hao, M.M., Obata, Y., Tack, J., Pachnis, V., Boesmans, W., and Vanden Berghe, P. (2021). Luminal nutrients activate distinct patterns in submucosal and myenteric neurons in the mouse small intestine. bioRxiv, 2021.2001.2019.427232.

Fung, T.C., Olson, C.A., and Hsiao, E.Y. (2017). Interactions between the microbiota, immune and nervous systems in health and disease. Nat Neurosci *20*, 145-155.

Furlan, A., La Manno, G., Lubke, M., Haring, M., Abdo, H., Hochgerner, H., Kupari, J., Usoskin, D., Airaksinen, M.S., Oliver, G.*, et al.* (2016). Visceral motor neuron diversity

delineates a cellular basis for nipple- and pilo-erection muscle control. Nat Neurosci *19*, 1331-1340.

Furness, J.B. (2000). Types of neurons in the enteric nervous system. J Auton Nerv Syst *81*, 87-96.

Furness, J.B. (2006). The Enteric Nervous System (Blackwell Publishing).

Furness, J.B. (2012). The enteric nervous system and neurogastroenterology. Nat Rev Gastroenterol Hepatol *9*, 286-294.

Furness, J.B., and Anderson, C.R. (1994). Origins of nerve terminals containing nitric oxide synthase in the guinea-pig coeliac ganglion. J Auton Nerv Syst *46*, 47-54.

Furness, J.B., Callaghan, B.P., Rivera, L.R., and Cho, H.J. (2014). The enteric nervous system and gastrointestinal innervation: integrated local and central control. Adv Exp Med Biol *817*, 39-71.

Furness, J.B., Rivera, L.R., Cho, H.J., Bravo, D.M., and Callaghan, B. (2013). The gut as a sensory organ. Nat Rev Gastroenterol Hepatol *10*, 729-740.

Gabanyi, I., Muller, P.A., Feighery, L., Oliveira, T.Y., Costa-Pinto, F.A., and Mucida, D. (2016). Neuro-immune Interactions Drive Tissue Programming in Intestinal Macrophages. Cell *164*, 378-391.

Gensel, J.C., Nakamura, S., Guan, Z., van Rooijen, N., Ankeny, D.P., and Popovich, P.G. (2009). Macrophages promote axon regeneration with concurrent neurotoxicity. J Neurosci *29*, 3956-3968.

Gerbe, F., Sidot, E., Smyth, D.J., Ohmoto, M., Matsumoto, I., Dardalhon, V., Cesses, P., Garnier, L., Pouzolles, M., Brulin, B.*, et al.* (2016). Intestinal epithelial tuft cells initiate type 2 mucosal immunity to helminth parasites. Nature *529*, 226-230.

Ghia, J.E., Li, N., Wang, H., Collins, M., Deng, Y., El-Sharkawy, R.T., Cote, F., Mallet, J., and Khan, W.I. (2009). Serotonin has a key role in pathogenesis of experimental colitis. Gastroenterology *137*, 1649-1660.

Gielkens, H.A., Verkijk, M., Lam, W.F., Lamers, C.B., and Masclee, A.A. (1998). Effects of hyperglycemia and hyperinsulinemia on satiety in humans. Metabolism *47*, 321-324.

Goehler, L.E., Relton, J.K., Dripps, D., Kiechle, R., Tartaglia, N., Maier, S.F., and Watkins, L.R. (1997). Vagal paraganglia bind biotinylated interleukin-1 receptor antagonist: a possible mechanism for immune-to-brain communication. Brain Res Bull *43*, 357-364.

Gombash, S.E., Cowley, C.J., Fitzgerald, J.A., Hall, J.C., Mueller, C., Christofi, F.L., and Foust, K.D. (2014). Intravenous AAV9 efficiently transduces myenteric neurons in neonate and juvenile mice. Front Mol Neurosci *7*, 81.

Gong, Z., Zhou, J., Zhao, S., Tian, C., Wang, P., Xu, C., Chen, Y., Cai, W., and Wu, J. (2016). Chenodeoxycholic acid activates NLRP3 inflammasome and contributes to cholestatic liver fibrosis. Oncotarget *7*, 83951-83963.

Gonkowski, S., and Rytel, L. (2019). Somatostatin as an Active Substance in the Mammalian Enteric Nervous System. Int J Mol Sci *20*.

Gorboulev, V., Schurmann, A., Vallon, V., Kipp, H., Jaschke, A., Klessen, D., Friedrich, A., Scherneck, S., Rieg, T., Cunard, R.*, et al.* (2012). Na(+)-D-glucose cotransporter SGLT1 is pivotal for intestinal glucose absorption and glucose-dependent incretin secretion. Diabetes *61*, 187-196.

Greenwood-Van Meerveld, B., Johnson, A.C., and Grundy, D. (2017). Gastrointestinal Physiology and Function. Handb Exp Pharmacol *239*, 1-16.

Gribble, F.M., and Reimann, F. (2016). Enteroendocrine Cells: Chemosensors in the Intestinal Epithelium. Annu Rev Physiol *78*, 277-299.

Grider, J.R. (2003). Neurotransmitters mediating the intestinal peristaltic reflex in the mouse. J Pharmacol Exp Ther *307*, 460-467.

Grunddal, K.V., Ratner, C.F., Svendsen, B., Sommer, F., Engelstoft, M.S., Madsen, A.N., Pedersen, J., Nohr, M.K., Egerod, K.L., Nawrocki, A.R.*, et al.* (2016). Neurotensin Is Coexpressed, Coreleased, and Acts Together With GLP-1 and PYY in Enteroendocrine Control of Metabolism. Endocrinology *157*, 176-194.

Gulbransen, B.D., Bashashati, M., Hirota, S.A., Gui, X., Roberts, J.A., MacDonald, J.A., Muruve, D.A., McKay, D.M., Beck, P.L., Mawe, G.M.*, et al.* (2012). Activation of neuronal P2X7 receptor-pannexin-1 mediates death of enteric neurons during colitis. Nat Med *18*, 600-604.

Gunawardene, A.R., Corfe, B.M., and Staton, C.A. (2011). Classification and functions of enteroendocrine cells of the lower gastrointestinal tract. Int J Exp Pathol *92*, 219-231.

Gunnarsdottir, A., Wierup, N., Larsson, L.T., Kuhar, M.J., and Ekblad, E. (2007). CART-peptide immunoreactivity in enteric nerves in patients with Hirschsprung's disease. Eur J Pediatr Surg *17*, 184-189.

Gupta, R., Ma, Y., Wang, M., and Whim, M.D. (2017). AgRP-Expressing Adrenal Chromaffin Cells Are Involved in the Sympathetic Response to Fasting. Endocrinology *158*, 2572-2584.

Gwynne, R.M., Ellis, M., Sjovall, H., and Bornstein, J.C. (2009). Cholera toxin induces sustained hyperexcitability in submucosal secretomotor neurons in guinea pig jejunum. Gastroenterology *136*, 299-308 e294.

Haber, A.L., Biton, M., Rogel, N., Herbst, R.H., Shekhar, K., Smillie, C., Burgin, G., Delorey, T.M., Howitt, M.R., Katz, Y.*, et al.* (2017). A single-cell survey of the small intestinal epithelium. Nature *551*, 333-339.

Hadis, U., Wahl, B., Schulz, O., Hardtke-Wolenski, M., Schippers, A., Wagner, N., Muller, W., Sparwasser, T., Forster, R., and Pabst, O. (2011). Intestinal tolerance requires gut homing and expansion of FoxP3+ regulatory T cells in the lamina propria. Immunity *34*, 237-246.

Han, L.P., Yuan, L.B., Shentu, Y.P., and Shao, J.D. (2013). Spermine reduced no-reflow size induced by ischemia-reperfusion through regulating autophagy. Int J Cardiol *168*, 3145-3147.

Han, W., Tellez, L.A., Perkins, M.H., Perez, I.O., Qu, T., Ferreira, J., Ferreira, T.L., Quinn, D., Liu, Z.W., Gao, X.B.*, et al.* (2018). A Neural Circuit for Gut-Induced Reward. Cell *175*, 665-678 e623.

Handa, A.K., Fatima, T., and Mattoo, A.K. (2018). Polyamines: Bio-Molecules with Diverse Functions in Plant and Human Health and Disease. Front Chem *6*, 10.

Hara, H., Seregin, S.S., Yang, D., Fukase, K., Chamaillard, M., Alnemri, E.S., Inohara, N., Chen, G.Y., and Nunez, G. (2018). The NLRP6 Inflammasome Recognizes Lipoteichoic Acid and Regulates Gram-Positive Pathogen Infection. Cell *175*, 1651-1664 e1614.

Hardbower, D.M., Asim, M., Luis, P.B., Singh, K., Barry, D.P., Yang, C., Steeves, M.A., Cleveland, J.L., Schneider, C., Piazuelo, M.B.*, et al.* (2017). Ornithine decarboxylase regulates M1 macrophage activation and mucosal inflammation via histone modifications. Proc Natl Acad Sci U S A *114*, E751-E760.

Hardbower, D.M., Singh, K., Asim, M., Verriere, T.G., Olivares-Villagomez, D., Barry, D.P., Allaman, M.M., Washington, M.K., Peek, R.M., Jr., Piazuelo, M.B.*, et al.* (2016). EGFR regulates macrophage activation and function in bacterial infection. J Clin Invest *126*, 3296-3312.

Havrankova, J., Roth, J., and Brownstein, M. (1978). Insulin receptors are widely distributed in the central nervous system of the rat. Nature *272*, 827-829.

Hayashi, A., Sato, T., Kamada, N., Mikami, Y., Matsuoka, K., Hisamatsu, T., Hibi, T., Roers, A., Yagita, H., Ohteki, T.*, et al.* (2013). A single strain of Clostridium butyricum induces intestinal IL-10-producing macrophages to suppress acute experimental colitis in mice. Cell Host Microbe *13*, 711-722.

Heiman, M., Kulicke, R., Fenster, R.J., Greengard, P., and Heintz, N. (2014). Cell type-specific mRNA purification by translating ribosome affinity purification (TRAP). Nat Protoc *9*, 1282-1291.

Heuckeroth, R.O. (2018). Hirschsprung disease - integrating basic science and clinical medicine to improve outcomes. Nat Rev Gastroenterol Hepatol *15*, 152-167.

Hibberd, T.J., Zagorodnyuk, V.P., Spencer, N.J., and Brookes, S.J. (2012). Identification and mechanosensitivity of viscerofugal neurons. Neuroscience *225*, 118-129.

Hine, A.M., and Loke, P. (2019). Intestinal Macrophages in Resolving Inflammation. J Immunol *203*, 593-599.

Hinoi, E., Gao, N., Jung, D.Y., Yadav, V., Yoshizawa, T., Myers, M.G., Jr., Chua, S.C., Jr., Kim, J.K., Kaestner, K.H., and Karsenty, G. (2008). The sympathetic tone mediates leptin's inhibition of insulin secretion by modulating osteocalcin bioactivity. J Cell Biol *183*, 1235-1242.

Holland, A.M., Bon-Frauches, A.C., Keszthelyi, D., Melotte, V., and Boesmans, W. (2021). The enteric nervous system in gastrointestinal disease etiology. Cell Mol Life Sci.

Holschneider, D.P., Bradesi, S., and Mayer, E.A. (2011). The role of experimental models in developing new treatments for irritable bowel syndrome. Expert Rev Gastroenterol Hepatol *5*, 43-57.

Holst, M.C., and Powley, T.L. (1995). Cuprolinic blue (quinolinic phthalocyanine) counterstaining of enteric neurons for peroxidase immunocytochemistry. J Neurosci Methods *62*, 121-127.

Holzer, P. (2009). Opioid receptors in the gastrointestinal tract. Regul Pept *155*, 11-17.

Holzer, P., and Farzi, A. (2014). Neuropeptides and the microbiota-gut-brain axis. Adv Exp Med Biol *817*, 195-219.

Holzer, P., Lippe, I.T., Bartho, L., and Saria, A. (1987). Neuropeptide Y inhibits excitatory enteric neurons supplying the circular muscle of the guinea pig small intestine. Gastroenterology *92*, 1944-1950.

Holzer, P., Reichmann, F., and Farzi, A. (2012). Neuropeptide Y, peptide YY and pancreatic polypeptide in the gut-brain axis. Neuropeptides *46*, 261-274.

Honda, K., and Littman, D.R. (2016). The microbiota in adaptive immune homeostasis and disease. Nature *535*, 75-84.

Horio, N., and Liberles, S.D. (2021). Hunger enhances food-odour attraction through a neuropeptide Y spotlight. Nature *592*, 262-266.

Howitt, M.R., Lavoie, S., Michaud, M., Blum, A.M., Tran, S.V., Weinstock, J.V., Gallini, C.A., Redding, K., Margolskee, R.F., Osborne, L.C.*, et al.* (2016). Tuft cells, taste-chemosensory cells, orchestrate parasite type 2 immunity in the gut. Science *351*, 1329-1333.

Hoytema van Konijnenburg, D.P., Reis, B.S., Pedicord, V.A., Farache, J., Victora, G.D., and Mucida, D. (2017). Intestinal Epithelial and Intraepithelial T Cell Crosstalk Mediates a Dynamic Response to Infection. Cell *171*, 783-794 e713.

Hsiao, E.Y., McBride, S.W., Hsien, S., Sharon, G., Hyde, E.R., McCue, T., Codelli, J.A., Chow, J., Reisman, S.E., Petrosino, J.F.*, et al.* (2013). Microbiota modulate behavioral and physiological abnormalities associated with neurodevelopmental disorders. Cell *155*, 1451-1463.

Huber, S., Gagliani, N., Zenewicz, L.A., Huber, F.J., Bosurgi, L., Hu, B., Hedl, M., Zhang, W., O'Connor, W., Jr., Murphy, A.J.*, et al.* (2012). IL-22BP is regulated by the inflammasome and modulates tumorigenesis in the intestine. Nature *491*, 259-263.

Hung, L.Y., Boonma, P., Unterweger, P., Parathan, P., Haag, A., Luna, R.A., Bornstein, J.C., Savidge, T.C., and Foong, J.P.P. (2019). Neonatal Antibiotics Disrupt Motility and Enteric Neural Circuits in Mouse Colon. Cell Mol Gastroenterol Hepatol *8*, 298-300 e296.

Hung, L.Y., Parathan, P., Boonma, P., Wu, Q., Wang, Y., Haag, A., Luna, R.A., Bornstein, J.C., Savidge, T.C., and Foong, J.P.P. (2020). Antibiotic exposure postweaning disrupts the neurochemistry and function of enteric neurons mediating colonic motor activity. Am J Physiol Gastrointest Liver Physiol *318*, G1042-G1053.

Hyland, N.P., and Cryan, J.F. (2016). Microbe-host interactions: Influence of the gut microbiota on the enteric nervous system. Dev Biol *417*, 182-187.

Ibiza, S., Garcia-Cassani, B., Ribeiro, H., Carvalho, T., Almeida, L., Marques, R., Misic, A.M., Bartow-McKenney, C., Larson, D.M., Pavan, W.J.*, et al.* (2016). Glial-cell-derived neuroregulators control type 3 innate lymphoid cells and gut defence. Nature *535*, 440-443.

Igarashi, K., and Kashiwagi, K. (2010). Modulation of cellular function by polyamines. Int J Biochem Cell Biol *42*, 39-51.

Ishifune, C., Maruyama, S., Sasaki, Y., Yagita, H., Hozumi, K., Tomita, T., Kishihara, K., and Yasutomo, K. (2014). Differentiation of CD11c+ CX3CR1+ cells in the small intestine requires Notch signaling. Proc Natl Acad Sci U S A *111*, 5986-5991.

Ismail, A.S., Severson, K.M., Vaishnava, S., Behrendt, C.L., Yu, X., Benjamin, J.L., Ruhn, K.A., Hou, B., DeFranco, A.L., Yarovinsky, F.*, et al.* (2011). Gammadelta intraepithelial lymphocytes are essential mediators of host-microbial homeostasis at the intestinal mucosal surface. Proc Natl Acad Sci U S A *108*, 8743-8748.

Jacobsen, E.A., Lesuer, W.E., Willetts, L., Zellner, K.R., Mazzolini, K., Antonios, N., Beck, B., Protheroe, C., Ochkur, S.I., Colbert, D.*, et al.* (2014). Eosinophil activities modulate the immune/inflammatory character of allergic respiratory responses in mice. Allergy *69*, 315-327.

Jacobson, A., Yang, D., Vella, M., and Chiu, I.M. (2021). The intestinal neuro-immune axis: crosstalk between neurons, immune cells, and microbes. Mucosal Immunol.

Janssen, S., and Depoortere, I. (2013). Nutrient sensing in the gut: new roads to therapeutics? Trends Endocrinol Metab *24*, 92-100.

Jarret, A., Jackson, R., Duizer, C., Healy, M.E., Zhao, J., Rone, J.M., Bielecki, P., Sefik, E., Roulis, M., Rice, T.*, et al.* (2020). Enteric Nervous System-Derived IL-18 Orchestrates Mucosal Barrier Immunity. Cell *180*, 50-63 e12.

Joly, A., Leulier, F., and De Vadder, F. (2020). Microbial Modulation of the Development and Physiology of the Enteric Nervous System. Trends Microbiol.

Jones, D.C., and Kuhar, M.J. (2008). CART receptor binding in primary cell cultures of the rat nucleus accumbens. Synapse *62*, 122-127.

Jones, J.G. (2016). Hepatic glucose and lipid metabolism. Diabetologia *59*, 1098-1103.

Joseph, N.M., He, S., Quintana, E., Kim, Y.G., Nunez, G., and Morrison, S.J. (2011). Enteric glia are multipotent in culture but primarily form glia in the adult rodent gut. J Clin Invest *121*, 3398-3411.

Kabouridis, P.S., Lasrado, R., McCallum, S., Chng, S.H., Snippert, H.J., Clevers, H., Pettersson, S., and Pachnis, V. (2015). Microbiota controls the homeostasis of glial cells in the gut lamina propria. Neuron *85*, 289-295.

Kaelberer, M.M., Buchanan, K.L., Klein, M.E., Barth, B.B., Montoya, M.M., Shen, X., and Bohórquez, D.V. (2018). A gut-brain neural circuit for nutrient sensory transduction. Science *361*.

Kaelberer, M.M., and Jordt, S.E. (2016). A Method to Target and Isolate Airway-innervating Sensory Neurons in Mice. J Vis Exp.

Kaestner, C.L., Smith, E.H., Peirce, S.G., and Hoover, D.B. (2019). Immunohistochemical analysis of the mouse celiac ganglion: An integrative relay station of the peripheral nervous system. J Comp Neurol *527*, 2742-2760.

Kalff, J.C., Schraut, W.H., Simmons, R.L., and Bauer, A.J. (1998). Surgical manipulation of the gut elicits an intestinal muscularis inflammatory response resulting in postsurgical ileus. Ann Surg *228*, 652-663.

Kayagaki, N., Warming, S., Lamkanfi, M., Vande Walle, L., Louie, S., Dong, J., Newton, K., Qu, Y., Liu, J., Heldens, S.*, et al.* (2011). Non-canonical inflammasome activation targets caspase-11. Nature *479*, 117-121.

Kayagaki, N., Wong, M.T., Stowe, I.B., Ramani, S.R., Gonzalez, L.C., Akashi-Takamura, S., Miyake, K., Zhang, J., Lee, W.P., Muszynski, A.*, et al.* (2013). Noncanonical

inflammasome activation by intracellular LPS independent of TLR4. Science *341*, 1246-1249.

Kenneth, N.S., Younger, J.M., Hughes, E.D., Marcotte, D., Barker, P.A., Saunders, T.L., and Duckett, C.S. (2012). An inactivating caspase 11 passenger mutation originating from the 129 murine strain in mice targeted for c-IAP1. Biochem J *443*, 355-359.

Kentish, S.J., O'Donnell, T.A., Isaacs, N.J., Young, R.L., Li, H., Harrington, A.M., Brierley, S.M., Wittert, G.A., Blackshaw, L.A., and Page, A.J. (2013). Gastric vagal afferent modulation by leptin is influenced by food intake status. J Physiol *591*, 1921-1934.

Kessmann, J. (2006). Hirschsprung's disease: diagnosis and management. Am Fam Physician *74*, 1319-1322.

Kiela, P.R., and Ghishan, F.K. (2016). Physiology of Intestinal Absorption and Secretion. Best Pract Res Clin Gastroenterol *30*, 145-159.

Kigerl, K.A., Gensel, J.C., Ankeny, D.P., Alexander, J.K., Donnelly, D.J., and Popovich, P.G. (2009). Identification of two distinct macrophage subsets with divergent effects causing either neurotoxicity or regeneration in the injured mouse spinal cord. J Neurosci *29*, 13435-13444.

Kim, M., Galan, C., Hill, A.A., Wu, W.J., Fehlner-Peach, H., Song, H.W., Schady, D., Bettini, M.L., Simpson, K.W., Longman, R.S.*, et al.* (2018). Critical Role for the Microbiota in CX3CR1(+) Intestinal Mononuclear Phagocyte Regulation of Intestinal T Cell Responses. Immunity *49*, 151-163 e155.

Kim, S., Covington, A., and Pamer, E.G. (2017a). The intestinal microbiota: Antibiotics, colonization resistance, and enteric pathogens. Immunol Rev *279*, 90-105.

Kim, S., Kim, H., Yim, Y.S., Ha, S., Atarashi, K., Tan, T.G., Longman, R.S., Honda, K., Littman, D.R., Choi, G.B.*, et al.* (2017b). Maternal gut bacteria promote neurodevelopmental abnormalities in mouse offspring. Nature *549*, 528-532.

Kimura, H., Imura, Y.K., Tomiyasu, H., Mihara, T., Kaji, N., Ohno, K., Unno, T., Tanahashi, Y., Jan, T.R., Tsubone, H.*, et al.* (2019). Neural anti-inflammatory action mediated by two types of acetylcholine receptors in the small intestine. Sci Rep *9*, 5887.

Kirchgessner, A.L., and Gershon, M.D. (1990). Innervation of the pancreas by neurons in the gut. J Neurosci *10*, 1626-1642.

Kleij, H.P., and Bienenstock, J. (2005). Significance of Conversation between Mast Cells and Nerves. Allergy Asthma Clin Immunol *1*, 65-80.

Klose, C.S.N., Mahlakoiv, T., Moeller, J.B., Rankin, L.C., Flamar, A.L., Kabata, H., Monticelli, L.A., Moriyama, S., Putzel, G.G., Rakhilin, N.*, et al.* (2017). The neuropeptide

neuromedin U stimulates innate lymphoid cells and type 2 inflammation. Nature *549*, 282-286.

Kockerling, F., Kockerling, D., and Lomas, C. (2013). Cornelius Celsus--ancient encyclopedist, surgeon-scientist, or master of surgery? Langenbecks Arch Surg *398*, 609-616.

Kodani, M., Fukui, H., Tomita, T., Oshima, T., Watari, J., and Miwa, H. (2018). Association between gastrointestinal motility and macrophage/mast cell distribution in mice during the healing stage after DSSinduced colitis. Mol Med Rep *17*, 8167-8172.

Koh, A., De Vadder, F., Kovatcheva-Datchary, P., and Backhed, F. (2016). From Dietary Fiber to Host Physiology: Short-Chain Fatty Acids as Key Bacterial Metabolites. Cell *165*, 1332-1345.

Kong, W., Stanley, S., Gardiner, J., Abbott, C., Murphy, K., Seth, A., Connoley, I., Ghatei, M., Stephens, D., and Bloom, S. (2003). A role for arcuate cocaine and amphetamine-regulated transcript in hyperphagia, thermogenesis, and cold adaptation. FASEB J *17*, 1688-1690.

Koomoa, D.L., Geerts, D., Lange, I., Koster, J., Pegg, A.E., Feith, D.J., and Bachmann, A.S. (2013). DFMO/eflornithine inhibits migration and invasion downstream of MYCN and involves p27Kip1 activity in neuroblastoma. Int J Oncol *42*, 1219-1228.

Korem, T., Zeevi, D., Zmora, N., Weissbrod, O., Bar, N., Lotan-Pompan, M., Avnit-Sagi, T., Kosower, N., Malka, G., Rein, M.*, et al.* (2017). Bread Affects Clinical Parameters and Induces Gut Microbiome-Associated Personal Glycemic Responses. Cell Metab *25*, 1243-1253 e1245.

Koylu, E.O., Couceyro, P.R., Lambert, P.D., and Kuhar, M.J. (1998). Cocaine- and amphetamine-regulated transcript peptide immunohistochemical localization in the rat brain. J Comp Neurol *391*, 115-132.

Koylu, E.O., Couceyro, P.R., Lambert, P.D., Ling, N.C., DeSouza, E.B., and Kuhar, M.J. (1997). Immunohistochemical localization of novel CART peptides in rat hypothalamus, pituitary and adrenal gland. J Neuroendocrinol *9*, 823-833.

Krashes, M.J., Koda, S., Ye, C., Rogan, S.C., Adams, A.C., Cusher, D.S., Maratos-Flier, E., Roth, B.L., and Lowell, B.B. (2011). Rapid, reversible activation of AgRP neurons drives feeding behavior in mice. J Clin Invest *121*, 1424-1428.

Krautkramer, K.A., Fan, J., and Backhed, F. (2021). Gut microbial metabolites as multi-kingdom intermediates. Nat Rev Microbiol *19*, 77-94.

Krisko, T.I., Nicholls, H.T., Bare, C.J., Holman, C.D., Putzel, G.G., Jansen, R.S., Sun, N., Rhee, K.Y., Banks, A.S., and Cohen, D.E. (2020). Dissociation of Adaptive

Thermogenesis from Glucose Homeostasis in Microbiome-Deficient Mice. Cell Metab *31*, 592-604 e599.

Kristensen, P., Judge, M.E., Thim, L., Ribel, U., Christjansen, K.N., Wulff, B.S., Clausen, J.T., Jensen, P.B., Madsen, O.D., Vrang, N.*, et al.* (1998). Hypothalamic CART is a new anorectic peptide regulated by leptin. Nature *393*, 72-76.

Kugler, S., Kilic, E., and Bahr, M. (2003). Human synapsin 1 gene promoter confers highly neuron-specific long-term transgene expression from an adenoviral vector in the adult rat brain depending on the transduced area. Gene Ther *10*, 337-347.

Kuhar, M.J., and Yoho, L.L. (1999). CART peptide analysis by Western blotting. Synapse *33*, 163-171.

Kuhn, R., Lohler, J., Rennick, D., Rajewsky, K., and Muller, W. (1993). Interleukin-10-deficient mice develop chronic enterocolitis. Cell *75*, 263-274.

Kuida, K., Lippke, J.A., Ku, G., Harding, M.W., Livingston, D.J., Su, M.S., and Flavell, R.A. (1995). Altered cytokine export and apoptosis in mice deficient in interleukin-1 beta converting enzyme. Science *267*, 2000-2003.

Kulkarni, S., Micci, M.A., Leser, J., Shin, C., Tang, S.C., Fu, Y.Y., Liu, L., Li, Q., Saha, M., Li, C.*, et al.* (2017). Adult enteric nervous system in health is maintained by a dynamic balance between neuronal apoptosis and neurogenesis. Proc Natl Acad Sci U S A *114*, E3709-E3718.

Kuno, T., Hirayama-Kurogi, M., Ito, S., and Ohtsuki, S. (2018). Reduction in hepatic secondary bile acids caused by short-term antibiotic-induced dysbiosis decreases mouse serum glucose and triglyceride levels. Sci Rep *8*, 1253.

Kuntz, A. (1938). The structural organization of the celiac ganglia. Journal of Comparative Neurology *69*, 1-12.

Kuo, H.S., Tsai, M.J., Huang, M.C., Chiu, C.W., Tsai, C.Y., Lee, M.J., Huang, W.C., Lin, Y.L., Kuo, W.C., and Cheng, H. (2011). Acid fibroblast growth factor and peripheral nerve grafts regulate Th2 cytokine expression, macrophage activation, polyamine synthesis, and neurotrophin expression in transected rat spinal cords. J Neurosci *31*, 4137-4147.

Kvetnansky, R., Sabban, E.L., and Palkovits, M. (2009). Catecholaminergic systems in stress: structural and molecular genetic approaches. Physiol Rev *89*, 535-606.

Lai, N.Y., Musser, M.A., Pinho-Ribeiro, F.A., Baral, P., Jacobson, A., Ma, P., Potts, D.E., Chen, Z., Paik, D., Soualhi, S.*, et al.* (2020). Gut-Innervating Nociceptor Neurons Regulate Peyer's Patch Microfold Cells and SFB Levels to Mediate Salmonella Host Defense. Cell *180*, 33-49 e22.

Lakhina, V., Arey, R.N., Kaletsky, R., Kauffman, A., Stein, G., Keyes, W., Xu, D., and Murphy, C.T. (2015). Genome-wide functional analysis of CREB/long-term memory-dependent transcription reveals distinct basal and memory gene expression programs. Neuron *85*, 330-345.

Lambert, P.D., Couceyro, P.R., McGirr, K.M., Dall Vechia, S.E., Smith, Y., and Kuhar, M.J. (1998). CART peptides in the central control of feeding and interactions with neuropeptide Y. Synapse *29*, 293-298.

Laranjeira, C., Sandgren, K., Kessaris, N., Richardson, W., Potocnik, A., Vanden Berghe, P., and Pachnis, V. (2011). Glial cells in the mouse enteric nervous system can undergo neurogenesis in response to injury. J Clin Invest *121*, 3412-3424.

Lasrado, R., Boesmans, W., Kleinjung, J., Pin, C., Bell, D., Bhaw, L., McCallum, S., Zong, H., Luo, L., Clevers, H.*, et al.* (2017). Lineage-dependent spatial and functional organization of the mammalian enteric nervous system. Science *356*, 722-726.

Latour, Y.L., Gobert, A.P., and Wilson, K.T. (2020). The role of polyamines in the regulation of macrophage polarization and function. Amino Acids *52*, 151-160.

Lau, J., and Herzog, H. (2014). CART in the regulation of appetite and energy homeostasis. Front Neurosci *8*, 313.

Lavin, Y., Mortha, A., Rahman, A., and Merad, M. (2015). Regulation of macrophage development and function in peripheral tissues. Nat Rev Immunol *15*, 731-744.

Lay, J., Carbone, S.E., DiCello, J.J., Bunnett, N.W., Canals, M., and Poole, D.P. (2016). Distribution and trafficking of the mu-opioid receptor in enteric neurons of the guinea pig. Am J Physiol Gastrointest Liver Physiol *311*, G252-266.

Lebrun, L.J., Lenaerts, K., Kiers, D., Pais de Barros, J.P., Le Guern, N., Plesnik, J., Thomas, C., Bourgeois, T., Dejong, C.H.C., Kox, M.*, et al.* (2017). Enteroendocrine L Cells Sense LPS after Gut Barrier Injury to Enhance GLP-1 Secretion. Cell Rep *21*, 1160-1168.

Lecci, A., Altamura, M., Capriati, A., and Maggi, C.A. (2008). Tachykinin receptors and gastrointestinal motility: focus on humans. Eur Rev Med Pharmacol Sci *12 Suppl 1*, 69-80.

Lemire, P., Robertson, S.J., Maughan, H., Tattoli, I., Streutker, C.J., Platnich, J.M., Muruve, D.A., Philpott, D.J., and Girardin, S.E. (2017). The NLR Protein NLRP6 Does Not Impact Gut Microbiota Composition. Cell Rep *21*, 3653-3661.

Leung, P.S. (2010). Overview of the pancreas. Adv Exp Med Biol *690*, 3-12.

Levy, M., Shapiro, H., Thaiss, C.A., and Elinav, E. (2017). NLRP6: A Multifaceted Innate Immune Sensor. Trends Immunol *38*, 248-260.

Levy, M., Thaiss, C.A., Zeevi, D., Dohnalova, L., Zilberman-Schapira, G., Mahdi, J.A., David, E., Savidor, A., Korem, T., Herzig, Y.*, et al.* (2015). Microbiota-Modulated Metabolites Shape the Intestinal Microenvironment by Regulating NLRP6 Inflammasome Signaling. Cell *163*, 1428-1443.

Li, C., Wu, X., Liu, S., Zhao, Y., Zhu, J., and Liu, K. (2019). Roles of Neuropeptide Y in Neurodegenerative and Neuroimmune Diseases. Front Neurosci *13*, 869.

Li, J., Meng, Y., Wu, X., and Sun, Y. (2020). Polyamines and related signaling pathways in cancer. Cancer Cell Int *20*, 539.

Lilla, J.N., Chen, C.C., Mukai, K., BenBarak, M.J., Franco, C.B., Kalesnikoff, J., Yu, M., Tsai, M., Piliponsky, A.M., and Galli, S.J. (2011). Reduced mast cell and basophil numbers and function in Cpa3-Cre; Mcl-1fl/fl mice. Blood *118*, 6930-6938.

Lin, E.E., Scott-Solomon, E., and Kuruvilla, R. (2021). Peripheral Innervation in the Regulation of Glucose Homeostasis. Trends Neurosci *44*, 189-202.

Liu, M.T., Kuan, Y.H., Wang, J., Hen, R., and Gershon, M.D. (2009). 5-HT4 receptor-mediated neuroprotection and neurogenesis in the enteric nervous system of adult mice. J Neurosci *29*, 9683-9699.

Liu, M.T., Rothstein, J.D., Gershon, M.D., and Kirchgessner, A.L. (1997). Glutamatergic enteric neurons. J Neurosci *17*, 4764-4784.

Longman, R.S., Diehl, G.E., Victorio, D.A., Huh, J.R., Galan, C., Miraldi, E.R., Swaminath, A., Bonneau, R., Scherl, E.J., and Littman, D.R. (2014). CX(3)CR1(+) mononuclear phagocytes support colitis-associated innate lymphoid cell production of IL-22. J Exp Med *211*, 1571-1583.

Love, J.A., Yi, E., and Smith, T.G. (2007). Autonomic pathways regulating pancreatic exocrine secretion. Auton Neurosci *133*, 19-34.

Love, M.I., Huber, W., and Anders, S. (2014). Moderated estimation of fold change and dispersion for RNA-seq data with DESeq2. Genome Biol *15*, 550.

Lu, V.B., Gribble, F.M., and Reimann, F. (2018). Free Fatty Acid Receptors in Enteroendocrine Cells. Endocrinology *159*, 2826-2835.

Lu, V.B., Rievaj, J., O'Flaherty, E.A., Smith, C.A., Pais, R., Pattison, L.A., Tolhurst, G., Leiter, A.B., Bulmer, D.C., Gribble, F.M.*, et al.* (2019). Adenosine triphosphate is co-secreted with glucagon-like peptide-1 to modulate intestinal enterocytes and afferent neurons. Nat Commun *10*, 1029.

Lundberg, J.M., Franco-Cereceda, A., Hemsen, A., Lacroix, J.S., and Pernow, J. (1990). Pharmacology of noradrenaline and neuropeptide tyrosine (NPY)-mediated sympathetic cotransmission. Fundam Clin Pharmacol *4*, 373-391.

Luo, J., Qian, A., Oetjen, L.K., Yu, W., Yang, P., Feng, J., Xie, Z., Liu, S., Yin, S., Dryn, D.*, et al.* (2018). TRPV4 Channel Signaling in Macrophages Promotes Gastrointestinal Motility via Direct Effects on Smooth Muscle Cells. Immunity *49*, 107-119 e104.

Luquet, S., Perez, F.A., Hnasko, T.S., and Palmiter, R.D. (2005). NPY/AgRP neurons are essential for feeding in adult mice but can be ablated in neonates. Science *310*, 683-685.

Ma, N.X., Yin, J.C., and Chen, G. (2019). Transcriptome Analysis of Small Molecule-Mediated Astrocyte-to-Neuron Reprogramming. Front Cell Dev Biol *7*, 82.

Mace, O.J., Tehan, B., and Marshall, F. (2015). Pharmacology and physiology of gastrointestinal enteroendocrine cells. Pharmacol Res Perspect *3*, e00155.

Maizels, R.M. (2020). Regulation of immunity and allergy by helminth parasites. Allergy *75*, 524-534.

Maizels, R.M., Smits, H.H., and McSorley, H.J. (2018). Modulation of Host Immunity by Helminths: The Expanding Repertoire of Parasite Effector Molecules. Immunity *49*, 801-818.

Maletinska, L., Maixnerova, J., Matyskova, R., Haugvicova, R., Sloncova, E., Elbert, T., Slaninova, J., and Zelezna, B. (2007). Cocaine- and amphetamine-regulated transcript (CART) peptide specific binding in pheochromocytoma cells PC12. Eur J Pharmacol *559*, 109-114.

Mamantopoulos, M., Ronchi, F., Van Hauwermeiren, F., Vieira-Silva, S., Yilmaz, B., Martens, L., Saeys, Y., Drexler, S.K., Yazdi, A.S., Raes, J.*, et al.* (2017). Nlrp6- and ASC-Dependent Inflammasomes Do Not Shape the Commensal Gut Microbiota Composition. Immunity *47*, 339-348 e334.

Man, A.L., Gicheva, N., Regoli, M., Rowley, G., De Cunto, G., Wellner, N., Bassity, E., Gulisano, M., Bertelli, E., and Nicoletti, C. (2017). CX3CR1+ Cell-Mediated Salmonella Exclusion Protects the Intestinal Mucosa during the Initial Stage of Infection. J Immunol *198*, 335-343.

Martin, A.M., Yabut, J.M., Choo, J.M., Page, A.J., Sun, E.W., Jessup, C.F., Wesselingh, S.L., Khan, W.I., Rogers, G.B., Steinberg, G.R.*, et al.* (2019). The gut microbiome regulates host glucose homeostasis via peripheral serotonin. Proc Natl Acad Sci U S A *116*, 19802-19804.

Martinez-Guryn, K., Leone, V., and Chang, E.B. (2019). Regional Diversity of the Gastrointestinal Microbiome. Cell Host Microbe *26*, 314-324.

Martinon, F., Burns, K., and Tschopp, J. (2002). The inflammasome: a molecular platform triggering activation of inflammatory caspases and processing of proIL-beta. Mol Cell *10*, 417-426.

Martins, R., Carlos, A.R., Braza, F., Thompson, J.A., Bastos-Amador, P., Ramos, S., and Soares, M.P. (2019). Disease Tolerance as an Inherent Component of Immunity. Annual review of immunology *37*, 405-437.

Maruyama, K., Takayama, Y., Sugisawa, E., Yamanoi, Y., Yokawa, T., Kondo, T., Ishibashi, K.I., Sahoo, B.R., Takemura, N., Mori, Y.*, et al.* (2018). The ATP Transporter VNUT Mediates Induction of Dectin-1-Triggered Candida Nociception. iScience *6*, 306-318.

Mawe, G.M. (2015). Colitis-induced neuroplasticity disrupts motility in the inflamed and post-inflamed colon. J Clin Invest *125*, 949-955.

Mawe, G.M., and Hoffman, J.M. (2013). Serotonin signalling in the gut--functions, dysfunctions and therapeutic targets. Nat Rev Gastroenterol Hepatol *10*, 473-486.

Mayer, E.A. (2011). Gut feelings: the emerging biology of gut-brain communication. Nat Rev Neurosci *12*, 453-466.

Mayer, E.A., Tillisch, K., and Gupta, A. (2015). Gut/brain axis and the microbiota. J Clin Invest *125*, 926-938.

McGinty, J.W., Ting, H.A., Billipp, T.E., Nadjsombati, M.S., Khan, D.M., Barrett, N.A., Liang, H.E., Matsumoto, I., and von Moltke, J. (2020). Tuft-Cell-Derived Leukotrienes Drive Rapid Anti-helminth Immunity in the Small Intestine but Are Dispensable for Anti-protist Immunity. Immunity *52*, 528-541 e527.

McKenzie, B.A., Dixit, V.M., and Power, C. (2020). Fiery Cell Death: Pyroptosis in the Central Nervous System. Trends Neurosci *43*, 55-73.

McVey Neufeld, K.A., Mao, Y.K., Bienenstock, J., Foster, J.A., and Kunze, W.A. (2013). The microbiome is essential for normal gut intrinsic primary afferent neuron excitability in the mouse. Neurogastroenterol Motil *25*, 183-e188.

McVey Neufeld, K.A., Perez-Burgos, A., Mao, Y.K., Bienenstock, J., and Kunze, W.A. (2015). The gut microbiome restores intrinsic and extrinsic nerve function in germ-free mice accompanied by changes in calbindin. Neurogastroenterol Motil *27*, 627-636.

Medzhitov, R., Schneider, D.S., and Soares, M.P. (2012). Disease tolerance as a defense strategy. Science *335*, 936-941.

Mei, Q., Mundinger, T.O., Kung, D., Baskin, D.G., and Taborsky, G.J., Jr. (2001). Fos expression in rat celiac ganglion: an index of the activation of postganglionic sympathetic nerves. Am J Physiol Endocrinol Metab *281*, E655-664.

Meng, C., Zhang, J., Zhang, L., Wang, Y., Li, Z., and Zhao, J. (2019). Effects of NLRP6 in Cerebral Ischemia/Reperfusion (I/R) Injury in Rats. J Mol Neurosci *69*, 411-418.

Meresse, B., Curran, S.A., Ciszewski, C., Orbelyan, G., Setty, M., Bhagat, G., Lee, L., Tretiakova, M., Semrad, C., Kistner, E.*, et al.* (2006). Reprogramming of CTLs into natural killer-like cells in celiac disease. J Exp Med *203*, 1343-1355.

Messenger, J.P., and Furness, J.B. (1992). Distribution of enteric nerve cells that project to the coeliac ganglion of the guinea-pig. Cell Tissue Res *269*, 119-132.

Metchnikoff, E. (1901). Dr. Metchnikoff on Microbes and the Human Body. Nature *63*, 621-622.

Mikkelsen, H.B., Thuneberg, L., Rumessen, J.J., and Thorball, N. (1985). Macrophage-like cells in the muscularis externa of mouse small intestine. Anat Rec *213*, 77-86.

Milstein, A.D., Bloss, E.B., Apostolides, P.F., Vaidya, S.P., Dilly, G.A., Zemelman, B.V., and Magee, J.C. (2015). Inhibitory Gating of Input Comparison in the CA1 Microcircuit. Neuron *87*, 1274-1289.

Mizuno, K., and Ueno, Y. (2017). Autonomic Nervous System and the Liver. Hepatol Res *47*, 160-165.

Moriyama, S., Brestoff, J.R., Flamar, A.L., Moeller, J.B., Klose, C.S.N., Rankin, L.C., Yudanin, N.A., Monticelli, L.A., Putzel, G.G., Rodewald, H.R.*, et al.* (2018). beta2-adrenergic receptor-mediated negative regulation of group 2 innate lymphoid cell responses. Science *359*, 1056-1061.

Mowat, A.M., and Agace, W.W. (2014). Regional specialization within the intestinal immune system. Nat Rev Immunol *14*, 667-685.

Mulder, W.J.M., Ochando, J., Joosten, L.A.B., Fayad, Z.A., and Netea, M.G. (2019). Therapeutic targeting of trained immunity. Nat Rev Drug Discov *18*, 553-566.

Muller, P.A., Koscso, B., Rajani, G.M., Stevanovic, K., Berres, M.L., Hashimoto, D., Mortha, A., Leboeuf, M., Li, X.M., Mucida, D.*, et al.* (2014). Crosstalk between muscularis macrophages and enteric neurons regulates gastrointestinal motility. Cell *158*, 300-313.

Muller, P.A., Matheis, F., Schneeberger, M., Kerner, Z., Jove, V., and Mucida, D. (2020a). Microbiota-modulated CART(+) enteric neurons autonomously regulate blood glucose. Science *370*, 314-321.

Muller, P.A., Schneeberger, M., Matheis, F., Wang, P., Kerner, Z., Ilanges, A., Pellegrino, K., Del Marmol, J., Castro, T.B.R., Furuichi, M.*, et al.* (2020b). Microbiota modulate sympathetic neurons via a gut-brain circuit. Nature *583*, 441-446.

Murphy, K.G., Abbott, C.R., Mahmoudi, M., Hunter, R., Gardiner, J.V., Rossi, M., Stanley, S.A., Ghatei, M.A., Kuhar, M.J., and Bloom, S.R. (2000). Quantification and synthesis of cocaine- and amphetamine-regulated transcript peptide (79-102)-like immunoreactivity and mRNA in rat tissues. J Endocrinol *166*, 659-668.

Nagashima, H., Mahlakoiv, T., Shih, H.Y., Davis, F.P., Meylan, F., Huang, Y., Harrison, O.J., Yao, C., Mikami, Y., Urban, J.F., Jr.*, et al.* (2019). Neuropeptide CGRP Limits Group 2 Innate Lymphoid Cell Responses and Constrains Type 2 Inflammation. Immunity *51*, 682-695 e686.

Netea, M.G., Dominguez-Andres, J., Barreiro, L.B., Chavakis, T., Divangahi, M., Fuchs, E., Joosten, L.A.B., van der Meer, J.W.M., Mhlanga, M.M., Mulder, W.J.M.*, et al.* (2020). Defining trained immunity and its role in health and disease. Nat Rev Immunol *20*, 375-388.

Netea, M.G., Joosten, L.A., Latz, E., Mills, K.H., Natoli, G., Stunnenberg, H.G., O'Neill, L.A., and Xavier, R.J. (2016). Trained immunity: A program of innate immune memory in health and disease. Science *352*, aaf1098.

Netea, M.G., Quintin, J., and van der Meer, J.W. (2011). Trained immunity: a memory for innate host defense. Cell Host Microbe *9*, 355-361.

Neuhuber, W.L., Appelt, M., Polak, J.M., Baier-Kustermann, W., Abelli, L., and Ferri, G.L. (1993). Rectospinal neurons: cell bodies, pathways, immunocytochemistry and ultrastructure. Neuroscience *56*, 367-378.

Newman, K.D., Mhalhal, T.R., Washington, M.C., Heath, J.C., and Sayegh, A.I. (2017). Peptide Tyrosine Tyrosine 3-36 Reduces Meal Size and Activates the Enteric Neurons in Male Sprague-Dawley Rats. Dig Dis Sci *62*, 3350-3358.

Niesler, B., Kuerten, S., Demir, I.E., and Schafer, K.H. (2021). Disorders of the enteric nervous system - a holistic view. Nat Rev Gastroenterol Hepatol.

Niess, J.H., Brand, S., Gu, X., Landsman, L., Jung, S., McCormick, B.A., Vyas, J.M., Boes, M., Ploegh, H.L., Fox, J.G.*, et al.* (2005). CX3CR1-mediated dendritic cell access to the intestinal lumen and bacterial clearance. Science *307*, 254-258.

Nijhuis, L.E., Olivier, B.J., and de Jonge, W.J. (2010). Neurogenic regulation of dendritic cells in the intestine. Biochem Pharmacol *80*, 2002-2008.

Nohr, M.K., Egerod, K.L., Christiansen, S.H., Gille, A., Offermanns, S., Schwartz, T.W., and Moller, M. (2015). Expression of the short chain fatty acid receptor GPR41/FFAR3 in autonomic and somatic sensory ganglia. Neuroscience *290*, 126-137.

Nowarski, R., Jackson, R., Gagliani, N., de Zoete, M.R., Palm, N.W., Bailis, W., Low, J.S., Harman, C.C., Graham, M., Elinav, E.*, et al.* (2015). Epithelial IL-18 Equilibrium Controls Barrier Function in Colitis. Cell *163*, 1444-1456.

O'Leary, C.E., Schneider, C., and Locksley, R.M. (2019). Tuft Cells-Systemically Dispersed Sensory Epithelia Integrating Immune and Neural Circuitry. Annu Rev Immunol *37*, 47-72.

Obata, Y., Castano, A., Boeing, S., Bon-Frauches, A.C., Fung, C., Fallesen, T., de Aguero, M.G., Yilmaz, B., Lopes, R., Huseynova, A.*, et al.* (2020). Neuronal programming by microbiota regulates intestinal physiology. Nature *578*, 284-289.

Obata, Y., and Pachnis, V. (2016). The Effect of Microbiota and the Immune System on the Development and Organization of the Enteric Nervous System. Gastroenterology *151*, 836-844.

Obermayr, F., Hotta, R., Enomoto, H., and Young, H.M. (2013). Development and developmental disorders of the enteric nervous system. Nat Rev Gastroenterol Hepatol *10*, 43-57.

Ohman, L., and Simren, M. (2010). Pathogenesis of IBS: role of inflammation, immunity and neuroimmune interactions. Nat Rev Gastroenterol Hepatol *7*, 163-173.

Ollmann, M.M., Wilson, B.D., Yang, Y.K., Kerns, J.A., Chen, Y., Gantz, I., and Barsh, G.S. (1997). Antagonism of central melanocortin receptors in vitro and in vivo by agouti-related protein. Science *278*, 135-138.

Palay, S.L., and Karlin, L.J. (1959). An electron microscopic study of the intestinal villus. I. The fasting animal. J Biophys Biochem Cytol *5*, 363-372.

Pavlov, V.A., Chavan, S.S., and Tracey, K.J. (2018). Molecular and Functional Neuroscience in Immunity. Annu Rev Immunol *36*, 783-812.

Peterson, L.W., and Artis, D. (2014). Intestinal epithelial cells: regulators of barrier function and immune homeostasis. Nat Rev Immunol *14*, 141-153.

Pham, T.D., Gershon, M.D., and Rothman, T.P. (1991). Time of origin of neurons in the murine enteric nervous system: sequence in relation to phenotype. J Comp Neurol *314*, 789-798.

Phillips, R.J., and Powley, T.L. (2012). Macrophages associated with the intrinsic and extrinsic autonomic innervation of the rat gastrointestinal tract. Auton Neurosci *169*, 12-27.

Pohl, J.M., Gutweiler, S., Thiebes, S., Volke, J.K., Klein-Hitpass, L., Zwanziger, D., Gunzer, M., Jung, S., Agace, W.W., Kurts, C*., et al.* (2017). Irf4-dependent CD103(+)CD11b(+) dendritic cells and the intestinal microbiome regulate monocyte and macrophage activation and intestinal peristalsis in postoperative ileus. Gut *66*, 2110-2120.

Poole, D.P., Godfrey, C., Cattaruzza, F., Cottrell, G.S., Kirkland, J.G., Pelayo, J.C., Bunnett, N.W., and Corvera, C.U. (2010). Expression and function of the bile acid receptor GpBAR1 (TGR5) in the murine enteric nervous system. Neurogastroenterol Motil *22*, 814-825, e227-818.

Portbury, A.L., Pompolo, S., Furness, J.B., Stebbing, M.J., Kunze, W.A., Bornstein, J.C., and Hughes, S. (1995). Cholinergic, somatostatin-immunoreactive interneurons in the guinea pig intestine: morphology, ultrastructure, connections and projections. J Anat *187 ( Pt 2)*, 303-321.

Pruss, H., Tedeschi, A., Thiriot, A., Lynch, L., Loughhead, S.M., Stutte, S., Mazo, I.B., Kopp, M.A., Brommer, B., Blex, C*., et al.* (2017). Spinal cord injury-induced immunodeficiency is mediated by a sympathetic-neuroendocrine adrenal reflex. Nat Neurosci *20*, 1549-1559.

Qin, J., Li, Y., Cai, Z., Li, S., Zhu, J., Zhang, F., Liang, S., Zhang, W., Guan, Y., Shen, D*., et al.* (2012). A metagenome-wide association study of gut microbiota in type 2 diabetes. Nature *490*, 55-60.

Quinson, N., Robbins, H.L., Clark, M.J., and Furness, J.B. (2001). Calbindin immunoreactivity of enteric neurons in the guinea-pig ileum. Cell Tissue Res *305*, 3-9.

Ran, W.Z., Dong, L., Tang, C.Y., Zhou, Y., Sun, G.Y., Liu, T., Liu, Y.P., and Guan, C.X. (2015). Vasoactive intestinal peptide suppresses macrophage-mediated inflammation by downregulating interleukin-17A expression via PKA- and PKC-dependent pathways. Int J Exp Pathol *96*, 269-275.

Rankin, L.C., and Artis, D. (2018). Beyond Host Defense: Emerging Functions of the Immune System in Regulating Complex Tissue Physiology. Cell *173*, 554-567.

Rao, M., and Gershon, M.D. (2016). The bowel and beyond: the enteric nervous system in neurological disorders. Nat Rev Gastroenterol Hepatol *13*, 517-528.

Rao, M., Nelms, B.D., Dong, L., Salinas-Rios, V., Rutlin, M., Gershon, M.D., and Corfas, G. (2015). Enteric glia express proteolipid protein 1 and are a transcriptionally unique population of glia in the mammalian nervous system. Glia *63*, 2040-2057.

Rao, M., Rastelli, D., Dong, L., Chiu, S., Setlik, W., Gershon, M.D., and Corfas, G. (2017). Enteric Glia Regulate Gastrointestinal Motility but Are Not Required for Maintenance of the Epithelium in Mice. Gastroenterology *153*, 1068-1081 e1067.

Rathinam, V.A., and Fitzgerald, K.A. (2016). Inflammasome Complexes: Emerging Mechanisms and Effector Functions. Cell *165*, 792-800.

Rathinam, V.A., Vanaja, S.K., Waggoner, L., Sokolovska, A., Becker, C., Stuart, L.M., Leong, J.M., and Fitzgerald, K.A. (2012). TRIF licenses caspase-11-dependent NLRP3 inflammasome activation by gram-negative bacteria. Cell *150*, 606-619.

Ridaura, V.K., Faith, J.J., Rey, F.E., Cheng, J., Duncan, A.E., Kau, A.L., Griffin, N.W., Lombard, V., Henrissat, B., Bain, J.R.*, et al.* (2013). Gut microbiota from twins discordant for obesity modulate metabolism in mice. Science *341*, 1241214.

Ridlon, J.M., Kang, D.J., Hylemon, P.B., and Bajaj, J.S. (2014). Bile acids and the gut microbiome. Curr Opin Gastroenterol *30*, 332-338.

Rivera-Chavez, F., Zhang, L.F., Faber, F., Lopez, C.A., Byndloss, M.X., Olsan, E.E., Xu, G., Velazquez, E.M., Lebrilla, C.B., Winter, S.E.*, et al.* (2016). Depletion of Butyrate-Producing Clostridia from the Gut Microbiota Drives an Aerobic Luminal Expansion of Salmonella. Cell Host Microbe *19*, 443-454.

Roder, P.V., Wu, B., Liu, Y., and Han, W. (2016). Pancreatic regulation of glucose homeostasis. Exp Mol Med *48*, e219.

Rogers, R.C., McTigue, D.M., and Hermann, G.E. (1995). Vagovagal reflex control of digestion: afferent modulation by neural and "endoneurocrine" factors. Am J Physiol *268*, G1-10.

Rogge, G., Jones, D., Hubert, G.W., Lin, Y., and Kuhar, M.J. (2008). CART peptides: regulators of body weight, reward and other functions. Nat Rev Neurosci *9*, 747-758.

Roider, H.G., Manke, T., O'Keeffe, S., Vingron, M., and Haas, S.A. (2009). PASTAA: identifying transcription factors associated with sets of co-regulated genes. Bioinformatics *25*, 435-442.

Rorsman, P., and Huising, M.O. (2018). The somatostatin-secreting pancreatic delta-cell in health and disease. Nat Rev Endocrinol *14*, 404-414.

Rosas-Ballina, M., Ochani, M., Parrish, W.R., Ochani, K., Harris, Y.T., Huston, J.M., Chavan, S., and Tracey, K.J. (2008). Splenic nerve is required for cholinergic antiinflammatory pathway control of TNF in endotoxemia. Proc Natl Acad Sci U S A *105*, 11008-11013.

Rosas-Ballina, M., Olofsson, P.S., Ochani, M., Valdes-Ferrer, S.I., Levine, Y.A., Reardon, C., Tusche, M.W., Pavlov, V.A., Andersson, U., Chavan, S.*, et al.* (2011). Acetylcholine-synthesizing T cells relay neural signals in a vagus nerve circuit. Science *334*, 98-101.

Rumessen, J.J., Thuneberg, L., and Mikkelsen, H.B. (1982). Plexus muscularis profundus and associated interstitial cells. II. Ultrastructural studies of mouse small intestine. Anat Rec *203*, 129-146.

Sang, Q., and Young, H.M. (1996). Chemical coding of neurons in the myenteric plexus and external muscle of the small and large intestine of the mouse. Cell Tissue Res *284*, 39-53.

Sanz, E., Yang, L., Su, T., Morris, D.R., McKnight, G.S., and Amieux, P.S. (2009). Cell-type-specific isolation of ribosome-associated mRNA from complex tissues. Proc Natl Acad Sci U S A *106*, 13939-13944.

Sayin, S.I., Wahlstrom, A., Felin, J., Jantti, S., Marschall, H.U., Bamberg, K., Angelin, B., Hyotylainen, T., Oresic, M., and Backhed, F. (2013). Gut microbiota regulates bile acid metabolism by reducing the levels of tauro-beta-muricholic acid, a naturally occurring FXR antagonist. Cell Metab *17*, 225-235.

Schaedler, R.W., Dubs, R., and Costello, R. (1965). Association of Germfree Mice with Bacteria Isolated from Normal Mice. J Exp Med *122*, 77-82.

Schiller, M., Ben-Shaanan, T.L., and Rolls, A. (2021). Neuronal regulation of immunity: why, how and where? Nat Rev Immunol *21*, 20-36.

Schmidt, R.E., Dorsey, D.A., Beaudet, L.N., Frederick, K.E., Parvin, C.A., Plurad, S.B., and Levisetti, M.G. (2003). Non-obese diabetic mice rapidly develop dramatic sympathetic neuritic dystrophy: a new experimental model of diabetic autonomic neuropathy. Am J Pathol *163*, 2077-2091.

Schridde, A., Bain, C.C., Mayer, J.U., Montgomery, J., Pollet, E., Denecke, B., Milling, S.W.F., Jenkins, S.J., Dalod, M., Henri, S.*, et al.* (2017). Tissue-specific differentiation of colonic macrophages requires TGFbeta receptor-mediated signaling. Mucosal Immunol *10*, 1387-1399.

Schulthess, J., Pandey, S., Capitani, M., Rue-Albrecht, K.C., Arnold, I., Franchini, F., Chomka, A., Ilott, N.E., Johnston, D.G.W., Pires, E.*, et al.* (2019). The Short Chain Fatty Acid Butyrate Imprints an Antimicrobial Program in Macrophages. Immunity *50*, 432-445 e437.

Sehgal, A., Donaldson, D.S., Pridans, C., Sauter, K.A., Hume, D.A., and Mabbott, N.A. (2018). The role of CSF1R-dependent macrophages in control of the intestinal stem-cell niche. Nat Commun *9*, 1272.

Selwyn, F.P., Csanaky, I.L., Zhang, Y., and Klaassen, C.D. (2015). Importance of Large Intestine in Regulating Bile Acids and Glucagon-Like Peptide-1 in Germ-Free Mice. Drug Metab Dispos *43*, 1544-1556.

Sender, R., Fuchs, S., and Milo, R. (2016). Revised Estimates for the Number of Human and Bacteria Cells in the Body. PLoS Biol *14*, e1002533.

Seregin, S.S., Golovchenko, N., Schaf, B., Chen, J., Eaton, K.A., and Chen, G.Y. (2017). NLRP6 function in inflammatory monocytes reduces susceptibility to chemically induced intestinal injury. Mucosal Immunol *10*, 434-445.

Sergeyev, V., Broberger, C., and Hokfelt, T. (2001). Effect of LPS administration on the expression of POMC, NPY, galanin, CART and MCH mRNAs in the rat hypothalamus. Brain Res Mol Brain Res *90*, 93-100.

Sharkey, K.A., Lomax, A.E., Bertrand, P.P., and Furness, J.B. (1998). Electrophysiology, shape, and chemistry of neurons that project from guinea pig colon to inferior mesenteric ganglia. Gastroenterology *115*, 909-918.

Shaw, T.N., Houston, S.A., Wemyss, K., Bridgeman, H.M., Barbera, T.A., Zangerle-Murray, T., Strangward, P., Ridley, A.J.L., Wang, P., Tamoutounour, S.*, et al.* (2018). Tissue-resident macrophages in the intestine are long lived and defined by Tim-4 and CD4 expression. J Exp Med *215*, 1507-1518.

Shcherbina, L., Edlund, A., Esguerra, J.L., Abels, M., Zhou, Y., Ottosson-Laakso, E., Wollheim, C.B., Hansson, O., Eliasson, L., and Wierup, N. (2017). Endogenous beta-cell CART regulates insulin secretion and transcription of beta-cell genes. Mol Cell Endocrinol *447*, 52-60.

Shechter, R., London, A., Varol, C., Raposo, C., Cusimano, M., Yovel, G., Rolls, A., Mack, M., Pluchino, S., Martino, G.*, et al.* (2009). Infiltrating blood-derived macrophages are vital cells playing an anti-inflammatory role in recovery from spinal cord injury in mice. PLoS Med *6*, e1000113.

Shen, L. (2009). Functional morphology of the gastrointestinal tract. Curr Top Microbiol Immunol *337*, 1-35.

Shutter, J.R., Graham, M., Kinsey, A.C., Scully, S., Luthy, R., and Stark, K.L. (1997). Hypothalamic expression of ART, a novel gene related to agouti, is up-regulated in obese and diabetic mutant mice. Genes Dev *11*, 593-602.

Silva, H.M., Kitoko, J.Z., Queiroz, C.P., Kroehling, L., Matheis, F., Yang, K.L., Ren-Fielding, C., Littman, D.R., Bozza, M.T., Mucida, D.*, et al.* (2021). c-MAF dependent perivascular macrophages regulate diet induced metabolic syndrome. bioRxiv, 2021.2002.2007.430147.

Silveira, M.R., Nunes, K.P., Cara, D.C., Souza, D.G., Correa, A., Jr., Teixeira, M.M., and Negrao-Correa, D. (2002). Infection with Strongyloides venezuelensis induces transient airway eosinophilic inflammation, an increase in immunoglobulin E, and hyperresponsiveness in rats. Infection and immunity *70*, 6263-6272.

Sjogren, K., Engdahl, C., Henning, P., Lerner, U.H., Tremaroli, V., Lagerquist, M.K., Backhed, F., and Ohlsson, C. (2012). The gut microbiota regulates bone mass in mice. J Bone Miner Res *27*, 1357-1367.

Skatchkov, S.N., Bukauskas, F.F., Benedikt, J., Inyushin, M., and Kucheryavykh, Y.V. (2015). Intracellular spermine prevents acid-induced uncoupling of Cx43 gap junction channels. Neuroreport *26*, 528-532.

Smith, B.N., Banfield, B.W., Smeraski, C.A., Wilcox, C.L., Dudek, F.E., Enquist, L.W., and Pickard, G.E. (2000). Pseudorabies virus expressing enhanced green fluorescent protein: A tool for in vitro electrophysiological analysis of transsynaptically labeled neurons in identified central nervous system circuits. Proceedings of the National Academy of Sciences of the United States of America *97*, 9264-9269.

Smith, S.M., and Vale, W.W. (2006). The role of the hypothalamic-pituitary-adrenal axis in neuroendocrine responses to stress. Dialogues Clin Neurosci *8*, 383-395.

Song, W.M., and Colonna, M. (2018). The Microglial Response to Neurodegenerative Disease. Adv Immunol *139*, 1-50.

Sonnenburg, J.L., and Bäckhed, F. (2016). Diet-microbiota interactions as moderators of human metabolism. Nature *535*, 56-64.

Sonoyama, K., Rutatip, S., and Kasai, T. (2000). Gene expression of activin, activin receptors, and follistatin in intestinal epithelial cells. Am J Physiol Gastrointest Liver Physiol *278*, G89-97.

Sousa-Valente, J., and Brain, S.D. (2018). A historical perspective on the role of sensory nerves in neurogenic inflammation. Semin Immunopathol *40*, 229-236.

Stacy, A., Andrade-Oliveira, V., McCulloch, J.A., Hild, B., Oh, J.H., Perez-Chaparro, P.J., Sim, C.K., Lim, A.I., Link, V.M., Enamorado, M.*, et al.* (2021). Infection trains the host for microbiota-enhanced resistance to pathogens. Cell *184*, 615-627 e617.

Stead, R.H., Dixon, M.F., Bramwell, N.H., Riddell, R.H., and Bienenstock, J. (1989). Mast cells are closely apposed to nerves in the human gastrointestinal mucosa. Gastroenterology *97*, 575-585.

Stead, R.H., Tomioka, M., Quinonez, G., Simon, G.T., Felten, S.Y., and Bienenstock, J. (1987). Intestinal mucosal mast cells in normal and nematode-infected rat intestines are in intimate contact with peptidergic nerves. Proc Natl Acad Sci U S A *84*, 2975-2979.

Stein, J., Steiner, D.F., and Dey, A. (2006). Processing of cocaine- and amphetamine-regulated transcript (CART) precursor proteins by prohormone convertases (PCs) and its implications. Peptides *27*, 1919-1925.

Steinert, R.E., and Beglinger, C. (2011). Nutrient sensing in the gut: interactions between chemosensory cells, visceral afferents and the secretion of satiation peptides. Physiol Behav *105*, 62-70.

Sternberg, E.M. (2006). Neural regulation of innate immunity: a coordinated nonspecific host response to pathogens. Nat Rev Immunol *6*, 318-328.

Studer, N., Desharnais, L., Beutler, M., Brugiroux, S., Terrazos, M.A., Menin, L., Schurch, C.M., McCoy, K.D., Kuehne, S.A., Minton, N.P.*, et al.* (2016). Functional Intestinal Bile Acid 7alpha-Dehydroxylation by Clostridium scindens Associated with Protection from Clostridium difficile Infection in a Gnotobiotic Mouse Model. Front Cell Infect Microbiol *6*, 191.

Sujino, T., London, M., Hoytema van Konijnenburg, D.P., Rendon, T., Buch, T., Silva, H.M., Lafaille, J.J., Reis, B.S., and Mucida, D. (2016). Tissue adaptation of regulatory and intraepithelial CD4(+) T cells controls gut inflammation. Science *352*, 1581-1586.

Sullivan, Z.A., Khoury-Hanold, W., Lim, J., Smillie, C., Biton, M., Reis, B.S., Zwick, R.K., Pope, S.D., Israni-Winger, K., Parsa, R.*, et al.* (2021). gammadelta T cells regulate the intestinal response to nutrient sensing. Science *371*.

Svendsen, B., Pais, R., Engelstoft, M.S., Milev, N.B., Richards, P., Christiansen, C.B., Egerod, K.L., Jensen, S.M., Habib, A.M., Gribble, F.M.*, et al.* (2016). GLP1- and GIP-producing cells rarely overlap and differ by bombesin receptor-2 expression and responsiveness. J Endocrinol *228*, 39-48.

Svendsen, B., Pedersen, J., Albrechtsen, N.J., Hartmann, B., Torang, S., Rehfeld, J.F., Poulsen, S.S., and Holst, J.J. (2015). An analysis of cosecretion and coexpression of gut hormones from male rat proximal and distal small intestine. Endocrinology *156*, 847-857.

Talbot, J., Hahn, P., Kroehling, L., Nguyen, H., Li, D., and Littman, D.R. (2020). Feeding-dependent VIP neuron-ILC3 circuit regulates the intestinal barrier. Nature *579*, 575-580.

Tang, F., Chen, Z., Ciszewski, C., Setty, M., Solus, J., Tretiakova, M., Ebert, E., Han, J., Lin, A., Guandalini, S.*, et al.* (2009). Cytosolic PLA2 is required for CTL-mediated immunopathology of celiac disease via NKG2D and IL-15. J Exp Med *206*, 707-719.

Tatemoto, K., Carlquist, M., and Mutt, V. (1982). Neuropeptide Y--a novel brain peptide with structural similarities to peptide YY and pancreatic polypeptide. Nature *296*, 659-660.

Teitelbaum, D.H., O'Dorisio, T.M., Perkins, W.E., and Gaginella, T.S. (1984). Somatostatin modulation of peptide-induced acetylcholine release in guinea pig ileum. Am J Physiol *246*, G509-514.

Teitelman, G., Alpert, S., Polak, J.M., Martinez, A., and Hanahan, D. (1993). Precursor cells of mouse endocrine pancreas coexpress insulin, glucagon and the neuronal proteins tyrosine hydroxylase and neuropeptide Y, but not pancreatic polypeptide. Development *118*, 1031-1039.

Theodoropoulou, M., and Stalla, G.K. (2013). Somatostatin receptors: from signaling to clinical practice. Front Neuroendocrinol *34*, 228-252.

Thim, L., Kristensen, P., Nielsen, P.F., Wulff, B.S., and Clausen, J.T. (1999). Tissue-specific processing of cocaine- and amphetamine-regulated transcript peptides in the rat. Proc Natl Acad Sci U S A *96*, 2722-2727.

Thim, L., Nielsen, P.F., Judge, M.E., Andersen, A.S., Diers, I., Egel-Mitani, M., and Hastrup, S. (1998). Purification and characterisation of a new hypothalamic satiety peptide, cocaine and amphetamine regulated transcript (CART), produced in yeast. FEBS Lett *428*, 263-268.

Thorens, B. (2014). Neural regulation of pancreatic islet cell mass and function. Diabetes Obes Metab *16 Suppl 1*, 87-95.

Thursby, E., and Juge, N. (2017). Introduction to the human gut microbiota. Biochem J *474*, 1823-1836.

Tong, Q., Ye, C.P., Jones, J.E., Elmquist, J.K., and Lowell, B.B. (2008). Synaptic release of GABA by AgRP neurons is required for normal regulation of energy balance. Nat Neurosci *11*, 998-1000.

Tracey, K.J. (2002). The inflammatory reflex. Nature *420*, 853-859.

Travagli, R.A., and Anselmi, L. (2016). Vagal neurocircuitry and its influence on gastric motility. Nat Rev Gastroenterol Hepatol *13*, 389-401.

Tropini, C., Earle, K.A., Huang, K.C., and Sonnenburg, J.L. (2017). The Gut Microbiome: Connecting Spatial Organization to Function. Cell Host Microbe *21*, 433-442.

Uesaka, T., Young, H.M., Pachnis, V., and Enomoto, H. (2016). Development of the intrinsic and extrinsic innervation of the gut. Dev Biol *417*, 158-167.

Uyama, N., Geerts, A., and Reynaert, H. (2004). Neural connections between the hypothalamus and the liver. Anat Rec A Discov Mol Cell Evol Biol *280*, 808-820.

Vallon-Eberhard, A., Landsman, L., Yogev, N., Verrier, B., and Jung, S. (2006). Transepithelial pathogen uptake into the small intestinal lamina propria. J Immunol *176*, 2465-2469.

van den Top, M., Lee, K., Whyment, A.D., Blanks, A.M., and Spanswick, D. (2004). Orexigen-sensitive NPY/AgRP pacemaker neurons in the hypothalamic arcuate nucleus. Nat Neurosci *7*, 493-494.

van Diest, S.A., Stanisor, O.I., Boeckxstaens, G.E., de Jonge, W.J., and van den Wijngaard, R.M. (2012). Relevance of mast cell-nerve interactions in intestinal nociception. Biochim Biophys Acta *1822*, 74-84.

Vanden Berghe, T., Hulpiau, P., Martens, L., Vandenbroucke, R.E., Van Wonterghem, E., Perry, S.W., Bruggeman, I., Divert, T., Choi, S.M., Vuylsteke, M.*, et al.* (2015). Passenger Mutations Confound Interpretation of All Genetically Modified Congenic Mice. Immunity *43*, 200-209.

Veiga-Fernandes, H., and Mucida, D. (2016). Neuro-Immune Interactions at Barrier Surfaces. Cell *165*, 801-811.

Veiga-Fernandes, H., and Pachnis, V. (2017). Neuroimmune regulation during intestinal development and homeostasis. Nat Immunol *18*, 116-122.

Vivier, E., Artis, D., Colonna, M., Diefenbach, A., Di Santo, J.P., Eberl, G., Koyasu, S., Locksley, R.M., McKenzie, A.N.J., Mebius, R.E.*, et al.* (2018). Innate Lymphoid Cells: 10 Years On. Cell *174*, 1054-1066.

Voisin, T., Perner, C., Messou, M.A., Shiers, S., Ualiyeva, S., Kanaoka, Y., Price, T.J., Sokol, C.L., Bankova, L.G., Austen, K.F.*, et al.* (2021). The CysLT2R receptor mediates leukotriene C4-driven acute and chronic itch. Proc Natl Acad Sci U S A *118*.

von Moltke, J., Ayres, J.S., Kofoed, E.M., Chavarria-Smith, J., and Vance, R.E. (2013). Recognition of bacteria by inflammasomes. Annu Rev Immunol *31*, 73-106.

von Moltke, J., Ji, M., Liang, H.E., and Locksley, R.M. (2016). Tuft-cell-derived IL-25 regulates an intestinal ILC2-epithelial response circuit. Nature *529*, 221-225.

Vuong, H.E., Pronovost, G.N., Williams, D.W., Coley, E.J.L., Siegler, E.L., Qiu, A., Kazantsev, M., Wilson, C.J., Rendon, T., and Hsiao, E.Y. (2020). The maternal microbiome modulates fetal neurodevelopment in mice. Nature *586*, 281-286.

Vuong, H.E., Yano, J.M., Fung, T.C., and Hsiao, E.Y. (2017). The Microbiome and Host Behavior. Annu Rev Neurosci *40*, 21-49.

Wallrapp, A., Burkett, P.R., Riesenfeld, S.J., Kim, S.J., Christian, E., Abdulnour, R.E., Thakore, P.I., Schnell, A., Lambden, C., Herbst, R.H.*, et al.* (2019). Calcitonin Gene-

Related Peptide Negatively Regulates Alarmin-Driven Type 2 Innate Lymphoid Cell Responses. Immunity *51*, 709-723 e706.

Wallrapp, A., Riesenfeld, S.J., Burkett, P.R., Abdulnour, R.E., Nyman, J., Dionne, D., Hofree, M., Cuoco, M.S., Rodman, C., Farouq, D.*, et al.* (2017). The neuropeptide NMU amplifies ILC2-driven allergic lung inflammation. Nature *549*, 351-356.

Wang, A., Huen, S.C., Luan, H.H., Yu, S., Zhang, C., Gallezot, J.D., Booth, C.J., and Medzhitov, R. (2016). Opposing Effects of Fasting Metabolism on Tissue Tolerance in Bacterial and Viral Inflammation. Cell *166*, 1512-1525 e1512.

Wang, P., Loh, K.H., Wu, M., Morgan, D.A., Schneeberger, M., Yu, X., Chi, J., Kosse, C., Kim, D., Rahmouni, K.*, et al.* (2020). A leptin-BDNF pathway regulating sympathetic innervation of adipose tissue. Nature *583*, 839-844.

Wang, X., Chan, A.K., Sham, M.H., Burns, A.J., and Chan, W.Y. (2011). Analysis of the sacral neural crest cell contribution to the hindgut enteric nervous system in the mouse embryo. Gastroenterology *141*, 992-1002 e1001-1006.

Waterson, M.J., and Horvath, T.L. (2015). Neuronal Regulation of Energy Homeostasis: Beyond the Hypothalamus and Feeding. Cell Metab *22*, 962-970.

Weems, W.A., and Szurszewski, J.H. (1977). Modulation of colonic motility by peripheral neural inputs to neurons of the inferior mesenteric ganglion. Gastroenterology *73*, 273-278.

Wendeln, A.C., Degenhardt, K., Kaurani, L., Gertig, M., Ulas, T., Jain, G., Wagner, J., Hasler, L.M., Wild, K., Skodras, A.*, et al.* (2018). Innate immune memory in the brain shapes neurological disease hallmarks. Nature *556*, 332-338.

Wexler, B.C., Dolgin, A.E., and Tryczynski, E.W. (1957). Effects of a bacterial polysaccharide (piromen) on the pituitary-adrenal axis: adrenal ascorbic acid, cholesterol and histologic alterations. Endocrinology *61*, 300-308.

White, J.P., Xiong, S., Malvin, N.P., Khoury-Hanold, W., Heuckeroth, R.O., Stappenbeck, T.S., and Diamond, M.S. (2018). Intestinal Dysmotility Syndromes following Systemic Infection by Flaviviruses. Cell *175*, 1198-1212 e1112.

Wichmann, A., Allahyar, A., Greiner, T.U., Plovier, H., Lunden, G.O., Larsson, T., Drucker, D.J., Delzenne, N.M., Cani, P.D., and Backhed, F. (2013). Microbial modulation of energy availability in the colon regulates intestinal transit. Cell Host Microbe *14*, 582-590.

Wierup, N., Kuhar, M., Nilsson, B.O., Mulder, H., Ekblad, E., and Sundler, F. (2004). Cocaine- and amphetamine-regulated transcript (CART) is expressed in several islet cell types during rat development. J Histochem Cytochem *52*, 169-177.

Wierup, N., Richards, W.G., Bannon, A.W., Kuhar, M.J., Ahren, B., and Sundler, F. (2005). CART knock out mice have impaired insulin secretion and glucose intolerance, altered beta cell morphology and increased body weight. Regul Pept *129*, 203-211.

Wikoff, W.R., Anfora, A.T., Liu, J., Schultz, P.G., Lesley, S.A., Peters, E.C., and Siuzdak, G. (2009). Metabolomics analysis reveals large effects of gut microflora on mammalian blood metabolites. Proc Natl Acad Sci U S A *106*, 3698-3703.

Wilhelm, C.L., and Yarovinsky, F. (2014). Apicomplexan infections in the gut. Parasite immunology *36*, 409-420.

Williams, E.K., Chang, R.B., Strochlic, D.E., Umans, B.D., Lowell, B.B., and Liberles, S.D. (2016). Sensory Neurons that Detect Stretch and Nutrients in the Digestive System. Cell *166*, 209-221.

Wlodarska, M., Thaiss, C.A., Nowarski, R., Henao-Mejia, J., Zhang, J.P., Brown, E.M., Frankel, G., Levy, M., Katz, M.N., Philbrick, W.M.*, et al.* (2014). NLRP6 inflammasome orchestrates the colonic host-microbial interface by regulating goblet cell mucus secretion. Cell *156*, 1045-1059.

Woods, S.C., Lotter, E.C., McKay, L.D., and Porte, D., Jr. (1979). Chronic intracerebroventricular infusion of insulin reduces food intake and body weight of baboons. Nature *282*, 503-505.

Worthington, J.J., Reimann, F., and Gribble, F.M. (2018). Enteroendocrine cells-sensory sentinels of the intestinal environment and orchestrators of mucosal immunity. Mucosal Immunol *11*, 3-20.

Wostmann, B.S. (1973). Intestinal bile acids and cholesterol absorption in the germfree rat. J Nutr *103*, 982-990.

Wouters, M.M., Vicario, M., and Santos, J. (2016). The role of mast cells in functional GI disorders. Gut *65*, 155-168.

Wu, Z., Autry, A.E., Bergan, J.F., Watabe-Uchida, M., and Dulac, C.G. (2014). Galanin neurons in the medial preoptic area govern parental behaviour. Nature *509*, 325-330.

Xu, H., Ding, J., Porter, C.B.M., Wallrapp, A., Tabaka, M., Ma, S., Fu, S., Guo, X., Riesenfeld, S.J., Su, C.*, et al.* (2019). Transcriptional Atlas of Intestinal Immune Cells Reveals that Neuropeptide alpha-CGRP Modulates Group 2 Innate Lymphoid Cell Responses. Immunity *51*, 696-708 e699.

Xu, J., Bartolome, C.L., Low, C.S., Yi, X., Chien, C.H., Wang, P., and Kong, D. (2018). Genetic identification of leptin neural circuits in energy and glucose homeostases. Nature *556*, 505-509.

Yamada, K., Yuan, X., Otabe, S., Koyanagi, A., Koyama, W., and Makita, Z. (2002). Sequencing of the putative promoter region of the cocaine- and amphetamine-regulated-transcript gene and identification of polymorphic sites associated with obesity. Int J Obes Relat Metab Disord *26*, 132-136.

Yang, D., He, Y., Munoz-Planillo, R., Liu, Q., and Nunez, G. (2015). Caspase-11 Requires the Pannexin-1 Channel and the Purinergic P2X7 Pore to Mediate Pyroptosis and Endotoxic Shock. Immunity *43*, 923-932.

Yanik, T., Dominguez, G., Kuhar, M.J., Del Giudice, E.M., and Loh, Y.P. (2006). The Leu34Phe ProCART mutation leads to cocaine- and amphetamine-regulated transcript (CART) deficiency: a possible cause for obesity in humans. Endocrinology *147*, 39-43.

Yano, J.M., Yu, K., Donaldson, G.P., Shastri, G.G., Ann, P., Ma, L., Nagler, C.R., Ismagilov, R.F., Mazmanian, S.K., and Hsiao, E.Y. (2015). Indigenous bacteria from the gut microbiota regulate host serotonin biosynthesis. Cell *161*, 264-276.

Yarandi, S.S., Kulkarni, S., Saha, M., Sylvia, K.E., Sears, C.L., and Pasricha, P.J. (2020). Intestinal Bacteria Maintain Adult Enteric Nervous System and Nitrergic Neurons via Toll-like Receptor 2-induced Neurogenesis in Mice. Gastroenterology *159*, 200-213 e208.

Yavorska, I., and Wehr, M. (2016). Somatostatin-Expressing Inhibitory Interneurons in Cortical Circuits. Front Neural Circuits *10*, 76.

Ydens, E., Demon, D., Lornet, G., De Winter, V., Timmerman, V., Lamkanfi, M., and Janssens, S. (2015). Nlrp6 promotes recovery after peripheral nerve injury independently of inflammasomes. J Neuroinflammation *12*, 143.

Yermolaieva, O., Chen, J., Couceyro, P.R., and Hoshi, T. (2001). Cocaine- and amphetamine-regulated transcript peptide modulation of voltage-gated Ca2+ signaling in hippocampal neurons. J Neurosci *21*, 7474-7480.

Yi, M., Li, H., Wu, Z., Yan, J., Liu, Q., Ou, C., and Chen, M. (2018). A Promising Therapeutic Target for Metabolic Diseases: Neuropeptide Y Receptors in Humans. Cell Physiol Biochem *45*, 88-107.

Yuan, X., Huang, Y., Shah, S., Wu, H., and Gautron, L. (2016). Levels of Cocaine- and Amphetamine-Regulated Transcript in Vagal Afferents in the Mouse Are Unaltered in Response to Metabolic Challenges. eNeuro *3*.

Zaiss, M.M., Jones, R.M., Schett, G., and Pacifici, R. (2019). The gut-bone axis: how bacterial metabolites bridge the distance. J Clin Invest *129*, 3018-3028.

Zarrinpar, A., Chaix, A., Xu, Z.Z., Chang, M.W., Marotz, C.A., Saghatelian, A., Knight, R., and Panda, S. (2018). Antibiotic-induced microbiome depletion alters metabolic homeostasis by affecting gut signaling and colonic metabolism. Nat Commun *9*, 2872.

Zeisel, A., Hochgerner, H., Lonnerberg, P., Johnsson, A., Memic, F., van der Zwan, J., Haring, M., Braun, E., Borm, L.E., La Manno, G.*, et al.* (2018). Molecular Architecture of the Mouse Nervous System. Cell *174*, 999-1014 e1022.

Zhang, J., Jiang, N., Zhang, L., Meng, C., Zhao, J., and Wu, J. (2020). NLRP6 expressed in astrocytes aggravates neurons injury after OGD/R through activating the inflammasome and inducing pyroptosis. Int Immunopharmacol *80*, 106183.

Zhang, M., Borovikova, L.V., Wang, H., Metz, C., and Tracey, K.J. (1999). Spermine inhibition of monocyte activation and inflammation. Mol Med *5*, 595-605.

Zhang, M., Caragine, T., Wang, H., Cohen, P.S., Botchkina, G., Soda, K., Bianchi, M., Ulrich, P., Cerami, A., Sherry, B.*, et al.* (1997). Spermine inhibits proinflammatory cytokine synthesis in human mononuclear cells: a counterregulatory mechanism that restrains the immune response. J Exp Med *185*, 1759-1768.

Zhang, M., Wang, H., and Tracey, K.J. (2000). Regulation of macrophage activation and inflammation by spermine: a new chapter in an old story. Crit Care Med *28*, N60-66.

Zhao, S., Gong, Z., Zhou, J., Tian, C., Gao, Y., Xu, C., Chen, Y., Cai, W., and Wu, J. (2016). Deoxycholic Acid Triggers NLRP3 Inflammasome Activation and Aggravates DSS-Induced Colitis in Mice. Front Immunol *7*, 536.

Zheng, D., Kern, L., and Elinav, E. (2021). The NLRP6 inflammasome. Immunology *162*, 281-289.

Zhou, L., Chu, C., Teng, F., Bessman, N.J., Goc, J., Santosa, E.K., Putzel, G.G., Kabata, H., Kelsen, J.R., Baldassano, R.N.*, et al.* (2019). Innate lymphoid cells support regulatory T cells in the intestine through interleukin-2. Nature *568*, 405-409.

Zigmond, E., Bernshtein, B., Friedlander, G., Walker, C.R., Yona, S., Kim, K.W., Brenner, O., Krauthgamer, R., Varol, C., Muller, W.*, et al.* (2014). Macrophage-restricted interleukin-10 receptor deficiency, but not IL-10 deficiency, causes severe spontaneous colitis. Immunity *40*, 720-733.